

Ingeniería e Investigación
Journal
Abbreviated Journal Title: **Ing. Investig.**

Editor-in-chief
Andrés Pava, Ph.D.

Editorial Assistants
Ingri Gisela Camacho, B.Sc.
Julian Arcila-Forero, M.Sc., B.Sc.

Editorial Board
Paulo César Narváez Rincón, Ph.D.
Universidad Nacional de Colombia - Bogotá
Julio Esteban Colmenares, Ph.D.
Universidad Nacional de Colombia - Bogotá
Luis Fernando Niño, Ph.D.
Universidad Nacional de Colombia - Bogotá
Óscar Germán Duarte, Ph.D.
Universidad Nacional de Colombia - Bogotá
Jaime Salazar Contreras, M.U.
Universidad Nacional de Colombia - Bogotá
Ignacio Pérez, Ph.D.
Escuela Colombiana de Ingeniería - Colombia
Nelly Cecilia Alba, Ph.D.
Universidad Autónoma de Occidente - Colombia
Heberto Tapia García, Ph.D.
Universidad de Antioquia - Colombia
Ricardo Llamasa Villalba, Ph.D.
UIS - Bucaramanga - Colombia
Gustavo Bolaños, Ph.D.
Universidad del Valle - Colombia
Dora Ángela Hoyos Ayala, Ph.D.
Universidad de Antioquia - Colombia
Lourdes Zumalacárregui, Ph.D.
Ciudad Universitaria José Antonio Echeverría -
Cujae, Cuba
Federico Méndez Lavielle, Ph.D.
Universidad Nacional Autónoma de México -
México
Mauricio Camargo, Ph.D.
Université de Lorraine - France
Laure Morel, Ph.D.
Université de Lorraine - France
Andrés Romero Quete, Ph.D.
Universidad Nacional de San Juan
San Juan - Argentina
Víctor Berrera Núñez, Ph.D.
Data Analytics Senior Manager - PwC
México D.F. - México

Frequency
Quarterly, three issues per year
April, August and December

Cover Layout
Carlos Andrés Ortiz Valle

Proofreader
José Daniel Gutiérrez-Mendoza

Layout Artist
David Mauricio Valero

**If you need additional information, please
contact**
revij_bog@unal.edu.co
Bogotá - Colombia
April - 2022

Table of Contents

Agricultural Engineering

Growth and Physiological Performance of Barley Plants Produced under Nitrogen Management
Bruno Oliveira Novais Araújo, Felipe Santos Zulli, Eduardo Goncalvez Borges, Manoela Andrade Monteiro, Jessica Mengue Rolim, Letícia Barão Medeiros, Angelita Celente Martin, Tiago Pedó, and Tiago Zanatta Aumonde

Chemical / Food / Environmental Engineering

Semicontinuous Lixiviation Process for Compound Extraction from *Cannabis sativa* grown in Colombia
Oscar Yecid Buitrago Suescún, and Miguel Augusto Santaella Serrano

Civil / Sanitary Engineering

Methodology for Classifying the Structural State of Uninspected Pipes in Sewer Networks Based on Support Vector Machines
Nathalie Hernández, Miguel Cañon, and Andrés Torres

The Self-Healing Effect on Bacteria-Enriched Steel Fiber- Reinforced SCC
Vasudev Raman, Nivin Philip, and Nijo Baven

Electrical / Electronic / Telecommunications Engineering

Low-Timing-Jitter and Low-Phase-Noise Microwave Signal Generation Using a VCSEL-Based Optoelectronic Oscillator
Christian Daniel Muñoz, Juan Coronel, Margarita Varón, Fabien Destic and Angélique Rissons

On the Optimal Reconfiguration of Radial AC Distribution Networks Using an MINLP Formulation: A GAMS-Based Approach
Oscar Danilo Montoya, Walter Julián Gil González, Luis Fernando Grisales-Noreña, Diego Giral, and Alexander Molina-Cabrera

Industrial Engineering

An Efficient Algorithm Applied to Optimized Billing Sequencing
Anderson Rogério Faia Pinto and Marcelo Seido Nagano

Mechanical Engineering / Mechatronics / Materials Science

Assessment of the Compressive Strength of Lime Mortars with Admixtures Subjected to Two Curing Environments
Andrés Felipe Espitia Morales and Nancy Torres Castellanos

Effect of the Colombian Renewable Energy Law on the Levelized Cost of a Substitute Gaseous Fuel Produced from MSW Gasification
Néstor D. Montiel-Bohórquez, Juan D. Saldarriaga-Loaiza and Juan F. Pérez

Systems / Computer Engineering

Automatic Personality Evaluation from Transliterations of YouTube Vlogs Using Classical and State-of-the-Art Word Embeddings
Felipe Orlando López Pabón and Juan Rafael Orozco Arroyave

Education in Engineering

First Aid Approaches, Teaching, and Knowledge and Technology Transfer to Undergraduate Engineering Students
Rosângela de Franca Bail, João Luiz Kovalski, Regina Negri Pagani, Daiane Maria de Genaro Chirolí, and Vander Luiz Silva

Typifying Students' Help-Seeking Behavior in an Intelligent Tutoring System for Mathematics
Roberto Ángel Meléndez-Armenta, Genaro Rebolledo-Méndez, and N. Sofía Huerta-Pacheco

**Facultad de Ingeniería
Universidad Nacional de Colombia**

María Alejandra Guzmán
Dean

Camilo Andrés Cortés Guerrero
Vice Dean of Research and Extension

Jesús Hernán Camacho Tamayo

Vice Dean of Academic Affairs

Sandra Liliana Rojas Martines

Director of the Students Welfare Service

Scientific Committee

Fabio González, Ph.D.

Universidad Nacional de Colombia - Bogotá

Miguel J. Bagajewicz, Ph.D.

University of Oklahoma, USA

Jayant Rajgopal, Ph.D.

University of Pittsburgh, USA

Ethics Committee

Óscar Fernando Castellanos, Ph.D.

Universidad Nacional de Colombia - Bogotá

Jullio César Cañón, Ph.D.

Universidad Nacional de Colombia - Bogotá

**Papers published in *Ingeniería e Investigación*
journal are abstracted/indexed in**

- Science Citation Index Expanded (SciSearch®), Clarivate Analytics
- Scopus - Elsevier
- Scientific Electronic Library Online - SciELO, Colombia
- Chemical Abstract
- Índice de Revistas Latinoamericanas en Ciencias Periódica
- Dialnet
- Sistema Regional de Información en Línea para Revistas Científicas de América Latina, El Caribe, España y Portugal - Latindex
- Ebsco Publishing
- DOAJ - Directory of Open Access Journals
- Redib - Red Iberoamericana de Innovación y Conocimiento Científico

The *Ingeniería e Investigación* journal was created in 1981. It is an entity in charge of spreading the teaching, scientific, and technical research conducted in the Department of Engineering of Universidad Nacional de Colombia and other national and international institutions. *Ingeniería e Investigación* deals with original, unedited scientific research and technological developments in the various disciplines related to engineering. *Ingeniería e Investigación* contributes to the development of knowledge, generating a global impact on academia, industry, and society at large, through an exchange of knowledge and ideas that maintains a set of serious and recognized quality standards.

The content of the articles published in this journal does not necessarily reflect the opinions of the Editorial Team. These texts can be totally or partially reproduced, provided that a correct citation of the source is given.

Ingeniería e Investigación publications are developed for the academic community who is interested in research and the development of engineering knowledge. We invite readers to be part of this journal and participate either as authors, peer reviewers, or subscribers.

If you need additional information, please contact:

www.revistas.unal.edu.co/index.php/ingenev

E-mail: revii_bog@unal.edu.co

Tel: 57(1) 3 16 5000 Ext. 13674

Tabla de Contenido

Ingeniería Agrícola

Crecimiento y rendimiento fisiológico de plantas de cebada producidas bajo manejo de nitrógeno

Bruno Oliveira Novais Araújo, Felipe Santos Zulli, Eduardo Goncalvez Borges, Manoela Andrade Monteiro, Jessica Mengue Rolim, Letícia Barão Medeiros, Angelita Celente Martin, Tiago Pedó, y Tiago Zanatta Aumonde

Ingeniería Química / Alimentos / Ambiental

Proceso semicontinuo de lixiviación para la extracción de compuestos a partir de Cannabis sativa cultivado en Colombia

Oscar Yecid Buitrago Suescún, y Miguel Augusto Santaella Serrano

Ingeniería Civil / Sanitaria

El efecto de autocuración en SCC reforzado con fibra de acero enriquecida con bacterias

Nathalie Hernández, Miguel Cañón, y Andrés Torres

Metodología para clasificar la condición estructural de tuberías no inspeccionadas de las redes de alcantarillado basada en máquinas de soporte vectorial

Vasudev Raman, Nivin Philip, y Nijo Baven

Ingeniería Eléctrica / Electrónica / Telecomunicaciones

Generación de señales microondas de bajo ruido y fluctuación de fase utilizando un oscilador optoelectrónico basado en VCSEL

Christian Daniel Muñoz, Juan Coronel, Margarita Varón, Fabien Destic, y Angelique Rissons

Sobre la reconfiguración óptima de redes radiales de distribución empleando un modelo de PNLEM: un enfoque basado en GAMS

Oscar Danilo Montoya, Walter Julián Gil González, Luis Fernando Grisales-Noreña, Diego Giral, y Alexander Molina-Cabrera

Ingeniería Industrial

Un algoritmo eficiente aplicado a la secuencia de facturación optimizada

Anderson Rogério Faia Pinto y Marcelo Seido Nagano

Ingeniería Mecánica / Mecatrónica / Ciencia de los Materiales

Evaluación de la resistencia a compresión de morteros de cal adicionados, sujetos a dos ambientes de curado

Andrés Felipe Espitia Morales y Nancy Torres Castellanos

Efecto de la ley colombiana de energías renovables en el costo nivelado del combustible gaseoso sustituto producido a partir de la gasificación de RSU

Néstor D. Montiel-Bohórquez, Juan D. Saldarriaga-Loaiza y Juan F. Pérez

Ingeniería de Sistemas / Informática

Evaluación automática de la personalidad a partir de las transliteraciones de los vlogs de YouTube mediante el uso de incrustaciones de palabras clásicas

Felipe Orlando López Pabón y Juan Rafael Orozco Arroyave

Educación en Ingeniería

Enfoques de primeros auxilios, enseñanza y transferencia de conocimiento y tecnología a estudiantes de pregrado en ingeniería

Rosangela de Franca Bail, João Luiz Kovalski, Regina Negri Pagani, Daiane Maria de Genaro Chirol, y Vander Luiz Silva

Tipificación de comportamientos de estudiantes relacionados con la búsqueda de ayuda en un sistema inteligente de tutorías para matemáticas

Roberto Ángel Meléndez-Armenta, Genaro Rebolledo-Méndez, y N. Sofía Huerta-Pacheco

Growth and Physiological Performance of Barley Plants Produced under Nitrogen Management

Crecimiento y rendimiento fisiológico de plantas de cebada producidas bajo manejo de nitrógeno

Bruno Oliveira Novais Araújo¹, Felipe Santos Zulli², Eduardo Goncalvez Borges³, Manoela Andrade Monteiro⁴, Jessica Mengue Rolim⁵, Leticia Barao Medeiros⁶, Angelita Celente Martins⁷, Tiago Pedó⁸, and Tiago Zanatta Aumonde⁹

ABSTRACT

This work aimed to evaluate the effect of nitrogen dose management on the growth responses and physiological performance of barley seeds. Two barley cultivars (BRS Brau and BRS Cauê) and four nitrogen doses were used. The experimental design consisted of randomized blocks in a 2 X 4 factorial scheme (cultivars BRS Brau and BRS Cauê x nitrogen doses 120, 150, 180, and 210 kg ha⁻¹). Successive collections of primary data were performed every fourteen days for growth analysis. The analyzed variables were total dry matter, dry matter production and relative growth rate, assimilated partition, and seed electrical conductivity. Increasing nitrogen doses caused a temporal-quantitative difference in growth, partition, and the accelerated aging test of barley seeds. The 150 kg ha⁻¹ N dose resulted in total dry matter over time (Wt) superiority for both evaluated cultivars. The variable dry matter production rate achieved an increase with the 150 kg ha⁻¹ N dose at 70 days after emergence (DAE) for BRS Brau and at 56 DAE for BRS Cauê supporting Wt. The 180 and 150 kg ha⁻¹ N doses increased the relative growth rate for BRS Brau and BRS Cauê.

Keywords: cereal, fertilizer, *Hordeum vulgare*

RESUMEN

Este trabajo tuvo como objetivo evaluar el efecto del manejo de las dosis de nitrógeno en las respuestas de crecimiento y el rendimiento fisiológico de las semillas de cebada. Se utilizaron dos cultivares de cebada (BRS Brau and BRS Cauê) y cuatro dosis de nitrógeno. El diseño experimental consistió en bloques al azar en un esquema factorial 2 X 4 (cultivares BRS Brau y BRS Cauê x dosis de nitrógeno 120, 150, 180 y 210 kg ha⁻¹). Se realizaron recolecciones sucesivas de datos primarios cada catorce días para el análisis de crecimiento. Las variables analizadas fueron materia seca total, producción de materia seca y tasa de crecimiento relativa, partición asimilada y conductividad eléctrica de las semillas. El aumento de las dosis de nitrógeno causa una diferencia cuantitativa-temporal en el crecimiento, partición y la prueba de envejecimiento acelerado de las semillas de cebada. La dosis de 150 kg ha⁻¹ N resultó en una superioridad total de la materia seca en el tiempo (Wt) para ambos cultivares evaluados. La tasa variable de producción de materia seca logró un aumento para la dosis de 150 kg ha⁻¹ N a los 70 días después de la germinación (DAE) para BRS Brau y a 56 DAE para BRS Cauê apoyando Wt. Las dosis de 180 y 150 kg ha⁻¹ N aumentaron la tasa de crecimiento relativo para BRS Brau y BRS Cauê.

Palabras clave: cereal, fertilizante, *Hordeum vulgare*

Received: July 13th 2020

Accepted: August 6th 2021

¹ Agronomist Engineer, Department of Crop Protection, Federal University of Pelotas – Pelotas, Rio Grande do Sul, Brazil. Affiliation: Master's student in the Crop Protection Graduate Program, Federal University of Pelotas, Pelotas, RS CEP 96160-000, Brazil. Email: bruno-tec@outlook.com

² Agronomy student, Federal University of Pelotas – Pelotas, Rio Grande do Sul, Brazil. Email: filipy@hotmai.com

³ Agronomist Engineer. Federal University of Pelotas – Pelotas, Rio Grande do Sul, Brazil. Email: eduardogborges@gmail.com

⁴ Agronomist Engineer, Ph.D. in Science, Department of Phytotechnics, Federal University of Pelotas – Pelotas, Rio Grande do Sul, Brazil. Email: manu_agro@hotmail.com

⁵ Forest engineer, M.Sc. in Forest engineer, Federal University of Santa Maria, RS, Brazil. Affiliation: Doctoral Student in Seed Science and Technology, Federal University of Pelotas. Pelotas, Rio Grande do Sul, Brazil. Email: eng.jessicarolim@gmail.com

⁶ Agronomist Engineer, M.Sc. in Agrobiolgy, Federal University of Santa Maria, RS, Brazil. Affiliation: Doctoral Student in Seed Science and Technology, Federal University of Pelotas. Pelotas, Rio Grande do Sul, Brazil. Email: lele-medeiros@hotmail.com

⁷ Biological Sciences, M.Sc., and Ph.D. in Plant Physiology. Federal University of Pelotas – Pelotas, Rio Grande do Sul, Brazil. Email: angel-celente@hotmail.com

⁸ Agronomist Engineer, Ph.D. in Science, Federal University of Pelotas – Pelotas, Rio Grande do Sul, Brazil. Affiliation: Associate Professor, Federal University of Pelotas (Brazil). Rio Grande do Sul, Brazil. Email: tiago.pedo@gmail.com

Introduction

Barley (*Hordeum vulgare* L.), a member of the *Poaceae* family, is grown in cold seasons. In the southern region of Brazil, the ideal time for sowing is between May and June, which is appropriate for winter growing (Texeira Filho *et al.*, 2008). The zoning for this cultivation aims to escape the times of frost occurrence when the crop is established and begins to grow, as well as the rainfall during the grain harvest period.

⁹ Agronomist Engineer, Ph.D. in Science, Federal University of Pelotas – Pelotas, Rio Grande do Sul, Brazil. Affiliation: Associate Professor, Federal University of Pelotas (Brazil). Rio Grande do Sul, Brazil. Email: tiago.aumonde@gmail.com

How to cite: Novais, B. O., Santos, F., Goncalvez, E., Monteiro, M., Mengue, J., Barao, L., Celente, A., Pedó, T. and Zanatta, T. (2022). Growth and Physiological Performance of Barley Plants Produced under Nitrogen Management. *Ingeniería e Investigación*, 42(2), e89116. <https://doi.org/10.15446/ing.investig.v42n2.89116>



Attribution 4.0 International (CC BY 4.0) Share - Adapt

The southern region of Brazil is the main producer of barley in the country, with beer production and animal feed being the largest end consumers of this production (De Mori and Minella, 2012). In the 2018 harvest, the area proposed for the cultivation of barley was just over 111 thousand ha, which represented a decrease of 3,2% compared to the previous year. In Rio Grande do Sul, there was a similar reduction in the area intended for grain growth - around 2,5% - decreasing from 57 thousand to 55,6 thousand ha.

The productivity achieved in Brazil during the 2019 harvest was 3 557 kg ha⁻¹: an increase of 12,6% compared to the previous year, which was 3 159 kg ha⁻¹. The crops of Rio Grande do Sul, however, reached the average yield of 2 370 kg ha⁻¹, also showing a 25,4% drop compared to 2018.

Although there was no change in the cultivated area in the country, national production decreased by 12,3% compared to the 2018 harvest. Rio Grande do Sul is the second largest producer in the country, with a production of 134,4 thousand tons in 2019, even with a 25,2% drop in production vs. the 2018 harvest. Paraná, which remained the largest barley producer in Brazil, showed a 3,1% reduction, which is equivalent to the production of 237,6 thousand tons (CONAB, 2020).

Nitrogen is considered essential for plants. In soil under adequate aeration conditions, this nutrient is absorbed as nitrate by the root system, and it can be accumulated in the cell vacuoles or transported, thus serving as a component of amino acids, proteins, and nucleic acids (Taiz and Zeiger, 2017).

The amount of nitrogen provided to plants, among other factors, depends on the nutritional requirement of the crop. There is a wide range of nitrogen sources on the market such as urea, Chile saltpeter (NaNO₃), Bengal saltpeter (KNO₃), ammonium sulfate ((NH₄)₂SO₄), cattle manure (1,7% N), and poultry litter (3,0% N). However, among the available nitrogen sources, the most widely employed in agriculture is urea since it is easily acquired and cost-effective.

The technical recommendations for fertilization and acidity correction in Brazilian soils aim to improve grain yield. However, the best nutritional condition or management for a good performance is not always equivalent to the one that prioritizes seed quality. Several factors affect physiological quality, including maturation, phytosanitary condition, and nutritional availability in the development of the embryonic axis, as well as the nutritional and the stressful conditions under which the seed was formed, which may change its weight and size, as evaluated by Soares et al. (2008).

Growth analysis allows quantifying vegetable carbon allocation in its variability along the crop cycle. In addition to being considered low-cost and accurate, this method can be applied throughout the growth and development of the species, and it is used to evaluate differences in response to management or environmental variations (Koch et al., 2017).

On the other hand, seed quality can be gauged by vigor, so that the immediate and uniform emergence of seedlings will favor early crop establishment. In this sense, the expression of seed vigor can be determined by means of several tests such as electrical conductivity, field seedling emergence, first germination count, and aging tests (Silva et al., 2014).

This work aimed to evaluate the effect of nitrogen doses on the growth responses and physiological performance of barley seeds.

Materials and methods

The experiment was performed in a didactic and experimental area at the Federal University of Pelotas (UFPEL), Department of Phytotechnics, PPG in Seed Science and Technology (31 ° 52 'S; 52 ° 21' W). The data of maximum and minimum temperature (°C), solar radiation (cal cm⁻² day⁻¹), rainfall (mm), and relative humidity (%) were obtained from a climate report from the Pelotas agroclimatological station (Figure 1), located near an UFPEL campus.

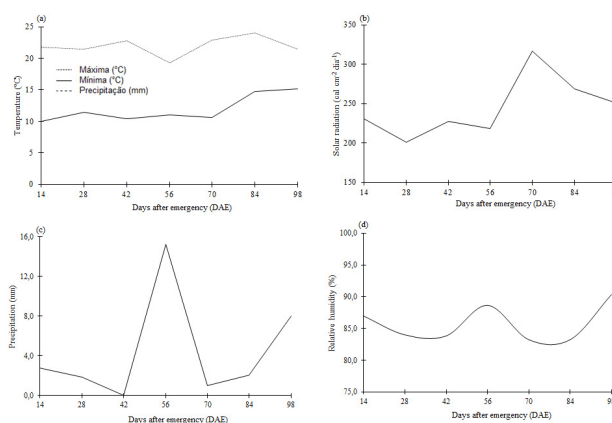


Figure 1. Maximum and minimum temperature (°C), solar radiation (cal cm⁻² day⁻¹), precipitation (mm), and relative humidity (%) data from the Pelotas agroclimatological station

Source: Authors

The seeds of two barley cultivars (BRS Cauê and BRS Brau) indicated for the states of Paraná, Santa Catarina, and Rio Grande do Sul were used. Sowing was carried out in a soil classified as *Solodic Eutrophic Haplic Planosol* (Streck et al., 2008).

Soil correction was performed according to the requirements determined in the soil analysis (Table 1), as well as the recommendations of the fertilization and liming manual of the states of Rio Grande do Sul and Santa Catarina (CQFS, 2016) for a productivity of four tons per ha.

Table 1. Chemical analysis of the soil used as a basis for the correction of acidity and fertility for the cultivation of barley (Pelotas, RS)

O.M.	pH	Clay	P	K	Ca	Mg	Al	H+Al	AEC	V	Ind.
%	H ₂ O	%	mg dm ⁻³			cmol dm ⁻³				%	SMP
2,07	4,8	14	21,5	27	3,3	1,1	0,3	6,2	4,9	42	5,7

Source: Authors

Regarding soil fertility correction, 60 kg ha⁻¹ of phosphorus and potassium were required, and they were obtained using triple super phosphate (41% P₂O₅) and potassium chloride (58% K₂O) as sources. Nitrogen fertilization required 120 kg ha⁻¹ as a control treatment, which was divided into two applications – sowing and tillering – sixteen days after emergence (DAE) with respective doses of 20 kg ha⁻¹ and 100 kg ha⁻¹, as well as urea being the nitrogen source (45% N).

The experiment consisted of a randomized block design in a 2 X 4 factorial scheme (two cultivars and four nitrogen doses) and four replications, with five lines spaced 0,17 m and 1,80 m in length. The corrected population density was 250 plants per m² as recommended (Embrapa, 2007).

The treatments consisted of nitrogen doses comprised by T1 100% (control), which received the 120 kg ha⁻¹ dose; T2 125% (150 kg ha⁻¹); T3 150% (180 kg ha⁻¹); and T4 175% (210 kg ha⁻¹). For growth evaluations, samples were collected throughout the crop cycle at regular intervals of fourteen days after emergence. In each collection, the plants were separated into different structures (roots, stalks, leaves, and ears). To determine the leaf area (A_l) the Liquor LI-3100 area meter was used, and the results were expressed in square meters (m²). Subsequently, the plant components were placed separately in brown paper envelopes and, to obtain the dry matter, the structures were taken to the greenhouse with forced ventilation at a temperature of 70° ± 2 °C until constant mass was achieved.

The total dry matter over time (W_t) data were adjusted using the simple logistic equation: $W_t = W_m / (1 + A \cdot e^{-Bt})$, where W_m is the asymptotic estimate of maximum growth; “A” and “B” are adjustment constants; “e” is the natural basis of the neperian logarithm; and “t” is the time in days after emergence (Richards, 1969). The primary dry matter data of leaves (W_l), roots (W_r), stalks (W_s), and ears (W_{esp}) were adjusted using orthogonal polynomials (Richards, 1969). The instantaneous dry matter production rate values (C_t) were obtained by derivative from the adjusted total dry matter equations (W_t). The equation $R_w = l/W_t \cdot d_w/d_t$ was used to determine the instantaneous values of the relative growth rate (R_w) (Radford, 1967).

The dry matter partition between the different organs was determined from the total dry mass allocated in each structure in relation to the total dry matter, and the results were expressed in percentage.

Electrical conductivity was determined from four samples containing four subsamples of 25 seeds for each treatment. The seeds were mass measured after being placed in polyethylene cups containing 80 mL of deionized water, which was kept in a *Biochemical Oxygen Demand* (BOD) type germinator at a temperature of 20°C with a 12-hour photoperiod. The electrical conductivity was determined after 3, 6, and 24 h of imbibition by means of a digital

conductivity meter. The results were expressed as μS cm⁻¹ g⁻¹ seeds (Ollson *et al.*, 2010).

Primary growth data were subjected to an analysis of variance at 5% probability, and the total dry matter was analyzed by simple logistic equation (Lopes and Lima 2015). Assimilated partition data were converted to percentage of dry matter allocated to each evaluated structure, whereas those related to germination and vigor were represented by orthogonal polynomials when significant at 5% probability.

Results and discussion

There was a significant difference for the primary values of leaf area, leaf, stalks, roots, and ear dry matter (Table 2). Total dry matter values (W_t) were adjusted for the simple logistic tendency for both cultivars submitted to nitrogen doses (Figure 2).

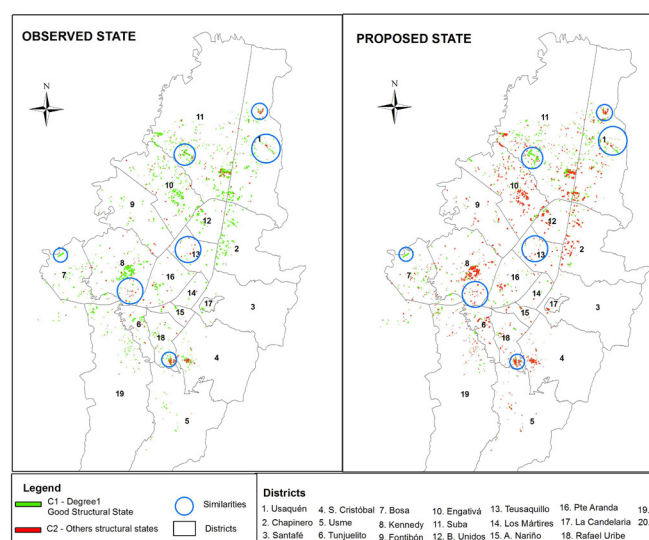


Figure 2. Total dry matter (a, b), dry matter production rate (c, d), and relative growth rate (e, f) in two barley cultivars (BRS Brau and BRS Cauê) in Pelotas, RS
Source: Authors

W_t was low at the beginning of the cycle until about 28 DAE (days after emergence), with a subsequent sharp increase in dry mass production. For cultivar BRS Brau, 82 days after nitrogen application, there was an increase of 8,66% and a decrease of 11,37 and 6,37% in the production of T2-weighted matter (150 kg ha⁻¹ N), T4 (210 kg ha⁻¹ N), and T3 (180 kg ha⁻¹ N) in relation to the control dose, respectively.

For cultivar BRS Cauê, 82 days after nitrogen application, there was an increase of 0,88% and a decrease of 18,82 and 11,50% in dry matter yield at doses of T2 (150 kg ha⁻¹ N), T3 (180 kg ha⁻¹ N), and T4 (210 kg ha⁻¹ N) in relation to the control dose, respectively. At the end of the development cycle of cultivars BRS Brau and BRS Cauê, plants under T2 application (150 kg ha⁻¹ N) reached a higher total dry matter production.

Table 2. Summary analysis of variance with mean squares for leaf dry matter (W_f), stem (W_c), root (W_r), and ear (W_{esp}) data of barley cultivars produced under application of nitrogen doses (Pelotas, RS)

Factor	DF	MS W_f	MS W_c	MS W_r	MS W_{esp}
CV	1	2 032,6392*	6 396,1151*	5 731,8153*	7 212,0514*
Times	6	1 3801,025	7 7588,403	14 083,167	351 514,63
Doses	3	572,86774 ^{ns}	591,31676 ^{ns}	118,60777 ^{ns}	568,91259 ^{ns}
CV X Times	6	1 156,7783*	368,70568*	470,46378 ^{ns}	5 993,0143*
Doses X Times	18	883,0618*	920,46653 ^{ns}	453,6561*	1 195,0103 ^{ns}
CV X Doses	3	706,54951 ^{ns}	671,5948 ^{ns}	340,72553 ^{ns}	3 327,483 ^{ns}
CV X Doses X Times	18	377,22714 ^{ns}	671,5948*	324,933 ^{ns}	2 477,5966 ^{ns}
Total	223				
Average		37,91	42	27	63
CV(%)		43,64	G	58	61

Note: (*) significance level 5%; (ns) not significant

Source: Authors

A lower initial plant growth is normal during development due to the low leaf area and low root volume. At this stage, the plants have a low assimilate production capacity, reduced respiratory demand, and low water and nutrient absorption, which limits their growth. Koch *et al.* (2017) observed a similar behavior while studying the response of wheat plants with nitrogen fertilization and growth regulator application.

The dry matter production rates (C_i) were low up to about 28 DAE (Figure 2c, d), which corroborates the total dry matter data for the same period. The maximum dry matter yield rates for both cultivars were obtained at approximately 56 DAE.

For cultivar BRS Brau, the maximum C_i was observed at 56 DAE for T3 (180 kg ha⁻¹ N), with an increase of 31,7%, and at 70 DAE for T2 (150 kg ha⁻¹ N) and T4 (210 kg ha⁻¹ N), which represented an increase of 9,97% and a decrease of 1,15%, respectively, according to the control dose. For the cultivar BRS Cauê, at 56 DAE, the T2-influenced plants (150 kg ha⁻¹ N) increased by 46,6%, and, at 70 DAE, the plants under the influence of T3 (180 kg ha⁻¹ N) and T4 (210 kg ha⁻¹ N) showed a decrease of 19,8 and 16,8%, for C_i in relation to the control dose.

The highest doses of nitrogen available in the soil did not have a direct relation to the maximum rate of dry matter production but obtained a temporal difference for cultivar BRS Brau. Cultivar BRS Cauê also presented variation according to the dose used. Thus, the adequate amount of nitrogen available to the plants could provide greater assimilation and conversion of this mineral into amino acids and proteins, which are related to the growth and development of the crop (Malavolta, 2006), that is, according to the capacity of the cultivar used.

The relative growth rate (R_w) for both cultivars showed maximum values at the beginning of development (14 DAE), with a subsequent systematic decrease until the end of the plant cycle (Figures 2d, e). It was observed that, at 14 DAE, cultivar BRS Brau obtained a difference in growth rate in relation to the different doses, in which treatments T2 (150 kg ha⁻¹ N), T3 (180 kg ha⁻¹ N), and T4 (210 kg ha⁻¹ N) resulted in an increase in R_w in the order of 17,9, 55,7, and 27,4% in relation to the control.

Cultivar BRS Cauê, evaluated at 14 DAE, showed a difference in R_w values for treatments: T2 (150 kg ha⁻¹ N) resulted in an increase of 76,2%; whereas the T3 (180 kg ha⁻¹ N) and T4 (210 kg ha⁻¹ N) treatments reported decreases of 2 and 6,3% in relation to the control.

When they are young, crop plants have high an assimilation capacity via photosynthesis. This kind of performance is partly due to the high amount of young tissues with high photosynthetic rate that favor relative growth (Aumonde *et al.*, 2013). The gradual decrease of R_w over the course of the plant cycle arises from the progressive increase of non-photosynthetic tissues and increased respiration of older tissues (Pedó *et al.*, 2015). This may also be caused by self-shading and loss in assimilate production efficiency (Aumonde *et al.*, 2013).

Dry matter partitioning of barley plants under application of nitrogen doses resulted in quantitative differences in their different organs in both cultivars. At 28 DAE, plants from treatments T4 (210 kg ha⁻¹ N) and T2 (150 kg ha⁻¹ N) in cultivar BRS Brau presented a higher W_f accumulation than the control treatment: approximately 4,57 and 0,63%, respectively. T3 (180 kg ha⁻¹ N) obtained a reduction of 3,38% compared to T1 (control). When W_c was analyzed, it could be observed that treatments T2 (150 kg ha⁻¹ N), T4 (210 kg ha⁻¹ N), and T3 (180 kg ha⁻¹ N) presented superiority of 118,10, 79,31, and 31,46% compared to T1. The results of the variable W_r showed that T3 (180 kg ha⁻¹ N) increased by 3,71%, while T2 (150 kg ha⁻¹ N) and T4 (210 kg ha⁻¹ N) decreased in the order of 12,6 and 29,65% in relation to T1 (Figure 3 a, c, e, g).

When the cultivar Cauê was analyzed for the variable W_f , a similar behavior at 28 DAE was observed, where T2 (150 kg ha⁻¹ N) and T4 (210 kg ha⁻¹ N) had higher increases of (9,23 and 4,26%). Yet, T3 (180 kg ha⁻¹ N) obtained a 7% decrease in relation to T1. For W_c , however, T3 (180 kg ha⁻¹ N) was the one with a superiority of 21,52%, whereas T2 (150 kg ha⁻¹ N) and T4 (210 kg ha⁻¹ N) presented inferior results: 23,62 and 14,82% in relation to T1. The same occurred while observing W_r , in which T3 (180 kg ha⁻¹ N) presented a 17,61% superiority to T1 (control), whereas T2 (150 kg ha⁻¹ N) and T4 (210 kg ha⁻¹ N) showed a reduction of 35,04 and 10,81% when compared to T1 (control) (Figure 3 a, c, e, g).

Adjustments in preferential metabolic drainage occur during the development of the culture, which will allocate products from photosynthesis. In the early stages of growth, leaf and

root accumulation is preferred, and, later, the allocation to the stalks, reproductive structures, and ears. Thus, the direction of assimilates from source leaves to seeds occurs in greater quantity and intensity according to the preference of the drain (Lopes *et al.*, 2011).

There was no significant difference when evaluating the electrical conductivity in seeds during the 3 h soaking period. However, for 24 h, it could be observed that the maximum flexion point occurred at 120 kg ha⁻¹ N (T1) for cultivar BRS Brau, while, for the cultivar BRS Cauê, the maximum point occurred with the 150 kg ha⁻¹ N dose (T2) (Figure 4b). Bazzo *et al.* (2018), while studying nitrogen doses on the physiological quality of wheat seeds, observed that increasing the dose results in changes in physiological quality.

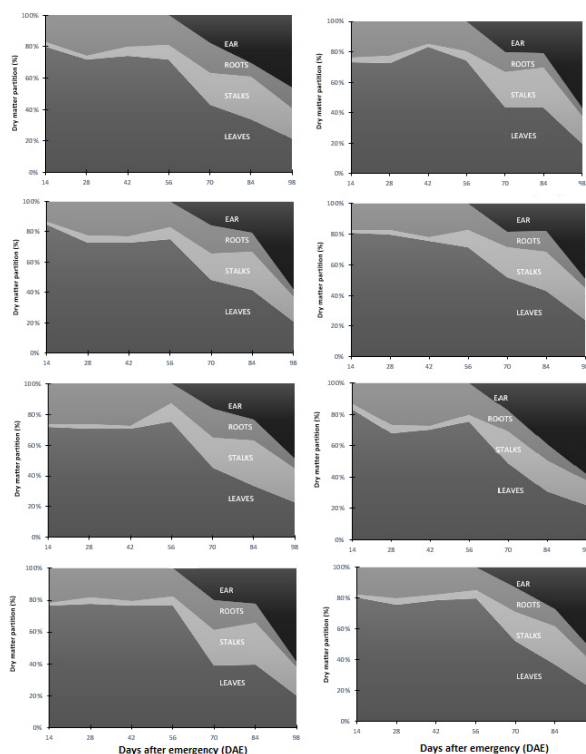


Figure 3. Dry matter partitioning of barley plants under application of nitrogen doses (control, 150, 180, and 210 kg ha⁻¹ N) in two barley cultivars (BRS Brau and BRS Cauê) (Pelotas, RS)

Source: Authors

Adjustments in preferential metabolic drainage occur during the development of the culture, which will allocate products from photosynthesis. In the early stages of growth, leaf and root accumulation is preferred, and, later, the allocation to the stalks, reproductive structures, and ears. Thus, the direction of assimilates from source leaves to seeds occurs in greater quantity and intensity according to the preference of the drain (Lopes *et al.*, 2011).

There was no significant difference when evaluating the electrical conductivity in seeds during the 3 h soaking period. However, for 24 h, it could be observed that the maximum flexion point occurred at 120 kg ha⁻¹ N (T1) for cultivar BRS Brau, while, for the cultivar BRS Cauê, the

maximum point occurred with the 150 kg ha⁻¹ N dose (T2) (Figure 4b). Bazzo *et al.* (2018), while studying nitrogen doses on the physiological quality of wheat seeds, observed that increasing the dose results in changes in physiological quality.

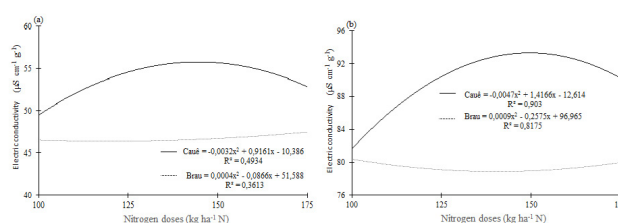


Figure 4. Results of the electrical conductivity analysis of the seeds after a 3- and 24-hour imbibition period (a, b), respectively (Pelotas, RS)

Source: Authors

It should be pointed out that the response to nitrogen fertilization might be due to the influence of the cultivar (genetic factors), the nitrogen source (availability to the crop) and the type of soil (factors linked to adsorption). It is possible that some cultivars in certain soil types and under different nitrogen sources direct most of the nitrogen to seeds and favor aspects related to their physiology in terms of vigor.

Conclusions

Increasing nitrogen doses causes temporal and quantitative difference in growth, partitioning, and accelerated aging test of barley seeds.

The 150 kg ha⁻¹ N dose resulted in a superiority of total dry matter over time (W_t) for both evaluated cultivars.

The variable dry matter production rate (C_t) increased by 31,7% for the 150 kg ha⁻¹ N dose at 70 DAE for BRS Brau, whereas BRS Cauê showed an increase of 46,6% at 56 DAE, thus corroborating W_t .

The 180 kg ha⁻¹ N and 150 kg ha⁻¹ N doses resulted in higher relative growth rates (R_w) for both BRS Brau and BRS Cauê.

Higher-than-recommended nitrogen doses did not change the harvest index in barley plants. However, depending on the dose, it changed the assimilated carbon partition.

References

- Aumonde, T. Z., Pedó, T., Martinazzo, E. G., Moraes, D. M., Vilela, F. A., and Lopes, N. F. (2013). Análise de crescimento e partição de assimilados em plantas de maria-pretinha submetidas a níveis de sombreamento. *Planta Daninha*, 31(1), 99-108. <https://doi.org/10.1590/S0100-83582013000100011>
- Bazzo, J. H. B., da Costa, D. S., Barbizan, T., Barbosa, A. P., de Oliveira, E. C., and Zucareli, C. (2018). Molybdenum application associated with nitrogen fertilization on yield and physiological potential of wheat seeds. *Semina: Ciências Agrárias*, 39(1), 67-76. <https://doi.org/10.5433/1679-0359.2018v39n1p67>

- CONAB (2019). Safra 2019/20: Décimo segundo levantamento. *Acompanhamento da Safra Brasileira de Grãos 2019/2020*, 7, 1-114. <https://www.conab.gov.br/info-agro/safras/graos/boletim-da-safra-de-graos?start=20>
- De Mori, C. and Minella, E. (2012). *Aspectos econômicos e conjunturais da cultura da cevada*. - Portal Embrapa. https://www.embrapa.br/busca-de-publicacoes/-/publicacao/969145/aspectos-economicos-e-conjunturais-da-cultura-da-aveia%0Ahttp://www.cnpt.embrapa.br/biblio/do/p_do139.htm
- Embrapa (2007). *Indicações técnicas para produção de cevada cervejeira nas safras 2007 e 2008*. Embrapa. <https://www.embrapa.br/busca-de-publicacoes/-/publicacao/821534/indicacoes-tecnicas-para-a-producao-de-cevada-cervejeira-nas-safras-2007-e-2008>
- Koch, F., Aisenberg, G. R., Monteiro, M. A., Pedó, T., Zimmer, P. D., Villela, F. A., and Aumonde, T. Z. (2017). Growth of wheat plants submitted to the application of the growth regulator trinexapac-ethyl and vigor of the produced seeds. *Agrociencia Uruguay*, 21(1), e167. <https://doi.org/10.31285/agro.21.1.4>
- Lopes, N. F. and Lima, M. da G. de S. (2015). *Fisiologia da produção*. UFV.
- Lopes, W. A. R., Negreiros, M. Z., Dombroski, J. L. D., Rodrigues, G. S. O., Soares, A. M., and Araújo, A. P. (2011). Análise do crescimento de tomate 'SM-16' cultivado sob diferentes coberturas de solo. *Horticultura Brasileira*, 29(4), 554-561. <https://doi.org/10.1590/S0102-05362011000400019>
- Malavolta, E. (2006). *Manual de nutrição mineral de plantas*. Editora Agronômica Ceres.
- Ohlson, O. C., Krzyzanowski, F. C., Caieiro, J. T., Panobianco, M. (2010). Teste de envelhecimento acelerado em sementes de trigo. *Revista Brasileira de Sementes*, 32(4). <https://doi.org/10.1590/S0101-31222010000400013>
- Pedó, T., Martinazzo, E. G., Aumonde, T. Z., and Villela, F. A. (2015). Plant growth analysis and seed vigor expression: Effects of soil waterlogging during rye plant development. *Acta Botanica Brasilica*, 29(1), 1-7. <https://doi.org/10.1590/0102-33062014abb3574>
- Radford, P. J. (1967). Growth analysis formulae - their use and abuse 1. *Crop Science*, 7(3), 171-175. <https://doi.org/10.2135/cropsci1967.0011183x000700030001x>
- Richards, F. J. (1969). The quantitative analysis of growth. In: F. C. Steward (Ed), *Plant physiology* (pp. 3-76). Academic Press. <http://dx.doi.org/10.4236/as.2011.23026>
- Silva, V. N., Zambiasi, C. N., Tillmann, M. A. A., Menezes, N. L., and Villela, F. A. (2014). Electrical conductivity test with parts of bean seeds. *Revista de Ciências Agrárias*, 37, 206-213. <https://www.cabdirect.org/cabdirect/FullTextPDF/2014/20143319097.pdf>
- Soares, M. M., Oliveira, G. L., Soriano, P. E., Sekita, M. C., and Sediya, T. (2013). Performance of soybean plants as function of seed size: II. Nutritional stress. *Journal of Seed Science*, 35(4), 419-427. <https://doi.org/10.1590/S2317-15372013000400002>
- Streck, E. V., Kämpf, N., and Dalmolin, R. S. D. (2008). *Solos do Rio Grande do Sul* (2nd ed.). EMATER/RS; UFRGS.
- Taiz, L., Zeiger, E., Moller, I. M., and Murphy, A. (2017). *Fisiologia e desenvolvimento vegetal* (vol. 6). Artmed.
- Teixeira Filho, M. C. M., Buzetti, S., Alvarez, R. de C. F., Freitas, J. G. de, Arf, O., and Sá, M. E. de. (2008). Desempenho agrônomo de cultivares de trigo em resposta a população de plantas e a adubação nitrogenada. *Científica*, 36(2), 97-106. <https://doi.org/10.15361/1984-5529.2008v36n2p97%20-%20106>

Semicontinuous Lixiviation Process for Compound Extraction from *Cannabis sativa* grown in Colombia

Proceso semicontinuo de lixiviación para la extracción de compuestos a partir de *Cannabis sativa* cultivado en Colombia

Oscar Y. Buitrago-Suescún¹ and Miguel A. Santaella-Serrano²

ABSTRACT

The extraction of compounds present in *Cannabis sativa* biomass from Colombian crops was studied using a semi-continuous lixiviation process. To this effect, three extraction stages were implemented, in which successive transfers were carried out at fixed times, seeking to emulate a continuous countercurrent process. In this way, the intention is to provide the Colombian agroindustry with an extraction method that is efficient and requires a lower initial investment than other techniques such as supercritical fluid extraction. Absolute ethanol was used as solvent, and constant temperature and stirring speed were applied. The obtained results indicate that, once the process is stabilized, extracted mass percentages (with respect to the total mass on a dry basis) of 10,5% at 40 °C and 9,5% at 19 °C are achieved, which are competitive compared to the 11,07% achieved through Soxhlet extraction. Besides, the proposed process is clearly a better alternative than a single-stage extraction method, through which it was possible to extract 5% of the mass. Five cannabinoids were identified in the obtained extract, and, with the proposed process, it was possible to extract 66% of cannabidiol present in the original biomass.

Keywords: *Cannabis sativa*, lixiviation, agroindustry, semicontinuous process, solvent extraction

RESUMEN

Se estudió la extracción de compuestos presentes en la biomasa de *Cannabis sativa* de cultivos colombianos mediante un proceso de lixiviación semicontinuo. Para tal fin se implementaron tres etapas de extracción, en las cuales se realizaron transvases sucesivos en tiempos determinados, buscando emular un proceso continuo a contracorriente. De esta forma se pretende proporcionar a la agroindustria colombiana un método de extracción que sea eficiente y requiera una inversión inicial más baja que otras alternativas tales como la extracción con fluidos supercríticos. Se empleó etanol absoluto como solvente y se aplicaron temperaturas y velocidades de agitación constantes. Los resultados obtenidos muestran que, una vez estabilizado el proceso, se logran porcentajes de masa extraída (con respecto a la masa total en base seca) del 10,5 % a 40 °C y de 9,5% a 19 °C, los cuales son competitivos frente al 11,07% alcanzado con extracción Soxhlet. Además, el proceso propuesto es una alternativa mejor que el método de extracción de una sola etapa, mediante el cual se logró extraer el 5% de la masa. Se identificaron cinco cannabinoides en el extracto obtenido y, con el proceso propuesto, se logró extraer el 66% del cannabidiol presente en la biomasa original.

Palabras clave: *Cannabis sativa*, lixiviación, agroindustria, proceso semicontinuo, extracción con solventes

Received: November 17th, 2020

Accepted: July 19th, 2021

Introduction

Although the *Cannabis sativa* plant comes from Central Asia and has been cultivated for more than 5 000 years (Booth and Bohlmann, 2019), it has been stigmatized for decades due to its psychoactive compounds. However, due to the use of these compounds for medicinal purposes and the presence of others, including phytocannabinoids, terpenes, and flavonoids, (Koltai and Namdar, 2020), that are of interest in other sectors such as the pharmaceutical, nutraceutical, cosmetic, and pesticide industries (Fiorini et al., 2019), many changes have begun worldwide in the legislation for the regulation for the growth and manufacture of its derivatives.

Particularly in Colombia, Decree 2467 of 2015 (which regulates growth, processes, possession of seeds, and manufacture of derivatives, among others) and Decree 613

of April 2017 (access to medical and scientific cannabis) have generated an attractive alternative that can contribute to the agro-industrial, technical, scientific, and economic development of the country.

¹ Chemical Engineer, Universidad Nacional de Colombia. MSc. in Industrial Engineering, Universidad de Los Andes, Colombia. Affiliation: Associate Professor, Industrial Engineering Program, Universidad Militar Nueva Granada, Colombia. Email: oscar.buitrago@unimilitar.edu.co

² Chemical Engineer, Universidad Nacional de Colombia. Ph.D. in Chemical Engineering, Universidad Nacional de Colombia. Affiliation: Research Assistant, Universidad Militar Nueva Granada, Colombia. Email: miguel.santaella@gmail.com

How to cite: Buitrago, O., Santaella, M. (2022). Semicontinuous Lixiviation Process for Compound Extraction from *Cannabis sativa* grown in Colombia. *Ingeniería e Investigación*, 42(2), e91616. <http://doi.org/10.15446/ing.investig.v42n2.91616>



Attribution 4.0 International (CC BY 4.0) Share - Adapt

The spectrum of compounds that can be extracted from the cannabis plant that are of interest in terms of their scientific, medicinal, and industrial use is very diverse. In fact, more than 500 compounds have been identified (Elkins *et al.*, 2019), which are distributed in different families. For example, Delgado-Povedano *et al.* (2019) analyzed 17 cultivars and identified 169 compounds in them (22 cannabinoids, 70 terpenoids, 31 lipids, 16 flavonoids, 6 amino acids, 5 organic acids, 4 benzenoids, 4 organic oxygen compounds, 3 hydrocarbons, 3 carbohydrates, 2 organoheterocyclic compounds, 2 organonitrogen compounds, and 1 alkaloid).

Additionally, for medicinal purposes, the extraction procedure is critical because it influences the profile of the preparations that can be obtained; in particular, hard decarboxylation conditions lead to not having terpenes, while milder conditions allow obtaining terpene-rich preparations (Ternelli *et al.*, 2020). Among the medicinal uses of cannabis derivatives, it is worth highlighting pain relief in patients with cancer, chronic pain, multiple sclerosis-related pain, inflammation reduction, and treatment of symptoms related to neurodegenerative disorders such as Parkinson's disease, Alzheimer's disease, and epilepsy (Koltai and Namdar, 2020).

It should also be considered that not only are the process conditions or the difference in cultivated varieties important, but the different growing conditions and the regions in which the sowing is done also influence the characteristics of the plants obtained (Amaducci *et al.*, 2008). In fact, even the position of the flower on the plant affects the composition of the extracts (Namdar *et al.*, 2018). Therefore, it is not correct to generalize the content of compounds in different varieties of cannabis that have been cultivated and characterized in different countries (or in different regions, even if they belong to the same variety or cultivar).

Regarding the procedures for the extraction of compounds, steam distillation and hydrodistillation are known alternatives, but there are other commonly available processes as well, such as mechanic techniques (cold-pressing), solvent extraction, ultrasonic-assisted extraction, microwave-assisted extraction, pressurized liquid extraction, and supercritical fluid extraction (SFE) (Baldino *et al.*, 2020). However, in comparison with conventional extraction methods, SFE has many advantages, such as a selective extraction, short processing times, a solvent-free product, low running costs, and low impact on the environment (Qamar *et al.*, 2021). Therefore, SFE is one of the most used techniques in commercial practice, due to the selectivity it allows, as well as the use of green solvents such as CO₂ (Moreno *et al.*, 2020; Da Porto *et al.*, 2012).

Specifically, SFE with supercritical CO₂ (SC-CO₂) is considered to be a green extraction technique, and it has been successfully employed in the extraction of different compounds from various vegetal matrices such as *Artemisia annua* L (to obtain antimalarial compounds), as well as in other fields such as micronization, nanonization, composite

microparticle formation, membrane production, and biomedical applications (Baldino *et al.*, 2017).

As for *Cannabis sativa* L, SFE with CO₂ has been used for compound extraction due to its characteristics. However, research still needs to be done in order to improve this extraction process. In particular, the different solubilities of the various compound families must be taken into account, since essential oil compounds show larger solubilities in SC-CO₂ than cannabinoids, and they are more soluble than other compounds with higher molecular weights. Therefore, it has been proposed to carry out extractions with sequential pressure increases (Baldino *et al.*, 2020).

For this research, the outlined aspects and the Colombian context are taken into account. The country has suffered the rigor of the war on drugs, and the regulation of cannabis crops is a great opportunity for farmers and local stakeholders to benefit from. Therefore, work is being done on finding alternatives that are not exclusive in terms of initial capital investment and technical understanding of the process. In particular, this research worked with vegetal material (biomass) from a plantation located in the department of Cauca in Colombia, and a solvent extraction process in several stages was carried out, emulating a continuous countercurrent process, which is efficient while relatively simple to understand and apply.

Solvent extraction

A simple process used in practice to extract compounds present in vegetal matrices is solvent extraction. The process of putting the solvent in direct contact with solids (in this case, flowers, leaves, stems, or other parts of the plant that have been previously dried and crushed) is also synonymous with lixiviation.

One way to evaluate the quantity of soluble compounds that are present in the solid and that can be extracted by means of the lixiviation is Soxhlet extraction. This procedure uses a device that allows the vapors of the boiling solvent in a container to ascend in a lateral arm and condense in such a way that they fall on a quantity of solid contained in a permeable cartridge, which is usually made of cellulose. When a sufficient volume of condensate is reached while in contact with the solid, and due to the siphoning effect, the lixivate returns to the solvent container (which is now the lixivate container) through another lateral detachment, and a new cycle begins (Figure 1).

An important characteristic of the Soxhlet process is that it requires a heat supply to bring the solvent to its boiling temperature in each of the cycles, and that the solvent/solid ratio is usually high, so the required energy consumption is quite high.

Even though solvent extraction usually has a higher yield than SFE with supercritical CO₂, (Marzorati *et al.*, 2020), it

does not mean that it is the best choice, since extraction with SFE is usually more selective, green, and it allows obtaining higher-purity extracts. On the other hand, single-stage solvent extraction processes are often time consuming and produce diluted extracts (da Silva *et al.*, 2016).

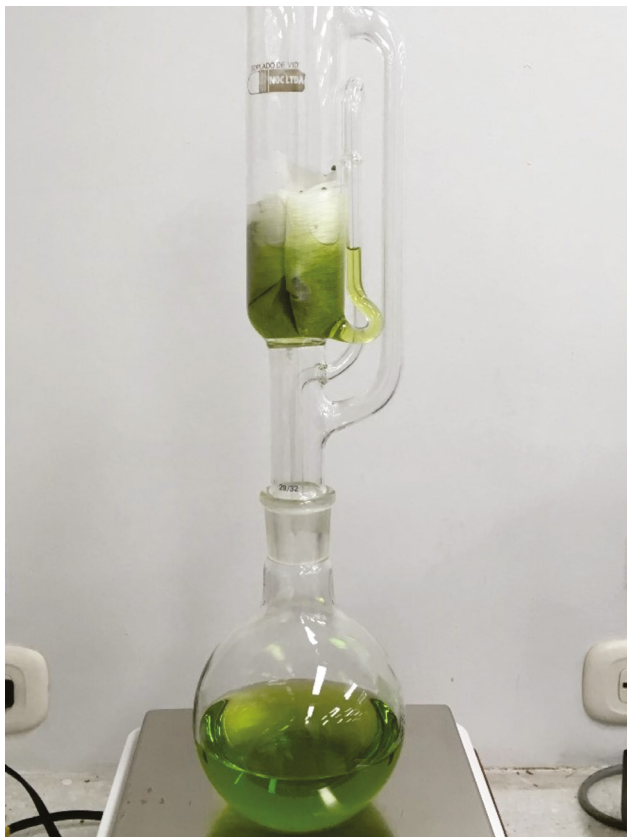


Figure 1. Soxhlet process to obtain compounds from cannabis biomass
Source: Authors

Although there are studies in which solvent extractions from cannabis material are analyzed with the purpose of calibrating analytical methods (Mudge *et al.*, 2017), they are only carried out in a single stage.

Despite the fact that a lixiviation process cannot be carried out continuously in countercurrent, it is possible to arrange a series of extraction tanks and adequately transfer the lixivate to emulate a continuous process, which is the foundation of the proposal presented in this work. Since there is no research that studies extraction from cannabis biomass with solvents in more than one stage, a three-stage process was designed, imitating a continuous countercurrent extraction process that seeks to increase the operation performance and decrease operating time. This three-stage process represents the main contribution of this work.

Selected solvent

Absolute ethanol was used as solvent because it is easy to obtain in Colombia, since, in Valle del Cauca, there are large sugar cane crops and sugar mills that produce ethanol.

This type of alcohol has also been used as a co-solvent in the extraction of compounds from cannabis using the SFE technique (Ribeiro Grijó *et al.*, 2019; Rovetto and Aieta, 2017; Gallo-Molina *et al.*, 2019). Furthermore, ethanol obtained through biotechnological processes from sugar cane is considered to be a green solvent.

Methodology

To extract compounds from the biomass of *Cannabis sativa* in Colombian crops, a ground mixture of stems, leaves, seeds, and some flower fragments was obtained, which was provided by the Finca Interactiva company, with potency of 3,24%. This biomass comes from the Colombian department of Cauca, and it was chosen for the ease of obtaining it and because there are many cannabis crops in the region (Figure 2a).

The cannabis biomass was dried at 70° C for 24 h before being used in the extractions, since the water content forms a barrier during the process (Baldino *et al.*, 2020). Particle size is another factor to consider because, if particles are too small, the caking and channeling phenomena are possible during extraction, thus affecting extraction performance (Baldino *et al.*, 2020).

A test was performed by grinding vegetal material 1 680 µm in size, detecting the inconvenience of the formation of a paste (Figure 2b), which hinders the precipitation of the biomass and makes it impossible to separate the lixivate from the solid to make the transfers. For this reason, it was decided to work with the crushed material as provided by the supplier (Figure 2a).

Regarding the extraction solvent, 99,5% ACS reagent-grade absolute ethanol was used, with a 0,789 g/mL density and 57,3 hPa vapor pressure at 20°C. It was manufactured by PanReac AppliChem S.L.U. and provided by Fisicoquímica Integral S.A.S.



Figure 2. a) Cannabis biomass from the department of Cauca, Colombia, and b) formed cake with ground material
Source: Authors

Three jacketed reactors mounted on heating plates with magnetic stirring were connected to perform the extractions (Figure 3). A water tank with a resistance in its interior, coupled with an automatic control, was used to keep the process temperature constant. Once the water reached the process temperature, it was pumped into the jacket of the

first reactor. From there, it went to the second, and then to the third, before returning to the tank. Additionally, the temperature of the stove was also set at a value equal to temperature of the tank, and the ethanol was preheated to that temperature before being used.

The amount of fresh and dry vegetal material that entered the reactors at each stage of the process was 2 g. Each time that fresh solvent was added, it was done in amounts of 40 g. The tests were carried out at room temperature in the city of Bogotá (19 °C) and at 40 °C. The latter was established in order not to move too far from room temperature (it can be 30 °C in the department of Cauca) and stay distant from the normal boiling point of ethanol.

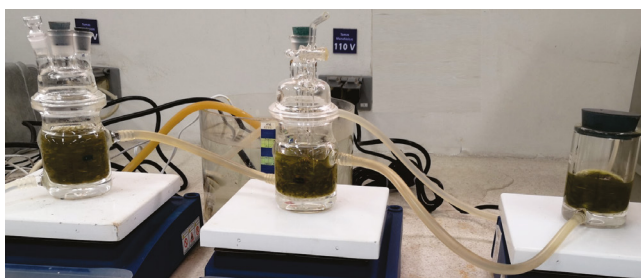


Figure 3. Assembly for the semicontinuous lixiviation of cannabis biomass

Source: Authors

The tests at room temperature were carried out with the purpose of determining if a suitable performance could be achieved, which allows omitting the heating of the solvent. A stirring value of 250 rpm was set. Each stage lasted five minutes and, once that time was completed, the transfers were made according to the scheme shown in Figure 4.

The number on the left in Figure 4 was called 'period' and corresponds to a five-minute interval for extraction plus the time taken by the respective transfers. T1, T2, and T3 refer to the three agitated tanks, FV is the fresh vegetal, FS is the fresh solvent, and the accompanying number refers to the order in which the vegetable and solvent batches entered the system. Each batch of vegetable remains in the system for three periods and does not change tanks. Each solvent batch also remains in the system for three periods but is transferred as indicated by the arrows in Figure 4.

In the same period, the smallest number identifies the exhausted vegetal (which leaves the system at the end of the period), and the largest refers to batch vegetal that has just entered the process. Something similar happens with the solvent (or lixivate): the smallest number identifies the concentrated liquid that leaves the process, and the largest one refers to the fresh solvent that enters to the process.

The three-stage extraction system is stabilized by repeated extraction periods. Eleven lixiviation periods were carried out according to the scheme shown in Figure 4. It is considered that, with this number of periods, the transition state is exceeded and there is a stable process. For comparison

purposes, Soxhlet extraction (for 2 h with a solvent/biomass ratio of 6:1) and single-stage extractions with absolute ethanol (40 g of solvent and 2 g of biomass) were performed.

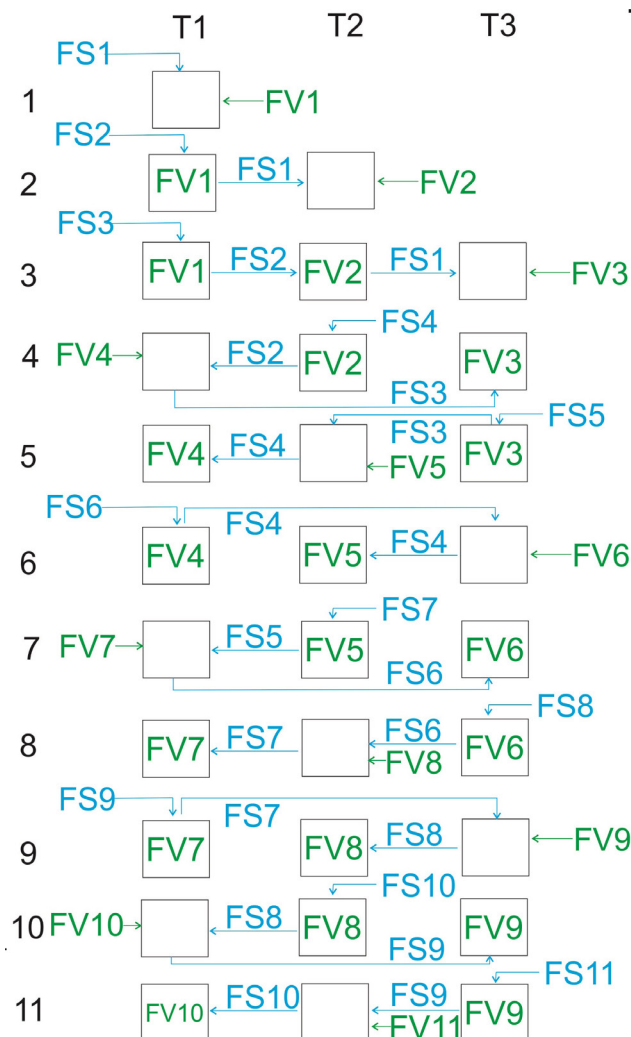


Figure 4. Implemented scheme for transfer between tanks; FS stands for Fresh Solvent and FV indicates Fresh Vegetal

Source: Authors

In the extract (FS9 in period 11) obtained through the proposed process, cannabinoids were identified and quantified, as they are compounds with high added value and with which comparisons can be established with other varieties of cannabis. High Performance Liquid Chromatography (HPLC), according to AOAC-SMPR, was used for this purpose.

Results and discussion

Although the product is described as dry by the supplier, drying tests were carried out on the biomass. The results shown in Table I indicate that the average moisture is 9,41%.

Initially, although it is a qualitative measure, and it is associated with the amount of chlorophyll extracted, the

difference in color can give an idea of the way in which the extraction process progresses. Figure 5 shows the result of a lixiviation carried out with a single stage at 19 °C for 20 min.

Table 1. Moisture of the biomass

Sample	Temperature	Time	Moisture
1	70 °C	48 h	9,38%
2	70 °C	48 h	9,27%
3	70 °C	48 h	9,27%
4	70 °C	48 h	9,73%

Source: Authors



Figure 5. Lixivate obtained by extraction with ethanol in a single stage at 20 °C

Source: Authors

The extracts obtained in the three stages of period 11 for the proposed process at 40 °C are shown in Figure 6. The contrast in tonality between the lixiviates from the stabilized process is evident.

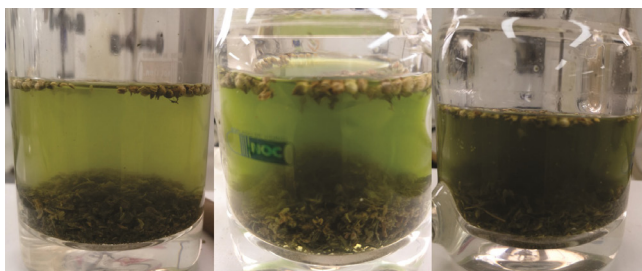


Figure 6. Color differences in each of the three stages of the stabilized process

Source: Authors

For all the extraction processes performed, the weight percentage of the total extracted compounds was calculated by using the weight difference between the initial dry biomass and the exhausted dry biomass, expressed as a percent of initial dry biomass.

The obtained percentage of extracted mass with the Soxhlet method was 11,07% (weight of extracted compounds/initial

dry biomass weight), whereas single-stage extraction (5 min) obtained a percentage of extracted mass of 2,41% at 19 °C and 3,47% at 40 °C. The performance was higher with increasing contact time; as for the test at 19 °C for 20 min, the percentage of extracted mass reached 5%.

For the proposed semicontinuous lixiviation process, the measurements carried out indicate that, from period six onwards, the process can be considered to be stabilized. However, for a greater certainty regarding a stable process, the reported results correspond to period eleven. With respect to the weight of the final lixivate obtained in each period, this corresponds to 81% of the weight of fresh solvent initially added in each tank. In other words, about 19% of the solvent remains impregnated in the biomass or is difficult to transfer. For this reason, designing a mechanism that allows increasing the percentage of liquid that can be passed from one tank to another can be an interesting matter to resolve.

For the lixiviates of the three stages of period 11, the percentage of extracted mass was calculated for the processes at 19 °C and 40 °C. The results are shown in Table 2. The initial stage refers to the tank in which the fresh vegetal is in contact with the oldest lixivate (this liquid leaves the process). In the intermediate stage, there are both vegetal and lixivate that have already passed through a stage, and, in the final stage, the exhausted vegetal (which has remained longer in the process and will leave it at the final period) and fresh absolute ethanol come in contact.

Table 2. Percentage of extracted mass in each stage of the proposed process (dry basis)

Stage	Description	Biomass	Lixivate	Yield 19°C	Yield 40°C
1	Initial	Fresh	Saturated	4,0%	4,0%
2	Intermediate	Intermediate	Intermediate	5,5%	6,0%
3	Final	exhausted	Fresh	9,5%	10,5%

Source: Authors

For both studied temperatures, the results indicate that, at the end of the process, a noticeably higher percentage of extracted mass is obtained by the three-stage extraction in comparison with a single-stage process. However, the difference between the process results at 40 °C and at 19 °C is one percentage point.

In comparison with the Soxhlet method, the proposed process (with any of the temperatures studied) exhibits a similar extraction performance, but it must be considered that it is more economic regarding energy consumption, since the vegetal/solvent ratio is lower, and it is not necessary to evaporate the solvent (referring only to the extraction operations). Additionally, the required equipment is simpler, and this process is carried out at lower temperature and pressure levels than the Soxhlet and SFE techniques. Additionally, for the 19 °C process, it seems convenient to run the process with three stages at room temperature and an increase in contact time.

The results of the quantification of identified cannabinoids present in the final extract are shown in Table 3. Since cannabinoids are normally found in the hemp flowers and not in the fiber, stem, or other parts of the plant, low amounts were expected in the extracts. However, the amounts found cannot be considered negligible. Also, surprisingly, a considerable amount (in comparison with non-psychotropic cannabinoids) of D-9 THC is present in the lixiviate.

Based on the results reported in Table 3 and the potency of the used biomass, the extraction yield can be calculated. For comparison purposes, the extraction yield is calculated as μg of compound/g of waste (or dry biomass). The obtained extraction yield is 1,77%, and, particularly for cannabidiol (CBD), it is 11 158 μg /g of waste, which corresponds to 66% of the one found in the original dry biomass.

On the other hand, since the biomass used is a hemp waste threshing, it is possible to compare our results with those obtained through SFE with CO₂ carried out on hemp waste, particularly the resulting dust in a processing plant by separating the fibers from the rest of the stem in hemp grown in North Yorkshire, UK (Attard *et al.*, 2018). In that case, the highest extraction crude yields are 1,57%, obtained with 65 °C and 400 bar.

Table 3. Identified cannabinoids and percentage in the final extract

Cannabinoid	%
Cannabidiol (CBD)	0,1284
Cannabidiolic Acid (CBDA)	0,0203
Cannabichromene (CBC)	0,0056
Cannabigerol (CBG)	0,0203
Delta-9-tetrahydrocannabinol (D9-THC)	0,0294

Source: Authors

The yield of 1,77% achieved with our semi-continuous extraction method does not seem to be significantly higher than the value of 1,57% reported by Attard *et al.* (2018), but it is indeed, since our yield only considers cannabinoids and theirs includes fatty acids, fatty aldehydes, hydrocarbons, sterols, wax esters, and cannabinoids. Considering cannabinoids specifically, the difference is more noticeable. In the case of North Yorkshire hemp dust, 5 832,5 \pm 118,9 μg CBD/g of dust with heptane as solvent and 1 138 μg CBD/g of dust with SFE-CO₂ at 50 °C and 350 bar were extracted (Attard *et al.*, 2018), compared to the 11 158 μg CBD/g of waste obtained with our method. Apart from the differences between the used methods, the characteristics of the vegetal material on which the extractions are made are a major cause of the gap in the results.

Conclusions

A proposal was made for the extraction of compounds from *Cannabis sativa* biomass using a multistage lixiviation process (with absolute ethanol as solvent). The proposed process seeks to imitate a continuous countercurrent

process through the successive transfer of lixiviates. Three extraction tanks with devices for temperature control were used, and the extractions were carried out at 40 °C and at room temperature in the city of Bogotá D.C (19 °C).

The results show that the proposed method is better than conventional single-stage extraction because the yield is more than double. In comparison with the Soxhlet process, our proposal achieves a slightly lower percentage of extracted mass (11,07% and 10,5%, respectively). However, it requires less energy consumption and shorter operation times. Finally, the results of the quantification carried out by HPLC indicate that the content of cannabinoids in the final extract of the stabilized process is 0,204%, with an extraction yield of 11 158 μg CBD/g of waste. This allows us to conclude that the proposed process extracts compounds of high added value that are present in the studied biomass.

Acknowledgements

This work is derived from project INV-ING-2989, funded by the Vice-Rectoría of Research at Universidad Militar Nueva Granada, in effect for 2019.

References

- Amaducci, S., Zatta, A., Pelatti, F., and Venturi, G. (2008). Influence of agronomic factors on yield and quality of hemp (*Cannabis sativa* L.) fibre and implication for an innovative production system. *Field Crops Research*, 107(2), 161-169. <https://doi.org/10.1016/j.fcr.2008.02.002>
- Attard, T. M., Bainier, C., Reinaud, M., Lanot, A., McQueen-Mason, S. J., and Hunt, A. J. (2018). Utilisation of supercritical fluids for the effective extraction of waxes and Cannabidiol (CBD) from hemp wastes. *Industrial Crops and Products*, 112, 38-46. <https://doi.org/10.1016/j.indcrop.2017.10.045>
- Baldino, L., Reverchon, E., and Della, G. (2017). An optimized process for SC-CO₂ extraction of antimalarial compounds from *Artemisia annua* L. *The Journal of Supercritical Fluids*, 128, 89-93. <https://doi.org/10.1016/j.supflu.2017.05.018>
- Baldino, L., Scognamiglio, M., and Reverchon, E. (2020). Supercritical fluid technologies applied to the extraction of compounds of industrial interest from *Cannabis sativa* L. and to their pharmaceutical formulations: A review. *Journal of Supercritical Fluids*, 165, 104960. <https://doi.org/10.1016/j.supflu.2020.104960>
- Booth, J. K. and Bohlmann, J. (2019). Terpenes in *Cannabis sativa* – From plant genome to humans. *Plant Science*, 284, 67-72. <https://doi.org/10.1016/j.plantsci.2019.03.022>
- da Porto, C., Voinovich, D., Decorti, D., and Natolino, A. (2012). Response surface optimization of hemp seed (*Cannabis sativa* L.) oil yield and oxidation stability by supercritical carbon dioxide extraction. *Journal of Supercritical Fluids*, 68, 45-51. <https://doi.org/10.1016/j.supflu.2012.04.008>
- da Silva, R. P. F. F., Rocha-Santos, T. A. P., and Duarte, A. C. (2016). Supercritical fluid extraction of bioactive compounds. *TrAC - Trends in Analytical Chemistry*, 76, 40-51. <https://doi.org/10.1016/j.trac.2015.11.013>

- Delgado-Povedano, M. M., Sánchez-Carnerero Callado, C., Priego-Capote, F., and Ferreiro-Vera, C. (2019). Untargeted characterization of extracts from *Cannabis sativa* L. cultivars by gas and liquid chromatography coupled to mass spectrometry in high resolution mode. *Talanta*, 208, 120384. <https://doi.org/10.1016/j.talanta.2019.120384>
- Elkins, A. C., Deseo, M. A., Rochfort, S., Ezernieks, V., and Spangenberg, G. (2019). Development of a validated method for the qualitative and quantitative analysis of cannabinoids in plant biomass and medicinal cannabis resin extracts obtained by super-critical fluid extraction. *Journal of Chromatography B: Analytical Technologies in the Biomedical and Life Sciences*, 1109, 76-83. <https://doi.org/10.1016/j.jchromb.2019.01.027>
- Fiorini, D., Molle, A., Nabissi, M., Santini, G., Benelli, G., and Maggi, F. (2019). Valorizing industrial hemp (*Cannabis sativa* L.) by-products: Cannabidiol enrichment in the inflorescence essential oil optimizing sample pre-treatment prior to distillation. *Industrial Crops and Products*, 128, 581-589. <https://doi.org/10.1016/j.indcrop.2018.10.045>
- Gallo-Molina, A. C., Castro-Vargas, H. I., Garzón-Méndez, W. F., Martínez-Ramírez, J. A., Rivera-Monroy, Z. J., King, J. W., and Parada-Alfonso, F. (2019). Extraction, isolation and purification of tetrahydrocannabinol from the *Cannabis sativa* L. plant using supercritical fluid extraction and solid phase extraction. *Journal of Supercritical Fluids*, 146, 208-216. <https://doi.org/10.1016/j.supflu.2019.01.020>
- Koltai, H. and Namdar, D. (2020). Cannabis phytomolecule "entourage": From domestication to medical use. *Trends in Plant Science*, 25(10), 976-984. <https://doi.org/10.1016/j.tplants.2020.04.007>
- Marzorati, S., Friscione, D., Picchi, E., and Verotta, L. (2020). Cannabidiol from inflorescences of *Cannabis sativa* L.: Green extraction and purification processes. *Industrial Crops and Products*, 155, 112816. <https://doi.org/10.1016/j.indcrop.2020.112816>
- Moreno, T., Montanes, F., Tallon, S. J., Fenton, T., and King, J. W. (2020). Extraction of cannabinoids from hemp (*Cannabis sativa* L.) using high pressure solvents: An overview of different processing options. *Journal of Supercritical Fluids*, 161, 104850. <https://doi.org/10.1016/j.supflu.2020.104850>
- Mudge, E. M., Murch, S. J., and Brown, P. N. (2017). Leaner and greener analysis of cannabinoids. *Analytical and Bioanalytical Chemistry*, 409(12), 3153-3163. <https://doi.org/10.1007/s00216-017-0256-3>
- Namdar, D., Mazuz, M., Ion, A., and Koltai, H. (2018). Variation in the compositions of cannabinoid and terpenoids in *Cannabis sativa* derived from inflorescence position along the stem and extraction methods. *Industrial Crops and Products*, 113, 376-382. <https://doi.org/10.1016/j.indcrop.2018.01.060>
- Qamar, S., Torres, Y. J. M., Parekh, H. S., and Falconer, J. R. (2021). Extraction of medicinal cannabinoids through supercritical carbon dioxide technologies: A review. *Journal of Chromatography B*, 1167, 122581. <https://doi.org/10.1016/j.jchromb.2021.122581>
- Ribeiro Grijó, D., Vieitez Osorio, I. A., and Cardozo-Filho, L. (2019). Supercritical extraction strategies using CO₂ and ethanol to obtain cannabinoid compounds from cannabis hybrid flowers. *Journal of CO₂ Utilization*, 30, 241-248. <https://doi.org/10.1016/j.jcou.2018.12.014>
- Rovetto, L. J. and Aieta, N. V. (2017). Supercritical carbon dioxide extraction of cannabinoids from *Cannabis sativa* L. *Journal of Supercritical Fluids*, 129, 16-27. <https://doi.org/10.1016/j.supflu.2017.03.014>
- Ternelli, M., Brighenti, V., Anceschi, L., Poto, M., Bertelli, D., Licata, M., and Pellati, F. (2020). Innovative methods for the preparation of medical Cannabis oils with a high content of both cannabinoids and terpenes. *Journal of Pharmaceutical and Biomedical Analysis*, 186, 113296. <https://doi.org/10.1016/j.jpba.2020.113296>

Methodology for Classifying the Structural State of Uninspected Pipes in Sewer Networks Based on Support Vector Machines

Metodología para clasificar la condición estructural de tuberías no inspeccionadas de las redes de alcantarillado basada en máquinas de soporte vectorial

Nathalie Hernández¹, Miguel A. Cañón², and Andrés Torres³

ABSTRACT

The nearly unmitigated growth of cities has placed ever-greater pressure on urban water systems regarding climate change, environmental pollution, resource limitations, and infrastructure aging. Therefore, the development of methods to classify and assess the structural state of urban drainage infrastructure becomes very important, given that they can be used as support tools for proactive management plans. This paper presents a method for predicting and classifying the structural state of uninspected sewer pipes using Support Vector Machines, based on the physical characteristics, age, and geographical location of the pipes. According to the results, the methodology: (i) correctly classified more than 75% of uninspected pipes; (ii) identified pipes in critical structural states, with low importance prediction error for 69% of pipes; and (iii) provided a guide for establishing the number or percentage of pipes that require inspection or intervention.

Keywords: Support Vector Machine, sewer asset management, structural state, sewer systems

RESUMEN

El crecimiento casi descontrolado de las ciudades ha puesto una creciente presión en los hidrosistemas urbanos en términos de cambio climático, contaminación ambiental, limitaciones presupuestales y envejecimiento de la infraestructura. Por lo tanto, la exploración de diferentes métodos para clasificar y evaluar la condición estructural de los alcantarillados ha adquirido gran importancia, dado que estos pueden ser utilizados para herramientas de apoyo para planes de gestión proactiva. Este trabajo presenta un método para predecir y clasificar la condición estructural de tuberías de alcantarillado no inspeccionadas usando Máquinas de Soporte Vectorial basado en las características físicas, edad y ubicación geográfica de las tuberías. De acuerdo con los resultados, la metodología: (i) clasificó correctamente más del 75 % de tuberías no inspeccionadas; (ii) identificó las tuberías que estaban en condiciones estructurales críticas, con errores de predicción de baja importancia para el 69 % de las tuberías; y (iii) proporcionó una guía para establecer el número o porcentaje de tuberías que requieren inspección o intervención.

Palabras clave: Máquina de Soporte Vectorial, gestión patrimonial de alcantarillados, condición estructural, sistemas de alcantarillado

Received: March 27th, 2020

Accepted: July 16th, 2021

Introduction

Urban drainage systems present alarming rates of aging and deterioration in both developed and developing countries (Osman *et al.*, 2012). Essentially, most sewer networks are more likely to fail each day (Ward and Savic, 2012) due to structural deterioration. In turn, this impacts the level of service and quality of life (Osman *et al.*, 2012; Micevski *et al.*, 2002; Liu and Kleiner, 2013; Caradot *et al.*, 2017).

Multiple factors affect pipe deterioration: physical characteristics (diameter, length, depth, material, joint type), installation-construction processes, external factors (soil fracture potential, soil use, and environmental characteristics), and other factors (e.g., age, sewer pipe use, and maintenance methods) (Davis *et al.*, 2001). Recently,

¹ Civil Engineer, Pontificia Universidad Javeriana, Colombia. M.Sc. Water Systems, Pontificia Universidad Javeriana, Colombia. Affiliation: Ph.D. Candidate in Engineering at Pontificia Universidad Javeriana and member of the research group "Ciencia e Ingeniería del Agua y el Ambiente" [Water and Environmental Science and Engineering]. E-mail: Nathalie_hernandez@javeriana.edu.co

² Environmental Engineer, Universidad Santo Tomás, Colombia. Affiliation: M.Sc. candidate in Water Systems, Pontificia Universidad Javeriana, Colombia. E-mail: miguel_canon@javeriana.edu.co

³ Civil Engineer and Specialist in Engineering Management, Pontificia Universidad Javeriana, Colombia. M.Sc. in Civil Engineering and Ph.D. in Urban Hydrology. University of Lyon – INSA Lyon, France. Affiliation: Full Professor at Pontificia Universidad Javeriana and member of the research group "Ciencia e Ingeniería del Agua y el Ambiente" [Water and Environmental Science and Engineering]. E-mail: andres.torres@javeriana.edu.co

How to cite: Hernández, N., Cañón, M., and Torres, A. (2022). Methodology for Classifying the Structural State of Uninspected Pipes in Sewer Networks Based on Support Vector Machines. *Ingeniería e Investigación*, 42(2), e85917. <https://doi.org/10.15446/ing.investig.v42n2.85917>



Attribution 4.0 International (CC BY 4.0) Share - Adapt

other factors have been reported, including climate change, land-use change, and demographic growth (Kleidorfer *et al.*, 2013). Numerous investigations have shown that older pipes have been structurally under-designed and thus do not meet the demands of urban growth. Likewise, past construction practices have been inadequate. These two factors have led to frequent failures in sewer pipes (Særgrov and Schilling, 2002). In short, underground urban service networks are considered to be complex systems due to the action and interaction of the aforementioned factors (Hao *et al.*, 2012), which have not been thoroughly studied (Lee *et al.*, 2013).

In light of the above, urban system stakeholders are faced with important challenges in order to achieve a rational, efficient, effective, and sustainable management and maintenance of this infrastructure, while also considering the diversity of actors involved (budget limitations, environmental regulations, and urban water infrastructure benefits) (Baik *et al.*, 2006; Cardoso *et al.*, 2012; Younis and Knight, 2012). Globally, some methodologies have been proposed for managing urban drainage systems, namely project CARE-S (Computer Aided Rehabilitation of Sewer and Storm Water Networks), which was integrated by and for various European cities. CARE-S entails methods and models for three levels of long-term sewage management (Særgrov and Schilling, 2002). Mashford *et al.* (2010) developed a methodology for the city of Adelaide (Australia) using information from CCTV inspections to classify the structural condition of pipes via Support Vector Machines (SVMs) and Artificial Neural Networks (ANNs). Machine learning tools have shown promise for predicting the service condition of sewer networks. These tools are based on a few physical pipe characteristics (diameter, pipe age, type of road over sewer pipelines, slope, and top of pipe level) (e.g., Mashford *et al.*, 2010). Moreover, various studies have shown that classifying through SVMs is adequate, and robust variables with non-linear processes are used. All this, in comparison with conventional methods such as ANNs (Zhang *et al.*, 2009) and Kernel independent component analysis (Zhang *et al.*, 2008).

In many countries, including Colombia, stakeholders have traditionally addressed the maintenance and operation of assets with a reactive focus (that is, acting after the failure). However, reactive maintenance can be significantly costlier than proactive maintenance (Rodríguez *et al.*, 2012). Wirahadikusumah *et al.* (2001) identify the primary reason for relying on a reactive approach: the lack of monitoring data. For example, in cities such as Bogotá and Medellín, more than 90% of the structural and operational sewer assets are unknown (Hernández *et al.*, 2020). This lack limits the development of predictive models and assessments of the effects of changes in maintenance policies (Rodríguez *et al.*, 2012). Despite the diversity of support models for the proactive maintenance of sewer systems worldwide (Særgrov and Schilling, 2002; Mashford *et al.*, 2010), the majority assume complete and timely information and, therefore, have only limited applicability in Colombia, given the scarcity and low coverage of sewer inspections, as well as the

unsecured quality of any inspections performed (Rodríguez *et al.*, 2012). Thanks to the great advantages of predicting through SVMs reported by the literature and the need to know the structural condition of the whole sewer network, this paper proposes a methodology based on Support Vector Machines to predict the structural condition of uninspected sewer assets. The methodology aims to provide support tools to the stakeholders' decision-making in order to plan rehabilitation and investment strategies. This contributes to developing more rational plans to invest in and rehabilitate the sewer network, leaving reactive maintenance aside and seeking to achieve sewer asset management (proactive maintenance).

Materials and methods

In 2001, a Colombian standard (EAAB, 2001) was developed to evaluate already inspected sewer networks via CCTV for the city of Bogotá. This standard assesses structural and operational conditions based on the failure types, as well as their severity, that are found during the inspections, thus assigning a defined score. According to the assessment of structural conditions, all failure scores are added and categorized into a grade for every single pipe. This categorization could be used for decision-making related to rehabilitation and preventive actions (Table 1).

Table 1. Structural states based on structural score NS 058 and description

Score	Condition	Description
<<10	1	Without structural failures
10-39	2	Failures of low importance
40-79	3	Failures that can generate structural and hydraulic problems
80-164	4	Failures of high importance; preventive and/or corrective steps required
165+	5	Collapsed or nearly collapsed pipes; emergency decisions required

Source: Adapted from EAAB (2001)

The CCTV data are related to inspections carried out between 2007 and 2011 by Bogotá's water and sewerage systems company, (Empresa de Acueducto y Alcantarillado de Bogotá, EAB) (Figure 1). This database contains the following information on the pipe: physical characteristics, location, score (assessment), and structural condition (grade). In total, 3563 inspections of waste and storm water pipes (local and main network) were included in the database.

According to data from the database and the literature (Davis *et al.*, 2001; Kleidorfer *et al.*, 2013), the following variables may be related to the structural condition of pipes: (i) slope, (ii) diameter, (iii) material type, (iv) age, (v) ground level at the beginning of the pipe, (vi) ground level at the end of the pipe, (vii) depth at the beginning of the pipe, (viii) depth at the end of the pipe, (ix) surface type at ground level,

(x) sewerage, and (xi) geographical coordinates (longitude, latitude). An exploratory statistical analysis of the inspected pipe data was performed to determine the relationship between these variables and the structural condition variable (Kruskal-Wallis test). The variables chosen were categorized to perform statistical tests (e.g., the Wilcoxon test), which require categorical variables. Thus, each variable was categorized according to the 33 and 67 percentiles.

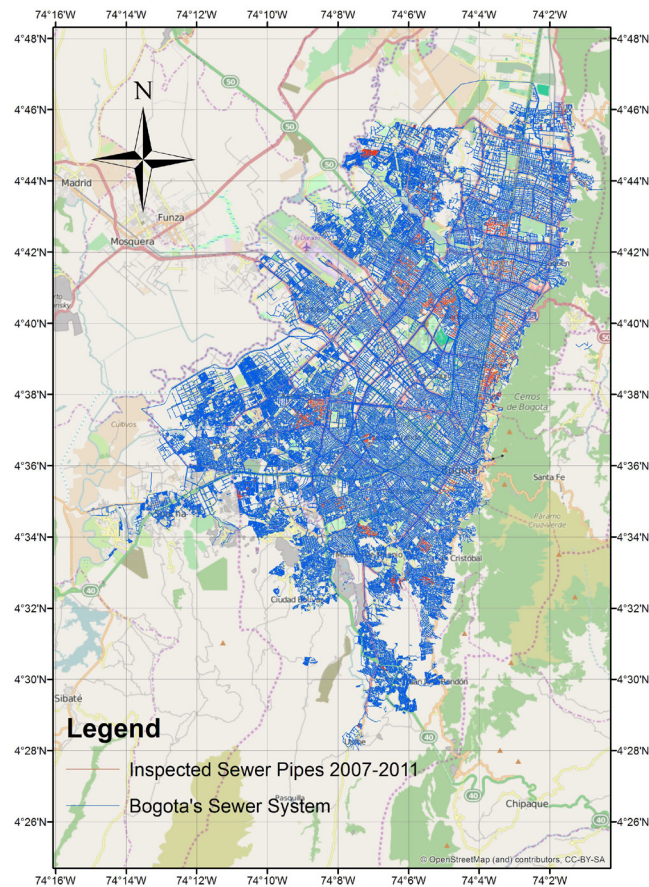


Figure 1. Map of sewer pipes in Bogotá D.C.

Source: Authors

The data did not have a normal distribution or variance homogeneity according to the Shapiro-Wilk and Bartlett tests, respectively. Therefore, the Kruskal-Wallis test was performed. Kruskal-Wallis is a nonparametric alternative to ANOVA and was used to determine which variables significantly influence the structural score of the pipes. According to this test, the variables with significant influence ($p\text{-value} < 0.05$) on structural score variability were age, material, slope, diameter, surface type, depth 2, pipe type, longitude, latitude, ground level 1, and ground level 2. With these results, the Wilcoxon test was applied for each chosen variable in order to determine significance difference ($p\text{-value} < 0.05$) between variable factors and structural score (Table 2): (i) slope, with significantly lower scores for low slopes (< 0.4113); (ii) diameter, with significantly higher scores for pipes with small diameters ($< 0.2\text{m}$) and significantly lower for pipes with large diameter ($> 2.4\text{m}$); (iii) ground level 1 and 2, with significantly higher scores for

category “2_medium” ground levels (between 2555-2606 m above sea level); (iv) depth 2, with significantly lower scores for shallow pipes ($< 1.13\text{ m}$); (v) age, with significantly higher scores for category “2_medium” (between 30 and 50 years) and significantly lower for category “3_new” (< 30 years); (vi) longitude, with significantly higher scores for the city’s west side ($74.06\text{--}74.02^\circ$); (vii) latitude, with significantly higher scores for the city center ($4.62\text{--}4.696^\circ$); (viii) surface type, with significantly higher scores for pipes under asphalt pavement; (ix) sewerage, with significantly higher scores for higher local wastewater pipes; and (x) material, with significantly higher scores for vitrified clay.

Table 2. Variable relationships that show significance differences ($p\text{-value} < 0.05$) in the Wilcoxon test.

Structural Scores	Variable
Low	Low slopes (slope < 0.4113)
	Long pipes ($> 2.4\text{ m}$)
	Shallow pipes (depths $< 1.13\text{ m}$)
High	Small pipes (diameter $< 0.2\text{ m}$)
	Intermediate ground levels (2555 – 2606 msl)
	Medium ages (30 years – 50 years)
	City’s west side (longitude: $74.06^\circ\text{--}74.02^\circ$)
	City center (latitude: $4.62^\circ\text{--}4.696^\circ$)
	Pipes under asphalt pave (Surface type)
	Local wastewater pipes (Sewerage)
	Vitrified clay pipes (Material)

Source: Authors

These results confirm the findings of other studies that estimated variables directly influencing the structural state of pipes. For example, vitrified clay pipes with small diameters had greater structural scores, which is consistent with findings reported in Niño *et al.* (2012). Similarly, slope and ground level were the variables most closely associated with the structural state of pipes (López-Kleine *et al.*, 2016). Nevertheless, certain tendencies were identified: the cause-effect rules given by the multivariate and nonlinear nature of structural scores cannot be formulated. Thus, tools that account for these characteristics must be utilized, such as SVMs.

SVMs are based on a supervised statistical learning method within the kernel family. This family consists of a class of algorithms for pattern analysis that finds and analyzes general types of relations (e.g., clusters, ranges, principal component correlations, and classifications) in databases (Shawe-Taylor and Cristianini, 2004). With the application of kernel functions, SVMs increase the data dimensionality to find a hyperplane that could separate them correctly (Jahed *et al.*, 2020; Hernández *et al.*, 2021). SVMs are used to solve nonlinear classification problems by means of pattern recognition and function estimation. The principal problem addressed using SVMs is the fit of a function describing a relation between an object X and response Y. Initially,

SVMs are used for two-category classifications, where Y is the categorical vector (or binary variable), by using S (the dataset). If the objects are within the P dimension, the relationship is described by Equation (1):

$$y = f(x) = w^T x + b \quad (1)$$

The hyperplane equation is defined by Equation (2):

$$|b + w^T x| = 1 \quad (2)$$

where b is the bias, w a weight vector, and x the support vectors. The distance between x and the hyperparameter is defined by Equation (3), and the hyperparameter margin is defined by Equation (4):

$$\frac{|b + w^T x|}{\|\beta\|} = \frac{1}{\|\beta\|} \quad (3)$$

$$M = \frac{2}{\|\beta\|} \quad (4)$$

The minimization function that maximizes the hyperparameter margin is defined by Equation (5):

$$\min_{w,b} L(\beta) = \frac{1}{2} \|\beta\|^2 \text{ depending of } y_i (w^T x_i + b) \geq 1 \forall i \quad (5)$$

where y is each category, and Lagrange multipliers are used to find the values w and b (Duda et al., 2012; Huang et al., 2018).

SVMs allow for classifications and regressions with parametric and nonparametric data (López-Kleine and Torres, 2014). The kernlab library (Karatzoglou et al., 2004) was used with R (R Core team, 2019) to build the SVM models. This library has a function that optimizes the hyperparameters of the kernel functions automatically, and the soft margin parameter C is taken as the value default (1).

After statistically analyzing the database, an SVM was used to classify pipes based on variables identified by the Kruskal-Wallis method. Independent variables (slope, age, etc.) of the SVM model must be numerical, and the dependent variable must be categorical (structural state). Still, given that some independent variables are categorical (material and road type), it is necessary to develop analysis alternatives that can be included in the model. These alternatives are the combination of the categorical variables for all variables, so that the database can be divided, that is, two categorical variables (material and road type). In turn, these are constituted by two factors for each one (concrete and vitrified clay pipes for the material; concrete and asphalt

pavement for surface type). By using pairwise combination of material and surface type, four possible alternatives were created: (i) vitrified clay pipes under concrete pavement; (ii) vitrified clay pipes under asphalt pavement; (iii) concrete pipes under concrete pavement; and (iv) concrete pipes under asphalt pavement. Doing so guaranteed that there were independent numerical variables and a categorical dependent variable for each alternative.

Furthermore, various structural grades were grouped into categories in line with the research done by López-Kleine et al. (2016). For example, one way of grouping structural grades into two categories would be: Category 1 with grades 1, 2, and 3 representing piped with acceptable structural conditions; and Category 2 with grades 4 and 5, meaning pipes with critical structural conditions. These categories correspond to the dependent variable vector for calibrating SVM models.

Once the previously described four alternatives were defined, each database was randomly divided into data for calibrating each SVM model (2/3 of total data) and data for validation (1/3 of total data). With calibration data for each alternative, SVM classification algorithms were employed with kernel functions whose application is associated with database characteristics. For this study, the characteristics found were as follows: insufficient *a priori* information for the data (Gaussian and Laplace kernel functions), binary categorization of input data (Vanilla linear function), and a classification that approximates neural networks taken from Mashford et al., (2010).

To arrive at the best classification model for each alternative, two approaches were used: (i) leave-one-out cross validation technique (Greisser, 1993) and (ii) Cohen's kappa coefficient (Carletta, 1996). The first approach was used to train the model with the calibration data, and the second one was used to evaluate the performance of the trained model with the validation data.

With the purpose of evaluating the performance of the prediction, comparing the estimated and observed categories, the authors suggest to classify the correct and wrong predictions by colors, as well as the Prediction Error Importance (Table 3). The latter (PEI) gives information about the severity of a wrong estimation compared to the observed information. According to Table 2, the percentages that are in 'GREEN' and Null-PEI are the percentage of pipes that were estimated correctly. The percentages in 'YELLOW' and Low-PEI show the percentage of pipes where the model underestimated the structural condition (it means that the model estimated the condition of the pipe in worse structural conditions than they really were). The percentages in 'ORANGE' and Medium-PEI represent the percentage of pipes where the model overestimated the structural condition, it means that the model estimated the condition of the pipe in better conditions than what they actually were. Finally, the percentage in 'RED' and High-PEI represents those pipes whose estimation was highly overestimated;

it means that the model estimated those pipes to be in excellent conditions while they were actually collapsed. Table 3 illustrates the possible error importance and the corresponding table of colors if the analysis is divided into three categories (e.g., if C1 corresponds to good structural conditions, C2 to regular structural conditions, and C3 to poor structural conditions).

Table 3. Description of the Prediction Error Importance levels and their corresponding color.

Estimated Category	Observed Category	Color	Prediction Error Importance (PEI)
C1	C3	RED	High
C1	C2	ORANGE	Medium
C2	C3		
C3	C1		
C3	C2	YELLOW	Low
C2	C1		
Pipes with the same estimated and observed category		GREEN	Null

Source: Authors

In light of the possible or inevitable financial limitations faced by the company in charge of sewer management, a minimum number or percentage of pipes classified by the tool was established in order to determine which of those were in critical structural conditions and required inspection or action. To this effect, a methodology was proposed to determine the percentage of pipes randomly selected over the total of those classified in a particular category by the tool to ensure that the expected percentage of proper classifications had a relatively acceptable uncertainty (e.g., less than 15%). The methodology consists of randomly selecting a certain percentage of pipes (between 1 and 100%) from those that received a given classification (e.g., good conditions or critical conditions) to apply the proposed tool and calculate the percentage of successful classifications using the inspection database. This process is repeated a given number of times for the same percentage of pipes, and the percentage of successful classifications is calculated each time. It is expected, then, that the dispersion of results obtained (percentage of successful classifications) is high for initial percentages, and that it gradually diminishes as more pipes are selected to finally achieve a null dispersion for 100%.

Results and discussion

Table 4 shows the functions selected for each analysis alternative according to Cohen's *kappa* coefficient, which was obtained using leave-one-out cross-validation (CV). This Table also includes category division for alternatives with the highest predictability (higher Cohen's *kappa* coefficient obtained for the proposed CV). As the Table demonstrates, there are two or three categories for which

predictability increases were observed, thus implying that the results are useful for classifying sections in three ways: (i) "excellent conditions" and "not excellent conditions" (C1 and C2, respectively, in alternatives 1 and 2, Table 4); (ii) "critical condition" and "not critical condition" (C2 and C1, respectively, in alternatives 4 and 5); and (iii) "excellent condition", "critical condition" and "nor excellent nor critical condition" (C1, C3, and C2, respectively, in alternative 3, Table 4). Furthermore, the Kernel functions that offer the best results in terms of predicting the classification of the categories of the pipe's structural states were RBF, Laplace, and Vanilla, which implies that the three functions rely on binary classification regardless of whether the function in the characteristic space is linear (Vanilla) or nonlinear (RBF and Laplace).

Table 4. Selected SVM models for each alternative

Alternatives	Categories	Function	K- cv
1. Concrete – Asphalt Pavement	C1: Grade 1 C2: Grades 2, 3, 4 and 5	RBF	0,305
2. Concrete – Concrete Pavement	C1: Grade 1 C2: Grades 2, 3, 4 and 5	Laplace	0,415
3. Vitrified Clay Pipes – Asphalt Pavement	C1: Grade 1 C2: Grades 2, 3 and 4 C3: Grade 5	RBF	0,071
4. Vitrified Clay Pipes – Concrete Pavement	C1: Grades 1, 2, 3 and 4 C2: Grade 5	Vanilla	0,213

Source: Authors

According to the confusion matrices (calibration and validation data) of the four analysis alternatives, it was found that:

- i. For the first two analysis alternatives (Concrete-Asphalt pavement and Concrete pavement), the calibration data's confusion matrices had similar prediction results (classifying more than 81% of pipes correctly in category C1 and more than 79% in category C2), while the validation data's confusion matrices differ (60 and 68% of pipes were properly classified in C1 and C2, respectively, for the first analysis alternative; and 38 and 80% were properly classified in C1 and C2 for the second analysis alternative). However, the results from the calibration and validation data for the first analysis alternative (Concrete-Asphalt Pavement) are consistent.
- ii. For the third analysis alternative (Vitrified clay pipes-Asphalt pavement), according to the calibration data from the confusion matrix, the model correctly classified between 58 and 65% of the three categories; whereas, in the validation data, the best classified category was C3 (50% match), followed by C2 (18%) and C1 (0%). This means that the model overestimated pipes in category C3 (classifying all pipes in excellent condition when, in reality, they were in critical structural conditions), and

underestimated pipes in category C1 (the pipes were worse than they actually were).

- iii. For the last analysis alternative (Vitrified clay-Concrete pavement), the results were similar to those of the first analysis alternative (Concrete-Asphalt pavement). The model classified approximately 70% of pipes in C1 and C2 in calibration and validation results.

In Figures 2, 3, and 4, maps of the pipes inspected in Bogotá are shown. In these Figures, the observed categories are compared to those obtained using SVM models.

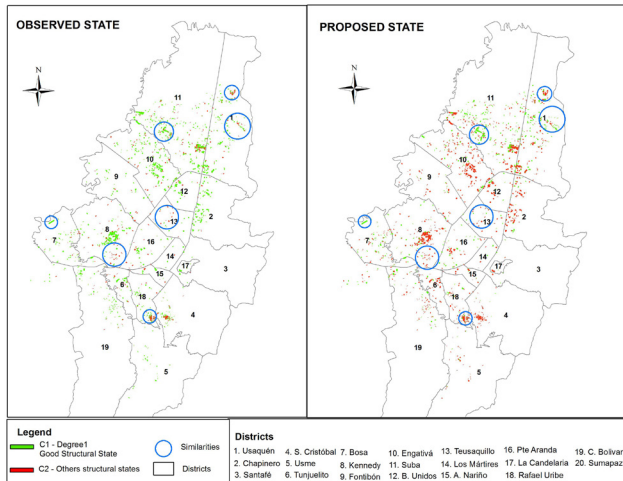


Figure 2. Category classification maps for inspected sewer pipes in Bogotá for alternatives (i) concrete pipes-asphalt pavement and (ii) concrete pipes-concrete pavement. *Left:* classification map of observed condition. *Right:* classification map of results when using the proposed methodology.

Source: Authors

Figure 2 demonstrates that, for these two alternatives, the structural condition of several pipes was underestimated by the proposed methodology. However, in certain parts of Bogotá (namely in the districts of Suba, Usaquén, Teusaquillo, Kennedy, Puente Aranda, and Bosa), the sewer's SVM-estimated overall condition matched the observed state. Moreover, in general terms, there were greater matches for categories classified as C1 by the proposed SVM. This finding suggests that the proposed methodology has potential applications for sewer system management in that it indicates which pipes are in excellent structural condition (category C1, corresponding to grade 1 in the NS-058 standard) because management efforts (inspection, rehabilitation, replacement, etc.) can be carried out only on pipes that are not classified as C1 by the SVM models. A similar behavior was observed for the proposed SVM models for vitrified clay pipes (Figures 3 and 4).

In Figure 5, the prediction error importance is seen to be generally null or low (green and yellow pipes). In other words, for the majority of pipes, the categories obtained using the proposed methodology matched the categories observed (green), or the methodology underestimated the

condition of the pipes (yellow or orange). Few pipes saw their structural state overestimated (red). In short, the proposed methodology proves to be conservative (more underestimation than overestimation), which is a plus from a safety perspective when it comes to deciding which pipes require priority management action. Table 4 summarizes the results presented in Figure 5.

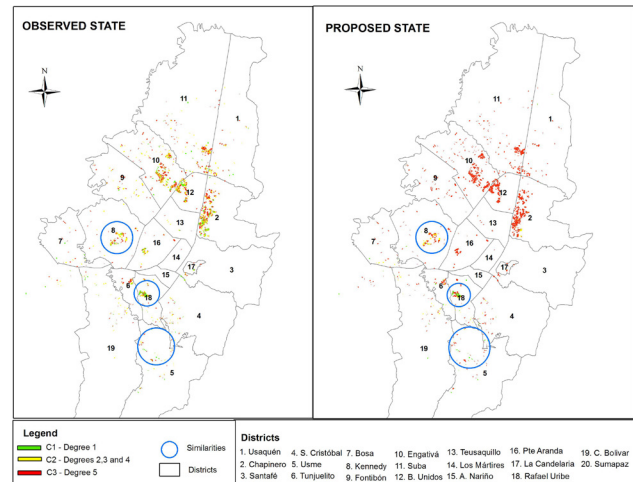


Figure 3. Category classification maps for inspected sewer pipes in Bogotá for vitrified clay-asphalt pavement. *Left:* classification map of observed condition. *Right:* classification map of results when using the proposed methodology.

Source: Authors

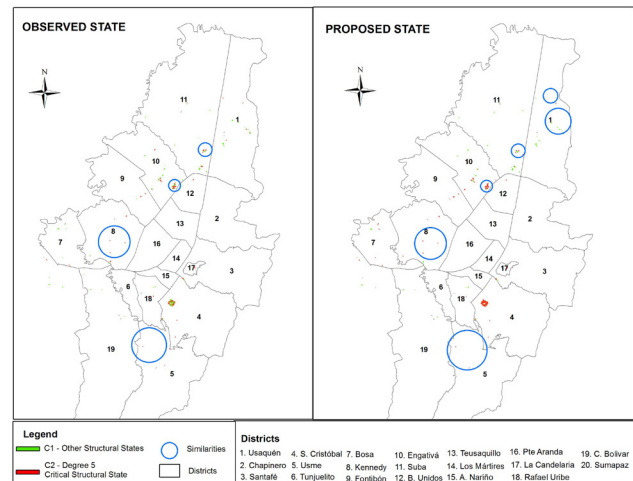


Figure 4. Category classification maps for inspected sewer pipes in Bogotá for vitrified clay-concrete pavement. *Left:* classification map of observed condition. *Right:* classification map of results when using the proposed methodology.

Source: Authors

In Figure 5, the prediction error importance is seen to be generally null or low (green and yellow pipes). In other words, for the majority of pipes, the categories obtained using the proposed methodology matched the categories observed (green), or the methodology underestimated the condition of the pipes (yellow or orange). Few pipes saw their structural state overestimated (red). In short, the

proposed methodology proves to be conservative (more underestimation than overestimation), which is a plus from a safety perspective when it comes to deciding which pipes require priority management action. Table 4 summarizes the results presented in Figure 5.

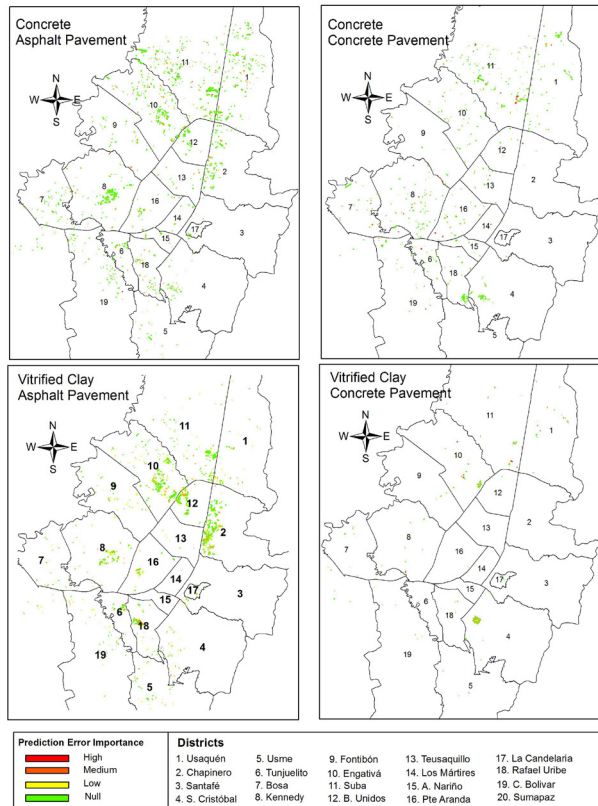


Figure 5. Prediction error importance maps for sewer pipes in Bogotá for the four proposed alternatives. Upper left: (i) concrete-asphalt pavement. Upper right: (ii) concrete-concrete pavement. Lower left: (iii) vitrified clay pipes-asphalt pavement. Lower right: (iv) vitrified clay pipes-concrete pavement.

Source: Authors

Table 5. Percentage of pipes per category for prediction error importance of each alternative

Alternative	Prediction error importance				Kappa
	Null	Low	Med	High	
Alternative 1: Concrete - Pavement in Asphalt	78		19	3	0,305
Alternative 2: Concrete - Concrete pavement	78		13	9	0,415
Alternative 3: Vitrified clay pipes - Asphalt pavement	55	31	14	1	0,071
Alternative 4: Vitrified clay pipes - Concrete pavement	69		27	4	0,213

Source: Authors

Table 5 shows that more than 78% of sewer pipes presented a null or low prediction error importance. Low prediction importance is considered favorable for decision-making

related to sewer management, provided that the percentage of pipes is not high. Despite the improper classification of some pipes, these were classified in the next most critical category. This suggests that, if these pipes were reviewed, they would likely be in better structural states than expected. It should be noted that low importance prediction error is possible when the selected model has more than two structural categories, as is the case for alternative 3 (vitrified clay pipes under asphalt pavement). Nevertheless, broadly speaking, satisfactory pipe classification was observed for the first three alternatives, with a successful classification between 78 and 86%. For the fourth alternative, this figure was 69%. Moreover, the percentage of pipes with high prediction error importance was less than 4% for all the alternatives studied, with the exception of alternative 2 (9%).

The results presented in Table 5 do not suggest a direct relation between proper classification with the proposed methodology for each alternative and the corresponding Cohen kappa coefficient, which implies that the latter is only useful for model selection.

The previously mentioned results represent the combination of results obtained for both calibration and validation databases. To distinguish the results obtained for the two databases, as well as to judge the predictive capacity of the proposed methodology, readers are directed to Figure 6.

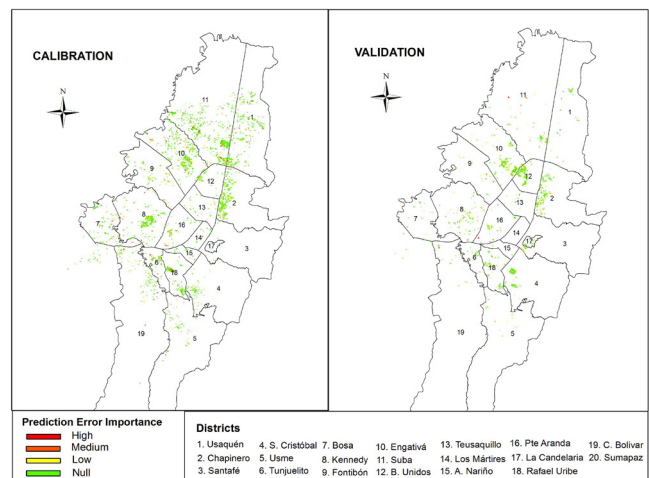


Figure 6. Prediction error importance for the calibration (left) and validation (right) databases

Source: Authors

Figure 6 evinces consistency among the results obtained for both databases (calibration and validation) in terms of prediction error importance. As was the case for the results shown in Figure 5, the majority of sewer pipes analyzed in both databases had null (green) or low prediction importance (yellow). Table 6 summarizes this information.

In Table 6, for the calibration data, 72% of pipes were properly classified (null prediction error importance-green), and 11% of pipes were improperly classified, but with a low prediction error importance (yellow). Therefore, it can be

said that, for the calibration database, the proposed SVM classification methodology provided satisfactory results for 83% of the pipes. Similarly, for the validation data, satisfactory classifications were obtained for 78% of analyzed pipes, thus opening the possibility of utilizing the proposed SVM classification methodology for sewer management decision-making to improve inspection processes, as well as maintenance, rehabilitation, and replacement. The validation data (78%) represent the proposed tool's performance concerning classifying the structural state of uninspected concrete or vitrified clay pipes.

Table 6. Prediction error importance of the proposed methodology's classification in calibration and validation databases

% Pipes	Prediction Importance			
	Null	Low	Medium	High
Calibration	72	11	14	3
Validation	58	20	20	2

Source: Authors

Although the results obtained are satisfactory for managing of Bogotá's sewer systems, it is essential not to lose sight of the limited public resources available for developing these activities. [Rodríguez et al. \(2012\)](#) discuss the budget for actions related to sewer pipe management, attributing the low inspection coverage in Bogotá to a meager budget that is too low to inspect all of the city's sewer pipes. In light of these restrictions, it is crucial to determine the percentage of the minimum number of pipes that should be selected (e.g., those that the proposed methodology classified in a critical structural state) to ensure a percentage of proper classifications with a satisfactory level of uncertainty (e.g., relative uncertainty $\leq 15\%$). This may serve a host of objectives, such as directing CCTV inspections as effectively as possible within budget constraints.

The proposed methodology was applied to a case study to select the minimum number or percentage of pipes classified via SVMs as being in critical structural states for purposes of inspection or action. Ten thousand random selections were performed for each percentage (1 to 100%, with 1% variations) of the total number of pipes in a critical structural state when applying the SVM classification methodology. The results of this case study can be found in Figure 7. This Figure demonstrates that (i) pipes in critical structural states were properly classified roughly 60% of the time by the methodology; and (ii) to obtain a relative uncertainty less than 15% of proper classifications, at least 10% of total pipes classified in this state must be randomly selected. According to the above, it is safe to say that decision-making regarding pipes that require inspection or action can be performed while meeting the budget assigned to these tasks. However, it must be clarified that the percentage of pipes selected is a decision to be made by stakeholders, and it requires the consideration of multiple variables (e.g., financial variables). Regardless, the results in [Figure 7](#) offer an accurate depiction of the analyzed case study.

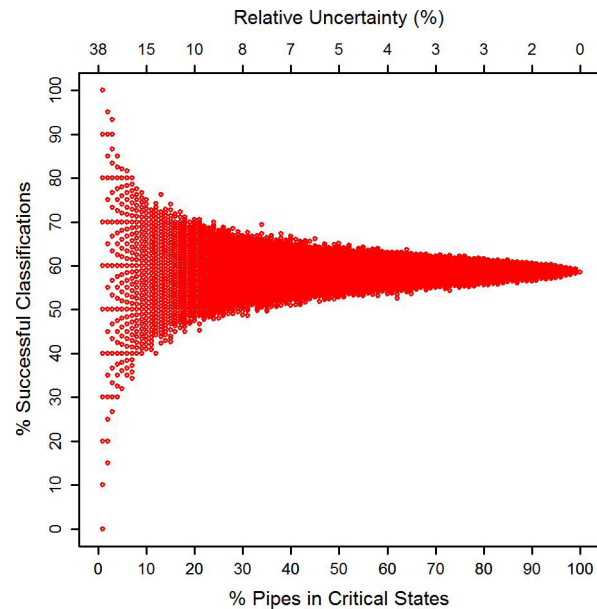


Figure 7. Relative uncertainty vs. percentage (%) of successful classifications and percentage (%) of pipes predicted to be in critical conditions

Source: Authors

Conclusions

In this article, the structural state of sewer pipes in a specific case study (database of pipes inspected via CCTV in Bogotá between 2007 and 2011) is shown to be related to physical characteristics, location, and pipe age. These findings match the results of previous studies on the same database ([Niño et al., 2012](#); [López-Kleine et al., 2016](#)).

A methodology for classifying the structural state of uninspected sewer pipes using SVMs was developed. The proposed methodology employed SVM functions, CV techniques, and an evaluation of results with Cohen's kappa coefficient. This coefficient proved to be especially useful for objectively selecting the best classification mode, for it emphasized model predictability and avoided overtraining.

When applied to the case study, this methodology correctly classified 78% of the inspected pipes (relative to validation data). Additionally, the results obtained were satisfactory; the methodology identified pipes in critical structural states with a low prediction error importance for 69% of the pipes studied. This provides an opportunity to develop more rational management strategies from a financial perspective for companies that provide sewer services and facilitate decision-making in system management for pipe inspection and action. Furthermore, this methodology identified which pipes require inspection or action based on the relative uncertainty of the expected percentage of proper classifications.

Comparing this methodology's results to those of [López-Kleine et al. \(2016\)](#), it can be confirmed that better results

are achieved when grouping structural states in a few groups that discriminate extreme structural states in the pipes.

In this study, other types of materials present in sewer networks (such as masonry and PVC) and other types of road (green surfaces or non-paved firm surfaces) over the sewer network were omitted because pipes with these configurations were not found in the inspection database provided by EAB.

In conclusion, the authors recommend that future studies use complete information on the types of roads over sewer pipes that have not been inspected in Bogotá, seeing as the methodology proposed in this paper could incorporate this information to classify all pipes in the city's sewer system.

Acknowledgements

This work was supported by the Administrative Department of Science, Technology, and Innovation (COLCIENCIAS) and Pontificia Universidad Javeriana (Ph.D. grant – Call 727 of 2015: Support for national doctorates).

Likewise, the authors would like to thank to Bogotá's Water and Sewerage Utility (Empresa de Acueducto de Bogota, EAB) for supplying the database information used in this research.

References

- Baik, H. S., Jeong, H. S., and Abraham, D. M. (2006). Estimating transition probabilities in Markov chain-based deterioration models for management of wastewater systems. *Journal of Water Resources Planning and Management*, 132(1), 15-24. [https://doi.org/10.1061/\(ASCE\)0733-9496\(2006\)132:1\(15\)](https://doi.org/10.1061/(ASCE)0733-9496(2006)132:1(15))
- Caradot, N., Sonnenberg, H., Kropp, I., Ringe, A., Denhez, S., Hartmann, A., and Rouault, P. (2017). The relevance of sewer deterioration modelling to support asset management strategies. *Urban Water Journal*, 14(10), 1007-1015. <https://doi.org/10.1080/1573062X.2017.1325497>
- Cardoso, M. A., Silva, M. S., Coelho, S. T., Almeida, M. C., and Covas, D. I. C. (2012). Urban water infrastructure asset management—a structured approach in four water utilities. *Water Science and Technology*, 66(12), 2702-2711. <https://doi.org/10.2166/wst.2012.509>
- Carletta, J. (1996). Assessing agreement on classification tasks: the kappa statistic. *Computational Linguistics*, 22(2), 249-254. <https://arxiv.org/abs/cmp-lg/9602004>
- Davies, J. P., Clarke, B. A., Whiter, J. T., and Cunningham, R. J. (2001). Factors influencing the structural deterioration and collapse of rigid sewer pipes. *Urban Water*, 3(1-2), 73-89. [https://doi.org/10.1016/S1462-0758\(01\)00017-6](https://doi.org/10.1016/S1462-0758(01)00017-6)
- Empresa de Acueducto y Alcantarillado de Bogotá (EAAB) (2001). *NS-058. Aspectos Técnicos para inspección y mantenimiento de redes y estructuras de alcantarillado*. EAAB-E.S.P.
- Geisser, S. (2017). *Predictive inference*. Routledge.
- Hernández, N., Caradot, N., Sonnenberg, H., Rouault, P., and Torres, A. (2021). Optimizing SVM models as predicting tools for sewer pipes conditions in the two main cities in Colombia for different sewer asset management purposes. *Structure and Infrastructure Engineering*, 17(2) 156-169. <https://doi.org/10.1080/15732479.2020.1733029>
- Hao, T., Rogers, C. D. F., Metje, N., Chapman, D. N., Muggleton, J. M., Foo, K. Y., Wang, P., Pennock, S. R., Atkins, P. R., Swingler, S. G., Parker, J., Costello, S. B., Burrow, M. P. N., Anspach, J. H., Armitage, R. J., Cohn, A. G., Goddard, P. L., Orlando, G., ... and Saul, A. J. (2012). Condition assessment of the buried utility service infrastructure. *Tunnelling and Underground Space Technology*, 28, 331-344. <https://doi.org/10.1016/j.tust.2011.10.011>
- Huang, S., Cai, N., Pacheco, P. P., Narrandes, S., Wang, Y., and Xu, W. (2018). Applications of support vector machine (SVM) learning in cancer genomics. *Cancer Genomics-Proteomics*, 15(1), 41-51. <https://doi.org/10.21873/cgp.20063>
- Jahed Armaghani, D., Asteris, P. G., Askarian, B., Hasanipanah, M., Tarinejad, R., and Huynh, V. V. (2020). Examining hybrid and single SVM models with different kernels to predict rock brittleness. *Sustainability*, 12(6), 2229. <https://doi.org/10.3390/su12062229>
- Karatzoglou, A., Smola, A., Hornik, K., and Zeileis, A. (2004). kernlab—an S4 package for kernel methods in R. *Journal of Statistical Software*, 11(9), 1-20. <https://doi.org/10.18637/jss.v011.i09>
- Kleidorfer, M., Möderl, M., Tscheikner-Gratl, F., Hammerer, M., Kinzel, H., and Rauch, W. (2013). Integrated planning of rehabilitation strategies for sewers. *Water Science and Technology*, 68(1), 176-183. <https://doi.org/10.2166/wst.2013.223>
- Lee, J., Jeong, Y., Oh, Y. S., Lee, J. C., Ahn, N., Lee, J., and Yoon, S. H. (2013). An integrated approach to intelligent urban facilities management for real-time emergency response. *Automation in Construction*, 30, 256-264. <https://doi.org/10.1016/j.autcon.2012.11.008>
- Liu, Z. and Kleiner, Y. (2013). State of the art review of inspection technologies for condition assessment of water pipes. *Measurement*, 46(1), 1-15. <https://doi.org/10.1016/j.measurement.2012.05.032>
- López-Kleine, L. and Torres, A. (2014). UV-vis in situ spectrometry data mining through linear and non linear analysis methods. *Dyna*, 81(185), 182-188. <https://doi.org/10.15446/dyna.v81n185.37718>
- López-Kleine, L., Hernández, N., and Torres, A. (2016). Physical characteristics of pipes as indicators of structural state for decision-making considerations in sewer asset management. *Ingeniería e Investigación*, 36(3), 15-21. <https://doi.org/10.15446/ing.investig.v36n3.56616>
- Mashford, J., Marlow, D., Tran, D., and May, R. (2010). Prediction of sewer condition grade using support vector machines. *Journal of Computing in Civil Engineering*, 25(4), 283-290. [https://doi.org/10.1061/\(ASCE\)CP.1943-5487.0000089](https://doi.org/10.1061/(ASCE)CP.1943-5487.0000089)
- Micevski, T., Kuczera, G., and Coombes, P. (2002). Markov model for storm water pipe deterioration. *Journal of Infrastructure Systems*, 8(2), 49-56. [https://doi.org/10.1061/\(ASCE\)1076-0342\(2002\)8:2\(49\)](https://doi.org/10.1061/(ASCE)1076-0342(2002)8:2(49))

- Niño, P., Angarita, H., Vargas, D., and Torres, A. (2012, 9-12 September). *Identificación factores de riesgo para la gestión patrimonial óptima de sistemas de drenaje urbano: Estudio Piloto en la Ciudad de Bogotá* [Conference presentation]. XXV Congreso Latinoamericano de Hidráulica San José, Costa Rica.
- Osman, H. (2012). Agent-based simulation of urban infrastructure asset management activities. *Automation in Construction*, 28, 45-57. <https://doi.org/10.1016/j.autcon.2012.06.004>
- Rodríguez, J. P., McIntyre, N., Díaz-Granados, M., and Maksimović, Č. (2012). A database and model to support proactive management of sediment-related sewer blockages. *Water Research*, 46(15), 4571-4586. <https://doi.org/10.1016/j.watres.2012.06.037>
- Sægrov, S. and Schilling, W. (2002). Computer Aided Rehabilitation of sewer and storm water networks. In E. W. Strecker and W. C. Huber (Eds.) *Global Solutions for Urban Drainage* (pp. 1-15). ASCE. [https://doi.org/10.1061/40644\(2002\)88](https://doi.org/10.1061/40644(2002)88)
- Shawe-Taylor, J. and Cristianini, N. (2004). *Kernel methods for pattern analysis*. Cambridge University Press. <https://doi.org/10.1017/CBO9780511809682>
- R Core Team (2019). R: A language and environment for statistical computing. <https://www.R-project.org/>
- Ward, B. and Savić, D. A. (2012). A multi-objective optimisation model for sewer rehabilitation considering critical risk of failure. *Water Science and Technology*, 66(11), 2410-2417. <https://doi.org/10.2166/wst.2012.393>
- Wirahadikusumah, R., Abraham, D., and Iseley, T. (2001). Challenging issues in modeling deterioration of combined sewers. *Journal of Infrastructure Systems*, 7(2), 77-84. [https://doi.org/10.1061/\(ASCE\)1076-0342\(2001\)7:2\(77\)](https://doi.org/10.1061/(ASCE)1076-0342(2001)7:2(77))
- Younis, R. and Knight, M. A. (2014). Development and implementation of an asset management framework for wastewater collection networks. *Tunnelling and Underground Space Technology*, 39, 130-143. <https://doi.org/10.1016/j.tust.2012.09.007>
- Zhang, X., Srinivasan, R., and Van Liew, M. (2009). Approximating SWAT model using artificial neural network and support vector machine 1. *Journal of the American Water Resources Association*, 45(2), 460-474. <https://doi.org/10.1111/j.1752-1688.2009.00302.x>
- Zhang, Y. (2008). Fault detection and diagnosis of nonlinear processes using improved kernel independent component analysis (KICA) and support vector machine (SVM). *Industrial and Engineering Chemistry Research*, 47(18), 6961-6971. <https://doi.org/10.1021/ie071496x>

The Self-Healing Effect on Bacteria-Enriched Steel Fiber-Reinforced SCC

El efecto de autorreparación en SCC reforzado con fibra de acero enriquecida con bacterias

Vasudev Raman¹, Nivin Philip², and Nijo Baven³

ABSTRACT

Steel fiber reinforced self-compacting concrete is well accepted due to its better resistance against segregation and its effective use in congested reinforcements. It has improved ductile properties, and crack propagation is minimal. As the need for sustainable materials increases all over the world, innovative techniques to make concrete more durable become relevant. Concrete is prone to cracks, which make it vulnerable as they debase it and erode the steel support. Bacterial concrete is a progression of current concrete innovation. Limestone-hastening microscopic organisms are brought into concrete during casting, and, when cracking happens due to dampness, microorganisms contribute to mending the breaks. Thereupon, a blend between self-healing attributes and the qualities of steel fiber-fortified self-compacting concrete is presented. In this paper, micro-silica is utilized to substitute Ordinary Portland Cement by up to 30%. Around 1.5% of steel fiber is used in the concrete mix. 20% is shown as an ideal amount for micro-silica substitution. The performance of self-compacting concrete under specific loads and their impact on healing are examined, as well as the quality of the recovered concrete. An overall increase in elasticity and durability over typical self-compacting concrete is seen.

Keywords: self-healing, mechanical properties, bacteria, micro-silica

RESUMEN

El concreto autocompactante reforzado con fibras de acero es comúnmente aceptado, dados su mejor resistencia a la segregación y su uso efectivo en refuerzos congestionados. Tiene mejores propiedades dúctiles y la propagación de roturas es mínima. A medida que aumenta la necesidad de materiales sostenibles alrededor del mundo, las técnicas innovadoras para hacer que el concreto sea más durable cobran importancia. El concreto es propenso a las roturas, las cuales lo hacen vulnerable, pues lo degradan y erosionan los soportes de acero. El concreto bacteriano es un avance de la innovación actual en concreto. Los organismos microscópicos que aceleran la piedra caliza se introducen en el concreto durante el colado y, cuando hay roturas por la humedad, los microorganismos contribuyen a repararlas. Por consiguiente, se presenta una mezcla entre los atributos de autorreparación y las cualidades del concreto autocompactante reforzado con fibras de acero. En este artículo se usa microsilíce para sustituir Cemento Portland Ordinario hasta en un 30 %. Se utiliza alrededor de 1,5 % de fibras de acero en la mezcla de concreto. Se muestra el 20 % como una cantidad ideal para la sustitución por microsilíce. Se examinan el rendimiento del concreto autocompactante bajo cargas específicas y su impacto en la reparación, así como la calidad del concreto recuperado. Se observa un aumento general en la elasticidad y la durabilidad por encima del concreto autocompactante típico.

Palabras clave: autorreparación, propiedades mecánicas, bacterias, microsilíce

Received: May 8th, 2020

Accepted: September 8th, 2021

¹ Civil Engineering, Bharathiar University, Tamil Nadu, India. MTech in Computer Aided Structural Engineering, Mar Athanasius College of Engineering, Kothamangalam & Mahatma Gandhi University, Kerala. PhD from Anna University, Tamil Nadu, India. Affiliation: Associate Professor & HOD, Department of Civil Engineering, Toc H Institute of Science and Technology, Cochin & APJ Abdul Kalam Technological University, Kerala, India. E-mail: vasu.vasudev@gmail.com

² Civil Engineering, Mahatma Gandhi University, Kerala, India. MTech in Computer Aided Structural Engineering, Mar Athanasius College of Engineering, Kothamangalam & Mahatma Gandhi University, Kerala. PhD from Vellore Institute of Technology, Vellore, India. Affiliation: Professor, Department of Civil Engineering, Saintgits College of Engineering, Kottayam & APJ Abdul Kalam Technological University, Kerala, India. E-mail: nivinadoor@gmail.com

³ Civil Engineering, Kerala University, Kerala, India. MTech in Construction Engineering & Management, Toc H Institute of Science and Technology, Cochin, Kerala. Affiliation: Research Scholar, Department of Civil Engineering, Toc H Institute of Science and Technology, Cochin & APJ Abdul Kalam Technological University, Kerala, India. E-mail: nijobaven@gmail.com

How to cite: Raman, V., Philip, N., and Baven, N. (2022). The Self-Healing Effect on Bacteria-Enriched Steel Fiber-Reinforced SCC. *Ingeniería e Investigación*, 42(2), e87120. <http://doi.org/10.15446/ing.investig.87120>

Introduction

Self-compacting concrete (SCC) is a streaming solid blend that can self-unite under its own weight. The profoundly liquid nature of SCC makes installing it under troublesome conditions and in areas with congested reinforcement a reasonable endeavor. The utilization of SCC can likewise limit hearing-related harms on the worksite that are due to the vibration of concrete. Another favorable feature of SCC is that the time required to install enormous segments is significantly diminished. Earlier, in order to increase the strength and durability of the structure, cracks were repaired using epoxy injection or latex treatment or by giving extra reinforcement to the structure during the design phase to ensure that the crack width stayed within permissible limits. The primary motivation



Attribution 4.0 International (CC BY 4.0) Share - Adapt

to prevent cracks or limit crack width is to upgrade the durability of the structure. Crack propagation can be restricted by including steel fiber into the concrete. Throughout the last three decades, noteworthy research has been conducted to analyze the effect of steel fibers as a fortifying framework on mechanical properties and impact resistance. Steel fibers overcome any issues between the nearby surfaces of existing micro-cracks, defer split development (Siddique *et al.*, 2016), and cut off break spread by diminishing the broken tip opening removal. This component is known as the spanning instrument. The vitality ingestion and the effect on the quality of cement can be furthered by the expansion of steel fiber (Wasim and Ehsan, 2016). Be that as it may, the expansion of steel fiber in high measure has the potential drawback of poor functionality and expanded expense (Ning *et al.*, 2015). Moreover, the use of micro-silica greatly influences and improves the bonding of the transition zone between the cement paste and the total aggregate since it consists of ultra-fine particles (Jeevetha *et al.*, 2014) and increases the bond strength. In addition, the use of silica fume significantly improves the holding said transition zone (Koksal *et al.*, 2008) and expands the bond quality between concrete glue and the total mix by densifying the interfacial zone (WSDOT FOP for ASTM C1621/C1621M). Due to pozzolanic movement, the mechanical qualities of the solid (Tasdemir and Bayramov, 2002) are improved. Another economic strategy could be a process that fixes break in solid and implies self-healing. This would expand the sturdiness of the structure. Microbiologically prompted calcite precipitation (Falguni and Darshika, 2016) is profoundly attractive given the fact that it is common and does not pollute. Appropriate selection of bacteria and dosage (Ghosh *et al.*, 2010; Jonkers *et al.*, 2010) must be ensured. Thus, incorporating these two techniques into steel fiber in concrete to minimize crack propagation (Sivakumar and Santhanam, 2007) would also improve tensile property (Tomaz, 2013; Nuruddin *et al.*, 2014), and, in particular, the technique involving the incorporation of bacteria for crack healing (Naveen and Sivakamasundari, 2016) would improve the overall properties and the durability of SCC. A micro-structure of concrete with an addition of bacteria was visualized by scanning electron microscopy (SEM).

Material properties

In this study, the ingredients of bacteria-enriched steel fiber reinforced SCC, namely Ordinary Portland cement (OPC), and cement-replacement materials acted as binders in the mixes, while manufactured sand was used as the fine aggregate. In addition, a superplasticizer based on polycarboxylate ether (PCE) was used (BASF MasterGlenium ACE 30IT); it is a second-generation superplasticizer for concrete that provides self-compacting abilities. Steel fiber was used in the mixes to give better ductility.

Binders

In this experimental work, OPC53 was used. Its main characteristics are shown in Table 1:

Table 1. Properties of the cement used

Cement fineness	5%
Standard consistency	36%
Specific gravity	3,15
Initial setting time	40 min

Source: Authors

Micro-silica is a fine pozzolanic material made out of undefined silica created by electric band heaters as a side-effect of the creation of basic silicon or ferro-silicon amalgams. It consists of spherical particles. Individual micro-silica particles have a diameter of less than 1 μm , which is approximately 1/100 of the size of an average cement particle. Its main field of application is as a pozzolanic material for high-performance concrete. Micro-silica can also be used in a variety of products such as grouts and mortars. The specific gravity of micro-silica is 2,21, its pack density 0,76 gm/cc, and its moisture 0,059%. It also has a white-colored, powdered appearance.

Bacteria

The microscopic organisms *Bacillus subtilis*, strain no. JC3, a soil bacterium refined in a research facility, was used for this research. An unadulterated culture was gathered from the Department of Agricultural Microbiology, College of Horticulture, Kerala Agricultural University, Vellanikkara, Thrissur. On a supplement agar plate, provinces of strain JC3 were round, raised, smooth, and translucent. The size of a settlement may reach up to 2-3 mm width after 24 h of hatching in dim, oxygen-consuming conditions at 37 °C. The life form delivered a pale blue green color that diffused into the medium. Singular cells of JC3 were Gram-positive, oval to poles, 0,6-0,8 μm wide, 2,0 to 3,0 μm long, motile, and duplicated by double parting. SEM was performed to recognize the precipitation in concrete.

Steel fiber

Loose snare finished steel fiber was utilized. It has more significant adaptability with all Portland concretes and admixtures. It additionally gives an even circulation in the blend and improves mechanical jetty, as well as the micro-crack mechanism, impact resistance, flexural strength, and fatigue strength of concrete. 50- and 30-mm length fibers with a diameter of 0,6 mm and tensile strength of 1100 MPa were used (aspect ratio 50). All the fibers were manufactured from high-strength steel. Specimens incorporated with 0,5-1,5% of steel fiber are shown in Figure 1 by volume fraction.

Calcium lactate

Calcium lactate is a dark or white crystalline salt generated by the activity of lactic corrosive on calcium carbonate. It is used for nourishment (as a fixing in heating powder) and given restoratively. It is made by the response of lactic corrosive to calcium carbonate or calcium hydroxide. The expansion builds the nearness of calcium in concrete. Only

the fuse of calcium lactate did not generously influence quality (curation of 3 and 7 days) or even brought about a slight increment (curation of 28 days) in compressive strength values (Henk *et al.*, 2010).

Fine and coarse aggregate

Manufactured sand (M-sand) is a better substitute for river sand because it has no silt or organic impurities and is mostly well graded. It was used in this project to cast the concrete. A fine aggregate of less than 4,75 mm was used. Coarse aggregates are commonly considered to be inert fillers. Their various properties play an important role in the strength, shape and texture, size gradation, moisture content, specific gravity, reactivity, soundness, bulk density, workability, and durability of concrete. Coarse aggregates of 12,5 mm and 6 mm in size were used for casting in a 60:40 ratio. The properties of aggregates used are shown in Table 3 and the sieve curve in Figure 2.



Figure 1. Hook-end steel fiber

Source: Authors

Table 3. Properties of fine and coarse aggregate

Fine aggregate	Specific gravity	2,73
	Water absorption	2,08%
Coarse aggregate	Specific gravity	2,85
	Water absorption	0,50%

Source: Authors

Table 4. Mix proportions

Content (kg/m ³)	MSCC-1	MSCC-2	MSCC-3	MSCC-4	MSCC-5	MSCC-6	MSCC-7
Cement	560,5	545,5	531	501,5	472	442,5	413
Micro-silica	29,5	44,25	59,0	88,5	118,0	147,5	177,0
F.A	900	900	900	900	900	900	900
C.A	770	770	770	770	770	770	770
W/C ratio	0,35	0,35	0,35	0,35	0,35	0,35	0,35
Superplasticizer	3,363	3,363	3,363	3,363	3,363	3,363	3,363
Calcium lactate	18	18	18	18	18	18	18

Source: Authors

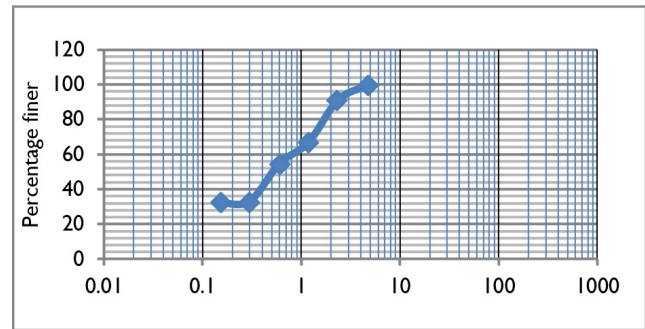


Figure 2. Gradation curve of fine aggregate

Source: Authors

Specimen preparation

The sizes of the concrete cube and cylinder are $150 \times 150 \times 150$ mm and 100×300 mm, respectively. These two were used to test compressive and split tensile strength. The M40 grade concrete mix design was carried out as per the European standards for SCC (EFNARC, 2002). A W/C ratio of 0,35 was used. The reinforced beam size used for testing flexural strength was $150 \times 150 \times 700$ mm, and advanced shafts of microscopic organisms were thrown. 8 mm reinforcement bars were used for stirrups, distribution, and main bars. Micro-silica was included by swapping the measure of concrete for an ideal fixation from 0 to 30%, with various groupings of steel filaments (0, 0,5, 1, and 1,5% of the total volume). The fortified shafts with microscopic organisms were cast and relieved for 28 days. Miniaturized-scale silica was included by incomplete substitution of concrete at convergences of 0, 5, 7,5, 10, 20, 25, and 30%. The concrete cubes, the cylinders with and without bacteria, and the steel fibers were casted and cured for 28 days.

Mixing procedures

The mixing proportions of SCC reinforced with bacteria-enriched steel fiber are shown in Table 4. An electric concrete mixer was employed, and the binders and sand were mixed for 2 min, followed by pouring 50% of the total mix in water

and then mixed again for 3 min. Next, 40% of water and 70% of SP were poured and then mixed for 5 min. Subsequently, the remaining water and SP were added and mixed until a uniform mix was achieved. Finally, the steel fibers were dispersed evenly to prevent fiber balling and mixed for 2 min.

Workability tests

In order to ensure the self-compacting abilities of the mix for on-site quality control, two test methods are sufficient to monitor the production quality. These tests yield results regarding two distinguished properties: flow ability and passing ability. Two workability tests were selected (slump flow and J-Ring) and conducted immediately after the mix was completed. The procedures of the tests were performed in accordance with BS EN 12350:2010 (BSI Standards, 2010). The acceptance criteria of self-compacting abilities in a slump flow test are a minimum diameter of 650 mm and maximum of 800 mm. The blocking assessment was determined using ASTM C1621/C1621M (Okamura and Ouchi, 2003), as shown in in Table 5.

Table 5. Blocking assessment

Difference between slump flow and J-Ring test	Blocking assessment
0-25 mm	No visible blocking
25-50 mm	Minimal to noticeable blocking
> 50 mm	Noticeable to extreme blocking

Source: Authors

Mechanical tests

Two mechanical tests were conducted to compare the control mix and the DSCC mixes with various cement-replacement materials. Compressive strength tests were performed at 7 and 28 days, while flexural quality tests were conducted at 28 days. The testing methods of both the compressive and flexural quality tests are in accordance with IS 516:1959 (Reaffirmed 2004) (Bureau of Indian Standards, 2004).

Ultra-sonic pulse velocity

The methodology includes estimating the time it takes for an ultrasonic heartbeat to go through the solid under study. A relatively higher speed is acquired when the solid quality is acceptable in terms of thickness, consistency, and homogeneity, among others. The values for the beams were taken before and after the flexural test. The velocity was also measured 28 days after the flexural testing, which gave an idea about the healing.

SEM and EDS

Scanning electron microscopy (SEM) and Energy-dispersive X-ray spectroscopy, sometimes called energy

dispersive X-ray analysis (EDXA) or energy dispersive X-ray microanalysis (EDXMA) were also conducted on the beam specimens for a detailed analysis.

Results and discussion

Micro-silica-based SCC

The mineral admixture micro-silica was employed as the concrete substitution material. Small-scale silica gives a progressively uniform dissemination and a more prominent volume of hydration items. As a channel, it diminishes the normal size of pores in the concrete glue. Smaller-scale silica is an exceptionally fine material with less explicit gravity than concrete, so it does not increase the density of concrete.

Workability

A slump flow test was conducted to evaluate the flat free stream without impediments. It is the most generally utilized test, and it gives a decent appraisal of the filling capacity. It gives no sign of the solid's ability to go between support without blocking, but it may give some sign of protection from isolation. The passing capabilities of SCC are measured by utilizing the J-Ring test in a mix with a droop cone form. The test strategy is restricted to concrete with a total size of 25 mm at most.

A highly flowable concrete does not simply have to do with prime point compacting, since SCC ought to stream under its own load as well as filling the whole frame and accomplishing a uniform consolidation without segregation. The superplasticizer content is kept constant as the binder content remains constant. The workability is determined using standard tests such as flow table testing and the J-Ring test, which are shown in Figure 3. The results are shown in Table 6.

Table 6. Workability of micro-silica-based SCC

Sl. No.	Mixes	SlumpFlow test (mm)	J-Ring flow(mm)	J-Ring(mm)
1	MSCC-1	685	673	12
2	MSCC-2	690	680	10
3	MSCC-3	680	671	9
4	MSCC-4	686	677	9
5	MSCC-5	695	687	8
6	MSCC-6	700	691	9
7	MSCC-7	712	701	11

Source: Authors

The obtained results fall under the range of 650 to 800 mm, which is recommended by EFNARC (2002). A visual inspection showed that the SCC had a good cohesion, so, from the workability results and the aforementioned inspection, the mix can be said to be an SCC. The results show that the increase in the addition of micro-silica causes the increase in the slump value. The circular molded particles of micro-silica go about as a smaller-than-expected metal roller inside the SCC blend, which prompts the improvement of the functionality of cement.



Figure 3. J-Ring test
Source: Authors

Miniaturized-scale silica also fundamentally lessens draining, given that the free water is spent in wetting the enormous micro-silica surface. Therefore, the free water left in the blend for draining was unexpectedly depleted. The expansion of smaller-scale silica in a blend modifies the concrete glue structure. The resulting paste contains a greater amount of the solid calcium-silicate hydrates and less of the feeble and effectively solvent calcium hydroxides than the common concrete glues. The miniaturized-scale silica particles are very little, and they scatter to cause the partition of the concrete particles. The upside of utilizing miniaturized-scale silica is that it very well may be considered to diminish the warm splitting brought about by the warmth of concrete hydration. It also results in the improvement of durability.

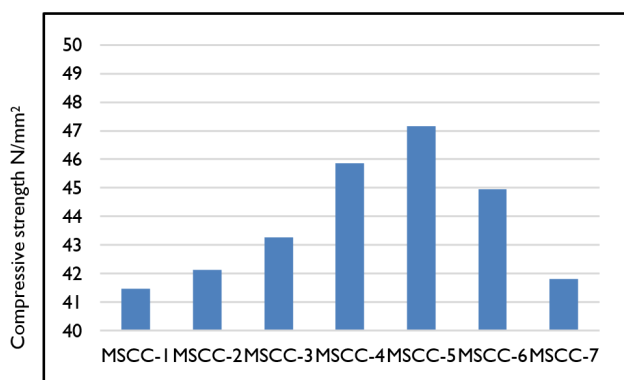


Figure 4. Compressive strength of micro-silica-based SCC
Source: Authors

Compressive strength

A compressive strength test was conducted on concrete specimens, cubes of Mix40 SCC, with micro-silica as a fractional substitution of cement. 150 mm cubes were used for the testing. Since it is a pozzolanic material, micro-silica improves the complete paste bond and enhances the bonding properties at the interface between the fiber and the network with a thick C-S-H gel in the strengthened self-compacting mixtures. The acquired outcomes are shown in Table 7, and a graphical representation is given in Figure 4.

The SCC mixes made with micro-silica showed a strength above 40 N/mm², which may suggest a medium-quality

cement. According to the results, the ideal measure of micro-silica that can be utilized as a concrete substitution in SCC is 20%. The improvement in mechanical properties improves the roots from the expansion of fine micro-silica to the concrete solid lattice, as well as the pozzolanic responses between the micro-silica and the free calcium hydroxide in the concrete matrix.

Table 7. Compressive strength of micro-silica-based SCC

Sl. No.	Mix	28-days split tensile strength (N/mm ²)
1	MSCC-1	3,28
2	MSCC-2	3,40
3	MSCC-3	3,52
4	MSCC-4	4,32
5	MSCC-5	4,50
6	MSCC-6	4,10
7	MSCC-7	3,56

Source: Authors

The compressive strength is improved as the average size of pores in the concrete matrix decreases due to the fineness of micro-silica. Hence, further studies should be carried out with this optimum amount of micro-silica.

Split tensile strength

The tensile strength of concrete is one of its essential and most significant properties. The solid is exceptionally frail under tractable power given its fragile nature, and it is not made to oppose immediate pressure. Concrete breaks when exposed to malleable powers. Thus, it is important to decide the tensile strength of concrete in order to determine the heap at which concrete members may crack.

The inclusion of micro-silica as a replacement of cement shows a slight increase in the split tensile strength throughout the variation in a definitive manner. However, there is no significant reduction in strength with an increase in the micro-silica content of up to MSCC-5 and a 20% addition of micro-silica. Beyond 20%, there is a decrease in split tensile strength.

The test results regarding compressive strength, split tensile strength, and workability show that the optimum micro silica content is observed to be 20%, i.e., MSCC-5. Further studies should focus on SCC specimens with this optimum content of micro-silica. The split tensile strengths of different micro-silica-based SCCs are shown in Table 8.

Bacteria-enriched self-compacting concrete

The MSCC-5 showed better workability and strength parameters. Self-healing of concrete is achieved by incorporating *Bacillus subtilis* in SCC. Microcracks of up to 0,2mm wide are autogenously recuperated because of the

hydration of non-responded concrete particles present in the grid, which interact with entering water. The mending process based on microscopic organisms has been found to feasibly recuperate up to 0,5 mm. A control mix was made with micro-silica (20% cement), a constant amount of *Bacillus subtilis*, and a constant amount of calcium lactate. Steel fiber and a constant amount of bacteria were added to the SCC containing a replacement of 20% cement with micro-silica.

Table 8. Split tensile strength of micro-silica-based SCC

Sl. No.	Mix	7-days compressive strength (N/mm ²)	28-days compressive strength (N/mm ²)
1	MSCC-1	25,29	41,47
2	MSCC-2	26,11	42,12
3	MSCC-3	27,25	43,26
4	MSCC-4	29,81	45,86
5	MSCC-5	30,46	47,17
6	MSCC-6	27,88	44,96
7	MSCC-7	26,35	41,81

Source: Authors

A constant amount of *Bacillus subtilis*, 10⁵ cells per mL of water, was added into the mix containing an optimum quantity of micro-silica, MSCC-5. The mix was labeled as MSCC-5 B₁, which is the SCC mix containing 20% micro-silica as cement replacement and 10⁵ cells per mL of water. Workability and mechanical strength tests were carried out. The SCC mix MSCC-5 B₁ was taken as the control mix for further comparative studies.

Workability

Workability tests on bacteria-enriched SCC were carried out as per BS EN 12350:2010 (BSI Standards, 2010). Acceptance criteria regarding self-compacting abilities in the slump flow test were a minimum diameter of 650 mm and a maximum of 800 mm. The blocking assessment was performed using ASTM C1621/C1621M-17 (ASTM International, 2017). Flow table and J-Ring tests showed no significant changes compared to MSCC-5. The MSCC-5 B₁ mix is a cohesive mix with less resistance to passing through the J-Ring. As the mix contains 20% of micro-silica, the effect of bleeding is reduced due to the large surface area. Hence, the bacteria seem to have no significant effect on the flow characteristics of SCC. The results are shown in Tables 9 and 10.

Table 9. Flow table test of bacteria-enriched SCC

Mixes	Samples	Slump flow diameter (mm)	Average slump flow diameter (mm)
MSCC-5 B ₁	1	695	697
	2	698	
	3	696	

Source: Authors

Table 10. J-Ring test of bacteria-enriched SCC

Mixes	Samples	Slump flow diameter (mm)	Average slump flow diameter (mm)
MSCC-5 B ₁	1	695	697
	2	698	
	3	696	

Source: Authors

Compressive strength

The compressive strength of microorganism-enhanced SCC was evaluated by pounding to the decimation of the test shapes using methods for compression testing machines in accordance with IS 516:1959 (Reaffirmed 2004) (Bureau of Indian Standards, 2004). The observed results are shown in Table 11.

Table 11. Compressive strength of bacteria-enriched SCC

Mixes	Samples	J-Ring flow diameter (mm)	J-Ring	Average J-Ring (mm)
MSCC-5 B ₁	1	690	5	9
	2	690	8	
	3	682	14	

Source: Authors

The results show that by the addition of *Bacillus subtilis* to MSCC-5 yields an increase of about 3,5% in compressive strength. Direct incorporation of bacteria also showed an increase in the compressive strength of concrete. This is due to the reduction in micropores by the calcite deposition of bacteria, which makes the concrete matrix more compact. The bacteria converts the calcium lactate into calcium carbonate crystals, which are not soluble in water. As the micro-silica takes up most of the micro pores due to its extreme fineness, there is only a slight increase in compressive strength due to the addition of *Bacillus subtilis*.

Split tensile strength

Split tensile strength testing was carried out on bacteria-enriched SCC. From the results shown in Table 12, only a very slight increase in the tensile strength of MSCC-5 was observed. Therefore, in general, it can be concluded that there is no significant variation in tensile strength from the parenting mix, MSCC-5. The results suggest that *Bacillus subtilis* has no effect on improvement or any adverse effect in the tensile strength of mix.

Table 12. Split tensile strength of bacteria-enriched SCC

Mix	28-days split tensile strength (N/mm ²)	Average 28-days split tensile strength (N/mm ²)
MSCC-5 B ₁	4,92	4,52
	4,34	
	4,30	

Source: Authors

Flexural strength

The flexural strength test was carried out in accordance with IS 516:1959 (Reaffirmed 2004) (Bureau of Indian Standards, 2004) on 700 mm long concrete beams with a 150×150 mm cross-section. During testing, the first crack loads were noted. It was observed that the crack width was wider (greater than 2 mm). Multiple cracks were more rarely noticed. MSCC-5 B₁ mixes possess a good flexural strength. The results show that bacteria enriched self-compacting concrete, as shown in Table 13 and Figure 5.

Table 13. Flexural strength of bacteria-enriched SCC

Mix	First crack load (kN)	Average Ultimate strength (N/mm ²)
MSCC-5 B ₁	48	20,92
	50	
	46	

Source: Authors



Figure 5. Flexural strength testing

Source: Authors

Bacteria-enriched SFRSCC

Bacteria-enriched SCC satisfies the requirements and has good mechanical properties. The crack width observed during the flexural strength testing highlights the need for limiting. The healing of SCC with the help of calcite-precipitating bacteria is effective up to 0,5 mm. The crack propagation and formation can be limited by incorporating fibers into SCC. In further experimental study, hook-ended steel fibers shall be incorporated into SCC enriched with bacteria. Steel fiber bridges the gap between surfaces, thus reducing crack width and ensuring an effective healing of SCC. The presence of steel fiber can affect the workability of the mix, even though it improves the split tensile strength, flexural strength, and ductile behavior of concrete.

Workability

The workability of bacteria-enriched steel fiber reinforced self-compacting concrete (SFRSCC) was tested regarding passing capabilities and flowability. Different volumes of steel fibers were added to SCC containing the aforementioned optimum amount of micro silica. The SCC mixes MSCC-5

C₁, MSCC-5 C₂, and MSCC-5 C₃ contain 0,5, 1, and 1,5% volumes of steel fiber, respectively. Workability is affected by the presence of steel fiber and micro silica. In essence, the spherical shape of micro silica improves the workability of SCC, but the presence of steel fiber hinders it. The J-Ring test results on bacteria-enriched SFRSCC shows that the MSCC-5 C₁ and MSCC-5 C₂ mixes have no visible blocking, as they were within the range of 0-25 mm. However, MSCC-5 C₃ showed minimal to noticeable blocking, as it was above 25 mm. Table 14 shows the workability of bacteria-enriched SFRSCC.

Table 14. Workability of bacteria-enriched SFRSCC

Sl. No.	Mix	Slump flow test (mm)	J-ring (mm)
1.	MSCC-5 C ₁	680	14
2.	MSCC-5 C ₂	668	18
3.	MSCC-5 C ₃	656	27

Source: Authors

Hook-end steel fibers cause sticking of the solid lattice all through the stream, which is dependent on steel fiber volume. As the volume of steel fibre increases, workability decreases. The filling ability of bacteria-enriched SFRSCC decreases with an increase in the concentration of steel fibre. The passing capabilities test also showed an impact caused by the increase in steel fibers. Bacteria-enriched SFRSCC mixes with lower steel fiber content are suitable to be used as self-compacting concrete.

Compressive strength

Compressive strength testing was conducted on SFRSCC, and the obtained results are shown in Table 15. Graphical representation of compressive strength is shown in Figure 6.

Table 15. Compressive strength of bacteria-enriched SFRSCC

Sl. No.	Mix	28-days compressive strength (N/mm ²)
1	MSCC-5 C ₁	50,80
2	MSCC-5 C ₂	56,12
3	MSCC-5 C ₃	52,76

Source: Authors

Due to its metabolic activity, *Bacillus subtilis* converts calcium lactate into calcium carbonates. The fine calcite also fills up the pores and densifies the SFRSCC, which in turn increases the compressive strength. The results of the compressive strength and workability tests show that MSCC-5 C₂ becomes progressively better in comparison with different blends with various rates of steel fiber expansion. This improvement is a direct result of the nearness of calcite creating microbes in the blend. This calcium carbonate constantly produced by the microbes and calcium lactate as an organic nutrient makes the interior structure of solid progressively conservative, which brings about an improvement in compressive strength.

From the results, it can be noted that the compressive strength values declined beyond MSCC-5 C₂ (1% of steel fiber), and that a further increase in steel content reduces the compressive strength. Steel fiber overcomes any barrier between adjoining surfaces of existing microcracks, thus causing imprisonment in the network. This builds up the break shutting powers, which invigorates an expansion of the compressive strength. The presence of pozzolanic material also results in a significant improvement for SFRSCC. There is a decrease in the strength of SCC made with 1,5% steel fiber (MSCC-5 C₃), which is due to the increase in the entrapped air in the concrete, which decreases the compressive strength. An increase in the steel fiber volume increases the porosity, as the distribution is not uniform and the matrix contains regions of only fiber.

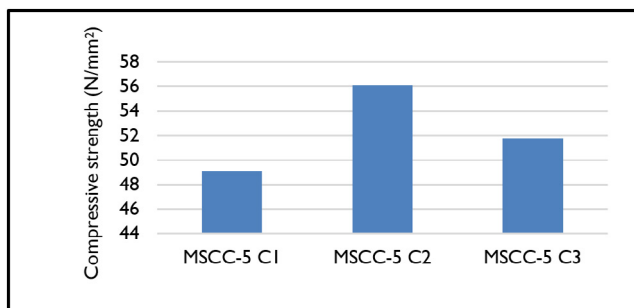


Figure 6. Compressive strength of bacteria-enriched SFRSCC

Source: Authors

Split tensile strength

The tensile strength is one of the basic and most important properties to be improved in concrete. Table 16 shows the results of split tensile strength testing.

Table 16. Split tensile strength of Bacteria enriched SFRSCC

Sl. No.	Mix	28-days split tensile strength (N/mm ²)
1.	MSCC-5 C ₁	4,92
2.	MSCC-5 C ₂	5,66
3.	MSCC-5 C ₃	6,24

Source: Authors

The addition of steel fiber resulted in an increase in split tensile strength. Because of the bridging action of steel fibers, the increase in the fiber content in the reinforced SCC mixtures showed improved results.

The spanning activity of reused steel fiber captured the split from further opening, and numerous breaks were thus shaped in the samples. Prior research likewise reported an increased rigidity in fortified SCC brought about by steel fibers.

Flexural strength

Two-points flexural strength testing of the self-compacting concrete mixes was conducted at 28 days. The reinforced

beams containing steel fiber were coated with a whitewash to facilitate the identification of cracks during loading. During testing, the load at which the first crack visible was noted. The flexural strength test was carried out in accordance with IS 516:1959 (Reaffirmed 2004) (Bureau of Indian Standards, 2004) on concrete beams 700 mm long and with a 150 x 150 mm cross-section. The results are shown in Table 17.

Table 17. Ultimate flexural strength of bacteria-enriched SFRSCC

Sl. No.	Mix	First crack load (kN)	Ultimate load (kN)	Ultimate flexural strength (N/mm ²)
1.	MSCC-5 C ₁	62	110	22,81
2.	MSCC-5 C ₂	85	135	28,00
3.	MSCC-5 C ₃	90	142	29,45

Source: Authors

As seen in Table 17, bacteria-enriched SFRSCC shows an enhanced flexural strength with an increased percentage of steel fiber volume by total volume. However, increasing the fiber content decreases the flexural stiffness, while the ultimate load carrying capacity and its corresponding deflection increases. The maximum flexural strength was 29,45 N/mm² (142 kN) for 1,5% of steel fiber (MSCC-5 C₃), which represents a 40% increase compared to the MSCC-5 B₁ mix. By comparing the results with bacteria-enriched SCC (MSCC-5 B₁), it is seen that the improvement in flexural behavior is due to the presence to steel fiber.

The flexural strength of concrete depends on the steel fiber volume and the aspect ratio of the fiber. With the increase in aspect ratio and volume of steel fiber, the flexural strength was improved. The bond between fiber and concrete, obtained by using hooked-end steel fibers, increased the flexural strength. The random distribution of steel fiber into self-compacting concrete, which controls the cracks and bridges them, resulted in an increased load carrying capacity for the beam. However, on considering the results of bacteria-enriched SFRSCC specimens in fresh and hardened state, MSCC-5 C₂ shows good workability and higher compressive strength than other mixes. MSCC-5 C₂ showed a 19% increase in compressive strength than MSCC-5 and a 15% increase compared to MSCC-5 B₁.

Visual inspection and discussion

By closely observing the beams after 28 days, the fact that the cracks were measured at less than 0,5 mm in width shows proper sealing of the cracks. Beyond 0,5 mm, the healing of concrete was rarer, even though white precipitates were seen on the inner surfaces. The majority of cracks between 0,1 and 0,2 mm wide were sealed off with calcium precipitate. The beams can take up more loads without forming many cracks because of the steel fiber content. A 10% increase over the first cracks showed more crack width, which were therefore not easy to heal. The first crack load and its 10% increment showed less crack width, thus facilitating healing (Figure 7).



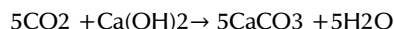
Figure 7. Healed bacteria-enriched SFRSCC

Source: Authors

Next, the structure of calcium carbonate-based minerals after the bacterial metabolic transformation of calcium lactate is presented, as indicated by the accompanying response:



The yield of calcium carbonate-based minerals increases when CO_2 molecules react with portlandite ($\text{Ca}(\text{OH})_2$) minerals, which are quantitatively huge hydration aftereffects of solid particles:



The last response is homologous to carbonation, a moderate procedure that normally happens in concrete because of the internal dissemination of environmental carbon dioxide, whose rate is considerably increased by the metabolic transformation of calcium lactate. Microscopic organisms in addition to calcium lactate intervene in the creation of plentiful measures of 20-80 μm -sized mineral-like accelerates on break surfaces of young, 7-days cured concrete stone specimens (Henk *et al.*, 2010).

Ultrasonic pulse velocity

An ultrasonic pulse velocity (UPV) test was conducted on the beams containing 0,5, 1 and 1,5% of steel fibers before and after being loaded for cracking, as well as after 56 days. The results gave an idea of the porosity of the concrete specimens. Cracked concrete specimens showed that waves took longer to travel than in the same concrete specimens before cracking. It was seen that, with the irregular distribution of steel fibers, the velocity of the SCC blends diminished due to more voids in the blends with steel strands than in the control blend. This reduction may be due to the fact that the steel fibers are arranged arbitrarily, and, when the waves go through the fibers, they do not travel in a straight line forward to the opposite end. The concrete specimen after 28 days showed less time for the passage of waves in comparison with the cracked beam before 56 days. ASTM C597-16 (ASTM International, 2016a) and IS 13311(part 1)-1992 (Bureau of Indian Standards, 1992) categorize the results as excellent, good, doubtful, poor, and very poor for >4,5, 3,5-4,5, 3-3,5, 2-3, and <2 km/s,

respectively. All the specimens under study fell under the good and excellent categories.

The UPV test results suggest that, at the age of 28 days, the bacteria-enriched SFRSCC shows traces of healing. Nevertheless, the uncracked areas in concrete were found to be much stronger than cracked parts. Even the white deposits in the cracks can be seen, as shown in Figure 5, and cracks below 0,5 mm wide are being sealed. Thus, the steel fibers take up more load and delay the formation, propagation, and width of cracks, which implies good conditions for bacteria-based healing.

SEM and EDS

Scanning electron microscopy (SEM) was used to recognize the morphology of the materials inside the breaks. Figure 8 shows the SEM analysis of a bacteria-enriched concrete specimen.

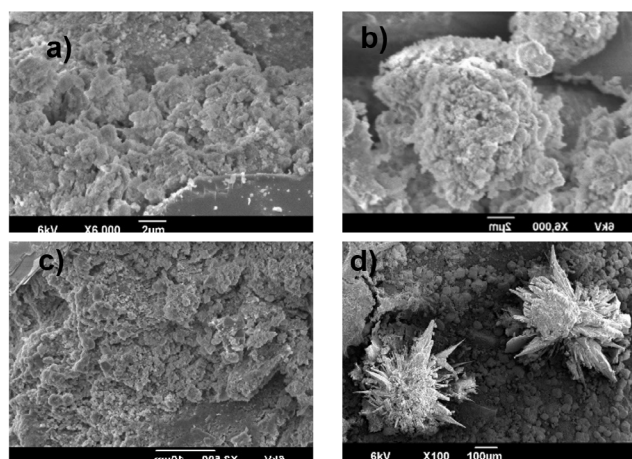


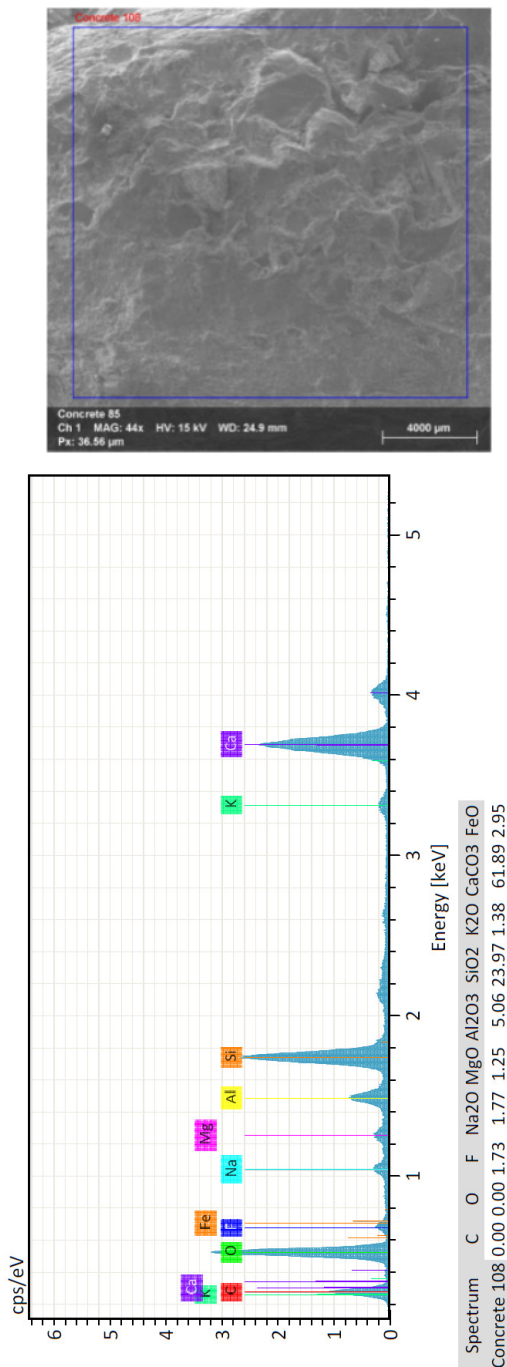
Figure 8. SEM images of a bacteria-enriched SFRSCC specimen

Source: Authors

These tests are generally conducted at a micro-scale in order to identify and characterize the materials deposited within the concrete cracks after self-healing. SEM analysis is carried out as per the guidelines of ASTM C1723-16 (ASTM International, 2016b) for examination of hardened concrete using SEM. This maximizes the reliability of the results obtained. The SEM shows the magnified image of calcite precipitation in concrete. The white color seen in Figures 8a and b is due to the lighting effect, which causes charging current. Those Figures are the magnified images of the powdered specimen. Figures 8c and d show the calcite precipitation in a solid specimen less than $1 \times 1 \times 0,5$ cm in size.

EDS is directly related to SEM; it shows the elements and chemicals present in the sample. The EDS was studied as per the guidelines of ASTM E1508-12a (ASTM International, 2019). The SEM images shown in Figure 9 correspond to the area of the specimen where the EDS was studied. The EDS test was conducted to determine the presence of calcite and silicate in the solid specimen. The EDS results shown in Table 8 show the elemental presence of silicon and calcium.

The presence of silicon indicates that the specimen contains silicate (SiO_2) which proves the presence of micro-silica and cement. The presence of calcium is an indication of calcite compounds. The quantification of chemical compounds in the sample using EDS showed that the presence of calcite is about 61,89%. The silicate compound contained in the specimen was about 23,97%. Hence, on combining the SEM and EDS results, the presence of calcite is confirmed, so bacteria-based healing in self-compacting concrete is practical and effective.



N/mm². When the fiber content increases beyond 1%, it has more and more entrapped air. In other words, the porosity increases, which, in turn, affects the strength.

- The flexural strength increases with the increase of steel fiber content. A maximum value of 29,45 N/mm² was recorded for 1,5% of steel fiber content, which is 40% more than MSCC-5 B₁. Flexural strength depends on the fiber content and the aspect ratio of the fiber. The increase is due to the bonding between aggregate-paste and fiber-matrix. Micro-silica enhances the interface of aggregate-paste.
- The UPV results show an increase in the time value for the cracked SFRSCC, which is due to the increase in the gap and the reflection effect by steel fiber. The UPV results after water curing the cracked specimens suggest that the crack is healed upon aging.
- Visual examination showed white deposits over cracks even at the age of 28 days (calcite crystals are white-colored). After 56 days, the specimens loaded with an initial crack load and 10 and 20% increments showed evidence of crack healing. Cracks less than 1 mm wide are effectively healed.
- As bacteria-based healing is more effective up to 0,5 mm. The bacteria enriched SCC shows wider cracks, which delays the healing process, whereas bacteria-containing SFRSCC has less crack width because of the bridging action of steel fiber. The first cracks and those due to the 10% load increment are effectively healed. As the first crack load of bacteria-enriched SFRSCC is far more than that of bacteria-enriched SCC, the former is better in terms of durability and ductile property.
- SEM images showed the presence of calcite crystals in the specimens. Similar images are seen in the literature. The presence of calcite compounds was confirmed by the EDS test results, which showed calcium and silicon ions.
- Bacteria-enriched SFRSCC is more efficient than normal self-compacting and self-healing concrete, as steel fiber helps in taking up more load without much cracking, thus favoring an effective environment for bacteria-based healing.

Bacteria-enriched SCC and steel fiber reinforced SCC are practical in its concepts, with good strength and workability compared to normal SCC. Bacteria-enriched SFRSCC has better strength and healing characteristics than bacteria enriched SCC.

References

- ASTM International (2016). *C597-16: Standard test method for pulse velocity through concrete*. ASTM International.
- ASTM International (2016b). *C1723-16: Standard guide for examination of hardened concrete using scanning electron microscopy*. ASTM International.
- ASTM International (2017). *C1621/C1621M-17: Standard test method for passing ability of self-consolidating concrete by J-ring*. ASTM International.
- ASTM International (2019). *E1508-12a: Standard guide for quantitative analysis by energy-dispersive spectroscopy*. ASTM International.
- BSI Standards (2010). *BS EN 12350:2010: Testing fresh concrete Self-compacting concrete. L box test*. BSI.
- Bureau of Indian Standards (1992). *IS 13311-1: Method of non-destructive testing of concrete, Part 1: Ultrasonic pulse velocity [CED 2: Cement and Concrete]*. Bureau of Indian Standards.
- Bureau of Indian Standards (2004). *IS 516(1959): Method of tests for strength of concrete (reaffirmed 2004)*. Bureau of Indian Standards.
- EFNARC (2002). *Specification and guidelines for self-compacting concrete*. <https://www.feb.unesp.br/pbastos/c.especiais/Efnarc.pdf>
- Falguni, S. and Darshika, P. (2016). An attempt to enhance the properties of concrete using bacteria. *Global Research and Development Journal for Engineering*, 2, 41-46. https://www.grdjournal.com/article?paper_id=GRDCF001009
- Ghosh, P., Mandal, S., Chattopadhyay, B., and Pal, S. (2010). Use of microorganism to improve the strength of cement mortar. *Cement and Concrete Research*, 35(10), 1980-1983. <https://doi.org/10.1016/j.cemconres.2005.03.005>
- Henk M. J., Thijssen, A., Muyzer, G., Copuroglu, O., and Schlangen, E. (2010). Application of bacteria as self-healing agent for the development of sustainable concrete. *Ecological Engineering*, 36(2), 230-235. <https://doi.org/10.1016/j.ecoleng.2008.12.036>
- Jeevetha, T., Krishnamoorthi, S., and Rampradheep, G. S. (2014). Study on the properties of Self-compacting concrete with Micro silica. *The International Journal of Innovative Research in Science, Engineering and Technology*, 3(4), 11239-11244. <http://citeseerx.ist.psu.edu/viewdoc/download?doi=10.1.1.1043.2498&rep=rep1&type=pdf>
- Jonkers, H. M., Thijssen, A., Muyzer, G., Copuroglu, O., and Schlangen, E. (2010). Application of bacteria as self-healing agent for the development of sustainable concrete. *Ecological Engineering*, 36(2), 230-235. <https://doi.org/10.1016/j.ecoleng.2008.12.036>
- Köksal, F., Altun, F., Yiğit, I., and Şahin, Y. (2008). Combined effect of silica fume and steel fibre on the mechanical properties of high strength concrete. *Construction and Building Materials*, 22(8), 1874-1880. <https://doi.org/10.1016/j.conbuildmat.2007.04.017>
- Naveen, B. and Sivakamasundari, S. (2016). *Study of strength parameters of bacterial concrete with controlled concrete and structural elements made with concrete enriched with bacteria* [Conference presentation]. International conference on engineering innovations and solutions CMS College of Engineering, Tamil Nadu, India.
- Ning, X., Ding, Y., Zhang, F., and Zhang, Y. (2015). Experimental study and prediction model for flexural behaviour of rein-

- forced SCC beam containing steel fibers. *Construction and Building Materials*, 93, 644-653. <https://doi.org/10.1016/j.conbuildmat.2015.06.024>
- Nuruddin, M. F., Chang K. Y, and Azmeen, N., M.(2014) Workability and compressive strength of ductile self-compacting concrete (DSCC) with various cement replacement materials. *Construction and Building Materials*, 55, 153-157. <https://doi.org/10.1016/j.conbuildmat.2013.12.094>
- Okamura, H., and Ouchi, M. (2003). Self compacting concrete. *Journal of Advanced Concrete Technology*, 1(1), 5-15. <https://doi.org/10.3151/jact.1.5>
- Siddique, R., Kaur, K., and Kunal (2016). Strength and permeation properties of self-compacting concrete containing fly ash and hooked steel fibres. *Construction and Building Materials*, 103, 15-22. <https://doi.org/10.1016/j.conbuildmat.2015.11.044>
- Sivakumar, A. and Santhanam, M. (2007). Mechanical properties of high strength concrete reinforced with metallic and non-metallic fibres. *Cement and Concrete Composites*, 29(8), 603-608. <https://doi.org/10.1016/j.cemconcomp.2007.03.006>
- Tomaz, P. J. (2013). Properties of SFRSCC for optimal rheological and mechanical properties in precast beams. *Procedia Engineering*, 65, 290-295. <https://doi.org/10.1016/j.proeng.2013.09.045>
- Wasim, K., and Ehsan, M. B. (2016). Crack healing in concrete using various bio influenced self-healing techniques. *Construction and Building Materials*, 102(Part 1), 349-357. <https://doi.org/10.1016/j.conbuildmat.2015.11.006>
- Tasdemir, M. A. and Bayramov, F. (2002). Mechanical behaviour of cement based composite materials. *ITU Journal, d/Engineering*, 1(2),125-144.

Low-Timing-Jitter and Low-Phase-Noise Microwave Signal Generation Using a VCSEL-Based Optoelectronic Oscillator

Generación de señales microondas de bajo ruido y fluctuación de fase utilizando un oscilador

Christian Daniel Muñoz¹, Juan Coronel², Margarita Varón³, Fabien Destic⁴, and Angélique Rissons⁵

ABSTRACT

This article presents the first results of the timing-jitter characterization of a VCSEL-based optoelectronic oscillator (VBO) at 2,5 GHz. For all implementations, vertical-cavity surface-emitting lasers (VCSEL) emitting in the O and C-bands were characterized. The resonant cavity was modified through the optical delay line length to verify its impact on timing-jitter and phase noise of the VBO. The lowest peak-to-peak jitter value obtained experimentally was 71 mUI when the optical fiber length was 1 km, whereas the lowest phase noise was -124 dBc/Hz with 5 km. This phase noise value, measured at 10 kHz offset, represents an 8 dB improvement compared to previous results, and it is the lowest value reported in the literature for the VBO architecture at 2,5 GHz.

Keywords: jitter, optoelectronic oscillator, phase noise, VCSEL, optical fiber

RESUMEN

Este artículo presenta los primeros resultados de la caracterización de la fluctuación de fase (*jitter*) de un oscilador optoelectrónico basado en VCSEL (VBO) a 2,5 GHz. Para todas las implementaciones, se caracterizaron láseres de emisión superficial con cavidad vertical (VCSEL) que emiten en las bandas O y C. La cavidad resonante se modificó a través de la longitud de la línea de retardo óptico para verificar su impacto en la fluctuación temporal y el ruido de fase del VBO. El valor de *jitter* pico a pico más bajo obtenido experimentalmente fue 71 mUI cuando la longitud de la fibra óptica era de 1 km, mientras que el ruido de fase más bajo fue -124 dBc/Hz con 5 km. Este valor de ruido de fase, medido a 10 kHz de la portadora principal, representa un mejoramiento de 8 dB con respecto a resultados previos y es el valor más bajo registrado en la literatura para la arquitectura VBO a 2,5 GHz.

Palabras clave: fluctuación de fase, oscilador optoelectrónico, ruido de fase, VCSEL, fibra óptica

Received: May 11th, 2020

Accepted: August 5th, 2021

Introduction

Nowadays, a wide range of applications, such as instrumentation (Wang *et al.*, 2020, Feng *et al.*, 2021), physical variable measurement (Zou *et al.*, 2016), and data transmission (Chi *et al.*, 2016), integrate electrical signals in the microwave and mm-wave range into their systems. Electronic oscillators have traditionally been used in telecommunications as high-frequency signal sources. However, the development of new and well-performing microwave signal generators is being boosted as a result of the emergence and evolution of some systems, e.g., radars and software-defined radio, as well as the use of higher frequencies in 5G (Ghosh *et al.*, 2019) and 6G cellular networks (Rappaport, Xing, Kanhere, Ju, Madanayake, Mandal, Alkhateeb and Trichopoulos, 2019). The systems based on optoelectronic components are a powerful alternative for microwave signal generation due to the high spectral purity that they can achieve (Sung *et al.*, 2007).

The optoelectronic oscillator (OEO) was developed in 1996 by Yao and Maleki (Yao and Maleki, 1996), and it is one

¹ Electronic Engineer, M.Sc. in Telecommunications Engineering, Universidad Nacional de Colombia, Colombia. Affiliation: Ph.D. candidate in Photonics and Optoelectronic Systems, ISAE-SUPAERO, Université de Toulouse, France. E-mail: 2cd.munoz@isae-supaero.fr

² Electronic Engineer, M.Sc. in Electrical Engineering, Universidad Nacional de Colombia, Colombia. Ph.D. Photonics and Optoelectronic Systems, ISAE-SUPAERO, France. Affiliation: Lead Laser Optics Researcher, Technology Innovation Institute, United Arab Emirates. E-mail: juan.coronel@tii.ae

³ Electronic Engineer, Pontificia Universidad Javeriana, Colombia. M.Sc. in Optical Communications and Photonic Technologies, Politecnico di Torino, Italy. Ph.D. in Optoelectronics and Microwave, ISAE-SUPAERO, France. Affiliation: Full-Professor, Universidad Nacional de Colombia, Colombia. E-mail: gmvarond@unal.edu.co

⁴ M.Sc. in Microwave and Optoelectronics, Université Paul Sabatier, France. Ph.D. Photonics and Optoelectronic Systems, ISAE-SUPAERO, France. Affiliation: Research Engineer, ISAE-SUPAERO, Université de Toulouse, France E-mail: f.destic@isae-supaero.fr

⁵ Degree in Physics-Chemistry, Université de Reims, France. M.Sc. and Ph.D. in Optoelectronics and Microwave, ISAE-SUPAERO, France. Affiliation: Full-Professor, ISAE-SUPAERO, Université de Toulouse, France. E-mail: a.rissons@isae-supaero.fr

How to cite: Muñoz, C. D., Coronel, J., Varón, M., Destic, F., and Rissons, A. (2022). Low-timing-jitter and Low-Phase-Noise Microwave Signal Generation Using a VCSEL-Based Optoelectronic Oscillator. *Ingeniería e Investigación*, 42(2), e87189. <http://doi.org/10.15446/ing.investig.v42n2.87189>



Attribution 4.0 International (CC BY 4.0) Share - Adapt

of the most sophisticated mechanisms for the generation of spectrally pure microwave signals (low phase noise). One of the main advantages of the OEO architecture is its high configuration flexibility, *i.e.*, it can be implemented in a wide variety of versions with different optical and electrical components in order to optimize its performance. In this topology, the cavity is an optical fiber delay line, and its length is related to the phase noise and the space between different non-oscillating modes. By increasing the optical fiber length, the phase noise decreases, but, at the same time, the mode spacing decreases. Multi-loop oscillators include several parallel delay lines into the cavity to guarantee an acceptable phase noise and a large mode spacing (Chen *et al.*, 2015).

In the OEO architecture proposed by Yao and Maleki (1996), the laser source is externally modulated through an intensity modulator driven by the generated microwave signal. The VCSEL-based optoelectronic oscillator (VBO) was introduced in 2006 (Varón *et al.*, 2006), and its architecture includes a directly modulated VCSEL. This type of laser, known for its low power consumption and low cost, is suitable for embedded aerospace applications (Rissons *et al.*, 2012). In addition to the advantages of VCSEL lasers, the implementation of VBOs is less expensive, smaller, and requires a smaller operating current than other implementations. The VCSEL bandwidth determines the highest oscillating frequency, and some authors have achieved frequencies up to 10 GHz with phase noises of -80 dBc/Hz (Hasegawa *et al.*, 2007) and -70 dBc/Hz (Koizumi *et al.*, 2010) at 10 kHz from the carrier.

The frequency stability of a clock or a microwave signal can be estimated through single-sideband (SSB) phase noise and jitter measurements (IEEE, 2021). On the one hand, phase noise is a frequency domain measurement of phase deviations that allows identifying some of the noise sources within the system (Rubiola, 2008). On the other hand, jitter is the time deviation of an event (usually the rise or fall event in digital systems and clocks) from an ideal reference time frame or sampling point (Da Dalt and Sheikholeslami, 2018). In digital transmission systems, increasing transfer rates are limited by mistiming in regeneration processes (Ryu *et al.*, 2020). For this reason, ultra-low jitter clocks must be implemented to meet the tolerance ranges of transmitting and receiving equipment (Choi *et al.*, 2019).

Some transmission systems such as optical transport networks (OTN) and Gigabit Ethernet networks include precise specifications regarding jitter tolerance and frequency accuracy (ITU, 2018). In this way, the application of an optoelectronic oscillator in a digital data transmission system can be established through jitter and phase noise measurements. As a contribution to this field, we present the first timing-jitter analysis for a VCSEL-based optoelectronic oscillator. The VBO implementation of this work uses the latest generation of VCSELs in the O and C-bands with reduced relative intensity noise (RIN) in comparison to VCSELs used in previous publications (Varón *et al.*, 2006; Rissons *et al.*, 2012; Koizumi *et al.*, 2009).

This paper is structured as follows: the first section comprises a detailed VCSEL description and an experimental laser characterization for both VCSELs used; then, the VBO architecture is described, and a phase noise predictive model is presented; the VBO implementation, in terms of phase noise and timing-jitter, is addressed in a third section; some performance comparisons between our systems and previous VBO implementations available in the literature are detailed in the fourth section; and, finally, the last section presents some conclusions about our work.

Vertical-cavity surface-emitting lasers -VCSEL

The vertical-cavity surface-emitting lasers are semiconductor lasers widely used in telecommunications at high transfer rates through different modulation formats, such as direct modulation (Malacarne *et al.*, 2017), discrete multitone modulation (DMT) (Wagner *et al.*, 2017) and four-level pulse amplitude modulation (PAM-4) (Lavernick *et al.*, 2017). While multimode VCSELs at short-wavelengths (850 - 1 050 nm) are employed in short-reach fiber links (Pavan, Lavrencik and Ralph, 2017) and visible light transmissions (Li-Fi) at 680 nm (Lu *et al.*, 2017), long-wavelength VCSELs (LW-VCSEL) in the 1,2 -1,6 μm range, are used in long-haul communications (Bacou *et al.*, 2010).

The development of LW-VCSELs has evolved in recent years according to their requirements and applications. Wafer-fused LW-VCSEL technology is the most applied for VCSEL manufacturing, covering the entire ITU-T single-mode spectral range (1 260 nm - 1 675 nm). The main drawback of this technology is the integration of the active region (which requires high optical gain) with the mirrors (high-reflectivity, low optical absorption, and high thermal conductivity) in a monolithic semiconductor (Belkin *et al.*, 2015).

VCSEL manufacturing has three particularities. First, the active cavity is grown on an InP substrate and incorporates InAlGaAs quantum wells (QW) covering both bands (Syrbu *et al.*, 2005). Secondly, the top and bottom AlGaAs/GaAs distributed Bragg reflectors (DBRs) are bonded to the active cavity using localized wafer fusion (Iakovlev *et al.*, 2005). This approach avoids VCSEL overheating problems. Finally, tunnel junctions (TJ) are grown to reduce free carrier absorption and mirror optical loss, as well as to ensure a single-mode transverse emission (Belkin *et al.*, 2015).

The O and C-band VCSELs used for this work were produced by the Korean manufacturer RayCan, and their structure is depicted in Figure 1. All layers were epitaxially grown by metal-organic chemical vapor deposition (MOCVD) on InP substrate (Park *et al.*, 2006). Each laser was placed inside a TO-56 package, and its output beam was coupled to a single-mode optical fiber.

The optical power versus bias current for both VCSELs is presented in Figure 2. The maximum emission powers of O and C-band VCSELs are 0,97 mW and 0,89 mW when the

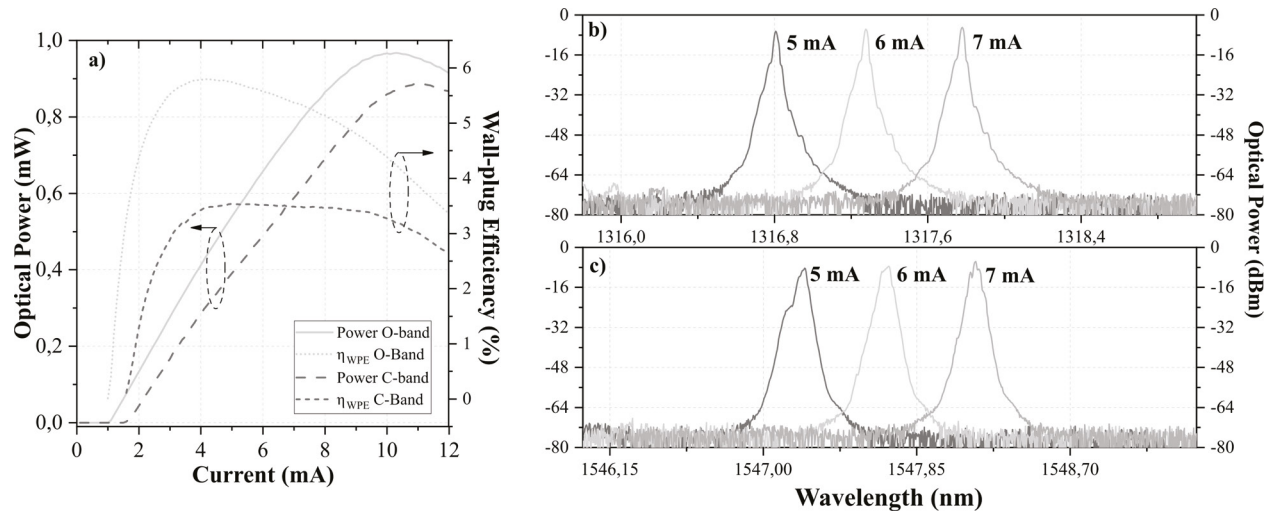


Figure 2. a) Bias current vs. output power and wall-plug efficiency (optical spectra at 5, 6 and 7; mA b) O-band c) C-band VCSEL)
Source: Authors

bias currents are 10,3 mA and 11,1 mA, respectively. The reduced threshold currents are close to each other (1 mA for O-band and 1,5 mA for C-band) and represent 10% of the current for a distributed feedback laser (DFB).

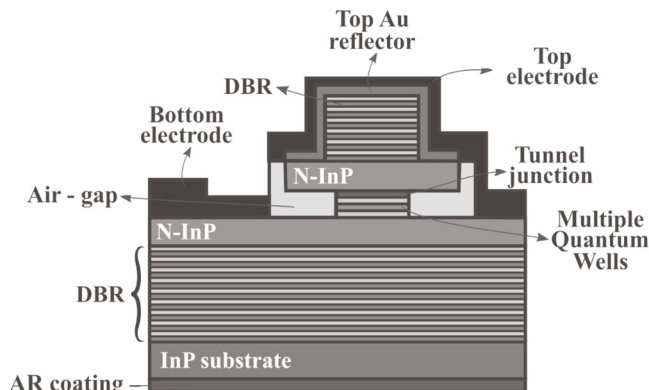


Figure 1. Cross-sectional VCSEL structure
Source: Adapted from (Park et al., 2006)

The selected bias current for the VBO implementations was 6 mA, given the linearity in this region, the constant wall-plug efficiency (WPE) after 4 mA, and the linear behavior of the dynamic resistance. Figure 2 shows the single-mode operation of VCSELs at different bias current and wavelengths around 1,31 μm and 1,54 μm .

Another relevant parameter for the VBO implementation is the relative intensity noise (RIN) due to its influence on the oscillator phase noise. RIN is expressed in dB/Hz and relates the photon density fluctuation to the mean photon square density. RIN measurements at 25 °C for both VCSELs are shown in Figure 3. Regardless of the optical band, the RIN decreases when the bias current increases, since the stimulated emission is higher than the spontaneous one when the bias current moves away from the threshold current. Under the same conditions, and considering the RIN

values at 2,5 GHz, the RIN is slightly lower in the O-band VCSEL for all bias currents. The RIN values for 5, 6 and 7 mA are -141, -144 and -146,5 dB/Hz, respectively, whereas, for the C-band VCSEL, they are -138, -142 and -143 dB/Hz. Considering the experimental results and the measurement uncertainty, both lasers impact the phase noise in the same proportion.

VCSEL-based optoelectronic oscillator

The VCSEL-based optoelectronic oscillator (VBO), which is illustrated in Figure 4, is a self-seeding ring oscillator composed of a directly modulated VCSEL that passes through a low-loss glass fiber, which acts as an optical delay line. Owing to the lower attenuation, long cavity length and a high-quality factor Q are possible, thus allowing low phase noise. Then, the optical signal is converted to the electrical domain by a photodetector. The electrical signal is amplified by a microwave amplifier to compensate loop losses and then filtered by a band-pass filter to select the oscillation frequency and remove the spur modes. Finally, the loop is closed using an electrical coupler, which allows extracting the generated microwave signal (Hayat et al., 2008).

The selectivity of the oscillation mode will depend on the resonant element through the optical delay τ_d produced by the optical fiber. The quality factor for the VBO is directly proportional to the optical fiber length, and it is expressed as follows:

$$Q = 2\pi f \tau_d \quad (1)$$

The oscillation mode is selected from the optical fiber frequency comb by the microwave band-pass filter. The mode spacing in the optical fiber is defined as the free spectral range (FSR), which is expressed as:

$$FSR = \frac{c}{n_f L} \quad (2)$$

where, c is the speed of light, n_f is the refractive index of the optical fiber core, and L is the optical fiber length. The longer the optical fiber, the closer the optical fiber oscillation modes. The selected mode lies inside the microwave filter band-pass bandwidth.

VBO phase noise is related to the phase fluctuation propagation of optical and electrical components inside the loop. By using Rubiola's linear feedback approach for delay-line oscillators (2008), the power spectral density (PSD) of phase fluctuations $S_\phi(s)$ can be expressed as follows:

$$S_\phi(j\omega) = \left| \frac{1}{1+B(j\omega)} \right|^2 (S_\psi(j\omega) + S_{\text{amplifier}}(j\omega)) \quad (3)$$

where $B(j\omega)$ is the transfer function of the resonator and the delay line, $S_\psi(j\omega)$ is the noise power spectral density due to components, and $S_{\text{amplifier}}(j\omega)$ the microwave amplifier noise. The main noise contributions from the components are the phase variation in the optical fiber, the thermal and shot noise, and the relative intensity noise of VCSELs. By definition, phase noise is the half of the one-sided PSD of phase fluctuations (IEEE, 2009); thus, the VBO phase noise $L(f)$ can be expressed as follows:

$$L(f) = \left(\left| \frac{1}{1+B(j\omega)} \right|^2 (S_\psi(j\omega) + S_{\text{amplifier}}(j\omega)) \right) / 2 \quad (4)$$

Another useful metric to verify frequency stability is timing-jitter, which corresponds to the short-term temporal variations of a signal relative to an ideal signal (International Telecommunication Union (ITU), 1996). Although phase noise is a frequency domain measurement and jitter is a time-domain measurement, both are related through Equation (5) (Da Dalt and Sheikholeslami, 2018):

$$\sigma_{RMS} = \frac{1}{2\pi f_c} \sqrt{2 \int_{f_{\min}}^{f_{\max}} L(f) df} \quad (5)$$

where σ_{RMS} corresponds to the root mean squared (RMS) jitter, f_c is the oscillation frequency, and f_{\min} and f_{\max} are the lower and upper frequency of the phase noise measurement, respectively. Jitter measurements can be composed of two individual contributions: random and deterministic jitter. On the one hand, random jitter (RJ) is caused by uncorrelated noise, e.g., thermal noise. Moreover, it generally follows a normal or Gaussian distribution. On the other hand, deterministic jitter (DJ) comes from systematic effects (intersymbol interference (ISI) and periodic jitter), and it can be predicted and reduced.

2,5-GHz VCSEL-based optoelectronic oscillator characterization

Setup description

Several VBOs at 2,5 GHz using 1,31 μm and 1,54 μm VCSELs were implemented and characterized through phase noise and jitter measurements. As stated before, the goal of using a direct modulated VCSEL is to develop a high spectral purity oscillator with low power consumption. For this oscillator, a cavity band-pass filter centered at 2,5 GHz, 3 MHz bandwidth at 3 dB, and insertion losses lower than 3 dB is used. A 39 dB gain low noise microwave amplifier is used to amplify the selected mode. The amplifier output is connected to a tunable attenuator in order to control the closed-loop gain, and the output is then connected to a bias tee to modulate the optical source.

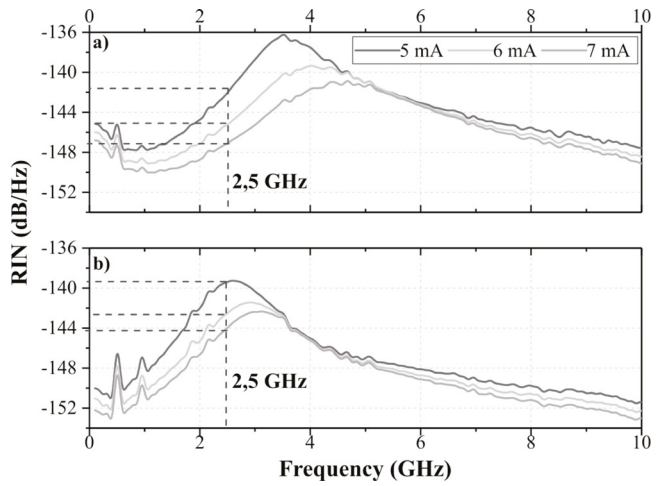


Figure 3. RIN measurements at 25 °C: a) O-band, b) C-band VCSEL
Source: Authors

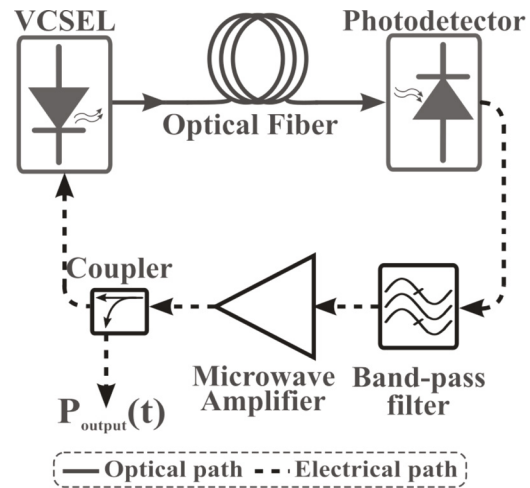


Figure 4. VCSEL based optoelectronic oscillator setup
Source: Adapted from (Hayat et al., 2008)

The optical fiber length is varied from 1 to 5 km in order to evaluate its effects on spectral purity and jitter variations. The measured and calculated FSR for each length are presented in

Table 1. Although a higher Q factor guarantees lower phase noise values, the reduced FSR can directly impact some sensitive parameters for telecommunications applications, such as jitter and residual phase modulation (PM), through the contribution of each non-oscillating mode.

Electrical output spectrum

Figure 5 shows the electrical spectrum taken from a 20-dB coupler output for 1 km. The measured FSR is 190 kHz, and the difference with the theoretical value corresponds to the fiber length uncertainty and the delay contribution of the electronic components. The oscillation power is -10 dBm, and the side mode suppression ratio (SMSR) to the first non-oscillating mode is 59 dB. The oscillation power can be improved by using an electrical coupler with a less attenuated output.

Table 1. Measured and calculated FSR values for several fiber lengths

Fiber length (km)	Calculated FSR (kHz)	Measured FSR (kHz)
1	204	190
2	102	98
3	68	65
5	41	40

Source: Authors

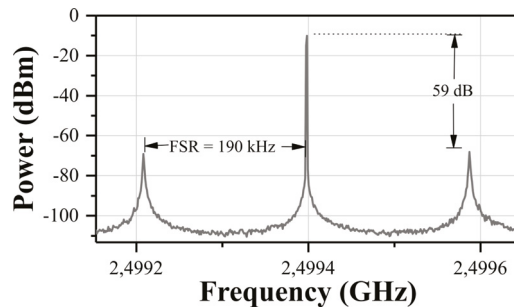


Figure 5. 2,5 GHz VCSEL-based optoelectronic oscillator output spectrum

Source: Authors

Phase noise characterization

The phase noise measurements for each VBO configuration are taken using a direct measurement method through an electrical spectrum analyzer ESA (R&S FSW50). For measurement validation purposes, a calibrated phase noise signal is implemented through frequency modulation (FM) of an ultra-low phase noise source (at 2,5GHz) with uniform noise (Gheen, 2012). According to the difference between the technical specifications of the ultra-low phase noise source and the phase noise measurements, the lowest of the latter, using direct method, is limited to -130 dBc/Hz at 10 kHz from the carrier.

Figure 6 shows the phase noise curves of the implemented VBOs using O and C-band VCSELs. In both cases, the phase noise is improved when the optical fiber delay line is enlarged, i.e., when the quality factor of the resonator is increased.

Additionally, the phase noise level difference between the optical bands is given by the zero chromatic dispersion of the standard single-mode optical fiber employed at 1,3 μ m. In this sense, the lowest phase noise values are achieved when a O-band VCSEL is used.

Regardless the optical fiber length, two noise processes are identified in the phase noise curves. The white phase noise process is located far from the carrier (from 20 kHz), and it is produced mainly by the white noise of the microwave amplifier. On the other hand, the white frequency noise process varies at a -20 dB/decade rate, and it results in the up-conversion process (also called Leeson effect) from the flicker noise of the amplifier inside the loop (Guo *et al.*, 2018). For the O-band VCSEL, white frequency noise is present in the two first decades (from 100 Hz to 10 kHz); for the C-band, the same slope is located only from 2 kHz to 10 kHz. In this decade, the slope becomes -25 dB/decade due to a more significant RIN contribution in this band.

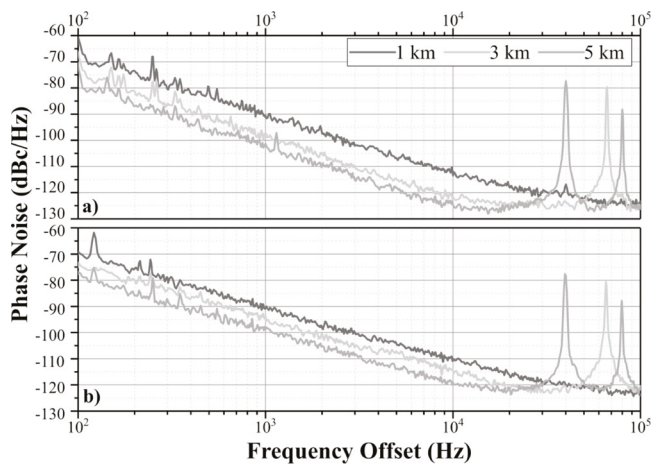


Figure 6. Phase noise curves for: a) O-band VCSEL, b) C-band VCSEL

Source: Authors

Timing-jitter characterization

For the phase noise curves using 3 and 5 km, the sharp peaks are spaced at 65 and 40 kHz, respectively. These values correspond to the FSR values summarized in Table 1. The frequency comb peaks are close to each other and cannot be rejected by the microwave band-pass filter. Consequently, these non-rejected peaks become secondary oscillation modes that can increase the timing-jitter. Figure 7 depicts the histograms (10 000 samples) of the time interval error (TIE) measurement using an O-band VCSEL and different fiber lengths.

In all cases, the histograms show a dominant Gaussian behavior, i.e., the main contribution comes from random jitter. The TIE RMS jitter was determined through the standard deviation of the Gaussian distribution of each histogram. Contrary to what was expected, the TIE RMS jitter increases as the fiber length increases. This phenomenon has two reasons. Firstly, the new non-rejected modes expand the profile of the Gaussian distribution due to additional periodic

jitter. Secondly, the amplifier input power decreases due to the higher optical attenuation, and, consequently, the white noise contribution of the amplifier is stronger. One way to reduce this effect is to use a band-pass filter with narrower bandwidth, therefore reducing the contribution of periodic jitter of each mode. Table 2 summarizes the measured phase noise at 10 kHz offset and the peak-to-peak jitter expressed in unit interval (UI) for each case.

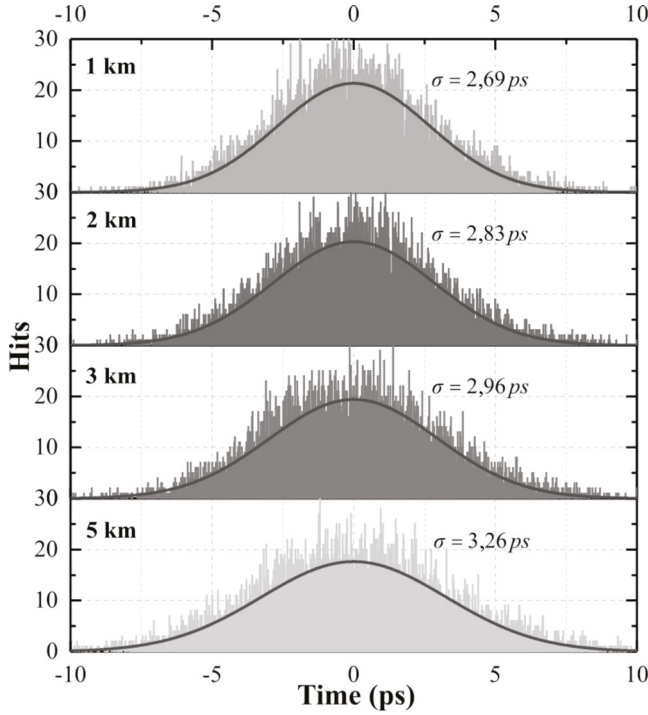


Figure 7. Jitter histograms of VBO using O-band VCSEL
Source: Authors

According to Table 2, and under the same conditions, the lowest phase noises and jitters are obtained using O-band VCSELs. This effect is mainly due to the zero-dispersion of the fiber at wavelengths close to 1,3 μm and the level power inside the loop. For both lasers, the phase noise improves proportionally when the resonator length increases, but, at the same time, the jitter deteriorates. Although the peak-to-peak jitter increases from 71 to 106 mUI, in any case, the values exceed the specifications of local clocks for OTN networks defined by the recommendation ITU-T G.8251 (ITU, 2018).

Table 2. VBO phase noise and peak-to-peak jitter

Fiber length (km)	Phase Noise (dBc/Hz) Oband	PkPk jitter (mUI) Oband	Phase Noise (dBc/Hz) Cband	PkPk jitter (mUI) Cband
1	-113,5	71	-110	88
2	-117	81	-112,8	91
3	-121,7	84	-114,5	95
5	-124,8	95	-119	106

Source: Authors

Phase noise model validation

The linear model of Equation 4 allows estimating the phase noise of the VBO considering different noise sources. The transfer function $B(j\omega)$ is determined using the Laplace transform to the phase impulse response of the optical delay ($B_d(j\omega) = e^{-j\omega\tau_d}$) and the microwave filter ($B_f(j\omega) = 1/(1 + j\omega\tau_f)$), where τ_f is the filter group delay. The noise power spectral density $S_\psi(j\omega)$ referred to the input impedance of the amplifier (Z_A) includes all the additive noise sources inside the loop (VCSEL RIN at the oscillating frequency RIN_{VCSEL} , shot and thermal noise, and the intensity-to-phase noise conversion process due to Rayleigh scattering RIN_{fiber}). $S_\psi(j\omega)$ can be expressed as:

$$S_\psi(j\omega) \left[\left(RIN_{VCSEL} + RIN_{fiber} \right) i_{ph}^2 + 2q i_{ph} + \frac{4k_B T}{R_{ph}} \right] * Z_{ph} \| Z_A \quad (6)$$

where i_{ph} is the photodetected current, k_B is the Boltzman constant, T is the operating temperature, and Z_{ph} is the photodetector impedance. The power spectral density of the microwave amplifier $S_{amplifier}(f)$ involves white noise and flicker noise (Rubiola, 2008). The white noise component is estimated from the equivalent noise spectral density ($N = FkT_0$) and the carrier power P_0 at the amplifier input (Rubiola and Giordano, 2007). In contrast, flicker noise is independent of carrier power at the amplifier input over a wide frequency range. Hence, $S_{amplifier}(f)$ corresponds to:

$$S_{amplifier}(f) = b_0 + \frac{b-1}{f} = \frac{FkT_0}{P_0} + \frac{b-1}{f} \quad (7)$$

where b_{-1} is a constant coefficient of flicker noise, F is the noise figure, and kT_0 is the thermal energy.

Figure 8 presents the estimated phase noise curves using the electrical power P_0 , which was experimentally obtained, and the technical characteristics of loop components summarized in Table 3. Figure 8a presents the estimated phase noise when the fiber length is 1, 2, 3, and 5 km, and the amplifier input power is constant. The phase noise at 10 kHz offset is reduced by 12 dB from -116,8 dBc/Hz to -128 dBc/Hz when the length is 1 km and 5 km, respectively. The estimated phase noise curves when P_0 ranges from -50 dBm to -35 dBm are plotted in Figure 8b. As expected, the input power modified the floor phase noise and the noise level far from the carrier. Therefore, the phase noise at 10 kHz from the carrier is improved by 14 dB (from -117,2 dBc/Hz to -131,5 dBc/Hz). The noise close to the carrier is also reduced, but it is limited by the additive noise sources and the flicker noise coming from the microwave amplifier. The level difference between the estimated and measured phase noise is caused by measurement uncertainty (around 3 dB for the direct method) and because some parameters are assumed from the literature.

The effect of the VCSEL RIN on the phase noise is represented in Figure 8c by assuming three different noise values: -120, -130, and -140 dB/Hz. For values below -130 dB/Hz, the phase noise at 10 kHz from the carrier is slightly enhanced (2 dB better when RIN = -140 dB/Hz). Conversely, when the RIN is -120 dB/Hz, the phase noise deteriorates rapidly by 8 dB from the value obtained for RIN = -130 dB/Hz (-116,64 dBc/Hz).

The RMS jitter can be also estimated by employing Equation 5 and the phase noise curves plotted in Figure 8a. By lengthening the optical fiber from 1 to 5 km, the RMS jitter is reduced from 1,37 ps to 0,33 ps, respectively. The difference between the estimated RMS jitter and the TIE jitter measurements is given by the aliasing and the noise floor of the oscilloscope used for the measurements.

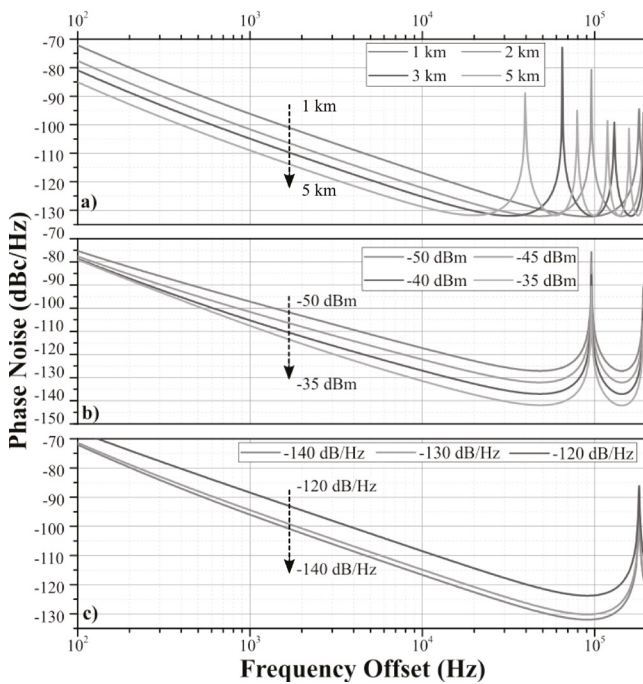


Figure 8. Phase noise simulation using different a) optical fiber lengths, b) amplifier input powers, and c) RIN values
Source: Authors

Table 3. Parameters used to estimate the theoretical phase noise

Parameter	Value
RIN @2,5 GHz	-140 dB/Hz
Z_{ph}	100 Ω
Z_A	50 Ω
P_o	-48 dBm
F	3 dB
T_o	25 °C
$b-1$	-100 rad ² /Hz

Source: Authors

Performance comparison

Table 4 presents some phase noise results obtained by different authors using short and long-wavelength VCSELs.

In all cases, the oscillating frequency is limited by the bandwidth laser and the electrical access. At 2,49 GHz, the highest phase noise is -100 dBc/Hz, and it was obtained when a multimode VCSEL emitting at 0,85 μ m and 120-m optical fiber were employed. Despite the reduced RIN of the multimode VCSEL (-130 dB/Hz), the phase noise of the VBO was deteriorated by the high attenuation and the reduced Q-factor provided by the multimode optical fiber.

When long-wavelength VCSELs are used, the phase noise of the generated microwave signal is improved in all cases. This event is mainly attributed to the RIN reduction resulting from the technological advances in VCSEL manufacturing, as well as the lengthening of single-mode optical fiber.

The lowest phase noise values of our work were obtained when the optical fiber length was 5 km. The phase noises were -124,8 dBc/Hz and -119 dBc/Hz when the emitting wavelengths were in the O and C-bands, respectively. To the best of our knowledge, these values are the lowest reported in the bibliography at 2,5 GHz when direct modulation is applied. According to the numerical results presented in the previous section and the experimental results (Table 4), we attribute the phase noise improvement to the reduction of the white phase noise through the amplifier input power P_o , and the lengthening of the optical fiber.

Conclusions

This paper presents the first time-domain stability characterization of several VBO implementations by performing timing-jitter measurements and their frequency-domain stability through phase noise measurements. As stated, both stability measurements are frequently used for establishing clock accuracy for several data transmission systems.

For all the experimental validations, the last generation of O and C-band VCSELs with reduced RIN levels were employed. In this way, VCSEL RIN and longer optical fiber have improved the phase noise by 8 dB in comparison with previously reported results. The best phase noise performance measured at 10 kHz from the carrier was -124,8 dBc/Hz, and it corresponds to the lowest value reported in the literature for a 2,5 GHz-VBO. It was experimentally demonstrated that the longer the optical fiber, the better the spectral purity, but, at the same time, the worse the timing-jitter deterioration. According to the application, a trade-off must be made between phase noise and timing-jitter.

Given the higher contribution from the non-oscillation modes, the peak-to-peak jitter increases from 71 to 106 mUI when the optical fiber length is enlarged from 1 to 5 km. In all cases, the electrical output of the VBO can be used as a recovery clock that meets the jitter tolerances of ITU-T G.813 for STM-16 transmissions and Telcordia GR-253-CORE for OC-48 transmissions.

Table 4. VCSEL based optoelectronic oscillator performance comparison

Reference	Laser wavelength (μm)	Frequency (GHz)	Phase noise (dBc/Hz)	Optical fiber length (m)
(Varón et al., 2006)	0,85	2,49	-100	120
(Hayat et al., 2008)	1,3	2,49	-107,5	1 000
(Rissons et al., 2012)	1,3	2,49	-116	2 000
(Belkin et al., 2015)	1,3	3	-106	65
This work (2020)	1,3	2,5	-124,8	5 000
This work (2020)	1,5	2,5	-119	5 000

Source: Authors

The phase noise estimation model agrees with the experimental characterization of the far-from-the-carrier microwave signal. The model can be improved by a complete characterization of the microwave amplifier and the addition of multiplicative noise sources such as the frequency noise and the low-frequency RIN of the VCSEL.

Considering the good phase noise performance and its lower power consumption, the VBO is suitable for embedded applications and an all-integrated solution can be explored. Additionally, high-bandwidth on-chip VCSELs can be employed to increase the oscillating frequency.

For future developments, it is recommended to employ other resonant elements such as fiber ring resonators, whispering gallery modes, or double feedback loop oscillator in order to explore the spectral purity performance in the frequency domain. A stability analysis in the time domain (long-term stability) is proposed, which uses a deviation.high-resolution frequency counter and the Allan standard deviation.

Acknowledgements

The authors would like to thank COLCIENCIAS and the French Ministry of Higher Education for funding the mobility and exchange of the researchers through the projects M301PR03F18 and C17P01, as well as the Departmental Government of Nariño for supporting this work through grant No. BPIN 2013000100092.

References

- Bacou, A., Hayat, A., Iakovlev, V., Syrbu, A., Rissons, A., Mollier, J., and Kapon, E. (2010). Electrical modeling of long-wavelength VCELS for intrinsic parameters extraction. *IEEE Journal of Quantum Electronics*, 46(3), 313-322. <https://doi.org/10.1109/JQE.2009.2031312>
- Belkin, M.-E., Belkin, L., Loparev, A., Sigov, A.-S., and Iakovlev, V. (2015). Long wavelength VCELS and VVCSEL-based processing of microwave signals. *IntechOpen*. <https://doi.org/10.5772/60480>
- Chen, H., Xia, M., Sun, M., and Sun, X. (2015). A high-speed tunable optoelectronic oscillator with a fine step based on semiconductor optical amplifier. *Microwave and Optical Technology Letters*, 57(2), 464-467. <https://doi.org/10.1002/mop.28868>
- Chi, Y.-C., Lin, G.-R., Chi, Y., and Lin, G. (2016). Optoelectronic oscillators. In J. G. Webster (Ed.) *Wiley Encyclopedia of Electrical and Electronics Engineering* (pp. 1-2). John Wiley & Sons. <https://doi.org/10.1002/047134608X.W8304>
- Choi, S., Yoo, S., Lee, Y., Jo, Y., Lee, J., Lim, Y., and Choi, J. (2019). An ultra-low-jitter 22.8-GHz ring-LC-hybrid injection-locked clock multiplier with a multiplication factor of 114.. *IEEE Journal of Solid-State Circuits*, 54(4), 927-936. <https://doi.org/10.1109/JSSC.2018.2883090>
- Da Dalt, N. and Sheikholeslami, A. (2018). *Understanding jitter and phase noise: A circuits and systems perspective*. Cambridge University Press. <https://doi.org/10.1017/9781316981238>
- Feng, D., Gao, Y., Zhu, T., Deng, M., Zhang, X., and Kai, L. (2021). High-precision temperature-compensated magnetic field sensor based on optoelectronic oscillator. *Journal of Lightwave Technology*, 39(8), 2559-2564. <https://doi.org/10.1109/JLT.2021.3050153>
- Gheen, K. (2012). *Phase noise measurements methods and techniques, technical report application note*. Agilent Technologies.
- Ghosh, A., Maeder, A., Baker, M., and Chandramouli, D. (2019). 5g evolution: A view on 5g cellular technology beyond 3GPP release 15. *IEEE Access*, 7, 127639-127651. <https://doi.org/10.1109/ACCESS.2019.2939938>
- Guo, J.-J., Jin, X.-D., Zhu, Y.-H., Jin, X.-F., Chi, H., Zheng, S., and Zhang, X. (2018). A comprehensive model for phase noise characteristics of an optoelectronic oscillator. *Microwave and Optical Technology Letters*, 60(9), 2194-2197. <https://doi.org/10.1002/mop.31327>
- Hasegawa, H., Oikawa, Y., and Nakazawa, M. (2007). A 10-ghz optoelectronic oscillator at 850 nm using a single-mode vcsel and a photonic crystal fiber. *IEEE Photonics Technology Letters*, 19(19), 1451-1453. <https://doi.org/10.1109/LPT.2007.903950>
- Hayat, A., Varón, M., Bacou, A., Rissons, A., and Mollier, J. C. (2008, September 30 – October 3). 2.49 GHz low phase-noise optoelectronic oscillator using 1.55 μm VCSEL for avionics and aerospace applications [Conference presentation]. 2008 IEEE International Meeting on Microwave Photonics, jointly held with the 2008 Asia-Pacific Microwave Photonics Conference, Gold Coast, Qld, Australia. <https://doi.org/10.1109/MWP.2008.4666644>
- Iakovlev, V., Suruceanu, G., Caliman, A., Mereuta, A., Mircea, A., Berseth, C., Syrbu, A., Rudra, A., and Kapon, E. (2005). High-performance single-mode VCSELs in the 1310-nm wa-

- veband. *IEEE Photonics Technology Letters*, 17(5), 947-949. <https://doi.org/10.1109/LPT.2005.845654>
- IEEE (2009). *IEEE standard definitions of physical quantities for fundamental frequency and time metrology—random instabilities (IEEE Std 1139-2008)*. IEEE. <https://doi.org/10.1109/IEEESTD.2008.4797525>
- IEEE (2021). *Standard for jitter and phase noise (IEEE Std 2414-2020)*. IEEE.
- International Telecommunication Union (ITU) (1996). *ITU-T recommendation G.810 (08/96), definitions and terminology for synchronization networks*. ITU.
- International Telecommunication Union (ITU) (2018). *G.8251: The control of jitter and wander within the optical transport network (OTN)*. ITU.
- Koizumi, K., Yoshida, M., and Nakazawa, M. (2009). 10-GHz 11.5-ps pulse generation from a single-mode gain-switched InGaAs VCSEL at 1.1 μm . *IEEE Photonics Technology Letters*, 21(22), 1704-1706. <https://doi.org/10.1109/LPT.2009.2031920>
- Koizumi, K., Yoshida, M., and Nakazawa, M. (2010). A 10-GHz optoelectronic oscillator at 1.1 μm using a single-mode VCSEL and a photonic crystal fiber. *IEEE Photonics Technology Letters*, 22(5), 293-295. <https://doi.org/10.1109/LPT.2009.2038892>
- Lavrencik, J., Thomas, V.-A., Varughese, S., and Ralph, S.-E. (2017). DSP-enabled 100 Gb/s PAM-4 VCSEL MMF links. *Journal of Lightwave Technology*, 35(15), 3189-3196. <https://doi.org/10.1109/JLT.2017.2683941>
- Lu, H., Li, C., Chen, H., Ho, C., Cheng, M., Yang, Z., and Lu, C. (2017). A 56 Gb/s PAM4 VCSEL-based LiFi transmission with two-stage injection-locked technique. *IEEE Photonics Journal*, 9(1), 1-8. <https://doi.org/10.1109/JPHOT.2016.2637564>
- Malacarne, A., Fresi, F., Meloni, G., Foggi, T., and Poti, L. (2017). Time-frequency packing directly applied to cost-effective IM/DD transmission based on directly modulated VCSEL. *Journal of Lightwave Technology*, 35(20), 4384-4391. <https://doi.org/10.1109/JLT.2017.2743529>
- Park, M., Kwon, O., Han, W., Lee, K., Park, S., and Yoo, B. (2006). All-epitaxial InAlGaAs-InP VCSELs in the 1.3-1.6- μm wavelength range for CWDM band applications. *IEEE Photonics Technology Letters*, 18(16), 1717-1719. <https://doi.org/10.1109/LPT.2006.879940>
- Pavan, S.-K., Lavrencik, J., and Ralph, S.-E. (2017). VCSEL-Based PAM-4 Links up to 62 Gbit/s over OM3, OM4, and WB-MMF: Performance Comparison at 850 nm and 1050 nm. *Journal of Lightwave Technology*, 35(9), 1614-1623. <https://doi.org/10.1109/JLT.2016.2647203>
- Rappaport, T. S., Xing, Y., Kanhere, O., Ju, S., Madanayake, A., Mandal, S., Alkhateeb, A., and Trichopoulos, G. C. (2019). wireless communications and applications above 100 GHz: Opportunities and Challenges for 6G and Beyond. *IEEE Access*, 7, 78729-78757. <https://doi.org/10.1109/ACCESS.2019.2921522>
- Rissons, A., Poulenard, S., Laurent, B., and Mollier, J. (2012, September 11-14). *Advances in VCSEL for satellite applications* [Conference presentation]. 2012 IEEE International Topical Meeting on Microwave Photonics, Noordwijk, Netherlands. <https://doi.org/10.1109/MWP.2012.6474110>
- Rubiola, E. (2008). *Phase noise and frequency stability in oscillators*. Cambridge University Press. <https://doi.org/10.1017/CBO9780511812798>
- Rubiola, E. and Giordano, V. (2007). On the 1/f frequency noise in ultra-stable quartz oscillators. *IEEE Transactions on Ultrasonics, Ferroelectrics, and Frequency Control*, 54(1), 15-22. <https://doi.org/10.1109/TUFFC.2007.207>
- Ryu, K., Lee, K.-H., Lim, J.-P., Kim, J., Pae, H., Park, J., Lim, H.-W., and Lee, J.-Y. (2020). An analytical jitter tolerance model for DLL-based clock and data recovery circuits. *IEEE Transactions on Very Large Scale Integration (VLSI) Systems*, 28(11), 2257-2267. <https://doi.org/10.1109/TVLSI.2020.3018794>
- Sung, H., Lau, E. K., Zhao, X., Parekh, D., Chang-Hasnain, C., and Wu, M. (2007, May 6-11). *Optically injection-locked optoelectronic oscillators with low RF threshold gain* [Conference presentation]. 2007 Conference on Lasers and Electro-Optics (CLEO), Baltimore, MD, USA. <https://doi.org/10.1109/CLEO.2007.4453176>
- Syrbu, A., Iakovlev, V., Suruceanu, G., Caliman, A., Mereuta, A., Mircea, A., Berseth, C.-A., Diechsel, E., Boucart, J., Rudra, A., and Kapon, E. (2005, January 22-27). *VCSELs emitting in the 1310-nm waveband for novel optical communication applications* [Conference presentation]. SPIE 5737, Vertical-Cavity Surface-Emitting Lasers IX, San José, CA, United States. <https://doi.org/10.1117/12.606964>
- Varón, M., Martin, J.-C., Le Kernec, A., and Mollier, C. (2006, October 2-4). *VCSEL based oscillator for harmonic frequency generation* [Conference presentation]. 5th Topical Meeting on Optoelectronic Distance/Displacement Measurements and Applications, Madrid, Spain.
- Wagner, C., Dochhan, A., Eiselt, M.-H., Grobe, K., Ortsiefer, M., Greus, C., Neumeyr, C., Paul, S., Cesar, J., Kuppers, F., Olmos, J.-J.-V., and Monroy, I.-T. (2017). 26-GB/s DMT transmission using full C-band tunable VCSEL for converged PONs. *IEEE Photonics Technology Letters*, 29(17), 1475-1478. <https://doi.org/10.1109/LPT.2017.2710323>
- Wang, W., Liu, Y., Du, X., Zhong, X., Yu, C., and Chen, X. (2020). Ultra-stable and real-time demultiplexing system of strong fiber bragg grating sensors based on low-frequency optoelectronic oscillator. *Journal of Lightwave Technology*, 38(4), 981-988. <https://doi.org/10.1109/JLT.2019.2949682>
- Yao, X. S. and Maleki, L. (1996). Optoelectronic oscillator for photonic systems. *IEEE Journal of Quantum Electronics*, 32(7), 1141-1149. <https://doi.org/10.1109/3.517013>
- Zou, X., Liu, X., Li, W., Li, P., Pan, W., Yan, L., and Shao, L. (2016). Optoelectronic oscillators (OEOs) to sensing, measurement, and detection. *IEEE Journal of Quantum Electronics*, 52(1), 1-16. <https://doi.org/10.1109/JQE.2015.2504088>

On the Optimal Reconfiguration of Radial AC Distribution Networks Using an MINLP Formulation: A GAMS-Based Approach

Sobre la reconfiguración óptima de redes radiales de distribución empleando un modelo de PNLEM: un enfoque basado en GAMS

Oscar D. Montoya-Giraldo ^{1,2}, Walter Gil-González ³, Luis F. Grisales-Noreña ⁴, Diego A. Giral-Ramírez ⁵, Alexander Molina-Cabrera ⁶

ABSTRACT

This paper addresses the problem of the optimal reconfiguration of medium-voltage distribution networks by proposing a mixed-integer nonlinear programming (MINLP) model. The objective function of this optimization model is the minimization of the total power losses in all the branches of the network, considering active and reactive power balance equations, voltage regulation bounds, and device capabilities, among others. The proposed MINLP formulation works with branch-to-node incidence that allows representing the active and reactive power flow in branches as a function of the real and imaginary components of the voltages and currents. The solution of the MINLP model is reached through the general algebraic modeling system widely known as the GAMS package while presenting it in the form of a tutorial. This software allows implementing the proposed model in a compact way, which is solved via branch and bound methods. Two test feeders comprising 5 and 14 nodes allow demonstrating the fidelity of the proposed MINLP model regarding power loss minimization when compared to that reported in the specialized literature.

Keywords: nonlinear optimization, general algebraic modeling system, distribution system reconfiguration, power loss minimization, mixed-integer nonlinear programming

RESUMEN

Este artículo aborda el problema de la reconfiguración óptima de redes de distribución de media tensión mediante la proposición de un modelo de programación no lineal entera mixta (PNLEM). La función objetivo de este modelo de optimización es la minimización de las pérdidas totales de potencia activa en todas las ramas del sistema, considerando las ecuaciones de balance de potencia activa y reactiva, los límites de regulación de voltaje y la capacidad de los diferentes dispositivos, entre otros. La formulación de PNLEM propuesto trabaja con la matriz de incidencia rama-nodo, la cual permite representar las ecuaciones de flujo de potencia en las ramas como una función de los componentes reales e imaginarios de los voltajes en los nodos y las corrientes en las ramas. La solución del modelo de PNLEM se obtiene a través del sistema de modelado algebraico general ampliamente conocido como el paquete GAMS, presentándolo en forma de tutorial. Este software permite implementar el modelo de optimización propuesto en forma compacta, el cual se resuelve mediante métodos de ramificación y corte. Dos alimentadores de prueba compuestos de 5 y 14 nodos permiten demostrar la fidelidad del modelo de PNLEM propuesto en relación con la minimización de pérdidas de potencia cuando se compara con reportes de la literatura especializada.

Palabras clave: optimización no lineal, sistema de modelado algebraico general, reconfiguración de sistemas de distribución, minimización de pérdidas de potencia, programación no lineal entera mixta

Received: October 26th, 2020

Accepted: September 14th, 2021

Introduction

General context

Electrical distribution networks correspond to the largest part of the power system that is responsible for the commercialization and distribution of electricity services to end-users at medium voltage levels (Sánchez-Zuleta *et al.*, 2012). The extensive longitude of these electrical networks combined with medium voltages is susceptible to high power losses in comparison with transmission networks (Anders, 1994). In the Colombian context, electrical networks typically operate between 11,4 kV and 13,8 kV, with power losses between 6 and 15% of the total energy bought in the spot market (Zuleta *et al.*, 2017). These percentage differences are related to the practices implemented by utilities regarding distribution system operation, as well as to the geographical location

¹ Electrical Engineer, M.Sc. Electrical Engineering, Ph.D. in Engineering. Affiliation: Assistant Professor, Department of Engineering, Universidad Distrital Francisco José de Caldas. Bogotá, Colombia. E-mail: odmontoyag@udistrital.edu.co.

² Electrical Engineer, M.Sc. Electrical Engineering, Ph.D. in Engineering. Affiliation: Research Professor, Universidad Tecnológica de Bolívar. Cartagena, Colombia. E-mail: omontoya@utb.edu.co.

³ Electrical Engineer, M.Sc. Electrical Engineering, Ph.D. in Engineering. Affiliation: Facultad de Ingeniería, Institución Universitaria Pascual Bravo. Medellín, Colombia. E-mail: walter.gil@pascualbravo.edu.co.

⁴ Electrical Engineer, M.Sc. Electrical Engineering, Ph.D. in Automatic Engineering. Affiliation: Facultad de Ingeniería, Institución Universitaria Pascual Bravo. Medellín, Colombia. E-mail: luis.grisales@pascualbravo.edu.co.

⁵ Electrical Engineer, M.Sc. Electrical Engineering, Ph.D. in Engineering. Affiliation: Assistant Professor, Technological Department, Universidad Distrital Francisco José de Caldas. Bogotá, Colombia. E-mail: dagiralr@udistrital.edu.co.

⁶ Electrical Engineer, M.Sc. Electrical Engineering, Ph.D. in Engineering. Affiliation: Facultad de Ingeniería, Universidad Tecnológica de Pereira. Pereira, Colombia. E-mail: almo@utp.edu.co.

How to cite: Montoya, O. D., Gil-González, W., Grisales-Noreña, L. F., Giral-Ramírez, D. A., and Molina-Cabrera, A., (2022). On the Optimal Reconfiguration of Radial AC Distribution Networks Using an MINLP Formulation: A GAMS-Based Approach. *Ingeniería e Investigación*, 42(2), e91192. <https://doi.org/10.15446/ing.investig.91192>

of the distribution grid, given that Colombia is essentially a rural country. This implies that the distribution networks have hundreds of kilometers of extension increment power losses due to the natural configuration of the grid (Marneni *et al.*, 2015). An additional fact that furthers power losses in the distribution stage corresponds to the radial structure of this network, which is largely adopted by utilities since it simplifies the coordination of protective devices (reclosers, sectionalizers, and fuses) and also reduces investments in infrastructure such as conductors and supports (Celli *et al.*, 2004; Cruz *et al.*, 2018), among others.

Optimal reconfiguration in distribution networks is a strategy to improve the operating conditions of power systems. It is a real-time operational task performed to minimize losses, improve voltage profiles, improve reliability indicators, balance the load, and minimize operating costs (Celli *et al.*, 2004; Cruz *et al.*, 2018).

Network operation and design standards have changed in recent years due to factors such as the need for new monitoring and control systems, the rational use of resources, the demand for high-quality service, and the deregulation of the electric power market (Augugliaro *et al.*, 2004; Azghandi *et al.*, 2021). Each of these factors represents a set of challenges that require technological advances. The aim is to improve the current scenarios and adapt to the challenges of the future energy industry by providing clean, economic, reliable, and safe electrical energy. Optimization applied to distribution networks plays a relevant role in adapting to these new challenges (Jafar-Nowdeh *et al.*, 2020; Vargas-Robayo *et al.*, 2021; Zhengzhong *et al.*, 2021).

Future scenarios for distribution networks need to include strategies that allow operating under unconventional conditions such as dynamic and probabilistic loads, renewable energy sources at distribution points, small-scale generation, bidirectional power flow, among others (Haitham and Helmi, 2021; Jafar-Nowdeh *et al.*, 2020; Raju and Sandeep, 2021). Operation scenarios can be adequately and efficiently addressed by proposing an optimal reconfigurable network (Sambaiah and Jaybarathi, 2021).

Motivation

The amount of power losses of distribution networks is undoubtedly an essential issue for electrical distribution companies, since it is the most direct quality indicator in the electrical service (Celli *et al.*, 2004). In order to minimize power losses in distribution networks, multiple strategies can be implemented, such as the optimal placement of distributed generators (Grisales-Noreña *et al.*, 2017; Grisales-Noreña *et al.*, 2018), shunt-capacitors (Elsheikh *et al.*, 2014), batteries (Grisales-Noreña *et al.*, 2019; Montoya *et al.*, 2020b), or the optimal reconfiguration of the network (Verma and Singh, 2018). Nevertheless, in the case of the optimal reconfiguration, most studies focus on the solution technique, glossing over the importance of an adequate mathematical formulation. This gap in the literature is the main motivation of this research. Our interest is to provide a correct mathematical formulation of the reconfiguration problem in distribution networks using a mixed-integer nonlinear programming model that can be solved with any optimization package (Montoya *et*

al., 2020a). This is especially important since engineers need to be formed in mathematical analysis, *i.e.*, with the capabilities of current adequate mathematical models that represent real-life problems. Moreover, they need to have the ability to solve them efficiently.

State of the art

The problem of the optimal reconfiguration of AC distribution feeders is a classical optimization problem in power systems analysis (Civanlar *et al.*, 1988). In general terms, this problem can be described as determining the best subset of lines that generates a radial configuration network from an initial solution space conformed by connected (existing) and tie lines (opened), which allows reducing the total active power losses into the network, fulfilling the devices' capabilities (current in lines and power generation in sources) and guaranteeing power balance and voltages bounds in all the nodes. In mathematical terms, this problem can be formulated by using a mixed-integer nonlinear programming structure, *i.e.*, an MINLP model (Lavorato *et al.*, 2012). To solve this problem, the specialized literature has proposed multiple approaches, most of them based on metaheuristic optimization, namely genetic algorithms (Su *et al.*, 2005; Zhang *et al.*, 2014), ant colony optimization (Ahuja and Pahwa, 2005; Su *et al.*, 2005), chaotic stochastic fractal search algorithms (The *et al.*, 2020), tabu search algorithms (García-Martínez and Espinosa-Juárez, 2013), binary particle swarm optimization (Arya *et al.*, 2011; Tandon and Saxena, 2014; Xiaozhi *et al.*, 2010), culture search algorithms (Verma and Singh, 2018), ant lion optimizer (Shokouhi *et al.*, 2017), and bat algorithms (Quintero-Durán *et al.*, 2019), among others.

The main characteristic of the aforementioned metaheuristic optimization approaches is that all of them concentrate efforts on solving the reconfiguration problem in sequential steps by proposing codification and evolution strategies. This implies that they have decomposed the problem into a master-slave strategy, where the metaheuristic approach is the master layer, and the slave stage corresponds to a conventional power flow approach (Su *et al.*, 2005). Even if these strategies are efficient to solve complex optimization problems implying binary variables (Verma and Singh, 2018), they have a recurrent problem from a theoretical perspective, since these neglect the importance of a correct mathematical representation of the problem and only focus on designing an algorithm to solve it (Grisales-Noreña *et al.*, 2018). To address the problem of reconfiguration correctly, Lavorato *et al.* (2012) presented a complete formulation to solve the problem regarding the optimal planning of distribution network systems that can be solved in the AMPL software. Nevertheless, the problem in that formulation is the representation of the voltage profiles, since the authors follow the classical representation that uses trigonometric functions, which clearly includes strong nonlinearities in the optimization model, thus increasing the possibilities of staying stuck in a local solution (Montoya *et al.*, 2020; Sultana and Roy, 2015). Hence, we present an alternative mathematical formulation to address this problem, which allows representing the problem of the



optimal reconfiguration in AC distribution networks without involving trigonometric functions (which is presented as a tutorial). This approach will be particularly interesting to introduce beginners to optimization problems, especially for power systems engineers (Soroudi, 2017).

Contributions and scope

The main contributions of this research can be summarized as follows:

- ✓ The mathematical formulation of the optimal reconfiguration problem in AC distribution networks using a rectangular representation of the voltage and current variables added to the inclusion of binary variables, which allows determining the subset of conductors needed to minimize the total power losses in all the branches of the network.
- ✓ The implementation of the proposed MINLP formulation in a specialized software known as the general algebraic modeling system (GAMS) in the form of a tutorial that allows introducing engineering students to mathematical optimization.

It is worth mentioning that the proposed MINLP model for optimal reconfiguration of AC distribution feeders has not been previously reported in the specialized literature, which corresponds to a gap that this research aims to fill. In addition, we introduce the general algebraic modeling system as a powerful optimization tool that helps solve large-scale nonlinear programming problems by focusing on the mathematical formulation and not on the solution technique. This is important since, in power systems optimization, when metaheuristic optimization is employed, the mathematical model is neglected by tackling the sequential step to solve the optimization problem. This practice is not advised when engineering students are introduced to mathematical optimization; the main focus must be the correct formulation of the problem under study and not the solution method. Therefore, this research concentrates on presenting a comprehensive formulation of the optimization reconfiguration of AC distribution feeders using an MINLP model.

Organization of the document

This paper is organized as follows: the MINLP formulation section presents the mathematical formulation of the optimal reconfiguration problem of AC distribution feeders by using a rectangular representation of the voltage and current variables, which produces a mixed-integer nonlinear programming model. The next section introduces the solution methodology based on the general algebraic modeling system that allows implementing the MINLP model in a compact structure. The numerical validation section presents numerical simulations for a classical 13-node test feeder using the GAMS software, as well as their comparisons with literature reports. The conclusions and future Work section presents the principal outcomes derived from this work, as well as some possible future developments.

MINLP formulation

The problem of the optimal reconfiguration of electrical distribution networks is indeed a complex optimization problem due to the presence of the power balance equations containing multiple products between voltage and currents (nonlinear expressions). Additionally, the nature of this optimization problem is binary, given the necessity of selecting a subset of conductors that minimizes the power losses of the distribution system for a particular load condition. The complete mathematical model of the reconfiguration problem in distribution networks is described below.

Objective function

The objective function of the optimal reconfiguration problem corresponds to the minimization of the active power losses in all the branches of the network p_{loss} , as expressed by Equation (1).

$$\min z = p_{\text{loss}} = \sum_{l \in \mathcal{L}} R_l I_l^2, \quad (1)$$

where R_l is the resistance value of the conductor associated to branch l , and I_l is the magnitude of the current that flows in said branch. Note that \mathcal{L} is the set containing all the branches (connected and non-connected).

Set of constraints

The set of constraints that defines the solution space of the optimal reconfiguration problem in AC distribution networks is defined as follows: first, the active and reactive power balance equations are presented using the real and imaginary parts of the voltage and current variables, as shown in Equations (2) and (3).

$$P_g^k - P_d^k = \sum_{l \in \mathcal{L}} \mathcal{A}_{kl} (V_k^r I_l^r + V_k^i I_l^i), \quad \forall k \in \mathcal{N}, \quad (2)$$

$$Q_g^k - Q_d^k = - \sum_{l \in \mathcal{L}} \mathcal{A}_{kl} (V_k^r I_l^i - V_k^i I_l^r), \quad \forall k \in \mathcal{N}, \quad (3)$$

where P_g^k and P_d^k are the active power generation and demands at node k , respectively; Q_g^k and Q_d^k represent the reactive power generation and consumption at node k , respectively; V_k^r and V_k^i are the real and imaginary parts of the voltage variable at node k ; and I_l^r and I_l^i correspond to the real and imaginary components of the current that flows in branch l . Note that \mathcal{A}_{kl} is the incidence node-to-branch matrix, and its components are defined as follows:

- ✓ $\mathcal{A}_{kl} = +1$ if the branch l is connected at node k and the current I_l leaves this node.
- ✓ $\mathcal{A}_{kl} = -1$ if the branch l is connected at node k and the current I_l arrives to this node.
- ✓ $\mathcal{A}_{kl} = 0$ if the branch l is non connected at node k .

Second, the real and imaginary currents are defined as function of the voltage drops at the ends of each branch

(Equations (4) and (5)).

$$I_l^r = \frac{y_l}{R_l^2 + X_l^2} \sum_{k \in \mathcal{N}} \mathcal{A}_{kl} (R_l V_k^r + X_l V_k^i), \quad \forall l \in \mathcal{L}, \quad (4)$$

$$I_l^i = \frac{y_l}{R_l^2 + X_l^2} \sum_{k \in \mathcal{N}} \mathcal{A}_{kl} (R_l V_k^i - X_l V_k^r), \quad \forall l \in \mathcal{L}, \quad (5)$$

where y_l is a binary variable that determines whether the branch l is connected to the distribution network ($y_l = 1$) or not ($y_l = 0$) and X_l is the reactance effect in the conductor l . Note that \mathcal{N} is the set that contains all the nodes of the network.

Third, the magnitudes of the voltages and currents are defined through Equations (6) and (7).

$$I_l = \sqrt{(I_l^r)^2 + (I_l^i)^2}, \quad \forall l \in \mathcal{L}, \quad (6)$$

$$V_k = \sqrt{(V_k^r)^2 + (V_k^i)^2}, \quad \forall k \in \mathcal{N}. \quad (7)$$

Fourth, the current capabilities and voltage regulation bounds are defined to ensure the useful life of the conductors and the regulatory policies regarding maximum voltage deviations (Equations (8) and (9)).

$$-I_l^{\max} \leq I_l \leq I_l^{\max}, \quad \forall l \in \mathcal{L}, \quad (8)$$

$$V_k^{\min} \leq V_k \leq V_k^{\max}, \quad \forall k \in \mathcal{N}, \quad (9)$$

where I_l^{\max} represents the maximum thermal limit of the conductor associated with branch l , and V_k^{\min} and V_k^{\max} represent the minimum and maximum voltage bounds allowed in all the nodes of the network.

Fifth, to ensure that the resulting configuration of the distribution network is radial, a constraint is imposed in the number of conductors that can be connected to the distribution (Equation (10)).

$$\sum_{l \in \mathcal{L}} y_l = |\mathcal{N}| - 1, \quad (10)$$

where $|\mathcal{N}|$ represents the cardinality of the set of nodes, i.e., the number of elements in this set.

The interpretation of the mathematical model in Equations (1) to (10) that represents the problem of the optimal reconfiguration of AC distribution networks has the following description: Equation (1) corresponds to the objective function associated with the power losses minimization in all the branches of the network. Equations (2) and (3) determine the active and reactive power balance in all the nodes of the network. These Equations are widely-known in the specialized literature as power flow constraints. Equations (4) and (5) calculate the real and imaginary components of the currents that flow at each branch. Equations (6) and (7) determine the magnitude of the network variables, i.e., voltages in all the nodes and currents in all the branches. Equations (8) and (9) allow for solutions that fulfill the thermal capabilities of the calibers associated with each branch and the voltage regulation bounds permitted in all the nodes. Finally, Equation (10) defines that the number of branches that can be connected produces a radial configuration. Nevertheless, this radial structure is ensured by the presence of the active

and reactive power balance equations in the mathematical model, i.e., Equations (2) and (3) and the number of conductors available for operation, i.e., constraint (10).

Remark 1. The mathematical formulation presented in Equations (1) to (10) is not unique, since multiple representations can be reached by representing the real and imaginary parts of the currents as a combination of magnitudes and angles, i.e., trigonometric functions. However, these trigonometric functions introduce complex nonlinearities that can make the solution to the problem difficult.

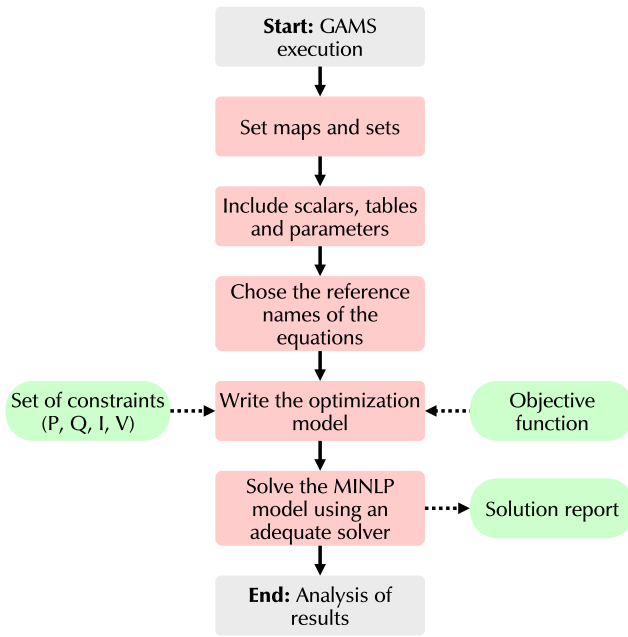
Solution methodology: GAMS software

This section presents the optimization strategy adopted to solve the problem of the optimal reconfiguration of AC networks with an MINLP model described in Equations (1) to (10). To this effect, the general algebraic modeling system is used as a solution technique. The GAMS software is a powerful tool that allows solving complex optimization models including linear and mixed-integer programming, quadratic programming and general nonlinear programming models with mixed variables (i.e., binary, integer) (Soroudi, 2017).

In the specialized literature, GAMS has been employed to solve complex optimization problems such as the optimal selection of conductors in distribution networks (Montoya et al., 2018), optimal planning of transmission networks (Aguado et al., 2017), optimal location of renewable generation in distribution networks (Babu and Singh, 2016; Gil-González et al., 2020; Montoya et al., 2020a), optimal operation of power systems with batteries (Soroudi, 2017; Montoya et al., 2020c), optimal design, and sizing of a pressure retarded osmosis power plant (Naghiloo et al., 2015), voltage stability analysis in direct current networks (Amin et al., 2019), multi-objective optimization of the stack of a thermoacoustic engine (Tartibu et al., 2015), multi-objective optimization of energy and water management in networked hubs (Pakdel et al., 2020), the optimal location of protective devices (Izadi et al., 2019; Gallego-Londoño et al., 2016), and so on.

The main advantages of using the GAMS software in mathematical optimization can be summarized as follows (Montoya et al., 2020c; Soroudi, 2017; Vargas-RObayo et al., 2021):

- ✓ It works with a compact structure, i.e., it employs sets that contain information regarding the number of variables as well as the dimension of the solution space.
- ✓ The information related to the system is introduced by using matrices, vectors, and scalars, and these can be assigned to the set's domain.
- ✓ It uses a symbolic representation of the variables to mathematically represent the optimization model under study, with the characteristic that the model has a pretty similar structure as presented in Equations (1) to (10).
- ✓ It is possible to differentiate the nature of the variables that intervene in the mathematical model, i.e., discrete



Source: Authors

Figure 1. Flowchart for optimal reconfiguration using GAMS

(integer), binary, continuous, and positive variables, among others.

- ✓ Multiple solution techniques based on interior point and branch and bounds methods can be selected to resolve the mathematical optimization model. Some of the classical natures of problems are linear programming (LP), nonlinear programming (NLP), mixed-integer programming (MIP), and mixed-integer nonlinear programming (MINLP).

Figure 1 presents the flowchart for the implementation of optimal reconfiguration in radial distribution networks using MINLP through GAMS. To illustrate an implementation of a mathematical model using the GAMS software, let us consider a small optimization example consisting of an AC distribution network operated at 13,2 kV with 5 nodes, 4 built lines, and 3 tie lines. The electrical configuration is depicted in Figure 2. The initial power losses in this system with the configuration depicted in said Figure are 222,842 kW, and the minimum voltage profile occurs in node 5 with a value of 0,952 pu.

The load information of this test feeder is reported in Table 1, and the branch data including connected and tie lines are presented in Table 2.

Table 1. Load information for the 5-node test feeder

Node	Active power [kW]	Reactive power [kVAr]
1	0	0
2	1 625	520
3	2 250	745
4	2 265	896
5	1 450	1 000

Source: Authors

It is worth mentioning that lines *e*, *f*, and *g* represent the subset of possible links to reconfigure the AC

Table 2. Branch information

Line	Resistance [Ω]	Reactance [Ω]
a	0,3414	0,4127
b	0,6467	0,6051
c	0,2540	0,5526
d	0,2469	0,8050
e	0,8245	0,9656
f	0,1525	0,4565
g	0,3548	0,6885

Source: Authors

distribution system by always guaranteeing a radial topology. In addition, the incidence node-to-branch matrix that represents this test feeder has the following structure:

$$\mathcal{A} = \begin{bmatrix} 1 & 0 & 0 & 0 & 1 & 0 & 0 \\ -1 & 1 & 1 & 1 & 0 & 0 & 0 \\ 0 & -1 & 0 & 0 & 0 & 1 & 0 \\ 0 & 0 & 0 & -1 & -1 & 0 & 1 \\ 0 & 0 & -1 & 0 & 0 & -1 & -1 \end{bmatrix}$$

where it was assumed that the currents flow from the smallest to the highest by rearranging the columns from lines *a* to *g* and the rows from node 1 to node 5.

The implementation of the mathematical model from Equations (1) to (10) to solve the reconfiguration problem in AC networks using GAMS is presented in Algorithm 1. Note that 13,2 kV and 1 000 kVA are used to obtain a per-unit (pu) representation of the system.

The information in Algorithm 1 can interpreted as follows:

- ✓ Lines 1 to 5 determine the sets in the optimization problems, i.e., nodes, lines, and generators, including the map that defines the location of the slack source.
- ✓ Lines 6 to 31 define all the constant information related to the test feeder, i.e., voltage ranges, and branch and load parameters.
- ✓ Lines 32 to 44 define the variables of the problem, i.e., voltages, currents, active and reactive power generations, and binary variables, as well as their constant bounds.
- ✓ Lines 45 to 61 are the necessary equations to solve the problem, starting by their names and followed by their mathematical structures.
- ✓ Lines 62 to 64 present the solution of the problem by defining its nature and selecting the minimization strategy. In addition, the variables of interest are extracted to analyze the final solution.

The solver used to reach the optimal solution of the AC reconfiguration problem in the 5-node test feeder corresponds to the DICOPT taking an average processing time of 1,40 s, which is fastest than any heuristic optimization approach. Figure 3 reports the final solution reached by GAMS, where lines *d* and *f* have been disconnected, and lines *c* and *e* are introduced in the final solution. The last power losses are 124,420 kW, which implies a reduction of about 44, 17% regarding the base case.

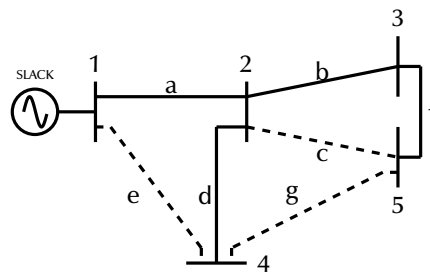
Algorithm 1 Implementation of the reconfiguration problem in the 5-node test feeder

```

1 SETS
2 k Set of nodes /N1*N5/
3 l Set of braches /a,b,c,d,e,f,g/
4 g Set of conv. generators /G1/
5 map(g,k) Association nodes-gen /G1.N1/;
6 SCALARS
7 Vmin Minimum voltage [pu] /0.90/
8 Vmax Maximum voltage [pu] /1.10/
9 TABLE LOAD(k,*) Active and reactive power loads [kVA]
10 Pd Qd
11 N1 0 0
12 N2 1.625 0.520
13 N3 2.250 0.745
14 N4 2.265 0.896
15 N5 1.450 1.000;
16 TABLE A(k,l)
17 a b c d e f g
18 N1 1 0 0 0 1 0 0
19 N2 -1 1 1 1 0 0 0
20 N3 0 -1 0 0 0 1 0
21 N4 0 0 0 -1 -1 0 1
22 N5 0 0 -1 0 0 -1 -1;
23 TABLE LINES(l,*) [Ohm]
24 Rl Xl
25 a 0.001959366391185 0.002368572084481
26 b 0.003711547291093 0.003472796143251
27 c 0.001457759412305 0.003171487603306
28 d 0.001417011019284 0.004620064279155
29 e 0.004731978879706 0.005541781450872
30 f 0.000875229568411 0.002619949494949
31 g 0.002036271808999 0.003951446280992;
32 VARIABLES
33 z Objective function value
34 v(k) Voltage magnitude at node k.
35 vr(k) Real part of the voltage at node k.
36 vi(k) Imag. part of the voltage at node k.
37 l(l) Current maginitude in brach l.
38 lr(l) Real part of the current in brach l.
39 li(l) Imag. part of the current in brach l.
40 Pg(g) Active power generation in the Conv. Gen.
41 Qg(g) Reactive power generation in the Conv. Gen.
42 BINARY VARIABLES
43 y(l) Selection of the branch l.;
44 v.lo(k) = Vmin; v.up(k) = Vmax; vr.lo(k) = Vmin/2; vi.fx('N1') = 0; vr.fx('N1') = 1;
45 EQUATIONS
46 ObjFun Objective function
47 BalP(k) Active power balance per node.
48 BalQ(k) Active power balance per node.
49 Curr(l) Real current in branch l.
50 Curi(l) Imag. current in branch l.
51 Cur(l) Magnitude of the current in branch l.
52 Vol(k) Magnitude of the voltage.
53 NLines Number of lines;
54 ObjFun.. z =E= sum(l,LINES(l,'Rl')*sqr(l(l)));
55 BalP(k).. SUM(g$map(g,k),Pg(g))-LOAD(k,'Pd')=E= SUM(l,A(k,l)*(vr(k)*lr(l) + vi(k)*li(l)));
56 BalQ(k).. SUM(g$map(g,k),Qg(g))-LOAD(k,'Qd')=E= -SUM(l,A(k,l)*(vr(k)*li(l) - vi(k)*lr(l)));
57 Curr(l).. lr(l) =E= (y(l)/(sqr(LINES(l,'Rl')) + sqr(LINES(l,'Xl'))))*SUM(k,A(k,l)*(LINES(l,'Rl')*vr(k)
+ LINES(l,'Xl')*vi(k)));
58 Curi(l).. li(l) =E= (y(l)/(sqr(LINES(l,'Rl')) + sqr(LINES(l,'Xl'))))*SUM(k,A(k,l)*(LINES(l,'Rl')*vi(k)
- LINES(l,'Xl')*vr(k)));
59 Vol(k).. v(k) =E= sqrt(sqr(vr(k)) + sqr(vi(k)));
60 Cur(l).. l(l) =E= sqrt(sqr(lr(l)) + sqr(li(l)));
61 NLines.. SUM(l,y(l)) =E= card(k) - 1;
62 MODEL Reconfiguration /ALL/;
63 SOLVE Reconfiguration us MINLP min z;
64 DISPLAY z.l, pg.l, y.l, v.l, vr.l, vi.l, l.l;

```

Source: Authors



Source: Authors

Figure 2. 5-node test system to illustrate the AC reconfiguration problem

Source: Authors

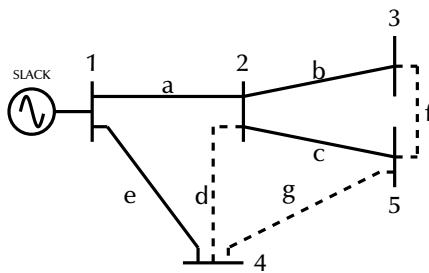


Figure 3. 5-node test system solution after optimal reconfiguration

Source: Authors

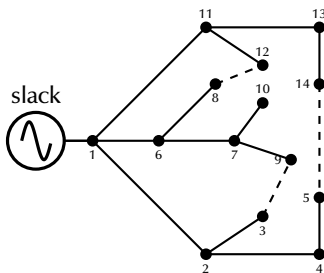


Figure 4. Electrical configuration of a radial distribution network

Source: Authors

It is important to mention that the implementation reported in Algorithm 1 can be applied to any AC distribution networks, regardless of the number of nodes and candidate lines, since it presents a compact structure for optimization, which is one of the most important and largely-known advantages of the GAMS software (Soroudi, 2017).

Numerical validation

In this section, in order to demonstrate the efficiency of the proposed approach for the optimal reconfiguration of AC distribution systems, the classical medium voltage distribution network composed by 14-nodes and 16 lines reported in (Tapia-Juárez and Espinosa-Juárez, 2013) is employed (Figure 4). This system is operated at 23 kV, and the based power is assumed to be 1 000 kVA. The initial active power losses for this test feeder are 512,165 kW. The information on the connected and candidate branches is reported in Table 3, and the load information is listed in Table 4.

Table 3. Branches information for the 14-node test feeder

Node i	Node j	Resistance [Ω]	Reactance [Ω]
Connected lines			
1	2	0,39675	0,5290
2	3	0,4232	0,5819
2	4	0,4761	0,9522
4	5	0,2116	0,2116
1	6	0,5819	0,5819
6	7	0,4232	0,5819
6	8	0,5819	0,5819
7	9	0,5819	0,5819
7	10	0,4232	0,5819
1	11	0,5819	0,5819
11	12	0,4761	0,6348
11	13	0,4232	0,5819
13	14	0,2116	0,2116
Tie lines			
3	9	0,2116	0,2116
8	12	0,2116	0,2116
5	14	0,4761	0,6348

Source: Authors

Table 4. Load information for the 14-node test feeder

Node	Active power [kW]	Reactive power [kVAr]
1	0,00	0,00
2	2 000	1 600
3	3 000	400
4	2 000	-400
5	1 500	1 200
6	4 000	2 700
7	5 000	1 800
8	1 000	900
9	600	-400
10	4 500	-1 700
11	1 000	900
12	1 000	-1 100
13	1 000	900
14	2 100	-800

Source: Authors

In this test system, we evaluate three simulation cases as follows:

- ✓ **Scenario 1 (S1):** The reconfiguration of this test feeder considering that all the tie lines are initially disconnected.

- ✓ **Scenario 2 (S2):** The reconfiguration of this test feeder considering the presence of a distributed generator at node 8 with a capacity of 10 MW operated with unity power factor.
- ✓ **Scenario 3 (S3):** The reconfiguration of this test feeder considering the presence of a large-scale capacitor compensation at node 6 with a size of 6 MVar.

Note that the first simulation scenario is the typical simulation case explored in the specialized literature for the optimal reconfiguration of the 14-node test feeder using metaheuristic techniques (Verma and Singh, 2018).

Table 5 presents the solution of the reconfiguration problem in the 14-node test feeder considering **S1**, where GA means genetic algorithm (Su et al., 2005), ACSA means ant colony search algorithm (Su et al., 2005), GAST means genetic algorithms based on spanning trees (Zhang et al., 2014), and MCA means modified culture algorithm (Verma and Singh, 2018). It is worth mentioning that Verma and Singh (2018) claim an optimal value of about 462 kW regarding power losses. However, this is not possible for this system, since, when we evaluated their solution, it turned out to be 466,47 kW.

From the results in Table 5, we can note the following. *i)* All the comparative methodologies, as well as the proposed MINLP model, solved in GAMS reach the same optimal solution (466,467 kW), which corresponds to a reduction of about 8,89% with respect to the base case. *ii)* Of the methods identified in the state of the art for the comparative analysis, none recorded the total calculation time. The state of the art was reviewed according to this work's contribution, objective, and motivation. It is relevant to highlight that the methods studied in this research are not the only strategies available for the optimal reconfiguration of radial networks. Therefore, it is likely that other solution methods do include runtime analysis. In the case of the proposed approach, this takes about 11,560 s, which is a short time for solving MINLP models. This is important since the utility can make multiple simulations before making a final decision regarding investment and grid intervention. *iii)* The solution reached by the GAMS package is obtained by using an interior-point optimization method combined with the branch and bound strategy, which makes it efficient in terms of quality response and computational effort (Kaur et al., 2014; Montoya et al., 2020c).

In the case of **S2**, the initial power losses considering the operation of the distributed generator with 10 MW with the initial topology of the system presented in Figure 4 are 364,057 kW. Once the mathematical formulation is solved by the GAMS package, the final power losses are 339,133 kW, which implies an improvement regarding power losses of about 24,924 kW. To reach this solution, the set of the disconnected lines are {4 – 5, 7 – 9, 11 – 12}, which is a solution found in approximately 15,50 s. This implies that the presence of the distributed generator does not significantly affect the complexity of the optimization problem under study in terms of the processing times.

As for **S3**, the initial power losses considering the initial topology depicted in Figure 4 and a capacitive compensation of 6 MVar at node 6 are 500,697. Once the proposed methodology for optimal reconfiguration in AC networks

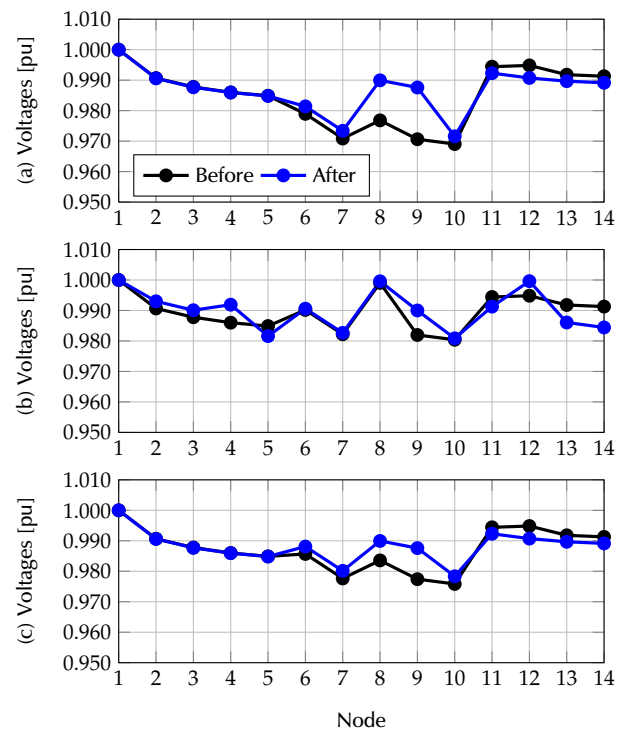


Figure 5. Voltage behavior in the nodes of the 14-node test feeder for each one of the simulation scenarios: (a) **S1**, (b) **S2**, and (c) **S3**

Source: Authors

is solved through GAMS, the resulting power losses are 463,039 kW, which means a reduction of 7,52% with respect to the initial case. Note that the disconnected lines are {6 – 8, 7 – 9, 5 – 14}, which agrees with the optimal solution for **S1**. In this problem, the GAMS package takes about 6 s to find the optimal solution, which confirms its effectiveness at analyzing complex MINLP models (Soroudi, 2017).

Remark 2. Note that the punctual injection of active and reactive power in specific nodes significantly influences the power loss behavior of the network, as it can be observed in the initial cases of **S2** and **S3**. However, the reconfiguration strategy applied to the test system considering these distributed energy resources can also help mitigate the negative effects produced by excessive injections of active and reactive power into the grid.

Figure 5 reports the voltage profiles for the 14-node test feeder in all the simulation scenarios including their base cases.

From Figure 5, we can observe that *i)* the reconfiguration of the AC distribution network allows improving the average voltages in all the nodes of the system, given that the reduction of power losses translates into lower voltage drops. Nevertheless, this does not imply that the worst voltage profile will improve, since the mathematical model presented in this paper is strongly nonlinear and non-convex, as seen in Figure 5b. *ii)* The presence of distributed generation and/or capacitor banks has a higher impact on the voltage profiles of the network (compare Figures 5b and 5c with 5a), which is expected in distribution networks since these largely modify the total power injection in the substation, whereas reconfiguration only redistributes those fluxes in a better way, regardless of the presence of shunt

Table 5. Solutions for S1

Method	Power losses [kW]	Disconnected lines	Proc. Time [s]
GA	466,470	{6 – 8, 7 – 9, 5 – 14}	–
ACSA	466,470	{6 – 8, 7 – 9, 5 – 14}	–
GAST	466,470	{6 – 8, 7 – 9, 5 – 14}	–
MCA	466,470	{6 – 8, 7 – 9, 5 – 14}	–
GAMS	466,467	{6 – 8, 7 – 9, 5 – 14}	11,560

Source: Authors

elements, *i.e.*, distributed generators and/or capacitor banks. *iii)* The reconfiguration of the network has positive impacts since it allows for further reduction in power losses, thus making it attractive for utilities regarding power quality and regulatory benefits via billing, as is the case of Colombian companies (Sánchez-Zuleta *et al.*, 2017).

Remark 3. *The effect of current constraints (6) and (8) can be considered for optimal reconfiguration in AC distribution networks if there is information available regarding the maximum thermal capabilities of the existing and tie lines, since the proposed rectangular representation of this problem allows evaluating it easily, due to the fact that our model is defined as a function of the branch currents, which implies that the information of the current magnitudes in all the branches is always available.*

In order to provide enough information to analyze the current flows in the 14-node test feeder, Table 6 presents the current magnitudes in this test system for each of the simulation scenarios.

From the results in Table 6, we can observe that each one of the reconfiguration planes provided by each simulation scenario effectively helps to redistribute the current flow in all the lines, which is directly connected to the power loss improvement. For example, in S1, if it is supposed that lines 1–6 have a current rate of 700 A, then, its loadability is about 98,95% in the initial case. Nevertheless, after the application of the reconfiguration strategy, the final loadability is about 88,03%, implying a liberation of capability of 10%, which can be used in the case of loads attended by this line that report increments in the near future. However, the discharge in this distribution line implies a loadability increment in some other lines to guarantee that the amount of power provided to the loads is satisfied. However, these increments in some lines are not a negative effect, since the global behavior of the network demonstrates that the power losses are reduced. This behavior is attributable to the nonlinear properties of the optimization problem analyzed in this research. Note that similar analyses can be made for S2 and S3 regarding their base cases.

Conclusions and future work

This paper proposes a new mathematical formulation to model the problem of the optimal reconfiguration of AC distribution feeders based on a rectangular representation of the voltage and current variables in nodes and branches, respectively. Due to the nature of the MINLP model's results, the GAMS package was selected as solution methodology since the main focus of this paper was indeed the mathematical formulation, not the solution technique. We presented the methodology in the style of a tutorial to

help engineering students understand the real complexity of the reconfiguration problem in AC distribution feeders.

The numerical results in the case under study (14-node test feeder) for all the simulation scenarios demonstrated that the reconfiguration of the system (modification of the topology) has positive impacts regarding power losses minimization, regardless of the presence of distributed energy resources in the grid, *i.e.*, distributed generators and/or capacitor banks. This implies that the proposed approach is suitable to be extended to electrical distribution networks with batteries and economic dispatch multi-period environments.

There is an alternative way to represent the reconfiguration problem in AC networks by using the magnitude of the nodal voltages and their angles. Nevertheless, that approach introduces complex characteristics in the model concerning trigonometric functions that relate voltages and currents in the power balance constraints. Said approach is less efficient than the rectangular representation proposed in this paper. It can multiply the possibilities of getting stuck in the local optimums, primarily when packages such as GAMS are used as solution methodology.

This work analyzes the problem of optimal reconfiguration in distribution networks using variables as electrical parameters, specifically power, voltage, and current. As future work, in the area of optimization for power systems, several variables can be implemented in the objective function and the constraints model. Likewise, criteria associated with social impacts can be included, thus allowing to analyze how the reconfiguration of networks, the inclusion of renewable energy sources, the implementation of storage systems, and others contribute to sustainable development.

References

- Aguado, J., de la Torre, S., and Triviño, A. (2017). Battery energy storage systems in transmission network expansion planning. *Electric Power Systems Research*, 145, 63-72. <https://doi.org/10.1016/j.epsr.2016.11.012>
- Ahuja, A., and Pahwa, A. (2005). Using ant colony optimization for loss minimization in distribution networks. In IEEE (Eds.) *Proceedings of the 37th Annual North American Power Symposium* (pp. 470-474). IEEE. <https://doi.org/10.1109/NAPS.2005.1560562>
- Amin, W. T., Montoya, O. D., and Grisales-Noreña, L. F. (2019). Determination of the voltage stability index in DC Networks with CPLs: A GAMS implementation. In J. Figueroa-García, M. Duarte-González, S. Jaramillo-Isaza, A. Orjuela-Caño, and Y. Díaz-Gutiérrez (Eds.) *Applied Computer Sciences in Engineering. WEA 2019. Communications in Computer and Information Science* (vol. 1052, pp.

Table 6. Current behavior in the 14-node test system

Node		S1		S2		S3	
<i>i</i>	<i>j</i>	Before	After	Before	After	Before	After
1	2	394,1332	414,5480	394,1332	337,6734	394,1332	414,5480
2	3	133,2162	158,4840	133,2162	158,0997	133,2162	158,4840
2	4	158,3968	158,4072	158,3968	89,4029	158,3968	158,4072
4	5	84,8000	84,8056	84,8000	—	84,8000	84,8056
1	6	692,6546	616,1869	279,5282	277,4053	680,2022	613,2501
6	7	453,3914	425,2542	448,1370	421,2268	450,2295	422,3069
6	8	59,8829	—	393,6306	348,0422	59,4720	—
7	9	32,3017	—	31,9286	—	32,0772	—
7	10	215,8304	215,2670	213,3294	213,2291	214,3254	213,7757
1	11	223,5337	270,2963	223,5337	265,6106	223,5337	270,2963
11	12	64,9702	88,2380	64,9702	—	64,9702	88,2380
11	13	136,0605	136,3538	136,0605	211,2690	136,0605	136,3538
13	14	98,5651	98,7775	98,5651	160,1499	98,5651	98,7775
3	9	—	31,7464	—	31,6694	—	31,7464
8	12	—	59,0878	—	64,6598	—	59,0878
5	14	—	—	—	85,0858	—	—

Source: Authors

- 552-564). Springer. https://doi.org/10.1007/978-3-030-31019-6_46
- Anders, G. J. (1994). Minimization of losses in transmission and distribution systems, integrated electricity resource planning. In A. T. de Almeida, A. H. Rosenfeld, J. Roturier, and J. Norgard (Eds.) *Integrated Electricity Resource Planning. NATO ASI Series (Series E: Applied Sciences)* (vol. 261, pp. 297-328). Springer. https://doi.org/10.1007/978-94-011-1054-9_17
- Arya, A., Kumar, Y., and Dubey, M. (2011). Reconfiguration of electric distribution network using modified particle swarm optimization. *International Journal of Computer Applications*, 34(6), 54-62. <https://doi.org/10.5120/4131-5994>
- Augugliaro, A., Dusonchet, L., Ippolito, M. G., and Riva-Sanseverino (2004). A new formulation of the optimal compensation and reconfiguration problem including minimum load nodes unavailability for automated distribution networks. *COMPEL - The International Journal for Computation and Mathematics in Electrical and Electronic Engineering*, 23(1), 104-118. <https://doi.org/10.1108/03321640410507581>
- Azghandi, M. N., Shojaei, A. A., Toosi, S., and Lotfi, H. (2021). Optimal reconfiguration of distribution network feeders considering electrical vehicles and distributed generators. *Evolutionary Intelligence*, 2021, s12065-021-00641-7. <https://doi.org/10.1007/s12065-021-00641-7>
- Babu, P. V. and Singh, S. (2016). Optimal placement of DG in distribution network for power loss minimization using NLP and PLS technique. *Energy Procedia*, 90, 441-454. <https://doi.org/10.1016/j.egypro.2016.11.211>
- Celli, G., Pilo, F., Pisano, G., Allegranza, V., Cicoria, R., and Iaria, A. (2004, October 10-13). *Meshed vs. radial MV distribution network in presence of large amount of DG* [Conference presentation]. IEEE PES Power Systems Conference and Exposition, New York, NY, USA. <https://doi.org/10.1109/PSCE.2004.1397664>
- Civanlar, S., Grainger, J. J., Yin, H., and Lee, S. S. H. (1988). Distribution feeder reconfiguration for loss reduction. *IEEE Transactions on Power Delivery*, 3(3), 1217-1223. <https://doi.org/10.1109/61.193906>
- Cruz, M., Fitiwi, D., Santos, S., Mariano, S., and Catalão, J. (2018). Prospects of a meshed electrical distribution system featuring large scale variable renewable power. *Energies*, 11(12), 3399. <https://doi.org/10.3390/en11123399>
- Elsheikh, A., Helmy, Y., Abouelseoud, Y., and Elsherif, A. (2014). Optimal capacitor placement and sizing in radial electric power systems. *Alexandria Engineering Journal* 53(4), 809-816. <https://doi.org/10.1016/j.aej.2014.09.012>
- Gallego-Londoño, J. P., Montoya-Giraldo, O. D., Hincapié-Isaza, R. A., and Granada-Echeverri, M. (2016). Ubicación óptima de reconectores y fusibles en sistemas de distribución. *ITECKNE*, 13(2), 113-126. <https://doi.org/10.15332/iteckne.v13i2.1476>
- García-Martínez, S. and Espinosa-Juárez, E. (2013). Optimal reconfiguration of electrical networks by applying tabu search to decrease voltage sag indices. *Electric Power Components and Systems*, 41(10), 943-959. <https://doi.org/10.1080/15325008.2013.801053>
- Gil-González, W., Montoya, O. D., Grisales-Noreña, L. F., Perea-Moreno, A. J., and Hernández-Escobedo, Q. (2020). Optimal placement and sizing of wind generators in AC grids considering reactive power capability and wind speed curves. *Sustainability*, 12(7), 2983. <https://doi.org/10.3390/su12072983>
- González, A., Echavarren, F., Rouco, L., Gómez, T., and Cabetas, J. (2012). Reconfiguration of largescale distribution networks for planning studies. *International Journal of Electrical Power & Energy Systems*, 37(1), 86-94. <https://doi.org/10.1016/j.ijepes.2011.12.009>
- Grisales-Noreña, L. F., Restrepo-Cuevas, B. J., and Jaramillo-Ramírez, F. E. (2017). Ubicación y dimensionamiento de generación distribuida: una revisión. *Ciencia e Ingeniería Neogranadina*, 27(2), 157-176. <https://doi.org/10.18359/rcin.2344>
- Grisales-Noreña, L. F., González-Montoya, D., and Ramos-Paja, C. A. (2018). Optimal sizing and location of distributed generators based on PBIL and PSO techniques. *Energies* 11(4), 1018. <https://doi.org/10.3390/en11041018>
- Grisales-Noreña, L., Montoya, O. D. and Gil-González, W. (2019). Integration of energy storage systems

- in AC distribution networks: Optimal location, selecting, and operation approach based on genetic algorithms. *Journal of Energy Storage*, 25, 100891. <https://doi.org/10.1016/j.est.2019.100891>
- Izadi, M., Safdarian, A., Moeini-Aghtaie, M., and Lehtonen, M. (2019). Optimal placement of protective and controlling devices in electric power distribution systems: A MIP model. *IEEE Access*, 7, 122827-122837. <https://doi.org/10.1109/ACCESS.2019.2938193>
- Jafar-Nowdeh, A., Babanezhad, M., Arabi-Nowdeh, S., Naderipour, A., Kamyab, H., Abdul-Malek, z. and Ramachandramurthy, V. K. (2020). Meta-heuristic matrix moth{flame algorithm for optimal reconfiguration of distribution networks and placement of solar and wind renewable sources considering reliability. *Environmental Technology & Innovation*, 20, 101118. <https://doi.org/10.1016/j.eti.2020.101118>
- Kaur, S., Kumbhar, G., and Sharma, J. (2014). A MINLP technique for optimal placement of multiple DG units in distribution systems. *International Journal of Electrical Power & Energy Systems*, 63, 609-617. <https://doi.org/10.1016/j.ijepes.2014.06.023>
- Lavorato, M., Franco, J. F., Rider, M. J., and Romero, R. (2012). Imposing radiality constraints in distribution system optimization problems. *IEEE Transactions on Power Systems*, 27(1), 172-180. <https://doi.org/10.1109/TPWRS.2011.2161349>
- Marneni, A., Kulkarni, A., and Ananthapadmanabha, T. (2015). Loss reduction and voltage profile improvement in a rural distribution feeder using solar photovoltaic generation and rural distribution feeder optimization using HOMER. *Procedia Technology*, 21, 507-513. <https://doi.org/10.1016/j.protcy.2015.10.036>
- Montoya, O. D., Garcés, A., and Castro, C. A. (2018). Optimal conductor size selection in radial distribution networks using a mixed-integer nonlinear programming formulation. *IEEE Latin America Transactions*, 16(8), 2213-2220. <https://doi.org/10.1109/TLA.2018.8528237>
- Montoya, O. D., Gil-González, W., and Grisales-Noreña, L. (2020a). An exact MINLP model for optimal location and sizing of DGs in distribution networks: A general algebraic modeling system approach. *Ain Shams Engineering Journal*, 11(2), 409-418. <https://doi.org/10.1016/j.asej.2019.08.011>
- Montoya, O. D., Gil-González, W. and Rivas-Trujillo, E. (2020b). Optimal location reallocation of battery energy storage systems in DC microgrids. *Energies*, 13(9), 2289. <https://doi.org/10.3390/en13092289>
- Montoya, O. D., Grisales-Noreña, L. F., Gil-González, W., Alcalá, G., and Hernández-Escobedo, Q. (2020c). Optimal location and sizing of PV sources in DC networks for minimizing greenhouse emissions in diesel generators. *Symmetry*, 12(2), 322. <https://doi.org/10.3390/sym12020322>
- Naghiloo, A., Abbaspour, M., Mohammadi-Ivatloo, B., and Bakhtari, K. (2015). GAMS based approach for optimal design and sizing of a pressure retarded osmosis power plant in Bahmanshir river of Iran. *Renewable and Sustainable Energy Reviews*, 52, 1559-1565. <https://doi.org/10.1016/j.rser.2015.08.018>
- Pakdel, M. J. V., Sohrabi, F., and Mohammadi-Ivatloo, B. (2020). Multiobjective optimization of energy and water management in networked hubs considering transactive energy. *Journal of Cleaner Production*, 266, 121936. <https://doi.org/10.1016/j.jclepro.2020.121936>
- Quintero-Durán, M. J., Candelo-Becerra, J. E., and Cabana-Jiménez, K. (2019). Distribution network reconfiguration with large number of switches solved by a modified binary bat algorithm and improved seed population. *Tehnicki vjesnik*, 26(5), 1284-1291. <https://doi.org/10.17559/TV-20180525204445>
- Sambaiah, K. S. and Jayabarathi, T. (2021). Optimal reconfiguration and renewable distributed generation allocation in electric distribution systems. *International Journal of Ambient Energy*, 42, 1018-1031. <https://doi.org/10.1080/01430750.2019.1583604>
- Sánchez-Zuleta, C. C., Fernandez-Gutiérrez, J. P., and Piedrahita-Escobar, C. C. (2017). Identification of the characteristics incident to the detection of nontechnical losses for two Colombian energy companies. *Revista Facultad de Ingeniería Universidad de Antioquia*, 84, 60-71. <https://doi.org/10.17533/udea.redin.n84a08>
- Shokouhi, M., Shojaeian, S., and Lotfi, M. (2017). Reconfiguration and capacitor allocation in distribution systems to reduce power losses and improve voltage profiles using ant lion algorithm. *International Journal of Digital Application & Contemporary Research*, 5(12), 1-6. http://ijdacr.com/uploads/papers/Shokouhi_51200-17-105.pdf
- Soroudi, A. (2017). *Power system optimization modeling in GAMS*. Springer. <https://doi.org/10.1007/978-3-319-62350-4>
- Su, C. T., Chang, C. F., and Chiou, J. P. (2005). Distribution network reconfiguration for loss reduction by ant colony search algorithm. *Electric Power Systems Research*, 75(2-3), 190-199. <https://doi.org/10.1016/j.epsr.2005.03.002>
- Sultana, S. and Roy, P. K. (2015). Oppositional krill herd algorithm for optimal location of distributed generator in radial distribution system. *International Journal of Electrical Power & Energy Systems*, 73, 182-191. <https://doi.org/10.1016/j.ijepes.2015.04.021>
- Tandon, A. and Saxena, D. (2014, December 26-28). *Optimal reconfiguration of electrical distribution network using selective particle swarm optimization algorithm* [Conference presentation]. 2014 International Conference on Power, Control and Embedded Systems (ICPCES), Allahabad, India. <https://doi.org/10.1109/ICPCES.2014.7062806>
- Tapia-Juárez, R., and Espinosa-Juárez, E. (2013, November 13-15). *Multiobjective reconfiguration of radial distribution networks considering voltage sags* [Conference presentation]. 2013 IEEE International Autumn Meeting on Power Electronics and Computing (ROPEC), Morelia, Mexico. <https://doi.org/10.1109/ROPEC.2013.6702754>
- Tartibu, L., Sun, B., and Kaunda, M. (2015). Multiobjective optimization of the stack of a thermoacoustic engine using GAMS. *Applied Soft Computing*, 28, 30-43. <https://doi.org/10.1016/j.asoc.2014.11.055>
- The, T. T., Ngoc, D. V., and Anh, N. T. (2020). Distribution network reconfiguration for power loss reduction and voltage profile

- improvement using chaotic stochastic fractal search algorithm. *Complexity*, 2020, 2353901. <https://doi.org/10.1155/2020/2353901>
- Vargas-Robayo, C. Y. and Blanco-Valbuena, D. F. (2021). Evaluación de modelos de programación lineal y no lineal para la planeación de sistemas de transmisión en el software GAMS. (69), 16-50. <https://doi.org/10.14483/22487638.17957>
- Verma, H. K. and Singh, P. (2018). Optimal reconfiguration of distribution network using modified culture algorithm. *Journal of The Institution of Engineers (India): Series B*, 99(6), 613-622. <https://doi.org/10.1007/s40031-018-0344-6>
- Xiaozhi, G., Linchuan, L., and Hailong, X. (2010). Network reconfiguration at the distribution system with distributed generators. In K. Li, M. Fei, L. Jia, and G. W. Irwin (Eds.) *Life System Modeling and Intelligent Computing. ICSEE 2010, LSMS 2010. Lecture Notes in Computer Science* (vol. 6329, pp. 400-409). https://doi.org/10.1007/978-3-642-15597-0_44
- Zhang, J., Yuan, X., and Yuan, Y. (2014). A novel genetic algorithm based on all spanning trees of undirected graph for distribution network reconfiguration. *Journal of Modern Power Systems and Clean Energy*, 2(2), 143-149. <https://doi.org/10.1007/s40565-014-0056-0>

An Efficient Algorithm Applied to Optimized Billing Sequencing

Un algoritmo eficiente aplicado a la secuencia de facturación optimizada

Anderson Rogério Faia Pinto¹ and Marcelo Seido Nagano²

ABSTRACT

This paper addresses the Optimized Billing Sequencing (OBS) problem to maximize billing of the order portfolio of a typical Distribution Center (DC). This is a new problem in the literature, and the search for the best billing mix has generated demands for better optimization methods for DCs. Therefore, the objective of this paper is to provide an effective algorithm that presents quick and optimized solutions for higher-complexity OBS levels. This algorithm is called Iterative Greedy Algorithm (IGA-OBS), and its performance is compared to the genetic algorithm (GA-OBS) by Pinto and Nagano. Performance evaluations were carried out after intense computational experiments for problems with different complexity levels. The results demonstrate that the GA-OBS is limited to medium-size instances, whereas the IGA-OBS is better adapted to reality, providing OBS with solutions with satisfactory time and quality. The IGA-OBS enables managers to make decisions in a more agile and consistent way in terms of the trade-off between the level of customer service and the maximization of the financial result of DCs. This paper fills a gap in the literature, makes innovative contributions, and provides suggestions for further research aimed at developing more suitable optimization methods for OBS.

Keywords: iterative greedy algorithm, genetic algorithm, maximized billing, distribution center

RESUMEN

Este documento aborda el problema de la Secuenciación Optimizada de Facturación (OBS) para maximizar la facturación de la cartera de pedidos de un centro de distribución (CD) típico. Este es un nuevo problema en la literatura, y la búsqueda de la mejor combinación de facturación ha exigido mejores métodos para optimizar los CD. Por lo tanto, el objetivo de este artículo es proporcionar un algoritmo eficaz que presente soluciones rápidas y optimizadas para niveles más altos de complejidad OBS. Este algoritmo se denomina Algoritmo Voraz Iterativo (IGA-OBS) y su rendimiento se compara con el del algoritmo genético (GA-OBS) de Pinto y Nagano. Se llevaron a cabo evaluaciones de desempeño después de intensos experimentos computacionales para problemas con diferentes niveles de complejidad. Los resultados demuestran que el GA-OBS se limita a instancias de tamaño medio, mientras que el IGA-OBS se adapta mejor a la realidad brindando soluciones en tiempo y calidad satisfactorias a OBS. El IGA-OBS permite a los gerentes tomar decisiones de una manera más ágil y consistente frente al *trade-off* entre el nivel de servicio al cliente y la maximización del resultado financiero de los CD. Este artículo llena un vacío en la literatura, aporta contribuciones innovadoras y proporciona sugerencias para futuras investigaciones destinadas a desarrollar métodos de optimización más adecuados para OBS.

Palabras clave: algoritmo voraz iterativo, algoritmo genético, facturación maximizada, centro de distribución

Received: November 6th, 2019

Accepted: July 6th, 2021

Introduction

During the last decades, most companies have started to aim for large production and distribution volumes focusing on reducing lead times and inventory (van den Berg and Zijm, 1999; Richards, 2011; Haq and Boddu, 2017). The majority of customers, according to Pinto and Nagano (2020), have reduced the size of their orders and started to place them in shorter time intervals and minimum amounts of multiple Stock Keeping Units (SKUs) in their Distribution Centers (DCs). This tendency has resulted in shorter order fulfillment deadlines, and, consequently, it has started to demand greater process agility in DCs (Seyedrezaei et al., 2012; Matthews and Visagie, 2013; Marchet et al., 2015). The fact is that there are still no tools that can foresee the exact demand volume for dynamic stochastic environments in an unequivocal way (Seyedrezaei et al., 2012; Sereshi and Bijari, 2013; Baud-Lavigne et al., 2014). The option to

maintain minimum levels in uncertain scenarios can cause, at a given billing moment, some SKU restrictions in the DC (Pinto et al., 2018). Additionally, most customers do not accept billings or receiving partial purchases, for example,

¹ Ph.D. in Production Engineering, São Carlos School of Engineering, University of São Paulo, Brazil. Affiliation: Professor and Senior Researcher, Production Engineering Department, University of Araraquara, Brazil. E-mail: anderson@life.com.br

² Ph.D. in Mechanical Engineering, São Carlos School of Engineering, University of São Paulo, Brazil. Affiliation: Associate Professor and Senior Researcher, São Carlos School of Engineering, University of São Paulo, Brazil. E-mail: drnagano@usp.br

How to cite: Pinto, A. R. F., and Nagano, M. S. (2022). An Efficient Algorithm Applied to Optimized Billing Sequencing. *Ingeniería e Investigación*, 42(2), e83394. <http://doi.org/10.15446/ing.investig.v42n2.83394>



Attribution 4.0 International (CC BY 4.0) Share - Adapt

in the e-commerce sector (Rim and Park, 2008). This fault will result in conflicting orders and the need to determine billing and fulfilment rankings for these SKUs (Rim and Park, 2008; Slotnick, 2011; Seyedrezaei *et al.*, 2012; Huang and Ke, 2017; Ledari *et al.*, 2018; Leung *et al.*, 2018; Boysen *et al.*, 2019; Pinto and Nagano, 2020). In this sense, this paper addresses a specific decision-making problem to maximize billing, which is called Optimized Billing Sequencing (OBS). This problem was initially approached by Pinto *et al.* (2018) and refers to the optimization of the billing processes of the order portfolio in a typical DC. In practice, OBS problems are usually very complex, and the pressure to maximize results and meet delivery deadlines demands agility in finding the best solution. However, dealing with a set of rules, restrictions, and decision variables without the help of a suitable quantitative tool becomes a complex task when the objective is to optimize the OBS. Fast decision-making based solely on experience or feeling may lead to waste of time and financial losses in the DC (Pinto *et al.*, 2018). The literature, however, is insufficient and does not provide optimization methods (OMs) that can arrive at time and quality solutions that are satisfactory to all OBS instances. The available research neglects important practical aspects or offers lengthy solutions that constitute limitations for DCs. Therefore, there is a demand for OMs that are more robust and suited for the reality of DCs, which basically consist of achieving two OBS targets: OM robustness and practical application in DCs. Thus, this paper focusses on adapting to real world demands in order to deal with practical dilemmas not yet addressed by the OMs proposed for OBS. The entire OBS configuration under study is the same as the one considered by Pinto and Nagano (2020). In this sense, the amount of available inventory for billing is always controlled at minimum levels based on SKU demands. There are therefore some uncertainties regarding the management of the demand, which is stochastic, and billings occur based on Variable Time Windows (VTW). Most delivery deadlines are tighter, and there is a high frequency of small orders containing minimum amounts of multiple SKUs. Billing decisions prioritize order fulfilment and payment dates by the Earliest Due Date (EDD) rule. The proposed approach aims to enable managers to make decisions in a more agile and consistent way regarding the trade-off between the level of customer service and the financial result maximization of the aforementioned DCs. Thus, the objective of this paper is to provide an efficient billing maximization algorithm that, in an agile and consistent manner, produces optimized solutions for higher levels of OBS complexity. This algorithm is called Iterative Greedy Algorithm (IGA-OBS), and its performance is compared to the genetic algorithm (GA-OBS) by Pinto and Nagano (2020). In technical terms, the latter is an extension and improvement of the first GA-OBS that was proposed in the literature by Pinto *et al.* (2018), whereas, in methodological terms, this is a quantitative research based on mathematical modeling and computational simulation. Performance evaluations of the IGA-OBS in this work are carried out by means of intense computational experiments for a set of problems with different OBS complexity levels.

We have focused our attention on the potential of IGA-OBS/GA-OBS for practical effectiveness and their capacity to adapt to the reality of current DCs. This paper is structured as follows: section 2 explains the OBS problem; section 3 presents the Literature review; section 4 expresses the model formulation of the OBS; section 5 presents the IGA-OBS; section 6 demonstrates the GA-OBS; section 7 brings the computational experiments and the performance assessments of the GA-OBS and the IGA-OBS; finally, the last section states the final considerations and the main suggestions for future studies and approaches to the OBS.

OBS problem

This section presents the OBS problem to maximize the billing of a typical DC. In this OBS, there are uncertainties regarding the management of the demand, which is stochastic, and SKU inventories available for billing are controlled at minimum levels in the DC. It is common for customers to place more than one order simultaneously, which constitutes a dynamic (online) input in the order portfolio regardless of SKU availability. These orders may have varied sizes and different quantities, or distinct unit selling prices for multiple combinations of different SKUs or of the same SKU. Most customers demand tighter delivery deadlines for a set of orders with multiple fulfilment and payment dates for a given VTW. Billing sequences are determined by analyzing the best combinations between fulfilment and payment dates, which are always prioritized by the EDD rule. All billings are generated after a certain number of orders accumulates in the order portfolio, which also occurs within time intervals pre-set by the VTW. Demands with partial inventory restrictions are billed according to customer approval, and those referring to total restrictions are billed when the SKUs are available. Every order that is not billed due to SKU restrictions is transferred to the following VTW until the quantities of the mentioned SKUs are available in the DC. Therefore, the OBS problem is caused by restrictions or management failures resulting from the dynamics of changes, uncertainties, and disorders, in addition the pressing emergency in the reality of current DCs (Pinto *et al.*, 2018). Decisions are usually made based on fulfillment rankings pre-defined by internal policies, which include a set of rules, constraints, and decision variables inherent to the OBS. In the literature, the mechanism to determine which SKUs are billed for each order was classified by Pinto *et al.* (2018) as a variation of the Knapsack Problem (KP). Thus, the OBS may be reduced to a decision-making problem, for which the ideal solution is to maximize the total billing of the order portfolio (Pinto and Nagano, 2020).

Literature Review

The available literature shows the research by Pinto *et al.* (2018) to be the first to approach and propose an OM for a specific problem of the so-called OBS. This OM is

formulated through a hybrid GA, whose structure is based on the canonic GA by [Holland \(1975\)](#) and programmed in Visual Basic for Applications (VBA) from Microsoft Office Excel 2013. The hybrid GA is called GA-OBS, and it is formulated by means of binary genetic structures that use an elitist selection and an aptitude function guided by penalties and repairs of individuals that are unfeasible to the OBS. This GA-OBS can deal with inventory restrictions and with customer acceptance criteria regarding billings of partial amounts of SKUs to attribute them in an optimized manner to the order portfolio demand in compliance with the First Come, First Served (FCFS) rule. Experiments demonstrated that the proposed GA-OBS provides solutions that optimize billing and expedite decision-making processes for the OBS.

More recently, an important innovation that aims to provide approaches to OBS that are better adapted to real-world needs was proposed by [Pinto and Nagano \(2020\)](#). This approach proposes an extension and enhancement of the OBS by [Pinto et al. \(2018\)](#), along with the Optimized Picking Sequence (OPS) by [Pinto and Nagano \(2019\)](#). These problems refer to the optimization of billing and manual picking processes, respectively, in a typical parts Warehouse (WA). The WA in question operates with a picking system that fits into the low-level picker-to-parts category with pick-and-sort process, and it has only one area known as Pick-up and Drop-off (P/D). The research objective was to provide a OM that integrated and offered optimized solutions for OBS/OPS in order to better deal with the trade-off between the level of customer service and the efficiency of said WA. The proposed OM was formulated by integrating two GAs called GA-OBS and GA-OPS. GA-OBS deals with inventory restrictions and possible partial billings, maximizes the total order portfolio billing by prioritizing the fulfilment and payment dates in compliance with the Earliest Due Date (EDD) rule, and generates a picking order for the GA-OPS. In the sequence, GA-OPS, which comprises the iteration of batch (GA_{BATCH}) and routing (GA_{TSP}) algorithms to satisfy all specificities of the problem and to minimize picking total time and cost for the OPS. Programming was done in Python, and both data inputs/outputs and results analyses were supported by Microsoft Office Excel 2016. Experiments with problems with different complexity levels showed that the proposed tool produces solutions of satisfactory quality and speeds up decision-making and operational processes so as to optimize financial results and productivity of the WAs.

Evidently, GA applications stand out for their robustness, implementation, and hybridization flexibility with other OMs ([Gen et al., 2008](#); [Bottani et al., 2012](#)). However, [Pinto et al. \(2018\)](#) applied the GA-OBS to solve only one single-size problem, and they did not include large OBS instances. The objective of the authors' approach was to gain insights into the best population size configuration and number of generations linked to variations in the genetic operator parameters that can maximize the solution potential of the GA-OBS. Therefore, the authors themselves recognize the need for tests in problems of higher instances, as well as the implementation of other parameters, operators, and genetic

representations or evolutionary designs that can improve performance. In [Pinto and Nagano \(2020\)](#), the proposal was to address the integration of problems by considering a series of practical dilemmas present in WAs. The solutions are of satisfactory quality for different instances and complexity levels configured for the OBS/OPS. However, solutions for problems in large instances demand considerable efforts in terms of checking and repairing chromosomes to be performed by GAs. These occurrences may result in an exponential increase of computational processing time and make the OM inefficient for some WAs.

Similar approaches to the OBS that presuppose inventory restrictions and uncertainties associated to the demand forecast were proposed by [Rim and Park \(2008\)](#) and [Seyedrezaei et al. \(2012\)](#). [Rim and Park \(2008\)](#) used the entire binary Linear Programming (LP) to deal with inventory restrictions in order to fulfil DC orders, aiming to maximize the Order Fill Rate (OFR). SKUs are only attributed to orders if there is available inventory in the DC; if there is not, orders are transferred to the next day and fulfilled according to SKU availability and priority rules to avoid excessive delays to the OFR. Experiments demonstrated that LP is better than the simple models in terms of order size and/or number of SKUs when compared to the FCFS rule. [Seyedrezaei et al. \(2012\)](#) applied the GA to a NP-complete inventory forecast and demand problem to plan and maximize the number of orders fulfilled according to Customer Importance, SKU Useful Life, and Back-Orders. This GA calculates the demand coefficient of each customer for a given time period and defines an inventory considering the DC's capacity and the useful life of the SKUs. Hence, orders that are not fulfilled due to SKU restrictions are transported to the next period (back-order). Compared to the Lingo software, the GA arrived at solutions with higher quality and satisfactory time to better manage DCs. In the search for more robust strategies and optimization methods, advanced technologies for intelligent decision making in manufacturing and logistics are presented by [Chien et al. \(2012\)](#). Other approaches focused on producing solutions that can maximize costs and/or maximize order fulfilment profit in an agile and flexible manner are found in high-impact journals ([Ghiami et al., 2013](#); [Mousavi et al., 2013](#); [Bandyopadhyay and Bhattacharya, 2014](#); [Diabat, 2014](#); [Park and Kyung, 2014](#); [Diabat and Deskoors, 2016](#); [Kumar et al., 2016](#); [Mousavi et al., 2017](#); [İnkaya and Akansel, 2017](#)).

Model formulation

In the OBS, the SKU notation refers to the registration number that distinguishes the n product types available in the DC stock. The quantity of each SKU in stock at a given t moment of the VTW is given by x_i , and it is represented by the set $X = \{x_1, x_2, \dots, x_n\}$, in which the subscript $i = (1, 2, \dots, n)$ denotes the i -th SKU. The Purchase Order Portfolio (POP) comprises n orders, represented by $POP = \{O_1, O_2, \dots, O_n\}$, and the subscript j refers to the j -th order $\forall j = (1, 2, \dots, n)$. These orders are from a set of m customers, represented

by $CG = \{C_1, C_2, \dots, C_m\}$, in which the subscript $a = (1, 2, \dots, m)$ denotes the a -th customer (C_a) of the POP. The total demand of x_i in the POP is given by Q_i , whereas the demand of x_i in O_j is given by q_{ij} , being $O_j = \{q_{1j}, q_{2j}, \dots, q_{nj}\} \forall i = (1, 2, \dots, n)$ attributes of C_a . If TV is the Total Value of the POP at the t instant of billing in the VTW, then, the TV will only be obtained if $x_i \geq Q_i$, in which y_i is the restriction of x_i and $w_i = (Q_i - y_i)$ is the availability of x_i in case $y_i > 0$. Thus, the notation $C_a^{w_{ij}}$ determines that the customer accepts w_i billing to O_j , whereas $C_a^{w_{ij}No}$ determines that the customer does not accept w_i billing to O_j . The insertion date of q_{ij} in the POP is denoted by id_{ij} , and, subsequently, the pre-defined priority criteria for the OBS are obtained: i) fd_{ij} – order fulfilment date of i in O_j ; ii) pd_{ij} – order payment date of i in O_j ; and; iii) pr_{ij} – unit selling price of i in O_j . The entire billing process of q_{ij} is carried out by comparing Q_i to the offer of x_i , so that, every non-billed q_{ij} will be transferred to t_{+1} to be processed again by the next VTW. Up next are the indexes, parameters and restrictions, as well as the decision criteria and variables that configure the OBS optimization problem:

• Indexes

i : denotes the i -th SKU of the n SKUs of the DC;
 j : denotes the j -th order of the n orders of the POP;
 α : denotes the a -th customer of the j -th order of POP.

• Parameters and restrictions

VTW: Variable Time Windows;
 t : VTW billing moment;
 O_j : refers to the j -th order of the POP in t ;
 C_a : refers to the a -th customer of the POP in t ;
 q_{ij} : SKU demand in the O_j of the POP in t ;
 Q_i : total demand of a SKU of the POP in t ;
 x_i : total number of a SKU in the DC in t ;
 y_i : restriction of x_i in the DC regarding the Q_i of the POP in t ;
 w_i : partial availability of x_i ($Q_i - y_i$) in the DC in case $y_i > 0$ in t .

• Decision criteria and variables

pr_{ij} : SKU unit price in the O_j ;
 fd_{ij} : SKU fulfilment date in the O_j ;
 pd_{ij} : SKU payment date in the O_j ;
 $C_a^{w_{ij}}$: determines if C_a accepts billings of w_i to O_j ;
 $C_a^{w_{ij}No}$: determines if C_a does not accept billings of w_i to O_j .

OBS optimization is subjected to the calculation of the possible Maximum Billing (MB) that can be obtained from the inventory of each SKU available in the DC versus the Q_i of the POP at a given t moment of the VTW. The calculation of the MB is then used to check the need for execution and of an IGA-OBS/GA-OBS search parameter to optimize the OBS. In cases where the $MB < TV$, i.e. if $x_i < Q_i$, so the MB will be the main parameter of the best possible solution for the OBS. The calculation criterion to obtain the MB, as demonstrated by Equation (1), prioritizes the highest pr_{ij} according to the following parameters: i) b_{wij} – billing value of w_{ij} and; ii) b_{qij} – billing value of q_{ij} .

$$\text{if } Q_i > x_i \rightarrow pr_{ij} \times w_{ij} = b_{wij} \text{ or if } Q_i \leq x_i \rightarrow pr_{ij} \times q_{ij} = b_{qij} \quad (1)$$

Then, MB can be obtained according to Equation (2). In the sequence, Table 1 demonstrates a calculation example of the MB for a given POP. In this example, we presuppose that the CD's inventory volume is represented by $X = \{3_a, 5_b, 3_c, 5_d, 0_e, 1_f, 0_g \text{ and } 5_h\}$.

$$MB = \sum_{j=1}^{O_j} \sum_{i=1}^n q_{ij} \times pr_{ij} + \sum_{j=1}^{O_j} \sum_{i=1}^n w_{ij} \times pr_{ij} \quad (2)$$

Table 1 shows that, given the availability of x_i , and prioritizing only the highest pr_{ij} according to b_{wij} and b_{qij} , the algorithm found the best billing mix, i.e., $MB = 1\,840,00$, then, $MB < TV$ ($x_i < Q_i$). For example, for “d”, despite $fd_{d200} < fd_{d250}$, the algorithm prioritized billing for O_{250} , given that, $pr_{d250} > pr_{d200}$ in POP. Note that the MB does not yet consider all the criteria and decision variables inherent to the OBS. Therefore, Total

Table 1. Maximum billing example

Number Order (O_j)	Code Customer (C_a)	Product Description (SKU)	Total SKU (Q_i)	Price Unit (pr_{ij})	Billing Order (b_{ij})	Order Date (id_{ij})	Fulfilment Date (fd_{ij})	Payment Date (pd_{ij})	Accepts partial q_i (w_{ij})	Stock Attribution (x_i)	Maximum Billing (MB)
100	10	a	3	50,00	150,00	10/05/2021	10/06/2021	10/07/2021	Yes	2	100,00
100	10	c	2	150,00	300,00	10/05/2021	10/06/2021	10/07/2021	Yes	2	300,00
150	15	c	1	155,00	155,00	15/05/2021	20/06/2021	20/07/2021	No	1	155,00
200	20	b	2	100,00	200,00	15/05/2021	10/06/2021	10/07/2021	No	2	200,00
200	30	c	2	150,00	300,00	15/05/2021	10/06/2021	10/07/2021	No	-	-
200	30	d	4	200,00	800,00	15/05/2021	10/06/2021	10/07/2021	No	3	600,00
250	10	d	2	212,50	425,00	18/05/2021	15/06/2021	10/07/2021	No	2	425,00
300	30	a	1	60,00	60,00	18/05/2021	10/06/2021	10/07/2021	No	1	60,00
300	30	e	2	25,00	50,00	18/05/2021	10/06/2021	10/07/2021	No	-	-
Total Value (TV)			19		2 440,00					13	1 840,00

Source: Authors

Billing (TB) maximization of the POP can be expressed as a mathematical programming model to maximize TB_{\max} :

$$\text{Maximize } TB_{\max} = \sum_{j=1}^{O_j} \sum_{i=1}^n q_{ij} \times pr_{ij} + \sum_{j=1}^{O_j} \sum_{i=1}^n w_{ij} \times pr_{ij} \quad (3)$$

Subjected to:

$$x_i > 0 \quad i = 1, 2, \dots, n \quad (4)$$

$$x_i \geq q_{ij} \quad \forall C_{\alpha}^{w_{ij}No} \quad j = 1, 2, \dots, n \quad (5)$$

$$w_{ij} > 0 \quad \forall C_{\alpha}^{w_{ij}Yes} \quad \alpha = 1, 2, \dots, m \quad (6)$$

$$O_n: \text{Fulfilment by priority } fd_{ij}, \text{ in POP} \quad (7)$$

$$O_n: \text{Fulfilment by precedent } pd_{ij} \text{ in POP} \quad (8)$$

$$O_n: \text{Fulfilment from highest to lowest } pr_{ij} \text{ in POP} \quad (9)$$

The objective function in Equation (3) is to find the maximum possible billing of the POP. **Restriction (4)** ensures that q_i will only be attributed to O_j if, in a t given moment of the VTW, the variable $x_i > 0$ in the DC. **Restriction (5)** ensures that, $\forall C_{\alpha}^{w_{ij}No}$, the total demand of q_{ij} can only be attributed to its corresponding O_j if, at a t given moment of VTW, the variable $x_i \geq q_{ij}$ in the DC. **Restriction (6)** will make sure that a given w_i can only be attributed to O_j if $w_i > 0$ in the POP and $C_{\alpha}^{w_{ij}Yes}$. **Variables (7), (8), and (9)** determine that the rules for fd_{ij} , pd_{ij} , and pr_{ij} are satisfied in the POP.

Iterative Greedy Algorithm (IGA-OBS)

The logic of the IGA-OBS is based on the verification and attribution technique through the iteration of a set of interdependent elements which configure the OBS. The first phase of its formulation is the sorting mechanism of the POP by the fulfilment priority levels defined by $fd_{ij}/pd_{ij}/pr_{ij}$. It is assumed that fd_{ij} and pd_{ij} have respectively higher priority levels than the pr_{ij} of the POP. Hence, q_{ij} and w_{ij} are attributed by automatically comparing and updating inventory balances after each SKU attribution. Therefore, q_i or w_i is attributed to O_j by the variable s_{ij} . Thus, $s_{ij} = q_i$ or w_i ; otherwise, $s_{ij} = 0$ to obtain the TB maximization according to Equation (10).

$$TB_{\max} = \sum_{j=1}^{O_j} \sum_{i=1}^n q_{ij} \times pr_{ij} + \sum_{j=1}^{O_j} \sum_{i=1}^n w_{ij} \times pr_{ij} \quad (10)$$

Thus, q_i or w_i may or may not be attributed to the j -th depending on parameters and restrictions, decision criteria, and variables inherent to the OBS. The attribution routine verifies whether there is a balance of x_i in the DC, and, after each execution, the IGA-OBS produces a solution that maximizes the TB of the POP. q_i or w_i to O_j is attributed according to the following conditions:

1. If $x_i = 0$, $s_{ij} = 0$ according to Equation (11).

$$\text{if } x_i = 0 \forall q_{ij} \rightarrow s_{ij} = 0 \quad (11)$$

2. If $x_i = w_{ij}$ in case $C_{\alpha}^{w_{ij}No}$, $s_{ij} = 0$ according to Equation (12).

$$\text{if } x_i = w_{ij} \leftrightarrow C_{\alpha}^{w_{ij}No} \rightarrow s_{ij} = 0 \quad (12)$$

3. If $fd_{t+1} < fd_t$, fd_{t+1} is prioritized over fd_t according to Equation (13).

$$\text{if } x_i = w_{ij} \forall C_{\alpha}^{w_{ij}Yes} \leftrightarrow O_j^{fd_{t+1}} < O_j^{fd_t} \rightarrow pr_{ij}^{fd_{t+1}} \times w_{ij} = b_{q_{ij}} \quad (13)$$

4. If $pd_{t+1} < pd_t$, pd_{t+1} has preference over pd_t according to Equation (14).

$$\text{if } x_i = w_{ij} \forall C_{\alpha}^{w_{ij}Yes} \wedge O_j^{fd_t} = O_j^{fd_{t+1}} \leftrightarrow O_j^{pd_{t+1}} < O_j^{pd_t} \rightarrow pr_{ij}^{pd_{t+1}} \times w_{ij} = b_{q_{ij}} \quad (14)$$

5. If $pr_{ij+1} > pr_{ij}$, pr_{ij+1} is prioritized over pr_{ij} according to Equation (15).

$$\text{if } x_i = w_{ij} \forall C_{\alpha}^{w_{ij}Yes} \wedge O_j^{fd_t} = O_j^{fd_{t+1}} \wedge O_j^{pd_t} = O_j^{pd_{t+1}} \leftrightarrow O_j^{pr_{ij+1}} > O_j^{pr_{ij}} \rightarrow pr_{ij}^{pr_{ij+1}} \times w_{ij} = b_{q_{ij}} \quad (15)$$

To exemplify the solution of the problem given by Table 1, Table 2 shows how the IGA-OBS performs both the POP ordering and the assignments of x_i to maximize TB. The following colors are used to demonstrate the attributions of q_{ij} and w_{ij} in order to exemplify the calculation that maximizes TB: i) *black*: it refers to the total attributions of q_{ij} ; ii) *green*: it corresponds to the attributions of w_{ij} ; and iii) *red*: it indicates the q_{ij} and w_{ij} that were not attributed due to the total restrictions of a given SKU.

On Table 2, it can be observed that, for “ α ”, O_{100} and O_{300} have identical fd_{ij} and pd_{ij} . However, $pr_{a300} > pr_{a100}$ and, if O_{100} has $C_{\alpha}^{w_{ij}Yes}$ as a criterion for billings of w_{ij} , $s_{i100} = 2\alpha$ and $s_{i300} = 1\alpha$. Note that for “ c ”, O_{150} , even having the highest pr_c among the orders, is discarded because fd_{150} is higher than fd_{100} and fd_{200} . In case of “ d ”, there is insufficient inventory of x_d to satisfy O_{200} and O_{250} , and both have $C_{\alpha}^{w_{ij}No}$ as a criterion for billings of w_{ij} . Thus, if $fd_{200} < fd_{250}$, the option is to satisfy O_{200} . As for “ e ”, there were no attributions as $x_d = 0$, that is, the entire IGA-OBS solution logic satisfies all demands inherent to the OBS to maximize the TB. Table 3 presents the list of q_{ij} to be billed, whereas the q_{ij} that will not be billed is represented by $y = \{1_a, 2_c, 2_d \text{ and } 2_e\}$ due to y_i restrictions. In sequence, Algorithm 1 shows the IGA-OBS pseudocode

Genetic algorithm (GA-OBS)

In the evolutive genetic structure of the GA-OBS, the representation of chromosome (C) is given by a binary string $\{0,1\}$, which attributes q_i or w_i to O_j by variable $s_{ij} = 1$; otherwise, $s_{ij} = 0$. Then, a C is divided into O_n genes, and q_{ij} or w_{ij} is an allele of the j -th gene according to Figure 1.

Table 2. IGA-OBS solution example

Number Order (O_j)	Code Customer (C_a)	Description Product (SKU)	Total SKU (Q_j)	Price Unit (pr_{ij})	Billing Order (b_{ij})	Order Date (id_j)	Fulfilment Date (fd_j)	Payment Date (pd_j)	Accepts partial q_i (w_{ij})	Stock Attribution (q_{ij} and w_{ij})	Total Billing (TB)
100	10	a	3	50,00	150,00	10/05/2021	10/06/2021	10/07/2021	Yes	2	100,00
300	30	a	1	60,00	60,00	18/05/2021	10/06/2021	10/07/2021	No	1	60,00
200	20	b	2	100,00	200,00	15/05/2021	10/06/2021	10/07/2021	No	2	200,00
100	10	c	2	150,00	300,00	10/05/2021	10/06/2021	10/07/2021	Yes	1	150,00
200	30	c	2	150,00	300,00	15/05/2021	10/06/2021	10/07/2021	No	2	300,00
150	15	c	1	155,00	155,00	15/05/2021	20/06/2021	20/07/2021	No	0	-
200	30	d	4	200,00	800,00	15/05/2021	10/06/2021	10/07/2021	No	4	800,00
250	10	d	2	212,50	425,00	18/05/2021	15/06/2021	10/07/2021	No	0	-
300	30	e	2	25,00	50,00	18/05/2021	10/06/2021	10/07/2021	No	0	-
Total Value (TV)			19		2 440,00					12	1 610,00

Source: Authors

Table 3. Billing list

Number Order (O_j)	Code Customer (C_a)	Product Description (SKU)	Total SKU (Q_j)	Price Unit (pr_{ij})	Billing Order (b_{ij})	Order Date (id_j)	Fulfilment Date (fd_j)	Payment Date (pd_j)	Accepts partial q_i (w_{ij})	Stock (x_i) Attribution (q_{ij} and w_{ij})	Total Billing (TB)
100	10	a	2	50,00	100,00	10/05/2019	10/06/2019	10/07/2019	Yes	2	100,00
100	10	c	1	150,00	150,00	10/05/2019	10/06/2019	10/07/2019	Yes	1	150,00
200	20	b	2	100,00	200,00	15/05/2019	10/06/2019	10/07/2019	No	2	200,00
200	30	c	2	150,00	300,00	15/05/2019	10/06/2019	10/07/2019	No	2	300,00
200	30	d	4	200,00	800,00	15/05/2019	10/06/2019	10/07/2019	No	4	800,00
300	30	a	1	60,00	60,00	18/05/2019	10/06/2019	10/07/2019	No	1	60,00
Total Value (TV)			12		1 610,00					12	1 610,00

Source: Authors

Attributions Chromosome for Billing									
Orders	O_{100}		O_{150}		O_{200}		O_{250}		O_{300}
SKUs	3 _a	2 _c	1 _c	2 _b	2 _c	2 _d	2 _d	1 _d	2 _e
Attributions	0	0	1	1	1	1	1	1	0
Orders (Genes - O_j) - - Demand (Bits - q_{ij})									

Figure 1. Assignment chromosome for billing (IGA-OBS)

Source: Authors

procedure: IGA-OBS // attribution iteration**input:** problem data and IGA-OBS parameters**output:** best solution**beginning****sort out POP**SKU: registration number of i in POP fd_j : fulfillment date of i in O_j pd_j : payment date of i in O_j **sort out SKU:** pr_{ij} : unit selling price of i in O_j **for each q_{ij} check:**if $x_i > 0$ e $x_i \geq q_{ij}$ bill \leftarrow update inventory (x_i) and check next SKU;if $x_i > 0$ e $q_{ij} > x_i$ and $C_a^{w_{ij}}$ bill $w_{ij} \leftarrow$ update x_i and check next SKU;if $x_i = 0 \leftarrow$ do not bill and check next SKUif $x_i > 0$ e $q_{ij} > x_i$ and $C_a^{w_{ij}No} \leftarrow$ do not bill and check next SKU;if $pr_t < pr_{t+1} \leftarrow$ bill $pr_{t+1} \leftarrow$ update x_i and check next SKU;**output:** the best solution;**end****Algorithm 1.** General implementation structure (IGA-OBS)

Source: Authors

The population is a matrix denoted by N_{pop} , with N_{bits} being the number of bits of C , and N_{ger} the total of generations in the execution of the GA-OBS (Haupt, R. and Haupt, S., 2004). The initial N_{pop} is generated randomly (Man et al., 1996), i.e., if $s_{ij} < 0,5$, $s_{ij} = 0$; otherwise, $s_{ij} = 1$, and N_{bits} is equal to the number of POP lines. Therefore, the Billing Obtained (BO) by C is given by Equation (16).

$$BO = \sum_{j=1}^{N_{bits}} \sum_{i=1}^{N_{pop}} s_{ij} \times q_{ij} \times pr_{ij} + \sum_{j=1}^{N_{bits}} \sum_{i=1}^{N_{pop}} s_{ij} \times w_{ij} \times pr_{ij} \quad s_{ij} = \{0,1\} \quad (16)$$

The fitness function ($F_{fitness}$) first penalizes every C that is not feasible to the OBS by assigning a negative value equal to the b_{qij} of the invalid bit, in which $\forall s_{ij} = 1$ according to the following conditions: If $s_{ij} = 1$ and $x_i = 0$: penalty Pe_x is imposed according to Equation (17).

$$Pe_{x_{ij}} = \sum_{j=i}^{N_{bits}} b_{q_{ij}} \text{ if } s_{ij} = 1 \forall x_i = 0 \rightarrow pr_{ij} \times q_{ij} = b_{q_{ij}} \quad (17)$$

1. If $s_{ij} = 1$ to w_{ij} in case $C_a^{w_{ij}No}$: penalty Pe_w is imposed according to Equation (18).

$$Pe_{w_{ij}} = \sum_{j=i}^{N_{bits}} b_{q_{ij}} \text{ if } s_{ij} = 1 \forall w_{ij} \leftrightarrow C_a^{w_{ij}No} \rightarrow pr_{ij} \times w_{ij} = b_{q_{ij}} \quad (18)$$

2. The $s_{ij} = 1$ must prioritize the first fd_{ij} in the POP: If $x_i < Q_i$, fd_i is preferred over fd_{t+1} ; otherwise, penalty Pe_{fd} is imposed according to Equation (19).

$$Pe_{fd_{ij}} = \sum_{j=1}^{N_{bits}} b_{q_{ij}} \text{ if } x_i < Q_i \leftrightarrow s_{ij} = 1 \forall O_j^{fd_{i+1}} \wedge s_{ij} = 0 \forall O_j^{fd_i} \rightarrow pr_{ij}^{fd_{i+1}} \times q_{ij} = b_{q_{ij}} \quad (19)$$

3. The $s_{ij} = 1$ must prioritize the first pd_{ij} in the POP: after checking the fd_{ij} , if $pd_{t+1} < pd_{it}$, pd_{t+1} is prioritized; otherwise, penalty Pe_{pd} is imposed according to Equation (20).

$$Pe_{pd_{ij}} = \sum_{j=1}^{N_{bits}} b_{q_{ij}} \text{ if } O_j^{pd_i} = O_j^{pd_{i+1}} \wedge s_{ij} = 1 \forall O_j^{pd_i} \leftrightarrow O_j^{pd_{i+1}} < O_j^{pd_i} \rightarrow pr_{ij}^{pd_{i+1}} \times q_{ij} = b_{q_{ij}} \quad (20)$$

4. The $s_{ij} = 1$ must prioritize the highest pr_{ij} in the POP: after checking the fd_{ij} and the pd_{ij} , if $pr_{ij+1} > pr_{ij}$, pr_{ij+1} is prioritized; otherwise, penalty Pe_{pr} is imposed according to Equation (21).

$$Pe_{pr_{ij}} = \sum_{j=1}^{N_{bits}} b_{q_{ij}} \text{ if } O_j^{pr_i} = O_j^{pr_{i+1}} \wedge s_{ij} = 1 \forall O_j^{pr_i} \leftrightarrow O_j^{pr_{i+1}} > O_j^{pr_i} \rightarrow pr_{ij}^{pr_{i+1}} \times q_{ij} = b_{q_{ij}} \quad (21)$$

Next, $F_{fitness}$ makes repairs by swapping “1” for “0” in bits with incidence of Pe_x and Pe_w by means of Re_x and Re_w repairs according to Equations (22) and (23).

$$Re_{x_{ij}} = Pe_{x_{ij}} \leftrightarrow s_{ij} = 1 \forall x_i = 0 \rightarrow s_{ij} = 0 \quad (22)$$

$$Re_{w_{ij}} = Pe_{w_{ij}} \leftrightarrow s_{ij} = 1 \forall w_{ij} \leftrightarrow C_a^{w_{ij}No} \rightarrow s_{ij} = 0 \quad (23)$$

Therefore, $b_{q_{ij}}$ and $b_{w_{ij}}$ for N_{bits} repaired are \$0,00, and \$1,00 is attributed to $F_{fitness}$ in case $F_{fitness} \leq 1$, i.e., $F_{fitness}$ may vary from \$0,00 to BO according to Equation (24).

$$F_{fitness} = \begin{cases} BO - \sum_{j=1}^{N_{bits}} (Pe_{fd_{ij}} + Pe_{pd_{ij}} + Pe_{pr_{ij}}) \\ \text{if } BO < \$1,00 \rightarrow F_{fitness} = \$1,00 \end{cases} \quad (24)$$

The roulette wheel by Holland (1975), linked to Elitism (E) by De Jong (1988), is used as a selection technique, in which only the best C (C_{Elite}) of each N_{ger} is transferred to become the first C of N_{ger+1} . The selection probability of each individual i is equivalent to a certain slice of the roulette wheel, as expressed by Equation (25).

$$P_{s_i} = \frac{F_{fitness_i}}{\sum_{i=1}^{N_{pop}} F_{fitness_i}} \quad (25)$$

To exemplify this, Table 4 shows the calculus of the selection probability for four individuals. Then, the select graphic by the roulette wheel with elitism is demonstrated by Figure 2.

Table 4. Evaluation calculus and selection percentage (GA-OBS)

Individual (String)	Fitness Function	Selection Percentage	Piece of Roulette
Chromosome (C ₁)	1 360,00	39%	138,70
Chromosome (C ₂)	1 250,00	35%	127,48
Chromosome (C ₃)	460,00	13%	46,91
Chromosome (C ₄)	460,00	13%	46,91
Total Population	3 530,00	100%	360,00

Source: Authors

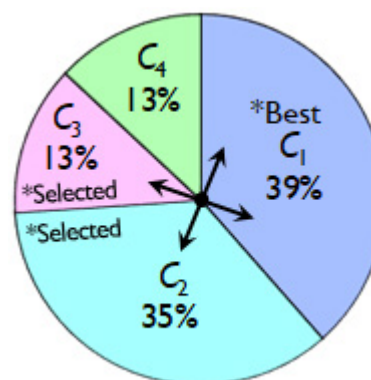


Figure 2. Graphic of the roulette wheel with elitism (GA-OBS)

Source: Authors

The implemented crossover operator is of the two-point kind, and the mutation is an adaptation of the flip type, both by Holland (1975). Figure 3 illustrates the crossover and mutation diagram implemented to GA-OBS.

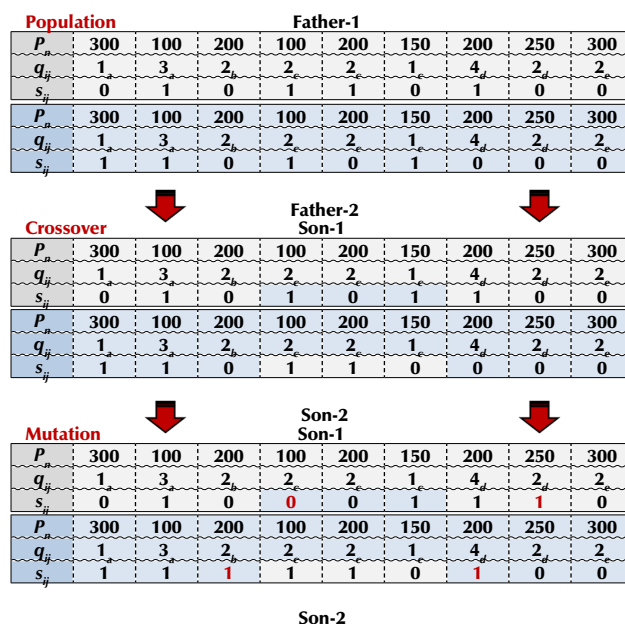


Figure 3. Crossover and mutation diagram (GA-OBS)

Source: Authors

Figure 3 shows that the crossover is applied to the “Parents” according to the crossover probability (p_c) pre-defined for the GA-OBS. In the crossover, each O_j and q_{ij} remain static, while permutations occur only for s_{ij} in order to form the “Sons” of N_{ger+1} . Figure 3 also shows that the mutation

affects the “Sons” resulting from the crossover, and it will be applied according to the mutation probability (p_m), whereas t_x is the rate for the exchange between the N_{bits} of C . Therefore, each bit to be mutated is randomly chosen and receives a value corresponding to the exchange between 0 and 1 for the s_{ij} of C . Note that the mutated bits (red) make changes in the genetic pattern of the “Sons”.

Thereupon, p_c , p_m , and t_x allow a parameterization that can vary from 0 to 100%. However, after being pre-defined, they remain fixed during all the N_{ger} in each execution of the GA-OBS. To generate N_{pop+1} , the N_{pop} swapping technique with elitism by [De Jong \(1988\)](#) is used. The termination criterion used, prevailing the first one obtained, is that the MB or N_{ger} is used. [Algorithm 2](#) shows the GA-OBS pseudocode.

procedure: GA-OBS // GA initial population generation
input: problem data and GA parameters
output: best solution (C_{Elite})
beginning
 random attributions $s_{ij} = 0$ or $s_{ij} = 1$ to q_{ij} of POP
 aptitude $eval(N_{pop})$ by decoding routine;
 for each bit $s_{ij} = 1$:
 check if total (q_{ij}) or partial (w_{ij}) billing is possible:
 if $x_i > 0$ and $q_i \geq q_j \leftarrow$ update inventory (x_i) and check next item;
 if $x_i > 0$ and $q_i > x_i$ and $C_{\alpha}^{w_{ij}}$ bill $w_i \leftarrow$ update x_i and check next item;
 if $x_i = 0 \leftarrow$ penalize $b_{ij} \leftarrow$ repair bit and check next item;
 if $x_i > 0$ and $q_i > x_i$ and $C_{\alpha}^{w_{ij}}$ penalize b_{ij} and repair item;
 if fd_{t+1} billed before $fd_t \leftarrow$ penalize b_{ij}
 if pd_{t+1} billed before $pd_t \leftarrow$ penalize b_{ij}
 if pr_{t+1} billed and $pr_t > pr_{t+1} \leftarrow$ penalize b_{ij}
 $F_{fitness} \leftarrow BO$ – total of penalties and repairs;
 if $F_{fitness} < 0$
 $F_{fitness} \leftarrow \$ 1,00$;
output: $F_{fitness}$ – individual’s aptitude value (C);
while (condition is **not** finished) **of**
 N_{pop} crossing to generate $C(g)$;
 N_{pop} mutation to modify $C(g)$;
 aptitude $eval(C)$ by codification routine;
 select $N_{pop}(g+1)$ for $N_{pop}(g)$ and $C(g)$;
 $g \leftarrow g+1$;
end
output: the best solution (C_{Elite});
end

Algorithm 2. General implementation structure (GA-OBS)

Source: Authors

Computational experiments and result analyses

This section and its subsections detail problem configurations, computational experiments, and analyses

of the results obtained by the GA-OBS and the IGA-OBS. These analyses focused on assessing performance and on the conditions to adapt GA-OBS/IGA-OBS to the reality of the aforementioned DC. Algorithm implementations and computational experiments were carried out in a microcomputer featuring a 2.0GHz i7 processor and 8GB of RAM. Programming was conducted in Python, and both data inputs/outputs and analyses were supported by Microsoft Office Excel 2016. Experiments included a set of problems with different complexity levels based on the literature and the reality of DCs. The entire problem configurations and the instances used in the experiments are identical to those considered by [Pinto and Nagano \(2020\)](#). Therefore, the problems are classified into three categories: i) Small (SM); ii) Medium (ME) and; iii) Large (LG).

Test problems and parameter setting

This subsection details problem formulations and parameter configurations for each OBS category. For a better comparative analysis of the algorithms, all the problems are configured so that the MB is the optimized solution for the OBS. Thus, in the DC under study, there is a total of 1 250 types of SKUs to satisfy the POP at a given t moment of the VTW. Depending on the OBS category, SKU restrictions in the DC are the following: i) $x_i = 0$ from 1 to 2,5% and; ii) $x_i = 2$ from 2 to 3%. All billing processes take place immediately after VTW = 8 (hours), where 50% of the POP orders contain $C_{\alpha}^{w_{ij}}$ and fr_{Yes} . The number of SKUs that repeat among the n orders of each POP range from 50 to 80%. However: i) if $x_i = 0$, there will be no SKU repeated in another order; ii) if $x_i = 2$, there will be only one SKU repeated in another order. Date configurations are shown next, and they presuppose that t refers to the date of the last order input in the POP. For id_{ij} : i) 50% have $id_{ij} = t$; and ii) 50% of the remaining id_{ij} range from $id_{ij} = t_{-5}$ days to $id_{ij} = t_{-1}$ days. For fd_{ij} : i) 30% ($fd_{ij} = t$); ii) 30% ($fd_{ij} = t_{+10}$ days); iii) 20% ($fd_{ij} = t_{+20}$ days); and iv) 20% ($fd_{ij} = t_{+30}$ days). For pd_{ij} : i) 20% ($pd_{ij} = t$); ii) 20% ($pd_{ij} = t_{+10}$ days); iii) 20% ($pd_{ij} = t_{+15}$ days); iv) 20% ($pd_{ij} = t_{+30}$ days); and v) 20% ($pd_{ij} = t_{+45}$ days). pr_{ij} is randomly determined by an even distribution function [100, 1 000]. However: i) if $x_i = 0$, $pr_{ij} = \$200,00$; ii) if $x_i = 2$, $pr_{ij} = \$100,00$; and iii) if SKU repeated among orders is $C_{\alpha}^{w_{ij}}$, then $pr_{ij} = \$120,00$. [Table 5](#) summarizes the problems formulated for the OBS.

Table 5. Summary of problem settings

OBS Problem	SM-1	SM-2	ME-3	ME-4	LG-6	LG-6
Number of orders of POP	10	15	20	30	40	50
Number of SKU in each O_j	2	2	4	4	6	6
Demand of each SKU in O_j	2	2	2	2	2	2
Different types of SKU in each O_j	20	30	80	120	240	300
Total demand of SKU in each O_j	40	60	160	240	480	600
Total Value (TV) of billing in each POP	15 000,00	20 000,00	54 908,00	9 836,00	209 408,00	250 274,00

Source: Authors

Computational results and analyses

This section describes the results of the computational experiments and the performance analyses of the GA-OBS/IGA-OBS proposed for the OBS. The analyses were carried out by means of Outcome Assessment Metrics (OAM), and the final assessment was substantiated by the set of average results obtained by the GA-OBS/IGA-OBS. GA-OBS computational experiments demonstrated that a critical factor in the generation of high-aptitude individuals is the calibration of the genetic operators. There is no standard formula to indicate which ideal parameter configuration will produce the appearance of C_{Elite} in the GA-OBS. While considering that the new generations are not deterministic, we sought to better deal with the trade-off between the quality of the solutions and the computational efficacy of the GA-OBS. The option was to use average parameters that better adjusted to the real situations and the design of the evolutive genetic structure of the GA-OBS. After the execution series for the each OBS problem category, combinations and parameter minimum and maximum limits that provided the best solutions to the GA-OBS are summarized in Table 6.

Table 6. Parameterization for genetic algorithms (GA-OBS)

Parameters	SM-1	SM-2	ME-3	ME-4	LG-5	LG-6
Population size (N_{pop})	200	400	800	1 000	1 500	2 000
Generation number (N_{ger})	200	400	2.000	5 000	8 000	12 000
Crossover probability (p_c)	80%	80%	80%	50%	50%	50%
Mutation probability (p_m)	80%	50%	20%	20%	20%	30%
Mutation rate of bits (t_x)	2%	1%	1%	1%	1%	1%

Source: Authors

In Table 6, it is possible to verify that the initial N_{pop} ranges from 200 to 2 000 individuals, and that the N_{ger} ranges from 200 to 12 000 individuals. Notice that p_c ranges from 50 to

80%, while p_m ranges from 20 to 80% using a t_x of 1 or 2% depending on OBS complexity. Tables 7 and 8 summarize the results obtained by the GA-OBS and IGA-OBS according to the following OAM: i) Tardiness in Customer Orders (TCO); ii) Number of Fulfilled Orders (NFO); iii) Total of Billed Products (TBP); iv) Computational Processing Time (CPT); v) Maximum Billing (MB); and vi) Total Billing (TB).

Tables 7 and 8 demonstrate that GA-OBS and IGA-OBS can satisfy all rules, restrictions, and decision criteria to maximize the TB for each OBS instance. The genetic structure implemented in the GA-OBS can conduct the search for C_{Elite} and meet all conditions attributed to the OBS. In general, the GA-OBS converges up to C_{Elite} from the third until the tenth generation at most for each OBS category. This demonstrates that the size of both the N_{pop} and the N_{ger} and that p_c , p_m , and t_x have proved to be sufficient to create a level of diversity capable of capturing all OBS specificities and allow the convergence of the GA-OBS.

However, obtaining the best results for instances of higher OBS levels is conditioned to significant increases in the size of the N_{pop} and the N_{ger} . Thus, there is a relative dependence on the size of the N_{pop} and the N_{ger} , which, if they are not large enough to expand the search space, will make the GA-OBS stagnate in a local solution that is distant from TB maximization. Note that, for a POP with more than 30 orders containing more than 80 lines and 200 SKUs, the GA-OBS obtained a much higher CPT than the IGA-OBS. This happens because the GA-OBS solutions require an exhaustive search for a large number of possible solutions, thus demanding intensive effort in verifications and repairs, which exponentially expands the CPT and can make it unfeasible for OBS reality. Probabilistic properties and the configuration of the genetic representation linked to an aptitude function guided by penalties and repairs are critical

Table 7. Results obtained by genetic algorithms (GA-OBS)

OAMs	Measures	SM-1	SM-2	ME-3	ME-4	LG -5	LG -6
TCO	Unit	–	–	–	–	–	–
NFO	Unit	10	15	20	30	40	50
TBP	Unit	34	50	134	200	402	500
CPT	Minutes	0,522	1 124	70 857	316 952	1 367 555	3 492 102
MB	Dollar (US\$)	14 400,00	19 000,00	52 908,00	94 336,00	201 608,00	240 274,00
TB	Dollar (US\$)	14 400,00	19 000,00	52 908,00	94 336,00	201 608,00	240 274,00

Source: Authors

Table 8. Results obtained by the Iterative Greedy Algorithm (IGA-OBS)

OAMs	Measures	SM-1	SM-2	ME-3	ME-4	LG -5	LG -6
TCO	Unit	–	–	–	–	–	–
NFO	Unit	10	15	20	30	40	50
TBP	Unit	34	50	134	200	402	500
CPT	Minutes	0,063	0,067	0,083	0,100	0,133	0,200
MB	Dollar (US\$)	14 400,00	19 000,00	52 908,00	94 336,00	201 608,00	240 274,00
TB	Dollar (US\$)	14 400,00	19 000,00	52 908,00	94 336,00	201 608,00	240 274,00

Source: Authors

factors for the evolution and convergence of the GA-OBS. We also verified that the GA-OBS is extremely sensitive to the calibration of genetic operators and the parameterization of p_c , p_m , and t_x , which is the best possible to favor the diffusion of positive genetic features for each new generation of the GA-OBS. Improper parameterizations can destroy the aptitude of the individuals or force the evolution to occur more slowly, as well as leading to a premature convergence or demanding a CPT that makes the GA-OBS unfeasible. The fact is that, the greater the OBS instance, the greater the number of penalties and repairs, thus the longer the GA-OBS solution will be.

In practical terms, the GA-OBS is limited to medium-size problems and differs from the needs of managers when faced with the complexities present in the daily reality of DCs. On the other hand, the experiments evidenced that the performance of the IGA-OBS was much better than that of the GA-OBS, and that it produced optimized solutions with a CPT that is less than one minute for any OBS category. The use of the IGA-OBS enables managers to deal more quickly and consistently with higher levels of OBS complexity; the faster the flow of information, the higher is the degree of negotiation accuracy, and the faster is the OBS decision-making. These actions result in less waste of time and greater flexibility and precision to schedule billing and picking processes within the DC. IGA-OBS solutions optimize the quality of order portfolio fulfilment and cash flow management by reducing the DC's eventual financial losses. In general terms, the IGA-OBS provides a tool that enables managers to make decisions in a more agile and consistent way regarding the trade-off between the level of customer service and the maximization of the DC's financial result. In addition to that, the IGA-OBS does not use penalties or repairs, and it can be implemented without major difficulties to other OBS and DC configurations. The option to use Excel allows the main current management software programs to extract .xls files to make uploads to the IGA-OBS. Analysis of SKU inventory specificities and the best VTW adjustment regarding the POP size also contribute to formulating OMs with practical designs that are more robust and suitable for OBS.

Final considerations

This paper proposes an efficient algorithm to solve a specific billing maximization problem called Optimized Billing Sequencing (OBS). Initially approached by [Pinto et al. \(2018\)](#), OBS refers to the optimization of order portfolio billing processes in a typical Distribution Center (DC). In the OBS under study, Stock Keeping Unit (SKU) inventories are controlled at minimum levels inside the DC. There are, however, uncertainties regarding the management of the demand, which is stochastic, and billings occur from Variable Time Windows (VTW). Most delivery deadlines are tight, and there is a high frequency of small orders containing minimum amounts of multiple SKUs. It is not uncommon that, when billing, determining fulfilment rankings may be

necessary, as well as analyzing whether customers accept partial amounts due to SKU restrictions. Decision making about billing prioritizes fulfilment and payment dates in compliance with the Earliest Due Date (EDD) rule. Thus, the new algorithm proposed for the OBS was called Iterative Greedy Algorithm (IGA-OBS) and its performance was compared to the genetic algorithm (GA-OBS) by [Pinto and Nagano \(2020\)](#). Experiments with problems with different levels of complexity demonstrated that the algorithms satisfy all rules, restrictions, and decision variables, and they obtain solutions of satisfactory quality for all OBS instances. It was evidenced that the GA-OBS is limited to medium-size problems, as it demands a high computational processing time that differs from those required to the reality of current DCs. However, the GA-OBS is capable of producing optimized solutions with a computational processing time of less than one minute for any OBS problem. This research fills a gap in the literature and makes valuable contributions to further studies on the development of algorithms with practical designs that are more robust and suitable for OBS. The proposed IGA-OBS enables managers to make decisions in a more agile and consistent way in terms of the trade-off between the level of customer service and the maximization of the financial result of the aforementioned DC. There is still a vast field of inquiries and assumptions for new optimization methods for many other approaches and configurations for the so-called OBS. The main limitation is that the literature does not yet provide an available database with different OBS problems to better test the IGA-OBS/GA-OBS. Suggestions for further researches are: i) to conduct studies with actual applications, so a comparative analysis of the processes adopted by managers versus those resulting from the IGA-OBS can be made; ii) to implement more efficient designs to elements, parameters, and genetic operators, or formulate evolutionary genetic representations that improve the GA-OBS performance; iii) to carry out extensive computational experiments by means of comparative studies among other renowned metaheuristics versus the IGA-OBS; iv) to assess the IGA-OBS with dynamic variables in order to deal with payment deadlines, cashflow, demand forecast, and production lead times that replenish DC inventories.

Acknowledgements

The research of the authors is partially supported by grants numbers 306,075/2017-2 and 430,137/2018-4 from the Conselho Nacional de Desenvolvimento Científico e Tecnológico (CNPq), as well as by grant 2700441 from the Fundação Nacional de Desenvolvimento do Ensino Superior Particular (FUNADESP), Brazil.

References

- Bandyopadhyay, S. and Bhattacharya, R. (2014). Solving a tri-objective supply chain problem with modified NSGA-II algorithm. *Journal of Manufacturing Systems*, 33(1), 41-50. <https://doi.org/10.1016/j.jmsy.2013.12.001>

- Baud-Lavigne, B., Bassetto, S., and Agard, B. (2014). A method for a robust optimization of joint product and supply chain design. *Journal of Intelligent Manufacturing*, 27(4), 741-749. <https://doi.org/10.1007/s10845-014-0908-5>
- Bottani, E., Cecconi, M., Vignali, G., and Montanari, R. (2012). Optimisation of storage allocation in order picking operations through a genetic algorithm. *International Journal of Logistics Research and Applications*, 15(2), 127-146. <https://doi.org/10.1080/13675567.2012.694860>
- Boysen, N., De Koster, R., and Weidinger, F. (2019). Warehousing in the e-commerce era: A survey. *European Journal of Operational Research*, 277(2), 396-411. <https://doi.org/10.1016/j.ejor.2018.08.023>
- Chien, C., Kim, K. H., Liu, B., and Gen, M. (2012). Advanced decision and intelligence technologies for manufacturing and logistics. *Journal of Intelligent Manufacturing*, 23(6), 2133-2135. <https://doi.org/10.1007/s10845-011-0559-8>
- De Jong, K. (1988). Learning with genetic algorithms: An overview. *Machine Learning*, 3(2-3), 121-138. <https://doi.org/10.1007/BF00113894>
- Diabat, A. (2014). Hybrid algorithm for a vendor managed inventory system in a two-echelon supply chain. *European Journal of Operational Research*, 238(1), 114-121. <https://doi.org/10.1016/j.ejor.2014.02.061>
- Diabat, A. and Deskoors, R. M. (2016). A hybrid genetic algorithm based heuristic for an integrated supply chain problem. *Journal of Manufacturing Systems*, 38, 172-180. <https://doi.org/10.1016/j.jmsy.2015.04.011>
- Gen, M., Cheng, R., and Lin, L. (2008). *Network models and optimization: Multiobjective genetic algorithms approach*. Springer. <https://doi.org/10.1007/978-1-84800-181-7>
- Ghiami, Y., Williams, T., and Wu, Y. (2013). A two-echelon inventory model for a deteriorating item with stock-dependent demand, partial backlogging and capacity constraints. *European Journal of Operational Research*, 231(3), 587-597. <https://doi.org/10.1016/j.ejor.2013.06.015>
- Haq, A. N. and Boddu, V. (2014). Analysis of enablers for the implementation of lean supply chain management using an integrated fuzzy QFD approach. *Journal of Intelligent Manufacturing*, 28(1), 1-12. <https://doi.org/10.1007/s10845-014-0957-9>
- Haupt, R. L. and Haupt, S. E. (2004). *Practical genetic algorithms* (2nd ed.). Wiley.
- Holland, J. H. (1975). *Adaptation in natural and artificial systems*. University of Michigan Press.
- Huang, H. and Ke, H. (2017). Pricing decision problem for substitutable products based on uncertainty theory. *Journal of Intelligent Manufacturing*, 28(3), 503-514. <https://doi.org/10.1007/s10845-014-0991-7>
- Inkaya, T. and Akansel, M. (2017). Coordinated scheduling of the transfer lots in an assembly-type supply chain: a genetic algorithm approach. *Journal of Intelligent Manufacturing*, 28(4), 1005-1015. <https://doi.org/10.1007/s10845-015-1041-9>
- Kumar, R. S., Tiwari, M., and Goswami, A. (2016). Two-echelon fuzzy stochastic supply chain for the manufacturer-buyer integrated production-inventory system. *Journal of Intelligent Manufacturing*, 27(4), 875-888. <https://doi.org/10.1007/s10845-014-0921-8>
- Ledari, A. M., Pasandideh, S. H. R., and Koupaei, M. N. (2018). A new newsvendor policy model for dual-sourcing supply chains by considering disruption risk and special order. *Journal of Intelligent Manufacturing*, 25(6), 1367-1376. <https://doi.org/10.1007/s10845-015-1104-y>
- Leung, K., Choy, K., Siu, P. K., Ho, G., Lam, H., and Lee, C. K. (2018). A B2C e-commerce intelligent system for re-engineering the e-order fulfilment process. *Expert Systems with Applications*, 91, 386-401. <https://doi.org/10.1016/j.eswa.2017.09.026>
- Man, K. F., Tang, K. S., and Kwong, S. (1996). Genetic algorithms: Concepts and Applications. *IEEE Transactions on Industrial Electronics*, 43(5), 519-534. <https://doi.org/10.1109/41.538609>
- Matthews, J. and Visagie, S. (2013). Order sequencing on a unidirectional cyclical picking line. *European Journal of Operational Research*, 231(1), 79-87. <https://doi.org/10.1016/j.ejor.2013.05.011>
- Marchet, G., Melacini, M., and Perotti, S. (2015). Investigating order picking system adoption: A case-study-based approach. *International Journal of Logistics Research and Applications*, 18(1), 82-98. <https://doi.org/10.1080/13675567.2014.945400>
- Mousavi, S. M., Bahreininejad, A., Musa, S. N., and Yusof, F. (2017). A modified particle swarm optimization for solving the integrated location and inventory control problems in a two-echelon supply chain network. *Journal of Intelligent Manufacturing*, 28(1), 191-206. <https://doi.org/10.1007/s10845-014-0970-z>
- Mousavi, S. M., Hajipour, V., Niaki, S. T. A., and Alikar, N. (2013). Optimizing multi-item multi-period inventory control system with discounted cash flow and inflation: two calibrated meta-heuristic algorithms. *Applied Mathematical Modelling*, 37(4), 2241-2256. <https://doi.org/10.1016/j.apm.2012.05.019>
- Park, K. and Kyung, G. (2014). Optimization of total inventory cost and order fill rate in a supply chain using PSO. *The International Journal of Advanced Manufacturing Technology*, 70(9-12), 1533-1541. <https://doi.org/10.1007/s00170-013-5399-6>
- Pinto, A. R. F., Crepaldi, A. F., and Nagano, M. S. (2018). A Genetic algorithm applied to pick sequencing for billing. *Journal of Intelligent Manufacturing*, 29(2), 405-422. <https://doi.org/10.1007/s10845-015-1116-7>
- Pinto, A. R. F. and Nagano, M. S. (2019). An approach for the solution to order batching and sequencing in picking systems. *Production Engineering Research and Development*, 13(3-4), 325-341. <https://doi.org/10.1007/s11740-019-00904-4>
- Pinto, A. R. F., and Nagano, M. S. (2020). Genetic algorithms applied to integration and optimization of billing and picking processes. *Journal of Intelligent Manufacturing*, 31(3), 641-659. <https://doi.org/10.1007/s10845-019-01470-3>
- Richards, G. (2011). *Warehouse Management: A complete guide to improving efficiency and minimizing costs in the modern warehouse*. Kogan Page.
- Rim, S. C. and Park, I. S. (2008). Order picking plan to maximize the order fill rate. *Computers and Industrial Engineering*, 55(3), 557-566. <https://doi.org/10.1016/j.cie.2008.01.012>

- Sereshti, N. and Bijari, M. (2013). Profit maximization in simultaneous lot-sizing and scheduling problem. *Applied Mathematical Modelling*, 37(23), 9516-9523. <https://doi.org/10.1016/j.apm.2013.05.004>
- Seyedrezaei, M., Najafi, S. E., Aghajani, A., and Valami, H. B. (2012). Designing a genetic algorithm to optimize fulfilled orders in order picking planning problem with probabilistic demand. *International Journal*, 1(2), 40-57. http://www.riejournal.com/article_47673_0bc47688fe20f8368d8d-6f2752146e3e.pdf
- Slotnick, S. A. (2011). Order acceptance and scheduling: a taxonomy and review. *European Journal of Operational Research*, 212(1), 1-11. <https://doi.org/10.1016/j.ejor.2010.09.042>
- van den Berg, J. P., and Zijm, W. H. M. (1999). Models for warehouse management: Classification and examples. *International Journal of Production Economics*, 59(1), 519-528. [https://doi.org/10.1016/S0925-5273\(98\)00114-5](https://doi.org/10.1016/S0925-5273(98)00114-5)

Assessment of the Compressive Strength of Lime Mortars with Admixtures Subjected to Two Curing Environments

Evaluación de la resistencia a compresión de morteros de cal adicionados sujetos a dos ambientes de curado

Andrés F. Espitia-Morales¹ and Nancy Torres-Castellanos²

ABSTRACT

This article presents the assessment of the compressive strength of three types of lime mortar, one without admixtures and the remaining two added with metakaolin and brick dust. The chemical composition of the lime and the pozzolans was evaluated using the X-ray fluorescence technique. The mortars were subjected to two curing conditions: a humidity and temperature-controlled chamber and an accelerated carbonation chamber. Then, they were tested at the ages of 7, 28, 60, and 90 days. The results showed that the samples cured in the carbonation chamber had higher compressive strength values than the ones cured in the humidity and temperature-controlled chamber because lime mortars increase their strength with the carbonation of the calcium hydroxide present in the lime. Likewise, when adding metakaolin to the lime mortars cured in the humidity and temperature-controlled chamber, the compressive strength values were close to those of the mortars with lime only, which were cured in the carbonation chamber. From the results of this research, it is worth noting that the use of pozzolans in lime mortars improves the short-term compressive strength, which is attractive for the rehabilitation of heritage buildings, given that, in short periods of time, it manages to match the strengths that lime mortars acquire over time.

Keywords: mortar, lime, metakaolin, brick dust, carbonation, compressive strength

RESUMEN

En este artículo se presenta la evaluación de la resistencia a compresión de tres tipos de morteros con cal, uno sin adición y los dos restantes adicionados con metacaolín y polvo de ladrillo. La composición química de la cal y las puzolanas se evaluó mediante la técnica de fluorescencia de rayos X. Los morteros fueron sometidos a dos condiciones de curado: una cámara de humedad y temperatura controladas y una cámara de carbonatación acelerada. Posteriormente fueron ensayados a las edades de 7, 28, 60 y 90 días. Los resultados mostraron que las muestras curadas en cámara de carbonatación presentaron resistencias a la compresión superiores a las de los especímenes curados en cámara de humedad y temperatura controladas, ya que los morteros de cal aumentan su resistencia con la carbonatación del hidróxido de calcio presente en la cal. De igual manera, al incorporar metacaolín a los morteros de cal curados en la cámara de humedad y temperatura controladas, los valores de resistencia a la compresión fueron cercanos a aquellos de los morteros con solo cal y curados en cámara de carbonatación. A partir de los resultados de esta investigación, se destaca que el uso de puzolanas en morteros de cal mejora la resistencia a la compresión a corto plazo, lo cual resulta atractivo para la rehabilitación de edificaciones patrimoniales, pues, en cortos periodos de tiempo, este logra igualar las resistencias que adquieren los morteros de cal a lo largo del tiempo.

Palabras clave: mortero, cal, metacaolín, polvo de ladrillo, carbonatación, resistencia a compresión

Received: November 4th, 2020

Accepted: November 9th, 2021

Introduction

Lime mortars are materials that have been frequently used throughout history, and their use has expanded since ancient times (Luo *et al.*, 2020; Luque *et al.*, 2010; Zhang, *et al.*, 2020; Zhang *et al.*, 2018). Thus, most masonry buildings built before the 20th century contain mostly lime mortars (Delgado Rodrigues, 2020; Pozo-Antonio, 2015). However, with the introduction of Portland cement in 1824 and its benefits, such as rapid hardening and high mechanical strength, the usage of lime binders decreased Radonjic *et al.*, 2001, as cited in Luque *et al.*, 2010; Zhang *et al.*, 2018).

A great number of masonry buildings that have lime mortar as a bond of their masonry units have begun to show

deterioration after a good part of their service life. This is due to the incidence of different factors, such as the changes in the use of the structure (Mercado, 2007; Peñaranda,

¹ C.E., MSc Department of Civil Engineering, Escuela Colombiana de Ingeniería, Bogotá, Colombia. Affiliation: Professor at Escuela Colombiana de Ingeniería Julio Garavito, Colombia. Email: andres.espitia@escuelaing.edu.co

² C.E., MSc, PhD(c), Department of Civil Engineering, Universidad Nacional de Colombia, Bogotá, Colombia. Affiliation: Professor at Escuela Colombiana de Ingeniería Julio Garavito, Colombia. Email: nancy.torres@escuelaing.edu.co

How to cite: Espitia-Morales, A. F., and Torres-Castellanos, N. (2022). Assessment of the Compressive Strength of Lime Mortars with Admixtures Subjected to Two Curing Environments. *Ingeniería e Investigación*, 42(2), e91364. <http://doi.org/10.15446/ing.investig.91364>



Attribution 4.0 International (CC BY 4.0) Share - Adapt

2011), partial demolition of the property (Peñaranda, 2011), foundation settlement (Maldonado *et al.*, 2011), the use of materials that are incompatible with the original ones (Lourenço *et al.*, 2014), or simply because of the effects of the passage of time (Maravelaki-Kalaitzaki *et al.*, 2005; Torney *et al.*, 2015).

This is how, during most of the 20th century, cement mortars were employed in the restoration of heritage buildings (Vejmelková *et al.*, 2012). Over time, different authors indicated that using cement mortars in heritage restorations resulted in some inconveniences for the structures, such as the crystallization of salts and the low flexibility of cement-based mortars (Pozo-Antonio, 2015; Vavříčuk *et al.*, 2018; Zhang *et al.*, 2020). Therefore, in some historical buildings, it has been observed that the deterioration process accelerates after restoration interventions (Gleize *et al.*, 2009; Vejmelková *et al.*, 2012), due to the incompatibility between cement mortars and the original materials (Aalil *et al.*, 2019; Lanás and Álvarez, 2003).

Certainly, at the moment of rehabilitating a heritage building, the starting point for an adequate selection of the repair materials is analyzing the ones that already exist in the structure (Forster, 2010; Gleize *et al.*, 2009; Maravelaki-Kalaitzaki *et al.*, 2005; Morillas *et al.*, 2019; Torney *et al.*, 2015). Hence, it is important to consider that historic structures have constructive characteristics and materials that differ from modern ones (Lucolano *et al.*, 2013).

Moreover, the materials vary in their composition, which is why there are uncertainties related to the environmental conditions to which they are exposed (Ball *et al.*, 2011; Koutník *et al.*, 2020). Thus, restoration mortars must be selected from the study of the ancient materials and their decay, as well as from the environmental factors affecting the structure (Apostolopoulou *et al.*, 2018).

Lime mortars, in turn, have certain advantages, such as physical-chemical compatibility with older binders; higher plasticity, which allows them to accommodate to the deformations implied by masonry; and good water vapor permeability (de Nardi *et al.*, 2017; Lanás and Álvarez, 2003; Pozo-Antonio, 2015; Vavříčuk *et al.*, 2018; Zhang *et al.*, 2018). On the other hand, there are some inconveniences when using lime binders, such as low strength, slow hardening, poor water resistance, high retraction, and low cohesion between the mortars and the masonry units (Vavříčuk *et al.*, 2018; Zhang *et al.*, 2018). To mitigate these problems, admixtures rich in aluminum-silicates (Zhang *et al.*, 2020) such as metakaolin or brick dust are employed (Nežerka *et al.*, 2016).

Furthermore, the hardening process of lime mortars stems from the reaction between the CO₂ present in the atmosphere and the Ca(OH)₂ of the lime (Pavlík *et al.*, 2012; Zhang *et al.*, 2020), which transforms into CaCO₃ (Arizzi *et al.*, 2011; Ergenç *et al.*, 2018; Luque *et al.*, 2010). Thus, the carbonation ratio of these mortars is a decisive

factor that influences the strength and durability of these mixtures (Arizzi *et al.*, 2011; El-Turki *et al.*, 2009; Pavlík *et al.*, 2012). This is due to the fact that the reaction with the environment generates changes in the structure of the mortars (Arandigoyen and Álvarez, 2006; Cazalla, 2002; Ergenç *et al.*, 2018). Moreover, it seems that, during the process, there is an increase in the mass and volume of the hardened particles (Pavlík *et al.*, 2012). Likewise, it has been observed that said phenomenon starts from the outer zone to the inner zone of the binders (Arizzi *et al.*, 2011; Delgado Rodríguez, 2020).

Therefore, different works of research have been conducted at an international level to evaluate lime mortars. These studies have found that the development of strength is related to the quality of the lime (Lanas and Álvarez, 2003) since it influences the mechanical and hydraulic properties of the mixtures (Vejmelková *et al.*, 2012). It has been noted that the hardening ratios of these mortars are low, which is reflected on the evolution of their mechanical properties (Moropoulou *et al.*, 2005). This is due to the fact that the maximum strength that these binders achieve is linked to the presence of non-carbonated portlandite (Garijo *et al.*, 2020; Lanás and Álvarez, 2003). Additionally, the stiffness of the mortars increases during the hydration of the materials' hydraulic components. Due to the chemical reactions that take place, the curing conditions influence the mechanical strength (Pozo-Antonio, 2015). Likewise, as the lime/aggregate ratio decreases, so does the strength (Lanas and Álvarez, 2003), which is why mortars with higher lime contents show higher strength values. This is explained by the fact that, as they are more porous, the carbonation process occurs at a higher rate, and, therefore, the development of the mechanical properties improves (Lanas *et al.*, 2006).

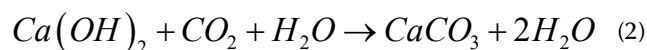
As mentioned before, using admixtures rich in aluminum-silicates can mitigate some problems encountered in lime mortars. Among these admixtures is metakaolin, a material that has several advantages when used in mortar mixtures, such as an increased mechanical strength, improved resistance to chemical attacks, increased durability, decreased retraction, and more (Cazalla, 2002; Siddique, 2008; Vavříčuk *et al.*, 2018). Accordingly, in lime mortars added with metakaolin, mechanical and micro-structural properties compatible with those found on traditional materials have been observed (Vejmelková *et al.*, 2012). Thus, they are useful for masonry rehabilitations (Aggelakopoulou *et al.*, 2011). On the other hand, some studies have evidenced a decrease in the long-term strength of this type of mortar, which is attributed to the emergence of micro-cracks due to the mixtures' retraction (Aggelakopoulou *et al.*, 2011; Velosa *et al.*, 2009). It seems that this decrease deepens as the metakaolin content increases (Vavříčuk *et al.*, 2018). Another relevant factor is the type of metakaolin, which can affect the properties of the mortar, as is the case of Velosa *et al.* (2009), who found that metakaolin rich in kaolinite and alumina can lead to mixtures with higher strength values.

Another material that has been used in lime mortar mixtures is brick dust, which can provide both economic and environmental benefits, considering that it has a high degradation resistance that hinders the conditioning of industrial waste (Matias *et al.*, 2008). Additionally, crushed brick particles have been identified in some historic mortars. Even the roman architect Vitruvius, in his work *The Ten Books on Architecture*, recommended adding a portion of crushed bricks to the mortar mixtures, with the objective of increasing their durability and strength (Nežerka *et al.*, 2016). Authors like Navrátilová Rovnaníková (2016), Matias *et al.* (2008), Nežerka *et al.* (2016), and Aalil *et al.* (2019) observed that adding brick dust to mortar mixtures improved their mechanical properties, which can be attributed to the reduction of retraction-related cracks, due to the presence of the brick grains (Nežerka *et al.*, 2016). Therefore, this type of binder may be acceptable for repair mortars (Matias *et al.*, 2008).

Considering the information provided above, the aim of this research was to evaluate the strength of mortars subjected to an accelerated carbonation process, in order to simulate the conditions of heritage building mortars. Furthermore, it was sought to evaluate the effect of admixtures such as metakaolin and brick dust, with the objective of obtaining the same properties of carbonated mixtures, therefore highlighting them as a rehabilitation alternative for lime mortar masonry in heritage buildings. This is important, as it opens the possibility of reinforcing existing structures by using materials with properties similar to those that are currently part of the structure.

Carbonation in lime mortars

The carbonation process of the mortars influences their hardening ratio, durability, and mechanical strength (Pavlík *et al.*, 2012) because the captured CO_2 fixes into a matrix to form calcites, thus improving its properties (Luo *et al.*, 2020). In general, five stages occur during this phenomenon (Arandigoyen and Álvarez, 2006; Papadakis *et al.*, 1991, as cited in Cazalla, 2002; Kang *et al.*, 2020; Pavlík *et al.*, 2012): diffusion of the CO_2 in the mixture, condensation of the water in the pores, dissolution of the $\text{Ca}(\text{OH})_2$, dissolution of the CO_2 in the pore solution, and the precipitation of CaCO_3 . To summarize, carbonation is represented as the transformation of $\text{Ca}(\text{OH})_2$ into CaCO_3 due to the presence of CO_2 . Equation (1) describes the entire process:



Reactions that occur between metakaolin and lime

Since metakaolin is a product based on silica and alumina, a reaction between the components of the pozzolan and the $\text{Ca}(\text{OH})_2$ of the lime is produced when mixing it with lime and water. In this way, calcium silicate hydrate (CSH) and crystalline products that include calcium aluminate hydrate (CAH), and aluminum silicate hydrates are produced

(Gameiroa *et al.*, 2014 as cited in Khatib *et al.*, 2018; Siddique, 2008; Tebbal and Abidine Rahmouni, 2019).

Reactions that occur between brick dust and lime

The reactivity of the pozzolan can be affected by different factors: the quantity of silica and alumina, the firing temperature of the ceramic materials, the quantity and type of the clay that constitutes the ceramic pieces, the granulometry of the admixture, and the fineness of the crushed material. Therefore, when mixing the $\text{Ca}(\text{OH})_2$ of the lime with water and the silico-aluminous components of the ceramic pieces, a reaction occurs which produces calcium silicates and calcium aluminates. However, some studies indicate that the pozzolanic reaction depends on the reaction of silica and alumina with the CaO of the lime (Matias *et al.*, 2014). This is analogous to the chemical phenomenon that occurs between metakaolin and lime when being hydrated with water. Moreover, the amorphous phase of the material has a large impact on its pozzolanicity.

Given the importance of preserving heritage buildings and using materials for their rehabilitation which are compatible with the existing ones, a project was developed to evaluate the evolution of the compressive strength of lime mortars subjected to two curing environments: a humidity and temperature chamber and an accelerated carbonation chamber. The mechanical behavior of lime mortar mixtures added with metakaolin (MK) and brick dust (BD) was assessed as well, with the objective of finding a short-term strength similar to that of the lime mortars in heritage buildings, which also increases due to the presence of CO_2 in the atmosphere.

Materials and experimental methodology

For this study, lime (hydraulic) and pit sand (yellow or washed) with a bulk density of $2,68 \text{ g/cm}^3$ and an absorption of 2,1% were acquired, which are representative of the typical Colombian heritage buildings. The metakaolin used as admixture was supplied by the Colombian company Insumos Industriales Corona, while the brick dust (maximum particle size of $300 \mu\text{m}$) was obtained from non-structural hollow clay bricks ($33 \text{ cm} \times 11,5 \text{ cm} \times 23 \text{ cm}$, 'No. 5' in the Colombian market) that were residues from other tests. These were initially fragmented with a crusher (Figures 1 and 2), and then pulverized in a Los Angeles abrasion machine. The obtained dust was sieved through a $300 \mu\text{m}$ sieve. The chemical composition of the materials was determined with a MagixPro PW-2440 (WDXRF) X-ray fluorescence spectrometer. Additionally, granulometric analyses of the sand and the brick dust were performed.

Physical and chemical properties of the materials

Table 1 shows the chemical composition of the lime, metakaolin (MK), and brick dust (BD) employed in this research.



Figure 1. Crushing process
Source: Authors



Figure 2. Crushed brick dust
Source: Authors

It can be observed that the lime has a high content of CaO, which is expected to transform into $\text{Ca}(\text{OH})_2$ when hydrated. This, in turn, will precipitate as CaCO_3 during the carbonation process. Likewise, it can be appreciated that the material contains SiO_2 and Al_2O_3 , compounds that intervene in the formation of CSH and CAH when the lime is hydrated.

Regarding the metakaolin, it is mainly composed of SiO_2 and Al_2O_3 , making up 96,18% of its composition. Thus, when incorporating the admixture to lime and water, the components of the pozzolan intervene in the formation of CSH, CAH, and hydrated aluminum-silicates. The chemical composition of the metakaolin is similar to the one registered by authors such as Aggelakopoulou *et al.* (2011), Velosa *et al.* (2009), Vavričuk *et al.* (2018), and Vejmelková *et al.* (2012).

Table 1. Chemical composition of the materials. XRF-148-16, XRF-024-17, and XRF-228-17 reports from the X-ray fluorescence laboratory of Universidad Nacional de Colombia, Bogotá.

Lime		MK		BD	
Component	%	Component	%	Component	%
CaO	86,83	SiO_2	58,04	SiO_2	67,27
SiO_2	6,67	Al_2O_3	38,14	Al_2O_3	23,13
Al_2O_3	2,36	Fe_2O_3	1,36	Fe_2O_3	5,56
Fe_2O_3	1,88	TiO_2	1,23	K_2O	1,59
MgO	0,88	K_2O	0,59	TiO_2	1,08
SO_3	0,60	MgO	0,20	MgO	0,43
K_2O	0,24	CaO	0,14	Na_2O	0,35
TiO_2	0,22	Na_2O	0,07	CaO	0,17
P_2O_5	0,16	SO_3	0,05	Ba	0,14
SrO	0,09	Ba	0,05	P_2O_5	0,08
MnO	0,06	P_2O_5	0,04	SO_3	0,06
ZnO	0,03	Zr	0,04	V	0,03
				Zr	0,03
				Cr	0,02
				Zn	0,02
				Sr	0,02
				Cl	0,01
				MnO	0,01

Source: Authors

Regarding brick dust, it can be observed that it is largely composed of SiO_2 and Al_2O_3 , which make up 90,40% of its composition. This agrees with the results reported by Böke *et al.* (2006) and Aail *et al.* (2019), who determined a high content of SiO_2 in brick composition. Moreover, Matias *et al.* (2014) indicated that the pozzolanic reaction depends mainly on the presence of SiO_2 and Al_2O_3 , and that, when these compounds are mixed with water and lime, they may intervene in the formation of calcium silicates and calcium aluminates.

Figure 3 shows the granulometric curve of the sand. It can be observed that it has a high content of material passing through the No. 100 sieve (34%) and 20% of material passing through the No. 200 sieve.

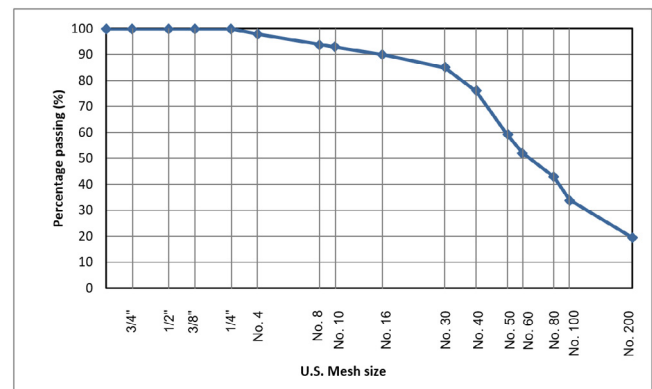


Figure 3. Granulometric curve of the sand

Source: Authors

Figure 4 presents the granulometric curve of the brick dust, which has approximately 42% of material passing through the No. 100 sieve and 12% passing through the No. 200 sieve.

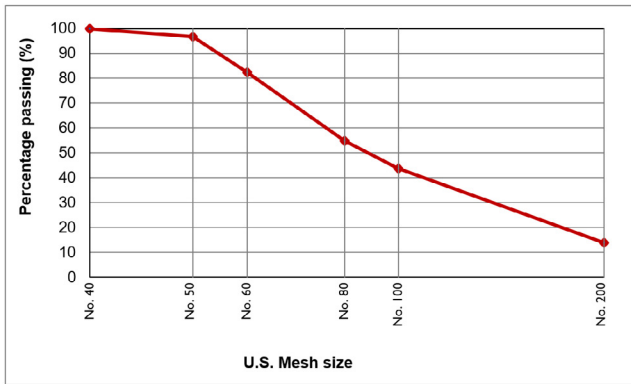


Figure 4. Granulometric curve of the brick dust

Source: Authors

Table 2 shows the weight proportions used in the elaboration of the mortars. These are typical dosages used in heritage buildings.

Table 2. Mortar weight proportions

Mortar	Denomination	Proportion
Lime : Sand	MLS	1:3
Lime : Sand : Metakaolin	MMK	1:3:0,2
Lime : Sand : Brick Dust	MBD	1:3:1

Source: Authors

Table 3 presents the amount of materials per cubic meter of each mortar mixture. Additionally, to determine the amount of water required, a fluidity close to 100% was sought. To that effect, fluidity tests were performed following the guidelines of the NTC 5784 (ICONTEC, 2017) standard, since no other regulation exists at a national level which applies to the type of mortars employed in this study.

Table 3. Dosages of the mortars per cubic meter

Mortar	Lime (kg)	Sand (kg)	MK (kg)	BD (kg)	Water (kg)	Fluidity (%)
MLS	450	1 350	-	-	405	101
MMK	430	1 290	86	-	452	97
MBD	360	1 080	-	360	454	100

Source: Authors

Figure 5 shows the fluidity test that guaranteed a proper workability of the mortars under study.

The compressive strength test specimens were mortar cubes with a 50 mm length, as shown in Figure 6. For their elaboration, the procedure described in the NTC 220 (ICONTEC, 2021) was used as reference. To that end, the materials were mixed, and the mixtures were placed on cubical molds. These were left for three days in a humidity and temperature chamber under the following controlled conditions: a temperature of 25 ± 2 °C and a relative humidity of $55 \pm 5\%$. Afterwards, the samples were taken out of the molds and then cured. In total, 72 cubes were elaborated.

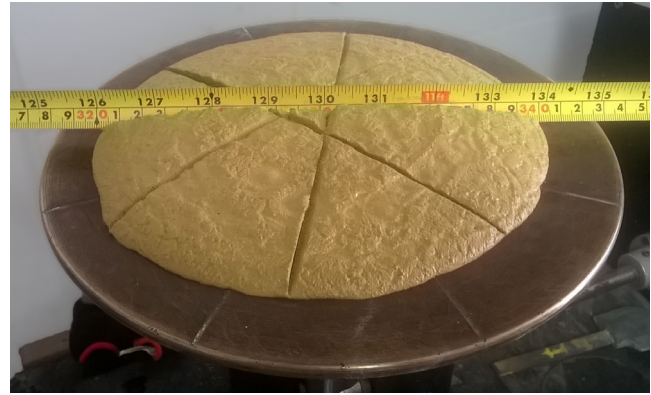


Figure 5. Mortar fluidity test

Source: Authors



Figure 6. Elaboration of the mortar cubes

Source: Authors

As mentioned before, two curing environments were evaluated: the first one consisted of a chamber with the humidity set at $55 \pm 5\%$ and a temperature of 25 ± 2 °C (Figure 7); the second one was an accelerated carbonation chamber (Figure 8) with the following controlled parameters: a temperature of 23 °C, a relative humidity of 65%, and a CO₂ concentration of 5%. This process was conducted to accelerate the aging process of the mixtures, with the objective of simulating the mortar of heritage buildings when exposed to the CO₂ of the environment.

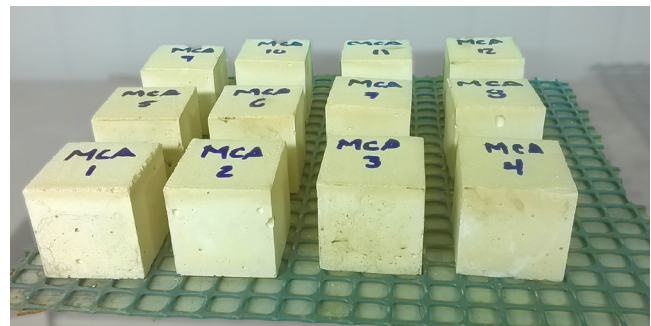


Figure 7. Curing environments

Source: Authors

The compressive strength tests were performed in a Shimadzu Universal Testing Machine with a load capacity of 1 000 kN. Three cubes were tested at each of the following ages: 7, 28, 60, and 90 days.



Figure 8. Curing environments
Source: Authors

Results and discussion

Compressive strength

Figure 9 shows the compressive strength results of the samples, which are identified as follows: MLS (sample with lime/sand), MMK (sample with metakaolin), and MBD (sample with brick dust). Moreover, the samples cured in the humidity chamber were identified as (NC), while (C) was for the samples cured in the accelerated carbonation chamber. There are records at ages 7, 28, 60, and 90 days, with three specimens from each age.

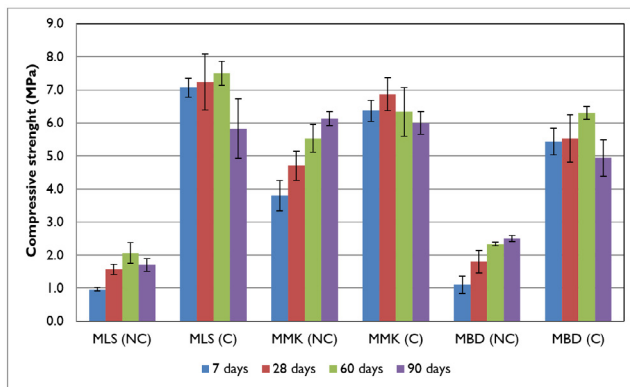


Figure 9. Evolution of the compressive strength of mortars cured in humidity chamber and accelerated carbonation chamber
Source: Authors

When assessing the results, a considerable increase in strength can be observed for the MLS (C) mixture with respect to the MLS (NC) mortar. At 7, 28, 60, and 90 days, said increase was of 631, 362, 263, and 243%, respectively. This phenomenon confirms the low hardening ratio of this type of mortar, which is favored by the CO₂ surrounding it over time, just as stated by Moropoulou *et al.* (2005). Likewise, in the carbonated cubes, a 22% decrease in strength was observed between days 60 and 90. In this regard, authors such as Velosa *et al.* (2009) and Aggelakopoulou (2011) attribute this decrease to the formation of micro-cracks caused by the retraction of the mortar. In the non-carbonated specimens, the decrease in strength was of 18%, which may be due to the presence of non-carbonated portlandite, as evidenced by Lanás and Álvarez (2003).

By comparing the strength values of the MMK (C) mortar samples with those of the MMK (NC) mixtures, the former reported values 68, 46, and 14% higher than the latter at the ages of 7, 28, and 60 days. However, at 90 days, their strength was 2% lower. Similarly, the strength of the carbonated samples showed a 13% decrease with respect to the maximum reached value, which is a phenomenon that was also observed by Velosa *et al.* (2009) and Aggelakopoulou (2011) in their research, due to the formation of micro-cracks as a result of retraction. On the other hand, the strength values of the MMK (NC) mortars were between 168 and 293% higher than those obtained in the samples made of MLS (NC) mortar. Also, the strength values of the MMK (C) mixture were between 5 and 16% lower than the ones of the MLS (C) mortar during the initial 60 days. At 90 days, that value was 3% higher.

As for the MBD (C) mortars, their strengths were 394, 207, 170, and 97% higher at the ages of 7, 28, 60, and 90 days, respectively, in comparison with those of the MBD (NC) mixtures. Regarding the carbonated samples, a 22% decrease in strength was observed, similar to the one observed for the MLS (C) mortar. Furthermore, the strength values of the MMK (NC) specimens were between 14 and 47% higher than those of the MLS (NC) mixture. The strength values of the MBD (C) mixtures were between 16 and 24% lower than those of the MLS (C) mortar.

With respect to the evolution of the compressive strength of the mortars, it was evidenced that the MMK (C) and MBD (C) mixtures presented strength values similar to those obtained for the MLS (C) mortar. This can be attributed to the accelerated aging process achieved in the carbonation chamber, since the components of the admixtures could react faster with the Ca(OH)₂ of the lime, thus forming other compounds like calcium silicates and calcium aluminates, which indicates that a lower amount of CaCO₃ may have precipitated in the added mixtures. In the case of the mixtures cured in the humidity chamber, the admixtures improved the compressive strength.

Carbonation depth

To study the carbonation process of the different samples, cylinders with a 10 cm diameter and 20 cm height were made using the same dosages as the mortars. These were taken to the carbonation chamber with the temperature set at 23 °C, a relative humidity of 65%, and a carbon dioxide concentration of 5%. Initially, the probes were left inside the chamber for a 5-day period. After that, a slice with a thickness of approximately 5 cm was taken from the samples. After that, phenolphthalein was applied to the sliced surface, and the depth of the carbonation front was measured. Afterwards, epoxy was applied to the affected surface of the cylinders, and then they were taken back to the chamber. The lime and sand samples, as well as those added with brick dust, were in the chamber for a 2-day period, and the specimens added with metakaolin were carbonated for 1 day more, since the initial carbonation was

higher on these samples. Once the samples reached those ages, the procedure was repeated to record the carbonation depth. Figure 10 shows the advancement of the carbonation front of the mortars under study.

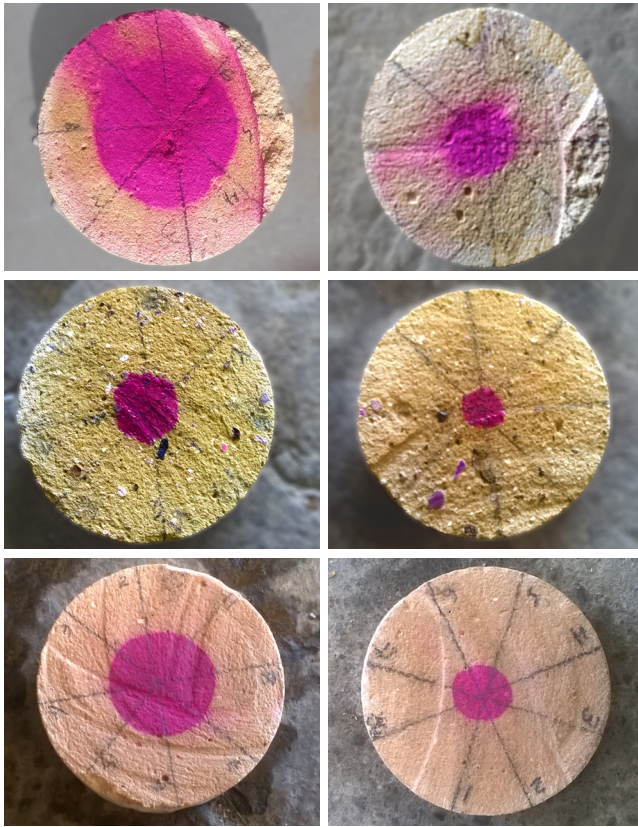


Figure 10. Advancement of the carbonation front
Source: Authors

The rapid penetration of CO_2 into the specimens is evident, and it accelerates the compressive strength gain. It can be observed that, at 7 days, values close to the compressive strengths at 90 days were already being obtained in the samples subjected to the carbonation process. Nevertheless, Garijo *et al.* (2020) indicate that the results of this method must be treated carefully because the reaction tends to advance along the cracks and voids beyond the front.

Conclusions

In general, the compressive strength values determined for the mortars added with metakaolin and cured in the humidity and temperature chamber tripled those registered for the lime and sand mixtures cured under the same conditions. They also matched the strength of the lime and sand mortars that were subjected to the accelerated carbonation chamber. This demonstrates the benefit of using metakaolin as an admixture in lime mortar mixtures for repairing or reinforcing heritage buildings since, in a very short period of time, it would match the properties of the mortars present in these structures, which have been subjected a carbonation process, thus improving their properties over time.

It was observed that the carbonated samples had similar strength values, which is explained by the fact that the carbonation process seeks to emulate the material properties through the passage of time, and it is known that strength increases with time. However, regarding the non-carbonated samples, the high variation between the metakaolin mixtures and the others was attributed to the early high pozzolanic activity of this material, which increases the strength of the mixture in short periods. This also implies that the carbonation process had less impact on the metakaolin samples, as most of its strength was gained due to its pozzolanic properties, and not by the simulation of the passage of time.

Acknowledgments

The authors express their gratitude to Escuela Colombiana de Ingeniería and the company Insumos Industriales Corona for the donation of the metakaolin.

References

- Aalil, I., Badreddine, D., Beck, K., Brunetaud, X., Cherkaoui, K., Chaaba, A., and Al-Mukhtar, M. (2019). Valorization of crushed bricks in lime-based mortars. *Construction and Building Materials*, 226, 555-563. <https://doi.org/10.1016/j.conbuildmat.2019.07.265>
- Aggelakopoulou, E., Bakolas, A., and Moropoulou, A. (2011). Properties of lime-metakaolin mortars for the restoration of historic masonries. *Applied Clay Science*, 53(1), 15-19. <https://doi.org/10.1016/j.clay.2011.04.005>
- Apostolopoulou, M., Delegou, E. T., Alexakis, E., Kalofonou, M., Lampropoulos, K. C., Aggelakopoulou, E., and Moropoulou, A. (2018). Study of the historical mortars of the Holy Aedicule as a basis for the design, application and assessment of repair mortars: a multispectral approach applied on the Holy Aedicule. *Construction and Building Materials*, 181, 618-637. <https://doi.org/10.1016/j.conbuildmat.2018.06.016>
- Arandigoyen, M. and Álvarez, J. (2006). Carbonation process in lime pastes with different water/binder ratio. *Materiales de Construcción*, 56, 5-18. <https://doi.org/10.3989/mc.2006.v56.i281.88>
- Arizzi, A., Martínez-Martínez, J., Cultrone, G., and Benavente, D. (2011). Mechanical evolution of lime mortars during the carbonation process. *Key Engineering Materials*, 465, 483-486. <https://doi.org/10.4028/www.scientific.net/KEM.465.483>
- Ball, R., El-Turki, A., and Allen, G. (2011). Influence of carbonation on the load dependent deformation of hydraulic lime mortars. *Materials Science and Engineering*, 528(7-8), 3193-3199. <https://doi.org/10.1016/j.msea.2010.12.070>
- Böke, H., Akkurt, S., and Elif, U. (2006). Characteristics of brick used as aggregate in historic brick-lime mortars and plasters. *Cement and Concrete Research*, 36, 1115-1122. <https://doi.org/10.1016/j.cemconres.2006.03.011>
- Cazalla, O. (2002). *Morteros de cal. Aplicación en el patrimonio histórico* [Doctoral thesis, Universidad de Granada]. <http://hdl.handle.net/10481/28626>

- de Nardi, C., Cecchi, A., Ferrara, L., Benedetti, A., and Cristofori, D. (2017). Effect of age and level of damage on the autogenous healing of lime mortars. *Composites Part B: Engineering*, 124, 144-157. <https://doi.org/10.1016/j.compositesb.2017.05.041>
- Delgado Rodrigues, J. (2020). Practical evidence and experimental demonstration of the Liesegang phenomenon in the carbonation process of lime mortars in exposed masonries. *Journal of Cultural Heritage*, 45, 169-179. <https://doi.org/10.1016/j.culher.2020.02.015>
- El-Turki, A., Ball, R., and Geoffrey, A. (2009, September 6-9). *The effect of carbonation on the mechanical and microstructural properties of lime and cement mortars* [Conference presentation]. 11th International Conference on Non-conventional Materials and Technologies (NOCMAT 2009), Bath, UK. http://opus.bath.ac.uk/21017/1/2009_NOCMAT_El_Turki_et_al_Paper_39.pdf
- Ergenç, D., Gómez-Villalba, L. S., and Fort, R. (2018). Crystal development during carbonation of lime-based mortars in different environmental conditions. *Materials Characterization*, 142, 276-288. <https://doi.org/10.1016/j.matchar.2018.05.043>
- Forster, A. M. (2010). Masonry repair options and their philosophical ramifications. In J. Válek, C. Groot, and J. J. Hughes (Eds.) *Proceedings of the 2nd Conference on Historic Mortars - HMC 2010 and RILEM TC 203-RHM final workshop* (pp. 937-982). RILEM. <https://researchportal.hw.ac.uk/en/publications/masonry-repair-options-and-their-philosophical-ramifications>
- Garijo, L., Zhang, X., Ruiz, G., and Ortega, J. J. (2020). Age effect on the mechanical properties of natural hydraulic and aerial lime mortars. *Construction and Building Materials*, 236, 117573. <https://doi.org/10.1016/j.conbuildmat.2019.117573>
- Gleize, P., Motta, E., Silva, D., and Roman, H. (2009). Characterization of historical mortars from Santa Catarina (Brazil). *Cement and Concrete Composites*, 31(5), 342-346. <https://doi.org/10.1016/j.cemconcomp.2009.02.013>
- ICONTEC (2017). NTC 5784:2017: Método para determinar la fluidez de morteros de cemento hidráulico. ICONTEC.
- ICONTEC (2021). NTC 220: 2021: Determinación de la resistencia de morteros de cemento hidráulico a la compresión, usando cubos de 50 mm o 2 pulgadas de lado. (ASTM C109). ICONTEC.
- Iucolano, F., Liguori, B., and Colella, C. (2013). Fibre-reinforced lime-based mortars: a possible resource for ancient masonry restoration. *Construction and Building Materials*, 38, 785-789. <https://doi.org/10.1016/j.conbuildmat.2012.09.050>
- Kang, S. H., Kwon, Y. H., and Moon, J. (2020). Controlling the hydration and carbonation in lime-based materials: Advantage of slow carbonation in CO₂ curable construction materials. *Construction and Building Materials*, 249, 118749. <https://doi.org/10.1016/j.conbuildmat.2020.118749>
- Khatib, J. M., Baalbaki, O., and Elkordi, A. A. (2018). Metakaolin. In R. Siddique and P. Cachim (Eds.) *Waste and supplementary cementitious materials in concrete: characterisation, properties and applications* (pp. 493-511). Woodhead Publishing. <https://doi.org/10.1016/B978-0-08-102156-9.00015-8>
- Koutník, P., Soukup, A., Bezucha, P., and Kohout, J. (2020). Properties of mortars based on β -belite-metakaolinite-hydrated lime binder system. *Construction and Building Materials*, 253, 119123. <https://doi.org/10.1016/j.conbuildmat.2020.119123>
- Lanas, J. and Álvarez, J. (2003). Masonry repair lime-based mortars: Factors affecting the mechanical behavior. *Cement and Concrete Research*, 33(11), 1867-1876. [https://doi.org/10.1016/S0008-8846\(03\)00210-2](https://doi.org/10.1016/S0008-8846(03)00210-2)
- Lanas, J., Pérez-Bernal, J., Bello, M., and Álvarez, J. (2006). Mechanical properties of masonry repair dolomitic lime-based mortars. *Cement and Concrete Research*, 36(5), 951-960. <https://doi.org/10.1016/j.cemconres.2005.10.004>
- Lourenço, P., Van Hees, R., Fernandes, F., and Lubelli, B. (2014). Characterization and Damage of Brick. In A. Costa, J. Miranda, and H. Varum (Eds.) *Structural rehabilitation of old buildings* (vol. 2, pp. 109-130). Springer. <https://doi.org/10.1007/978-3-642-39686-1>
- Luo, K., Li, J., Han, Q., Lu, Z., Deng, X., Hou, L., and Cai, P. (2020). Influence of nano-SiO₂ and carbonation on the performance of natural hydraulic lime mortars. *Construction and Building Materials*, 235, 117411. <https://doi.org/10.1016/j.conbuildmat.2019.117411>
- Luque, A., Cultrone, G., and Sebastian, E. (2010). The use of lime mortars in restoration work on architectural heritage. In M. Bosternaru, R. Přikryl, and Á. Török (Eds.) *Materials, technologies and practice in historic heritage structures* (pp. 197-207). Springer. https://doi.org/10.1007/978-90-481-2684-2_11
- Maldonado, N., Martin, P., and Maldonado, I. (2011). Seismic mitigation of a historic masonry building. *The Open Construction and Building Technology Journal*, 5, 61-70. <https://doi.org/10.2174/1874836801105010061>
- Maravelaki-Kalaitzaki, P., Bakolas, A., Karatasios, I., and Kilikoglou, V. (2005). Hydraulic lime mortars for the restoration of historic masonry in Crete. *Cement and Concrete Research*, 35(8), 1577-1587. <https://doi.org/10.1016/j.cemconres.2004.09.001>
- Matias, G., Faria, P., and Torres, I. (2008, September 24-26). *Lime mortars with brick dust and ground particles for ancient masonry: development and evaluation* [Conference presentation]. HMC08 - 1st Historical Mortars Conference: Characterization, Diagnosis, Conservation, Repair and Compatibility, Lisbon, Portugal. <http://hdl.handle.net/10362/11325>
- Matias, G., Faria, P., and Torres, I. (2014). Lime mortars with heat treated clays and ceramic waste: a review. *Construction and Building Materials*, 73, 125-136. <https://doi.org/10.1016/j.conbuildmat.2014.09.028>
- Mercado, E. (2007). Patrimonio edificado de propiedad privada: relación compleja y contradictoria entre lo público y lo privado en el Centro Histórico de Morelia. *Intervención (México DF)*, 2(4) 27-34. <https://www.redalyc.org/articulo.oa?id=355632771006>
- Morillas, H., Hualparimachi, G., Maguregui, M., Marcaida, I., Gallego Cartagena, E., Astete, F., and Madaraiga, J. M. (2019). Characterization of restoration lime mortars and decay by-products in the Meditation area of Machu Picchu archaeological site. *Science of the Total Environment*, 692, 23-31. <https://doi.org/10.1016/j.scitotenv.2019.07.256>

- Moropoulou, A., Bakolas, A., Moundoulas, P., Aggelakopoulou, E., and Anagnostopoulou, S. (2005). Strength development and lime reaction in mortars for repairing historic masonries. *Cement and Concrete Composites*, 27(2), 289-294. <https://doi.org/10.1016/j.cemconcomp.2004.02.017>
- Navrátilová, E. and Rovnaníková, P. (2016). Pozzolan properties of brick powders and their effect on the properties of modified lime mortars. *Construction and Building Materials*, 120, 530-539. <https://doi.org/10.1016/j.conbuildmat.2016.05.062>
- Nežerka, V., Antoš, J., Litoš, J., Tesárek, P., and Zeman, J. (2016). An integrated experimental-numerical study of the performance of lime-based mortars in masonry piers under eccentric loading. *Construction and Building Materials*, 114, 913-924. <https://doi.org/10.1016/j.conbuildmat.2016.04.013>
- Pavlík, Z., Benešová, H., Matiašovský, P., and Pavlíková, M. (2012). Study on carbonation process of several types of advanced lime-based plasters. *International Journal of Materials and Metallurgical Engineering*, 6(10), 963-967. <https://zenodo.org/record/1055934/files/1834.pdf>
- Peñaranda, L. (2011). *Manual para la conservación del patrimonio arquitectónico habitacional de Sucre*. https://www.aecid.es/Centro-Documentacion/Documentos/Publicaciones%20coeditadas%20por%20AECID/Manual_de_Intervencixn_PRAHS.pdf
- Pozo, A. (2015). Evolution of mechanical properties and drying shrinkage in lime-based and lime cement-based mortars with pure limestone aggregate. *Construction and Building Materials*, 77, 472-478. <https://doi.org/10.1016/j.conbuildmat.2014.12.115>
- Siddique, R. (2008). *Waste materials and by-products in concrete*. Springer. https://doi.org/10.1007/978-3-540-74294-4_2
- Tebbal, N. and Abidine Rahmouni, Z. (2019). Rheological and mechanical behavior of mortars with metakaolin formulation. *Procedia Computer Science*, 158, 45-50. <https://doi.org/10.1016/j.procs.2019.09.026>
- Torney, C., Forster, A. M., Banfill, P. F., and Szadurski, E. M. (2015). The effects of site practice on the physical properties of proprietary stone restoration mortar. *Construction and Building Materials*, 75, 359-367. <https://doi.org/10.1016/j.conbuildmat.2014.11.040>
- Vavričuk, A., Bokan-Bosiljkov, V., and Kramar, S. (2018). The influence of metakaolin on the properties of natural hydraulic lime-based grouts for historic masonry repair. *Construction and Building Materials*, 172, 706-716. <https://doi.org/10.1016/j.conbuildmat.2018.04.007>
- Vejmelková, E., Keppert, M., Keršner, Z., Rovnaníková, P., and Černý, R. (2012). Mechanical, fracture-mechanical, hydric, thermal, and durability properties of lime-metakaolin plasters for renovation of historical buildings. *Construction and Building Materials*, 31, 22-28. <https://doi.org/10.1016/j.conbuildmat.2011.12.084>
- Velosa, A. L., Rocha, F., and Veiga, R. (2009). Influence of chemical and mineralogical composition of metakaolin on mortar characteristics. *Acta Geodynamica et Geomaterialia*, 6(1), 121-126. https://www.irsm.cas.cz/materialy/acta_content/2009_01/9_Rocha.pdf
- Zhang, D., Zhao, J., Wang, D., Wang, Y., and Ma, X. (2020). Influence of pozzolanic materials on the properties of natural hydraulic lime based mortars. *Construction and Building Materials*, 244, 118360. <https://doi.org/10.1016/j.conbuildmat.2020.118360>
- Zhang, D., Zhao, J., Wang, D., Xu, C., Zhai, M., and Ma, X. (2018). Comparative study on the properties of three hydraulic lime mortar systems: Natural hydraulic lime mortar, cement-aerial lime-based mortar and slag-aerial lime-based mortar. *Construction and Building Materials*, 186, 42-52. <https://doi.org/10.1016/j.conbuildmat.2018.07.053>

Effect of the Colombian Renewable Energy Law on the Levelized Cost of a Substitute Gaseous Fuel Produced from MSW Gasification

Efecto de la ley colombiana de energías renovables en el costo nivelado del combustible gaseoso sustituto producido a partir de la gasificación de RSU

Néstor D. Montiel-Bohórquez¹, Juan D. Saldarriaga-Loaiza², and Juan F. Pérez³

ABSTRACT

Colombian municipal solid waste (MSW) production trends indicate that sanitary emergencies could occur in the largest cities of the country by 2030 because of the end of their landfills' useful life. In this work, the energy recovery from different MSW through the updraft plasma gasification process to produce syngas as a substitute gaseous fuel was assessed from an economic viewpoint. The study was carried out using the results of an implemented model under a thermochemical approach using Aspen Plus. The economic assessment was conducted using the levelized cost of syngas production (LCOS), which was regarded as an economic indicator that considers tax incentives in the context of the Colombian renewable energy regulations (Law 715 of 2014). The combination between operational conditions (air flow and plasma temperature) allowed finding the maximum efficiency by means of a sensitivity analysis. The maximum efficiency ranged from 79,22 to 83,46%, highlighting the flexibility of the plasma gasification process to treat MSW. The lowest levelized syngas production cost reached with tax incentives varied from 13,19 to 22,95 ¢US\$/kWh. Therefore, a waste disposal charge was proposed to make these projects feasible, which must range between 11,25 and 23,56 ¢US\$/kWh (123-259 US\$/t).

Keywords: waste to energy, syngas, plasma gasification, law 1715 of 2014, economic analysis

RESUMEN

Las tendencias de la producción de residuos sólidos urbanos (RSU) en Colombia indican que podrían producirse emergencias sanitarias en las ciudades más grandes del país para 2030 debido a la finalización de la vida útil de sus rellenos sanitarios. En este trabajo se evaluó, desde un punto de vista económico, la recuperación de energía de los diferentes RSU mediante el proceso de gasificación por plasma en contracorriente para producir un gas de síntesis como combustible gaseoso sustituto. El estudio se llevó a cabo utilizando los resultados de un modelo implementado bajo un enfoque termoquímico en Aspen Plus. La evaluación económica se realizó mediante el costo nivelado de la producción de gas natural sintético (LCOS), que se consideró como un indicador económico que considera los incentivos fiscales en el contexto de la legislación colombiana sobre energía renovable (Ley de 1715 de 2014). La combinación entre las condiciones operativas (flujo de aire y temperatura de plasma) permitió encontrar la máxima eficiencia mediante un análisis de sensibilidad. La eficiencia máxima varió entre 79,22 y 83,46 %, destacando la flexibilidad del proceso de gasificación de plasma para el tratamiento de los RSU. El menor costo nivelado de la producción de gas natural sintético alcanzado con los incentivos fiscales varió de 13,19 a 22,95 ¢US\$/kWh. Por lo tanto, se propuso un cobro por disposición de residuos para hacer factibles estos proyectos, que debe oscilar entre 11,25 y 23,56 ¢US\$/kWh (123-259 US\$/t).

Palabras clave: residuos a energía, gas de síntesis, gasificación por plasma, ley 1715 de 2014, análisis económico

Received: November 16th, 2020

Accepted: August 17th, 2021

Introduction

In the last decade, the global increase in primary energy consumption has been between 1,5 and 2,2% per year, where the share of fossil fuels was ~85% of the 1 3511 Mtoe consumed in 2017 (British Petroleum, 2018; International Energy Agency, 2018). In Colombia, the primary energy mix is composed of oil (39,1%), natural gas (20%), coal (9,4%), hydro (30,4%), and renewable energy (1,0%) (British Petroleum, 2018); whereas the power mix is composed by hydro (63,9%), natural gas (26,3%), coal (4,8%), and cogeneration and others (5,1%) (Unidad de Planeación Minero-Energética, 2015). Currently, the country faces several challenges such as maintaining a rate of economic

¹ Mechanical Engineer, Universidad de Antioquia, Colombia. Master of Science, Universidad de Antioquia, Colombia. Affiliation: Graduate student, Universidad de Antioquia, Colombia. E-mail: nestor.montiel@udea.edu.co

² Electrical Engineer, Universidad de Antioquia, Colombia. Master of Science, Universidad de Antioquia, Colombia. Affiliation: Assistant Professor, Universidad de Antioquia, Colombia. E-mail: juand.saldarriaga@udea.edu.co

³ Mechanical Engineer, Universidad Nacional de Colombia – Sede Medellín, Colombia. Ph.D. in Energy and Fluid-mechanics Engineering, Universidad de Valladolid, Spain. Affiliation: Full Professor, Universidad de Antioquia, Colombia. E-mail: juanpb@udea.edu.co

How to cite: Montiel-Bohórquez, N. D., Saldarriaga-Loaiza, J. D., and Pérez J. F. (2022). Effect of the Colombian Renewable Energy Law on the Levelized Cost of a Substitute Gaseous Fuel Produced from MSW Gasification. *Ingeniería e Investigación*, 42(2), e92410. <https://doi.org/10.15446/ing.investig.v42n2.92410>



Attribution 4.0 International (CC BY 4.0) Share - Adapt

growth under sustainability criteria and environmental preservation, which implies guaranteeing the energy supply with fewer environmental impacts. Therefore, the finite life span of fossil energy resources such as oil, natural gas, and coal, which represent 68,6% of the Colombian energy mix and have a local reserves/production ratio of 5,4, 10,8, and 55 years, respectively (British Petroleum, 2018), requires exploration to increase the energy resource reserves of oil and natural gas, as well as the development and implementation of renewable energy technologies (Unidad de Planeación Minero-Energética, 2015).

In most developing countries, landfills are the main disposal pathway for municipal solid waste (MSW). This has several disadvantages, such as extensive land use, greenhouse gas emissions, groundwater pollution, and detrimental effects on human health. In Colombia, the average production of MSW was ~30 100 t/day in 2017. 83% of the total MSW produced in the country is disposed in landfills. The waste production trends indicate that sanitary emergencies could occur in the largest cities of the country by 2030 because of the end of the landfills' useful life (Superintendencia de Servicios Públicos Domiciliarios, 2017). The thermochemical treatment of MSW for energy uses has been recognized as a promising alternative for efficient MSW management. In this work, the energy recovery from different types of MSW by means of the updraft plasma gasification process to produce syngas as a substitute gaseous fuel was assessed from an economic viewpoint. According to the energy and waste scenarios in the country, this process could contribute to addressing the aforementioned issues while seeking to expand the energy mix by producing a substitute gaseous fuel and using MSW as feedstock (Unidad de Planeación Minero-Energética, 2015). The substitute gaseous fuel could be used as an energy source for residential, hotel, and commercial sectors to produce heat for energy requirements such as cooking tasks, heating water, low-medium pressure steam, and others (Unidad de Planeación Minero-Energética, 2015). Therefore, this work assesses the effect of tax incentives promoted by Law 1715 of 2014 (Colombian law of renewable energies) on the Levelized cost of syngas (LCOS) produced from MSW plasma gasification; the aim is to analyze the pre-feasibility of these projects under the current Colombian regulations. The assessment was conducted based on a previous work, where the plasma gasification model and its validation were presented in detail. Furthermore, the MSW plasma gasification process was thermodynamically characterized, and the operational parameters leading to reach the highest cold gas efficiency as a function of the MSW type were found (Montiel-Bohórquez et al., 2021).

Methodology

MSW as feedstock

The economic assessment of syngas production by plasma gasification (Plasma-G) of MSW was conducted with the five types of MSW produced in Medellín-Colombia. The MSW

generation rate of the city was ~1 970 t/day (TPD) in 2019 (SGCT-UM, 2015). The residential (74,5 wt%), commercial (11,8 wt%), industrial (7,9 wt%), and institutional (5,8 wt%) sectors make up the city's MSW, which is coded here as 'Mixed'. In Medellín, only ~16% of the produced MSW is recycled, and the remaining waste is disposed in La Pradera, a landfill located ~57 km from the city (Vélez and Mora, 2016). In general, the chemical composition of MSW is different for each sector (SGCT-UM, 2015). The chemical composition of MSW from each sector that makes up the MSW from the city is presented in Table 1. The calculation of the MSW's chemical composition is presented in detail in previous works (Montiel-Bohórquez and Pérez, 2019; Montiel-Bohórquez et al., 2021). Besides, the HHV of each waste type was estimated using the correlation proposed by Channiwala and Parikh (2002). Herein, inert waste such as glass, metal, and dangerous wastes were excluded from the MSW stream to be gasified (Couto et al., 2016; Lozano et al., 2017).

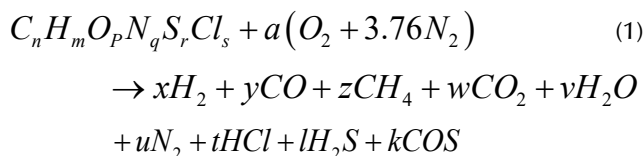
Table 1. Generation rate, heating value, and ultimate and proximate analyses of MSW produced in Medellín, Colombia

Waste properties and characterization	MSW type (by sector)				
	Res.	Mix.	Inst.	Com.	Ind.
Generation rate [t/day] wet base	1 121	1 468	75	168	104
HHV wet base [MJ/kg]	8,55	10,12	13,42	15,10	16,41
Ultimate analysis (wt% dry base)					
C	53,01	53,64	55,04	56,05	54,98
H	6,91	7,03	7,04	7,47	7,43
O	36,85	36,37	36,16	34,6	34,70
N	2,65	2,38	1,41	1,47	1,87
S	0,34	0,32	0,26	0,26	0,35
Cl	0,24	0,26	0,09	0,15	0,67
Proximate analysis (wt% dry base)					
Fixed Carbon	12,36	11,90	10,92	10,19	10,82
Volatile Matter	77,53	78,49	80,73	81,38	81,58
Ash	10,11	9,61	8,35	8,43	7,60
MC (wt%)	57,90	51,33	37,92	32,95	26,61

Com: Commercial, Ind: Industrial, Inst: Institutional, Mix: Mixed, Res: Residential
Source: (Montiel-Bohórquez and Pérez, 2019; Montiel-Bohórquez et al., 2021)

Plasma gasification

The Plasma-G process was successfully modelled under a thermo-chemical equilibrium approach (Montiel-Bohórquez et al., 2021). There, the syngas composition and torch power consumption associated with MSW Plasma-G, as well as the energy and exergy efficiencies of the process, were estimated. The Plasma-G was modeled by means of a thermochemical equilibrium approach, simulating a moving bed updraft plasma gasifier, which works at atmospheric pressure and uses air as plasma gas in the DC torches (Figure 1). The global gasification equation modelled is presented in Equation (1) (Minutillo et al., 2009).



In the moving bed updraft plasma gasifier, the solid waste is fed through an input port located at the top of the reactor. Thus, the solid absorbs energy from the gaseous phase (syngas) as the waste travels from the top to the bottom, while the syngas flows from the bottom to the top (Figure 1). The drying process of MSW is conducted when its temperature reaches 105 °C, which leads to the evaporation of the moisture that is mixed with the syngas stream (Indrawan *et al.*, 2019; Janajreh *et al.*, 2013; Minutillo *et al.*, 2009). Downstream (from top to bottom), the dried solid continues to be heated by the gaseous phase until the waste reaches the high energy-density stage (plasma), where plasma jet impacts the solid phase, and consequently, it is thermally degraded for producing the syngas and slag.

Montiel-Bohórquez *et al.* (2020) validated the Plasma-G model with experimental and numeric data from the literature. There, the data reported by Minutillo *et al.* (2009) and Perna *et al.* (2016) were used to assess the Plasma-G model's accuracy regarding numeric and experimental results, which was found satisfactory given the low average relative errors of 5,24 and 6,23% for the numeric and experimental validations, respectively. Furthermore, the combination between operational conditions (air flow and plasma temperature) that allowed to reach the maximum efficiency was found through a sensitivity analysis. The power consumption of the plasma torch was one of the main process parameters that affected the energy and exergy efficiencies. Despite the fact that the moisture content of MSW increased from 26,61 to 57,9% (Table 1), the energy and exergy efficiencies increased on average by 1,5 and 5,4%, respectively.

This behavior was ascribed to the updraft technology; when the raw MSW fed to the reactor is dried by the gaseous stream, a high MC leads to a reduction of the dry MSW fraction to be thermally decomposed by the torches, and, consequently, the power torch consumption decreases. On the other hand, when the plasma temperature increased (from 2 500 to 4 000 °C), the energy and exergy gasification efficiencies diminished because the torch power consumption increased by 28,3% on average. The maximum cold gas efficiency (CGE) of the Plasma-G process ranged from 79,22 to 83,46%, highlighting the flexibility of the process in treating MSW (Montiel-Bohórquez *et al.*, 2021). The maximum Plasma-G CGEs reached for each waste type (sector) are considered here to analyze the effect of the renewable energy law (tax incentives) on LCOS from MSW Plasma-G (Figure 2).

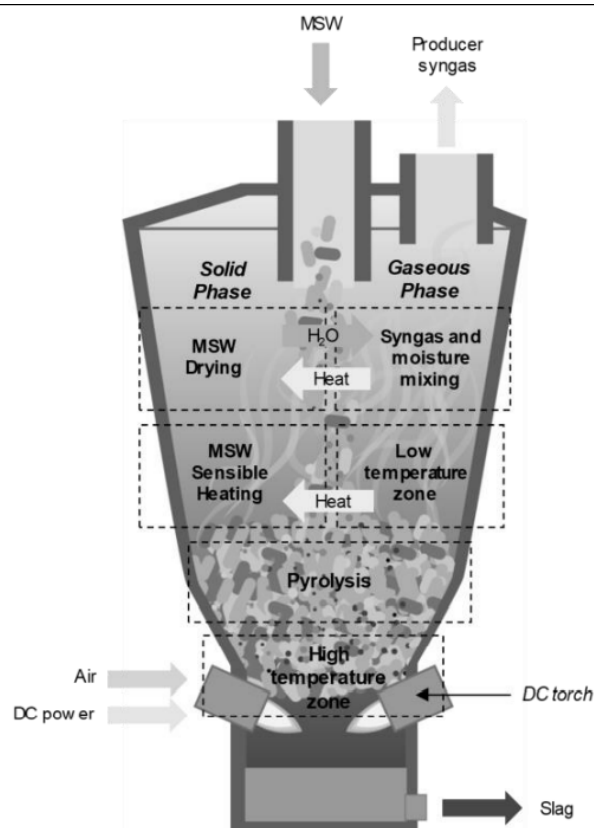


Figure 1. Updraft plasma gasifier scheme with considered solid phase-gaseous phase interactions

Source: Authors

Levelized cost of syngas as substitute gaseous fuel

Law 1715 of 2014 includes the energy content of waste as a non-conventional renewable energy source (Article 18), specifically waste without recycling or recovery strategies. Thereupon, given the low recycling and recovery rate in the city of Medellín (~15%), we have proposed that all the generated waste could be used in the plasma gasification plant to produce gaseous fuel as an energy recovery strategy. The LCOS produced by Plasma-G of the five different types of MSW was calculated. These calculations were carried out based on the optimal conditions for each waste found (plasma gasification section), whose development and analysis were presented in detail by Montiel-Bohórquez *et al.* (2021). The LCOS is the cost per unit of energy that includes all costs of an energy (gaseous fuel) generation project during its lifetime. Therefore, LCOS determines the constant price at which the energy must be sold to guarantee a net present value equal to zero and a minimum acceptable rate of return. LCOS (US\$/kWh) considers the investment costs, the fixed and variable costs for operating and maintenance, the fuel costs, and externality costs. It is calculated according to Equations (2) and (3) (Bruck *et al.*, 2018; Castillo-Ramírez *et al.*, 2016; Saldarriaga-Loaiza *et al.*, 2019; Zang *et al.*, 2019).

$$LCOS = LCOS_I + LCOS_V + LCOS_F + LCOS_G + LCOS_E \quad (2)$$

where, $LCOE_i$ (US\$/kWh) represents the investment costs per energy unit, $LCOE_v$ (US\$/kWh) denotes the variable operating and maintenance costs per energy unit, $LCOE_f$ (US\$/kWh) is the fixed operating and maintenance costs per energy unit, $LCOE_G$ (US\$/kWh) represents the fuel costs per energy unit, and $LCOE_E$ (US\$/kWh) denotes the externality costs per energy unit. It is worth noting that, while calculating the LCOS for MSW plasma gasification, the fuel cost was assumed to be zero, since the plant does not pay for the fuel. Meanwhile, the externality costs were considered as the amount of money (USD/t of MSW) that the plant receives for the treatment of MSW.

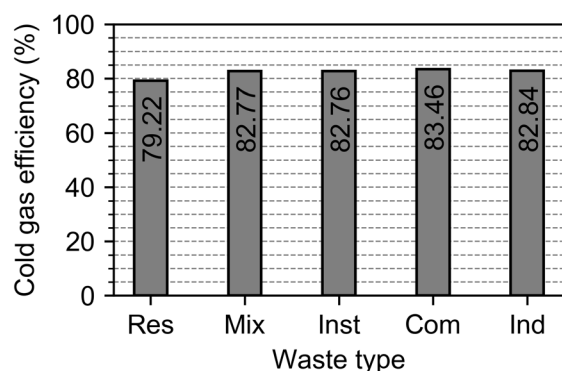


Figure 2. The best Plasma-G behavior (CGE) as a function of operational parameters for each MSW type
Source: Authors

$$LCOS = \frac{I_o + \sum_{t=1}^n \frac{C_t}{(1+i)^t}}{\sum_{t=1}^n \frac{E_t}{(1+i)^t}} \quad (3)$$

where, I_o (US\$) represents the initial investment, C_t (US\$) is the net costs for operating, maintenance, fuels, and externalities in year t , E_t (kWh) is the yearly energy production, i (effective annual interest rate, %) denotes the discount rate that is calculated by the weighted average cost of capital (WACC), and n (years) is the lifetime of the project.

Law 1715 of 2014 encourages investment in projects involving non-conventional energy sources (NCES) through four tax incentives (*Ley 1715 de 2014*), namely 1) a deduction of up to 50% of the investment through income tax during the first five years of operation (Investment Tax Credit, ITC); 2) exemption from VAT on national or imported equipment, elements, machinery, and services that are destined to the pre-investment and investment of NCES; 3) exemption from the payment of import on the previously named components; 4) an accelerated depreciation of assets, which will not be greater than 20% per year as a global rate. Nevertheless, under the National Development Plan 2018-2022, the ITC can be exercised during the first fifteen years of operation. Therefore, the concept of the tax factor (Δ) is applied to evaluate the effect of tax incentives on LCOS. Equations (4)

and (5) show the modified LCOS considering tax incentives (López-Lezama *et al.*, 2017). Thus, Δ is a factor affecting the initial investment cost of the project, and it stems from the tax incentives given by Law 1715 of 2014.

$$LCOS = \Delta LCOS_i + LCOS_v + LCOS_f + LCOS_G + LCOS_E \quad (4)$$

$$\Delta = \frac{1}{1-t} \left[1 - t \left(\sum_{j=1}^{j=t_1} \frac{I_j}{(1+i)^j} + \sum_{j=1}^{j=t_2} \frac{d_j}{(1+i)^j} \right) \right] \quad (5)$$

Herein, the five types of waste produced in the city of Medellín have been considered as potential feedstock for plasma gasification plants. The capacity of each plant depends on the production of each waste type. The methodology followed for estimating the capital cost of each plant, as well as O&M cost was presented in detail by Montiel-Bohórquez *et al.* (2020). Table 2 shows the costs updated to December 2019 for the syngas plants as a function of waste type and its processing capacity (in tons per day, TPD). The energy behavior and technical parameters of each plasma gasification plant were previously calculated and analyzed (Montiel-Bohórquez *et al.*, 2021). It was assumed that the treatment system of the plasma gasification plant completely removes the undesirable compounds from the syngas (H_2S , COS, HCl, etc.) (Figure 1), and also that a fraction of syngas is used to produce the torch power requirements by its combustion in an internal combustion engine (ICE) with a thermal efficiency of 36% (Medina-Jiménez *et al.*, 2019).

Table 2. Capital and O&M cost for five analyzed cases

Case	1	2	3	4	5
Waste type	Res.	Mix.	Inst.	Com.	Ind.
Plant capacity (TPD)	1 000	1 000	75	150	100
Capital cost (MMUS\$)	232,852	232,852	27,594	50,091	39,488
O&M cost (MMUS\$/yr)	27,525	27,525	3,934	7,868	5,245

Source: Authors

Results and discussion

The LCOS was calculated for each MSW type (sector) named as 'plant case' considering tax incentives. Thereby, the tax incentives of Law 1715 of 2014 and the benefits of the National Development Plan 2018-2022 were evaluated on LCOS (Congreso de la República, 2018; Ley 1715 de 2014). Table 3 presents additional technical and financial data of the Plasma-G plants for each case, which was used for calculating LCOS. The O&M cost includes the fixed and variable costs. The fuel cost was set to zero because, in the business model proposed here, the plants do not have to pay for solid waste (Lozano *et al.*, 2017; Zang *et al.*, 2019). Furthermore, the cost of MSW transportation was also set as zero since the plant is assumed to be located within the current landfill facility; the transportation cost is assumed to be paid by the waste generators (city residents, companies, commercial centers, and institutions), which is the actual condition of waste management in Medellín. Conversely, the

externality costs represent an income (¢US\$/kWh) for the project from disposal of solid waste. For LCOS calculation, a discount rate of 8,1% was considered, which was estimated according to the WACC.

Additionally, the cash flows were calculated considering constant the following parameters: a lifetime of 20 years, a cost of 8,7 US\$/t for solid waste disposal (Empresas Varias de Medellín E.S.P, 2019), a market representative rate of 3 300 COP/US\$ (December 29th, 2019), an accelerated depreciation on assets of 10 years, and the constant prices methodology [16].

The LCOS without and with tax incentives is presented in Figure 3 for each plant case. The LCOS, regardless of MSW type, diminished by ~4,3% on average when the tax benefits of Law 1715 of 2014 and of the National Development Plan 2018-2022 were applied. Case 2 (mixed wastes) reached the lowest LCOS (14,37 ¢US\$/kWh) because that plant has the highest yearly energy production and the lowest O&M cost, as shown in Table 3.

Table 3. Technical and financial parameters for each plant case

Case	1	2	3	4	5
Waste type	Res.	Mix.	Inst.	Com.	Ind.
Syngas HHV (MJ/kg)	9,64	13,72	13,77	14,77	13,85
Syngas for selling (Sm ³ /s) - [MMSCFD]	2,94 [8,98]	3,34 [10,18]	0,34 [1,05]	0,76 [2,33]	0,57 [1,75]
Plant efficiency (%)	26,19	38,51	40,84	44,04	41,55
Capacity Factor	0,9	0,9	0,9	0,9	0,9
O&M costs (¢US\$/kWh)	13,4	7,7	10,4	8,6	8,4
Externality (¢US\$/kWh)	1,4	0,8	0,57	0,47	0,46

*MMSCFD: Million standard cubic feet per day of syngas produced

Source: Authors

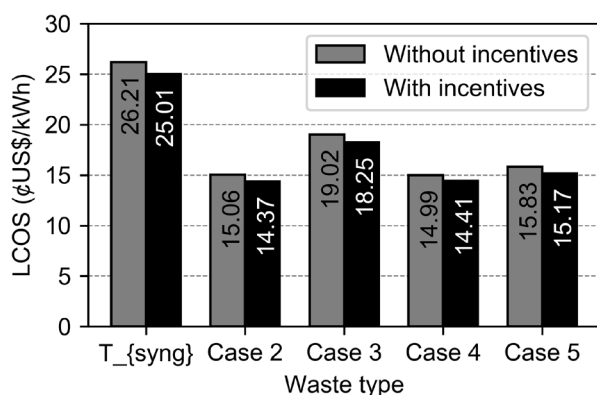


Figure 3. LCOS without and with the tax incentives of Law 1715 of 2014

Source: Authors

Case 2 has associated the highest investment cost that is compensated by the two mentioned variables (high energy production and low O&M costs). Thereby, case 2 could generate a unity of energy with the lowest cost. This result is highlighted because it represents the mixture of all waste types, which is the main MSW problem due to the increasing

production rate (Superintendencia de Servicios Públicos Domiciliarios, 2017).

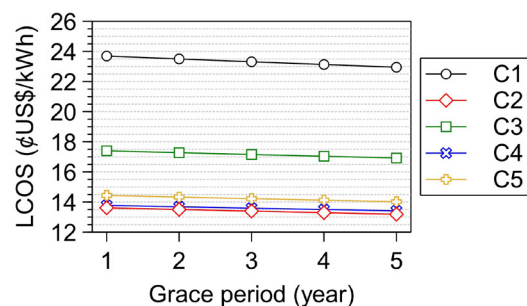
On the other hand, the reduction percentage of LCOS increases if the investment costs and the pre-tax earnings of the plant increase. This is attributed to the effect of tax incentives on LCOS that depends on the ITC, as shown in Equations (4) and (5). Therefore, cases 1 and 2 reached the highest reduction on LCOS (4,59%), which is ascribed to their high investment costs and the pre-tax earnings. According to the highest investment costs for cases 1 and 2 (residential and mixed), these cases can take advantage to reduce the LCOS. The benefits are related to the ITC during the first fifteen years of operation, which allow recovering up to the 50% of the initial investment through the income tax (Congreso de la República, 2018; Ley 1715 de 2014). Seeking to further reduce LCOS of Plasma-G plants, an alternative investment plan is proposed herein, which consists of financing 70% of the initial investment considering different grace periods between 1 and 5 years, as well as the tax incentives. Figure 4a shows the LCOS variation of each plant case with regard to the grace periods.

The LCOS of each Plasma-G plant decreases if the grace period increases (Figure 4a). This behavior is related to the effect of the effective corporate tax income rate on the net present value. LCOS decreases when the financial interests are paid in some periods of the cash flow, where there is no deduction for accelerated depreciation. The LCOS of the five cases (waste types) for a grace period of 5 years is 22,95 ¢US\$/kWh, 13,19 ¢US\$/kWh, 16,92 ¢US\$/kWh, 13,42 ¢US\$/kWh, and 14,02 ¢US\$/kWh, respectively. Consequently, case 2 reached the lowest LCOS, with a 12,43% reduction with respect to LCOS without tax incentives (Figure 3). For this investment alternative, the effect of the tax incentives will be greater on projects with high investment costs and high pre-tax earnings, as well as within the projects where there is no financing.

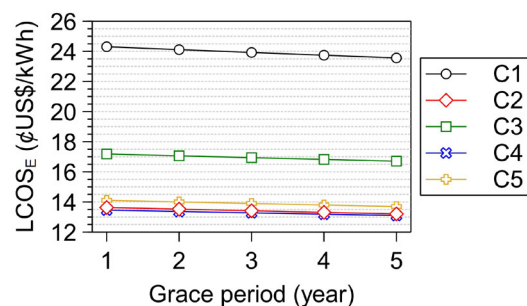
Regarding economic pre-feasibility, in the international and national markets, natural gas is traded at 2,3 US\$/MMBTU (LCOS=0,78 ¢US\$/kWh) (US Energy Information Administration, 2020) and 7,72 US\$/MMBTU (LCOS=2,6 ¢US\$/kWh) (Unidad de Planeación Minero-Energética, 2017), respectively. Aiming for the syngas to match these levelized costs (LCOS), it is required that the Plasma-G plants receive an income from waste disposal charge that is represented by the $LCOS_e$ externality, which is defined as the income per unit of generated energy (¢US\$/kWh) associated with the waste disposal charge. As the international and national prices of natural gas are different, one value of $LCOS_e$ must be calculated for each price of reference, thus finding an $LCOS_e$ for the international price and another one for the national price, which are named international $LCOS_e$ and national $LCOS_e$, respectively (Figure 4a b, c).

Figure 4b and Figure 4c show the international and national $LCOS_e$ considering tax incentives as a function of the grace period. According to these results, and considering a grace

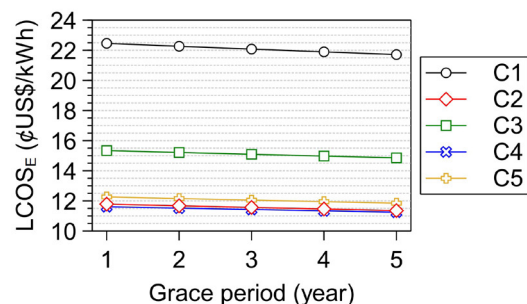
period of 5 years as reference, the $LCOS_E$ of plant cases 1, 2, 3, 4, and 5 must be equal to 23,56 ¢US\$/kWh, 13,20 ¢US\$/kWh, 16,71 ¢US\$/kWh, 13,1 ¢US\$/kWh, and 13,96 ¢US\$/kWh, respectively, in order to obtain an international natural gas price of 0,78 ¢US\$/kWh (2,3 US\$/MMBTU). For a national natural gas price of 2,6 ¢US\$/kWh (7,72 US\$/MMBTU), the $LCOS_E$ of the plants must be 21,71 ¢US\$/kWh, 11,36 ¢US\$/kWh, 14,86 ¢US\$/kWh, 11,25 ¢US\$/kWh, and 11,84 ¢US\$/kWh, respectively. When the national and international prices of natural gas (LCOS) are lower than that of the Plasma-G plants, the waste disposal charge must raise in order to obtain greater incomes from externalities and be able to reduce the LCOS. On the other hand, judging from Figure 4b and Figure 4c, the $LCOS_E$ of each plant diminishes when the grace period increases. This behavior stems from the influence of the effective corporate tax income rate on the net present value, since the net present value decreases when the financial interest payment is deferred to a longer time, while the tax incentives are considered. This was previously analyzed in Figure 4a.



a) LCOS as function of the grace period



b) International $LCOS_E$ as function of the grace period



c) National $LCOS_E$ as function of the grace period

Figure 4. Effect of the grace period on LCOS and $LCOS_E$ of each study case associated with the five waste types

Source: Authors

The plant of case 4 reached the lowest $LCOS_E$ for both scenarios (national and international), since it had the highest ratio between incomes from energy generation and total incomes (sum of incomes from externalities and from energy generation), and, likewise the lowest LCOS without incentives, as shown in Figure 3. Therefore, the incomes from gaseous fuel (syngas) production, together with the low cost of the technology per unit of net power, allow a greater reduction of the cost of solid waste disposal than the other plants. Finally, and according to the cash flows, the plant of case 2 (mixed waste type) showed the highest reduction percentage in $LCOS_E$, which is associated with the highest ratio between pre-tax earnings and externalities incomes, thus allowing it to take greater advantage of the tax incentives by means of the ITC.

Conclusions

The LCOS was estimated and used as an economic indicator in order to assess the economic pre-feasibility of syngas production by means Plasma-G on MSW in the Colombian context. The five plant cases were considered according to the studied waste types: case 1 - Residential, case 2 - Mixed, case 3 - Institutional, case 4 - Commercial, and case 5 - Industrial. The LCOS found without tax incentives were 26,21, 15,06, 19,02, 14,99, and 15,83 ¢US\$/kWh for cases from 1 to 5, respectively. Nevertheless, when the tax incentives of the renewable energy Law 1715 of 2014 and the National Development Plan 2018-2022 were applied, the LCOS were reduced down to 22,95, 13,19, 16,92, 13,42, and 14,02 ¢US\$/kWh for cases from 1 to 5, respectively. These reduced values were reached considering the following conditions: an accelerated depreciation on assets of 10 years, a financing of 70% of the initial investment, and a grace period of 5 years. It is highlighted that the plants 1 and 2 achieved the greatest LCOS reduction percentage (12,43%), which is attributed to their high investment costs and the pre-tax earnings, thus allowing them to exercise the investment tax credit in a greater proportion during the first fifteen years of operation. However, these projects involving syngas production (as a substitute gaseous fuel) from solid waste are not yet financially feasible in Colombia, as the LCOS for each case is higher than the average national price of natural gas 2,6 ¢US\$/kWh (7,72 US\$/MMBTU – December 29th, 2019). Therefore, it is necessary to implement new tax policies and incentives to diminish the LCOS, thus ensuring financial pre-feasibility and competitiveness of Plasma-G plants in the country. As it was proposed here, an increase in the waste disposal charge through an $LCOS_E$ ranging between 11,25 and 23,56 ¢US\$/kWh (123-259 US\$/t) on average contributes to the economic pre-feasibility of these waste-to-energy (WtoE) projects. It is a relevant result since it shows two main facts: first, plasma gasification technology requires further commercial development to overcome the current limitations associated with high technological costs; and second, more policies are required for encouraging the energy recovery of wastes through high-efficiency technologies in the Colombian context. On the other hand, it is worth noting that the high

waste disposal charge (123-259 USD/t) also stems from comparing the LCOS with the price of natural gas, which is a fuel with a higher quality and more mature production and distribution chains. Although waste generators should pay a tax for MSW management and treatment, other mechanisms must be considered while seeking to enhance the economic performance of WtoE projects and reduce taxes. For instance, including green bonds and reliability charges. New assessments on WtoE systems could be carried out including these factors in future work.

Acknowledgements

The authors acknowledge the financial support of CODI-Universidad de Antioquia through research project ES25190102, and Néstor D. Montiel-Bohórquez acknowledges the tutor student program.

Nomenclature

Abbreviations

HHV	Higher heating value, MJ/kg
LCOS	Levelized cost of syngas, US\$/kWh

Symbols

C_t	Net cost for operating, US\$/year
d_j	Accelerated depreciation rate, %
E_t	Amount of energy produced in a year, GWh
i	Discount rate, %
I_j	Effective annual rate, %
I_0	Initial investment, US\$
n	Lifetime of the project, years
t_1	Maximum number of years to apply the investment tax credit, years
t_2	Lifetime of the project accelerated depreciation purpose, years

Subscripts

E	Externalities
F	Fixed operating and maintenance
G	Fuel
I	Investment
V	Variable operating and maintenance

Greeks

β	Factor defined for the fuel
ρ	Tax rate, %
η	Efficiency
Δ	Tax factor



References

- British Petroleum (2018). *BP statistical review of world energy 2018*.
- Bruck, M., Sandborn, P., and Goudarzi, N. (2018). A Levelized Cost of Energy (LCOE) model for wind farms that include Power Purchase Agreements (PPAs). *Renewable Energy*, 122, 131-139. <https://doi.org/10.1016/j.renene.2017.12.100>
- Castillo-Ramírez, A., Mejía-Giraldo, D., and Giraldo-Ocampo, J. D. (2016). Geospatial levelized cost of energy in Colombia: GeoLCOE. In IEEE (Eds.) *2015 IEEE PES Innovative Smart Grid Technologies Latin America, ISGT LATAM 2015* (pp. 298-303). IEEE. <https://doi.org/10.1109/ISGT-LA.2015.7381171>
- Channiwala, S. A. and Parikh, P. P. (2002). A unified correlation for estimating HHV of solid, liquid and gaseous fuels. *Fuel*, 81(8), 1051-1063. [https://doi.org/10.1016/S0016-2361\(01\)00131-4](https://doi.org/10.1016/S0016-2361(01)00131-4)
- Congreso de la República (2014, May). Ley 1715 de 2014: Por la cual se regula la integración de energías renovables no convencionales al Sistema Energético Nacional.
- Congreso de la República (2018). *Plan Nacional de Desarrollo 2018-2022 "Pacto por Colombia, Pacto por la Equidad"*. Gobierno de Colombia.
- Couto, N. D., Silva, V. B., and Rouboa, A. (2016). Thermodynamic evaluation of portuguese municipal solid waste gasification. *Journal of Cleaner Production*, 139, 622-635. <https://doi.org/10.1016/j.jclepro.2016.08.082>
- Empresas Varias de Medellín E.S.P. (2019). *Charges for the second semester of 2019*.
- Indrawan, N., Mohammad, S., Kumar, A., and Huhnke, R. L. (2019). Modeling low temperature plasma gasification of municipal solid waste. *Environmental Technology and Innovation*, 15, 100412. <https://doi.org/10.1016/j.eti.2019.100412>
- International Energy Agency (2018). *World energy balances: database documentation*.
- Janajreh, I., Raza, S. S., and Valmundsson, A. S. (2013). Plasma gasification process: Modeling, simulation and comparison with conventional air gasification. *Energy Conversion and Management*, 65, 801-809. <https://doi.org/10.1016/j.enconman.2012.03.010>
- López-Lezama, J. M., Villada, F., and Muñoz-Galeano, N. (2017). Effects of Incentives for Renewable Energy in Colombia. *Ingeniería y Universidad*, 21(2), 257-272. <https://doi.org/10.11144/javeriana.iyu21-2.eire>
- Lozano, A. M., Lora, E. E. S., Palacio, J. C. E., Rocha, M. H., Restrepo, J. C., Venturini, O. J., and Ratner, A. (2017). Refuse Derived Fuel (RDF) production and gasification in a pilot plant integrated with an otto cycle ICE through Aspen Plus™ modelling: Thermodynamic and economic viability. *Waste Management*, 69, 187-201. <https://doi.org/10.1016/j.wasman.2017.08.006>
- Medina-Jiménez, A. C., Bereche, R. P., and Nebra, S. (2019). Three municipal solid waste gasification technologies analysis for electrical energy generation in Brazil. *Waste Management and Research*, 37(6), 631-642. <https://doi.org/10.1177/0734242X19841126>
- Minutillo, M., Perna, A., and Di Bona, D. (2009). Modelling and performance analysis of an integrated plasma gasification combined cycle (IPGCC) power plant. *Energy Conversion and Management*, 50(11), 2837-2842. <https://doi.org/10.1016/j.enconman.2009.07.002>
- Montiel-Bohórquez, N. D. and Pérez, J. F. (2019). Generación de energía a partir de residuos sólidos urbanos. Estrategias termodinámicas para optimizar el desempeño de centrales térmicas. *Información Tecnológica*, 30(1), 273-284. <https://doi.org/10.4067/s0718-07642019000100273>

- Montiel-Bohórquez, N. D., Saldarriaga-Loaiza, J. D., and Pérez, J. F. (2021). A techno-economic assessment of syngas production by plasma gasification of municipal solid waste as a substitute gaseous fuel. *Journal of Energy Resources Technology*, 43(9). <https://doi.org/10.1115/1.4049285>
- Perna, A., Minutillo, M., and Jannelli, E. (2016). Hydrogen from intermittent renewable energy sources as gasification medium in integrated waste gasification combined cycle power plants: A performance comparison. *Energy*, 94, 457-465. <https://doi.org/10.1016/j.energy.2015.10.143>
- Saldarriaga-Loaiza, J. D., Villada, F., and Pérez, J. F. (2019). Análisis de Costos Nivelados de Electricidad de Plantas de Cogeneración usando Biomasa Forestal en el Departamento de Antioquia, Colombia. *Información Tecnológica*, 30(1), 63–74. <https://doi.org/10.4067/s0718-07642019000100063>
- Secretaría de gestión y control territorial and Universidad de Medellín (SGCT-UM) (2015). *Plan de gestión integral de residuos sólidos del municipio de Medellín. Documento de actualización - parte 1*.
- Superintendencia de Servicios Públicos Domiciliarios. (2017). *Informe de Disposición Final de Residuos Sólidos – 2017*.
- US Energy Information Administration (2020). *Natural gas weekly update*.
- Unidad de Planeación Minero-Energética. (2015). *Plan Energético Nacional Colombia: Ideario energético 2050*.
- Unidad de Planeación Minero-Energética. (2017). *Proyección de los precios de los energéticos para la generación eléctrica 2018-2040*.
- Vélez, S. L. P. and Mora, N. E. (2016). System dynamics model for the municipal solid waste management system in the metropolitan area of Medellín, Colombia. *International Journal of Environment and Waste Management*, 18(2), 161. <https://doi.org/10.1504/ijewm.2016.080404>
- Zang, G., Jia, J., Shi, Y., Sharma, T., and Ratner, A. (2019). Modeling and economic analysis of waste tire gasification in fluidized and fixed bed gasifiers. *Waste Management*, 89(1), 201-211. <https://doi.org/10.1016/j.wasman.2019.03.070>

Automatic Personality Evaluation from Transliterations of YouTube Vlogs Using Classical and State-of-the-Art Word Embeddings

Evaluación automática de la personalidad a partir de transliteraciones de vlogs de YouTube mediante el uso de incrustaciones de palabras clásicas y del estado del arte

Felipe O. López-Pabón ¹, Juan R. Orozco-Arroyave ²

ABSTRACT

The study of automatic personality recognition has gained attention in the last decade thanks to a variety of applications deriving from this field. The Big Five model (also known as OCEAN) constitutes a well-known method to label different personality traits. This work considered transliterations of video recordings collected from YouTube (originally provided by the Idiap research institute) and automatically generated scores for the Big Five personality traits, which were also in the database. The transliterations were modeled with three different word embedding approaches (Word2Vec, GloVe, and BERT) and three different levels of analysis, namely a regression to predict the score of each personality trait, a binary classification between the strong vs. weak presence of each trait, and a tri-class classification according to three different levels of manifestations in each trait (low, medium, and high). According to our findings, the proposed approach provides similar results to others reported in the specialized literature. We believe that further research is required to find better results. Our results, as well as others reported in the literature, suggest that there is a big gap in the study of personality traits based on linguistic patterns, which highlights the need to work on collecting and labeling data considering the knowledge of expert psychologists and psycholinguists.

Keywords: personality, word embeddings, YouTube, regression, classification

RESUMEN

El estudio del reconocimiento automático de la personalidad ha ganado atención en la última década gracias a las diversas aplicaciones que se derivan de este campo. El modelo de los cinco grandes (también conocido como OCEAN) constituye un método ampliamente conocido para etiquetar diferentes rasgos de personalidad. Este trabajo consideró transliteraciones de grabaciones de vídeo recogidas de YouTube (proporcionadas originalmente por el instituto de investigación Idiap) y puntuaciones generadas automáticamente para los cinco grandes rasgos de personalidad, las cuales también se encontraban en la base de datos. Las transliteraciones se modelaron con tres enfoques diferentes de incrustación de palabras (Word2Vec, GloVe y BERT) y se incluyeron tres niveles diferentes de análisis, a saber: regresión para predecir la puntuación de cada rasgo de personalidad, clasificación binaria entre presencia fuerte y débil de cada rasgo, y una clasificación tri-clase según tres niveles diferentes de manifestaciones en cada rasgo (bajo, medio y alto). Según nuestros resultados, el enfoque propuesto proporciona resultados similares a otros reportados en la literatura especializada. Creemos que es necesario seguir investigando para encontrar mejores resultados. Nuestros resultados, así como otros reportados en la literatura, sugieren que existe un gran vacío en el estudio de los rasgos de personalidad basados en patrones lingüísticos, lo cual resalta la necesidad de trabajar en la recolección y etiquetado de datos considerando el conocimiento de psicólogos y psicolingüistas expertos.

Palabras clave: personalidad, incrustaciones de palabras, YouTube, regresión, clasificación

Received: February 21th, 2021

Accepted: August 18th, 2021

Introduction

Text analysis and natural language processing have emerged as a very useful sub-area of artificial intelligence, which allows extracting valuable information from text and performing a specific task. Some applications of these areas include web page classification (Onan, 2015), text document classification (Onan *et al.*, 2016a; Onan, 2017a), text genre classification (Onan, 2016), text document clustering (Onan, 2017b), and, more recently, topic extraction modeling (Onan, 2019a) and opinion mining (Onan, 2019b). Similarly, one of the most frequent tasks in text analysis is sentiment classification (Onan and Korukoğlu, 2015; Onan *et al.*, 2016b; Onan *et al.*, 2016c; Onan, 2018; Onan, 2020). Regarding the most used types of features in text analysis, we found: Bag of Words (BoW) (Onan and Korukoğlu, 2015;

Korukoğlu and Bulut, 2016c), latent topics obtained with Latent Dirichlet Allocation (LDA) (Onan *et al.*, 2016b), five

¹Electronics Engineer, Universidad de Antioquia, Colombia. Affiliation: Master's student in Telecommunications Engineering and teaching assistant, Universidad de Antioquia, Colombia. E-mail: forlando.lopez@udea.edu.co

²Electronics Engineer, Universidad de Antioquia, Colombia. M.Sc Telecommunications Engineering, Universidad de Antioquia, Colombia. Ph.D. in Computer Science, Friedrich-Alexander-Universität, Erlangen, Germany. Affiliation: Associate Professor, Universidad de Antioquia, Colombia and Adjunct Researcher the the Pattern Recognition Lab, Friedrich-Alexander-Universität, Erlangen, Germany. E-mail: rafael.orozco@udea.edu.co

How to cite: López-Pabón, F. O., Orozco-Arroyave, J. R. (2022). Automatic Personality Evaluation from Transliterations of YouTube Vlogs Using Classical and State-of-the-Art Word Embeddings. *Ingeniería e Investigación*, 42(2), e93803. <https://doi.org/10.15446/ing.investig.93803>



Attribution 4.0 International (CC BY 4.0) Share - Adapt

main categories from Linguistic Inquiry and Word Count (LIWC) (Onan, 2018), and, more recently, word embeddings such as Word2Vec, FastText, GloVe, LDA2vec, DOC2vec, and Term Frequency - Inverse Document Frequency (TF-IDF) weighted Global Vectors for word representation (GloVe) (Onan, 2020). Regarding the use of machine learning methods, the following have been widely used in the literature: i) classical learning methods such as Naive Bayes (NB) (Onan, 2015; Onan et al., 2016a), K-Nearest Neighbors (KNN) (Onan, 2016), Support Vector Machines (SVMs) (Onan, 2017a, 2017b), and Logistic Regression (LR) (Onan, 2019b); and ii) deep learning methods such as Convolutional Neural Networks (CNNs), Recurrent Neural Networks (RNNs), Bidirectional RNNs with attention mechanisms (RNNAM), Gated Recurrent Units (GRUs), Long short-term memory (LSTMs) (Onan, 2019b), and a combination of CNNs and LSTMs (Onan, 2020). Ensemble learning methods such as bagging, adaptive boosting, and random subspace have also been used (Onan et al., 2016b; Onan et al., 2016c; Onan, 2018).

Another important task related to text analysis which has emerged in the last decade is the study of personality, which plays an important role in human interaction and is defined as the combination of the various behavioral characteristics, emotions, motivations, and thinking patterns of an individual (Allport, 1937). Personality not only reflects the consistent patterns of behavior, thinking, and interpersonal communication; it also influences important aspects of life, including happiness, motivation to address tasks, preferences, emotions, and mental-physical health (White et al., 2004; Vinciarelli and Mohammadi, 2014; Xue et al., 2017). Nowadays, the increasing amount of information that users publish online allow the study of different personality traits with considerable volumes of data. One of the specific sources of information is the text that people publish in their status updates, tweets, blogs, vlogs (video-blogs), and reviews (Mohammad and Kiritchenko, 2013). From the psychological point of view, one suitable and accepted way of assessing personality traits is the Big Five Factor Model of personality dimensions. This is a well-known scale that evaluates the presence of five personality traits (John et al., 2008). The list below shows the five basic traits included in it and their corresponding social aspects (John et al., 1991; Celli et al., 2014). Note that the resulting acronym is OCEAN, which gives the other widely used name of the model.

Openness to experience: intellectual vs. unimaginative.

Conscientiousness: self-disciplined vs. careless.

Extraversion: sociable vs. shy.

Agreeableness: friendly vs. uncooperative.

Neuroticism (the inverse of emotional stability): neurotic vs. calm.

The automatic classification of personality traits has a wide variety of applications ranging from cognitive-based market segmentation to human health evaluation (Cambria et al., 2017). Different methods to model personality traits from texts directly generated by the person (i.e., social media posts) or from transliterations generated from audio or video

recordings have been proposed in the literature. Celli (2012) classified the five personality traits of the OCEAN model considering linguistic features extracted from status updates of a social network called FriendFeed. The author found an average accuracy of 61,3% for the five traits. Similarly, in Hassanein et al. (2018), the authors classified the presence vs. absence of the same five personality traits in posts belonging to the myPersonality dataset (Kosinski et al., 2015). The authors extracted semantic and morphological features and reported an average accuracy of 64%. Different machine learning methods were used in Pratama and Sarno (2015) to classify different personalities from different datasets. The authors created models based on TF-IDF and reported accuracies of up to 60% with data from Facebook posts and 65% with Twitter posts (Tweets). Later, also working with the myPersonality dataset, Mao et al. (2018) used different classifiers, including KNN, NB, and Decision Trees (DT), in order to classify the personality traits. The features considered by the authors include temporal measures (e.g., frequency of status updates per day), social network measures (e.g., network size), morphological features (e.g., frequency of adjectives), and TF-IDF-based features. According to their findings, TF-IDF features are suitable for classifying personality traits and the best reported F-measure was 79% for the 'openness to experience' trait.

In the same year, da Silva and Paraboni (2018) presented a study where different features were extracted, including BoW, psycholinguistics, Word2Vec (600-dimensional Continuous BoW and Skipgram embedding models), Doc2Vec, and LSTM (600-dimensional Keras-based embedding layer) to recognize the personality of approximately one thousand Facebook Brazilian users. The highest F1-score reported by the authors was 61% for the 'extraversion' trait. According to them, there is no single model capable of providing the best results for all five traits, which may suggest that not all personality traits are equally modeled from text. They also noticed that word embeddings seem to outperform other models based on lexical resources.

Among the works about language model features, Mehta et al. (2020a) used language model embeddings obtained from Bidirectional Encoder Representations from Transformers (BERT) models, as well as psycholinguistic features obtained with Mairesse, SenticNet, NRC Emotion Lexicon, and other methods to predict the personality traits of the Big Five model in the Essays dataset (Pennebaker and King, 1999). In their fine-tuned setup, they experimented with LR, SVM, and Multilayer Perceptron (MLP). Their results showed that language modeling features (based on BERT embeddings) consistently outperformed conventional psycholinguistic features for personality prediction. In another work with the same dataset (Kazameini et al., 2020), the authors used the BERT linguistic model to extract contextualized word embeddings from textual data and psycholinguistic features obtained with Mairesse for automatic author personality detection. Their extensive experiments led them to develop a new model that feeds contextualized embeddings along with psycholinguistic features to a bagged-SVM classifier for personality trait prediction. Their model outperformed previous results in the state of the art by 1,04% while being significantly more efficient. Similarly, Jiang et al. (2020) analyzed the Essays dataset using the pre-trained

contextual embeddings obtained from BERT and RoBERTa while also using different linguistic features obtained with LIWC. The authors tested several types of neural networks: HCNN (Hierarchical CNN model), ABCNN, and ABLSTM, which represent CNN and Bidirectional LSTM models with attention mechanism and HAN (Hierarchical Attention Network). They concluded that, in comparison with LIWC-based models and different Neural Networks (HCNN, ABCNN, ABLSTM), their model improved the performance by approximately 2,5% for the five traits on average when using BERT embeddings: 'agreeableness' by 2,2%, 'conscientiousness' by 2,8%, 'extraversion' by 2,5%, 'openness to experience' by 3,1%, and 'neuroticism' by 1,6%. With RoBERTa, the authors achieved the best accuracy in four out of the five traits: 59,7% for 'agreeableness', 60,6% for 'extraversion', 65,9% for 'openness to experience', 61,1% for 'neuroticism', and 60,1% for 'conscientiousness'.

In addition to the studies mentioned above, there are works where transliterations obtained from YouTube videos are considered as the input to the model in order to evaluate different personality traits. Our work is focused on the automatic evaluation of personality traits based on the transliterations provided in Biel *et al.* (2013) (see the *Data* subsection for further details). The authors that originally introduced the dataset extracted features from the texts using LIWC and TF-IDF features, which were extracted from bi-grams and tri-grams. The authors proposed an approach based on a Random Forest (RF) regressor to predict the label of each trait. The authors report coefficients of determination of 0,04, 0,18, 0,13, 0,31, and 0,17 for each trait in the OCEAN model, respectively. Later, also working with the same dataset, Sarkar *et al.* (2014) considered each trait as a separate bi-class problem (i.e., they performed the automatic classification of presence vs. absence of each trait). Their model was based on uni-gram BoW and TF-IDF features, and the classification was performed with a LR classifier. The average F1-score reported for the OCEAN traits was 60,1%, and the highest value was obtained for the 'agreeableness' trait (65,8%). A similar study was presented in Alam and Riccardi (2014), where the best result was obtained with part-of-speech (POS) tagging features, and the classification was performed using an SVM for each separate trait. In this case, the authors reported an average F1-score of 60,2% for the five traits in the OCEAN model, and the highest F1-score was 69,6% for 'agreeableness'.

Das-Kumar and Das-Dipankar (2017) considered transliterations from the same dataset and used 69-dimensional LIWC vectors to represent the texts. The authors reported accuracies of up to 62,3% to classify different traits of the OCEAN model. Sun *et al.* (2019) started to approach the problem of personality detection based on unsupervised learning methods. The authors reported RMSE values of 0,68, 0,69, 0,89, 0,77, and 0,69 for the OCEAN traits, respectively. More recently, also working with unsupervised methods based on the skip-gram algorithm, Guan *et al.* (2020) reported MAE values of 0,58, 0,57, 0,72, 0,67, and 0,60 for the same traits. In the same year, also working upon the same dataset with transliterations from YouTube vlogs, Salminen *et al.* (2020) considered 300-dimensional embedding vectors obtained from the Google-News Word2Vec pre-trained model. The authors created a neural network architecture that combined convolutional and recurrent layers to perform the classification of the traits.

The reported average F1-score value for the OCEAN traits was 54,74%.

Other works have addressed the study of personality considering different biosignals and also merging information in a multimodal approach. For instance, Mehta *et al.* (2020b) reviewed different machine learning methods according to the input modality, including text, audio, video, and multimodal. For the specific case of modeling personality through text, the authors mentioned that the labels are usually created through questionnaires and surveys. The authors also highlight the importance of data pre-processing to find better models that are more robust and stable. The authors also mention that open vocabulary methods (e.g., Word2Vec, GloVe, BERT) are more robust and have a better generalization capability than others based on a prior judgment of words or categories such as those that rely on lexicons or dictionaries (e.g., LIWC, SenticNet, or NRC Emotion Lexicon). Finally, the authors criticize the use of machine learning methods as the only way to model personality through text, given that those methods highly depend on the data used to train them.

Aiming to make progress in the field of automatic recognition of personality traits, in this study, we focused on extracting information from transliterations of the YouTube database presented in Biel *et al.* (2013). The proposed approach considers two classical word embeddings, namely Word2Vec and GloVe and state-of-the-art word embeddings obtained from the BERT-base and BERT-large language models. Machine learning systems based on support vector regression and support vector machines are used to estimate and classify the personality traits. Different performance metrics are included in the results. The rest of this paper is organized as follows: first, the methodology and database used in the paper are described; later, the experiments and the discussion of the results are presented; and, in the final section, conclusions and future work are presented.

Methodology

Figure 1 illustrates the main components of the implemented methodology. Details are included in the next subsections.

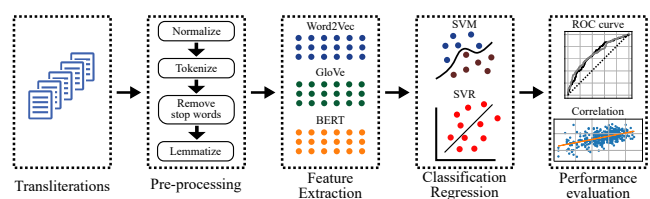


Figure 1. Block diagram of the methodology proposed in this study
Source: Authors

Data

The dataset consists of manual transliterations of audio-visual recordings generated by 404 YouTube vloggers that explicitly show themselves in front of a webcam talking about a variety of topics including personal issues, politics, movies, and books. The corpus was originally presented in Biel *et al.* (2013). There are no content-related restrictions in the videos, and the language is natural, diverse, and informal. The transliterations contain approximately 10

000 unique words and 240 000 word tokens. The data is gender-balanced (52% female). The transliterations were originally produced in the English language, and the videos in the database were automatically labeled according to the five traits of the OCEAN model. The labeling process was performed using the Amazon Mechanical Turk (Buhrmester et al., 2016) and the Ten-Item Personality Inventory (Gosling et al., 2003). Figure 2 shows histograms with the scores assigned to each trait. Some statistical information on the scores is also provided in Table 1.

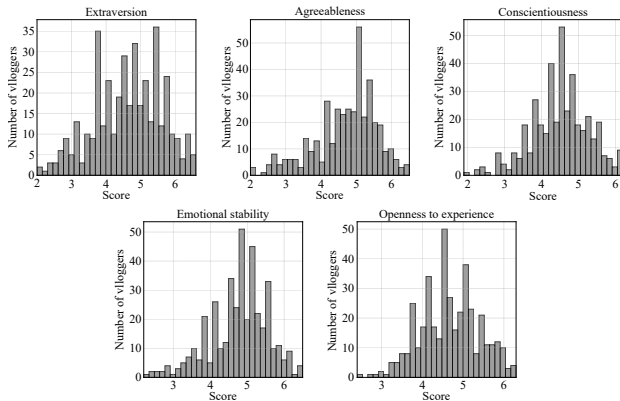


Figure 2. Histogram for the score in the five traits
Source: Authors

Table 1. Statistical information of the personality scores

Trait	Min.	T1	Med.	T2	Max.	Var.
Extraversion	2	4,2	4,7	5,2	6,6	0,95
Agreeableness	2	4,4	4,9	5,1	6,5	0,77
Conscientiousness	1,9	4,2	4,5	4,8	6,2	0,59
Emotional stability	2,2	4,5	4,8	5,1	6,5	0,61
Openness to experience	2,4	4,4	4,7	5,0	6,3	0,51

Med.: Median; Min.: Minimum; Max.: Maximum;
T1: 1st tertile; T2: 2nd tertile; Var.: Variance.

Source: Authors

Pre-processing

Before feature extraction, the data need to be cleaned and standardized in order to remove the 'noise' and prepare them for analysis. The steps followed during the text pre-processing include: i) removal of non-content words like 'xxx', 'um', 'uh', and others; ii) conversion of all texts to lower case, removal of punctuation, numbers, and stop-words; and iii) lemmatization, which is applied to transform words into their root form. Figure 3 shows the number of words per text before and after pre-processing.

Feature extraction

One of the goals of Natural Language Processing (NLP) is to mathematically represent words of a text in a vector space. This vector representation is such that similar words are represented by nearby points. In this work, we consider three different techniques to create said vectors: Word2Vec, Global Vectors (GloVe), and BERT. Details of each model are presented below.

Word2Vec: Word2Vec considers information from nearby words to represent target words with a shallow

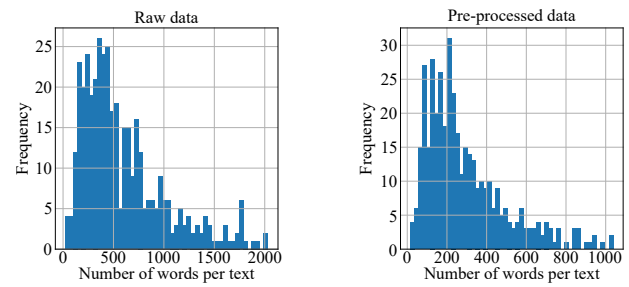


Figure 3. Number of words per text before and after pre-processing
Source: Authors

neural network whose hidden layer encodes the word's representation (Mikolov et al., 2013). The network contains one hidden layer, whose dimension is equal to the embedding size, which is smaller than the one at the input/output vector. A softmax activation function is applied at the output layer, so that each element of the output vector represents the probability of a given word appearing in the context. Word embeddings are obtained from the hidden layer following the Continuous Bag of Words (CBow) method, which considers information from the neighboring words to model the probability of the target word appearing in a given context. In this case, the input is the words around in the given context and the output is the target word. For example, assuming a context of 2 and 'drink' as the target word, in the sentence 'I will drink orange juice', the input would be 'I', 'will', 'orange', and 'juice', while the output would be 'drink'.

All inputs and output data have the same dimension and are coded as *one-hot* vectors. The length of the vector is equal to the size of the vocabulary in the corpus, which considers unique words. Typically, these unique words are coded in alphabetical order, that is, *one-hot* vectors for words beginning with 'a' are expected to have the target '1' in a lower index, while words beginning with 'z' are expected to have the target '1' in a higher index. Figure 4 shows the structure of the network for the CBow method, where $W \in \mathbb{R}^{V \times N}$ refers to the weight matrix that maps inputs x_i to the hidden layer, and $W' \in \mathbb{R}^{N \times V}$ is the weight matrix that maps outputs of the hidden layer to the final output layer. The neurons in the hidden layer copy the weighted sum of inputs to the next layer (i.e., linear activation function).

GloVe: The Global Vectors for Word Representation (GloVe) model creates word vectors by examining the co-occurrences of words within a corpus (Pennington et al., 2014). Before the model is trained, an X co-occurrence matrix is created, where each element X_{ij} represents the frequency for the i -th word to appear in the context of the j -th word. The corpus is traversed only once to create the X matrix, and these co-occurrence data are then used instead of the corpus. Once X is created, the task is to generate the vectors in a continuous space for each word of the corpus. Vectors with a smooth constraint will be produced for each pair of words (w_i, w_j):

$$\vec{w}_i^T \vec{w}_j + b_i + b_j = \log(X_{ij}) \quad (1)$$

where w_i and w_j are word vectors and b_i and b_j are scalar biases associated with the i -th and j -th word, respectively.

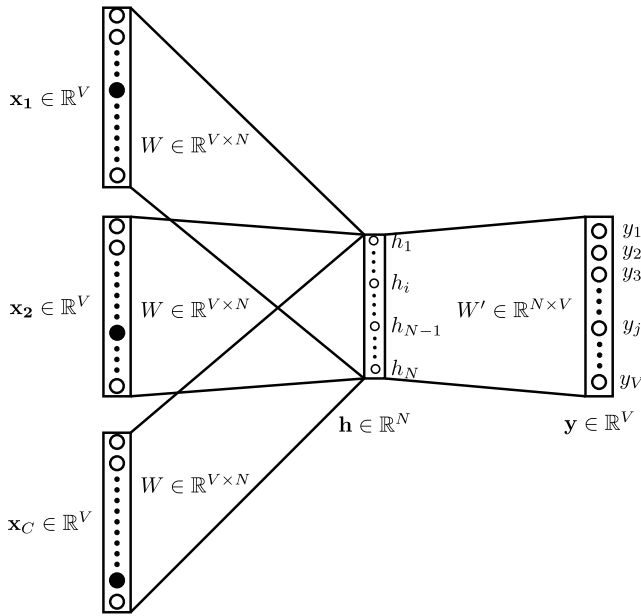


Figure 4. CBoW topology used in Word2Vec. \mathbf{x} : one-hot vectors; V : size of the vocabulary; C : number of context words; \mathbf{h} : hidden layer with N neurons, where N is also the number of dimensions to represent the word; \mathbf{y} : one-hot vector for target word.

Source: Modified from Bellei (2018)

This model creates word vectors with relevant information about how each pair of words coexist. The objective function of the optimization problem is called J , and it evaluates the mean square error of Equation 1, weighted by the function f :

$$J = \sum_{i=1}^V \sum_{j=1}^V f(X_{ij})(\vec{w}_i^T \vec{w}_j + b_i + b_j - \log(X_{ij}))^2 \quad (2)$$

From Equation 2, $f(X_{ij})$ is chosen in such a way that common word pairs are not considered (those with large X_{ij} values) because they would deviate too much from regular words:

$$f(X_{ij}) = \begin{cases} \left(\frac{X_{ij}}{x_{\max}}\right)^\alpha & \text{if } X_{ij} < x_{\max} \\ 1 & \text{in other case.} \end{cases} \quad (3)$$

In Equation 3, x_{\max} refers to the maximum co-occurrence value between the i -th and j -th word. When common word pairs are found (such that $X_{ij} > x_{\max}$), the function limits its output to 1. For all other word pairs, a weight in the range $[0 - 1]$ is computed. The distribution of weights depends on α , which is a hyper-parameter that controls the sensitivity of the weights to increased co-occurrence counts.

BERT makes use of transformers, which are attention mechanisms that learn contextual relations between words (or sub-words) in a text (Devlin et al., 2018). In its general form, a transformer includes two separate mechanisms: an encoder that reads the text input and a decoder that produces a prediction for the task. BERT allows both left and right contexts to influence many language representations that include word predictions (Devlin et al., 2018). To effectively train a bidirectional transformer, BERT uses two techniques called Masked Language Model (MLM) and Next

Sentence Prediction (NSP). The transformer architecture comprises a stack of encoders and a stack of decoders, where the encoders are composed of a self-attention layer and a Feed-Forward Neural Network (FFNN). Encoders are identical in structure and are connected to decoders, which include all the elements present in an encoder, in addition to an encoder-decoder attention layer between the self-attention layer and the feed-forward layer. Figure 5 shows the architecture of the transformer in BERT.

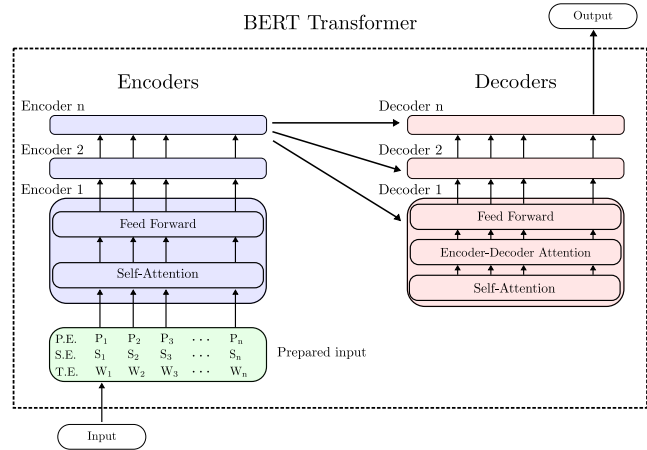


Figure 5. Architecture of the transformer used in BERT. **T.E.** text embedding; **S.E.** segment embedding; **P.E.** positional embedding. Source: Modified from Alammari (2018)

Pre-trained models were used for Word2Vec, GloVe, and BERT. For Word2Vec and GloVe, we considered the Python gensim module (Rehurek and Sojka, 2010). In the case of Word2Vec, the word2vec-google-news-300 model was employed, which was trained with Google News, with a corpus of around 100 billion words and a vector dimension of 300 (Mikolov, 2015). For GloVe, the model glove-wiki-gigaword-300 was employed, which was trained with the Wikipedia 2014 + Gigaword 5 corpus. In this case, there are 5,6 Billion tokens, a vocabulary of 400 000 words, and a vector dimension of 300 as well (Pennington, 2014). To obtain word embeddings based on BERT, we used the WEBERT Toolkit (Pérez, 2020), which is a Python tool typically used to obtain pre-trained BERT embeddings in English and Spanish. To train the BERT word embeddings in the English language, the Multi-Genre Natural Language Inference corpus was used. We considered two different pre-trained BERT models: (i) BERT-base and ii) BERT-large, where the last layer (768 units for BERT-base and 1 024 units for BERT-large) was taken as the word-embedding representation.

Vector representations for each transcript are created per word, so that $\mathbf{x} \in \mathbb{R}^{300}$ for Word2Vec and GloVe, $\mathbf{x} \in \mathbb{R}^{768}$ for Bert-base, and $\mathbf{x} \in \mathbb{R}^{1024}$ for Bert-large. Since texts correspond to spontaneous speech, they have a different number of words per individual. To obtain vectors of a fixed dimension per text, six statistics are computed along the vectors: mean, standard deviation, skewness, kurtosis, minimum, and maximum. The resulting feature matrix is given by $\mathbf{X} \in \mathbb{R}^{N \times 1800}$ for Word2Vec and GloVe, $\mathbf{X} \in \mathbb{R}^{N \times 4608}$ for BERT-base, and $\mathbf{X} \in \mathbb{R}^{N \times 6144}$ for BERT-large. Where N is the number of transliterations ($N = 404$).

Classification and regression models

Since Support Vector Machines (SVM) are one of the most used classification methods in the state of the art, and considering their robustness regarding high-dimensional representation spaces (Schölkopf et al., 2002), we decided to adopt this as our main framework for the classification and regression experiments. The following subsections provide some details of the mathematical background of the methods. However, we recommend that the reader refer to Schölkopf et al. (2002) for a more comprehensive description of the methods.

Bi-class classification: In this case, the goal is to discriminate data samples by finding a separating hyperplane that maximizes the margin between classes. Soft-margin SVMs allow errors in the process of finding the optimal hyper-plane. These allowed errors are data samples located on the wrong side of the hyper-plane but within the optimal margin. An example of a soft-margin SVM is shown in Figure 6.

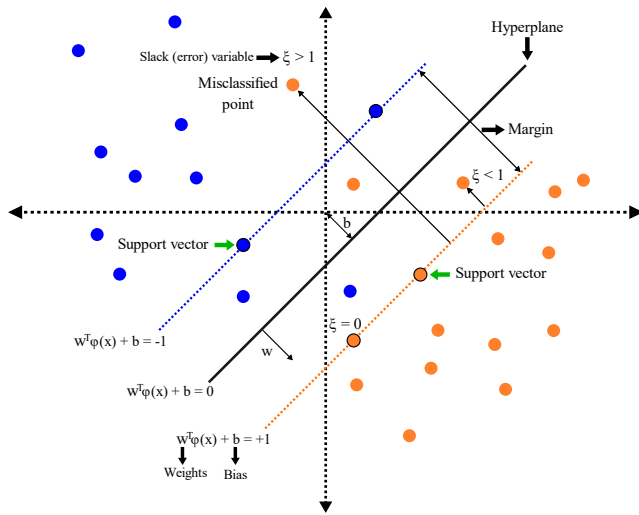


Figure 6. Soft-margin SVM
Source: Modified from Dey (2018)

The decision function of a soft-margin SVM is expressed according to Equation 4, where ξ_n is a slack variable that penalizes the number of errors allowed in the optimization process; $y_n \in \{-1, +1\}$ are class labels; $\phi(x_n)$ is a kernel function that transforms the feature space x into a higher dimensional space, where a linear solution to the problem can be found; and the weight vector w and the bias b define the separating hyperplane.

$$y_n \cdot (w^T \phi(x_n) + b) \geq 1 - \xi_n, \quad n = 1, 2, 3, \dots, N \quad (4)$$

The optimization problem is defined in Equation 5, where the hyper-parameter C controls the offset between ξ_n and the margin width. Samples x_n that satisfy the condition of equality in Equation 4 are called 'support vectors' (x_m).

$$\begin{aligned} &\underset{w, b}{\text{minimize}} && \frac{1}{2} \|w\|^2 + C \sum_{n=1}^N \xi_n \\ &\text{subject to} && y \cdot (w^T x_n + b) \geq 1 - \xi_n \\ &&& \xi_n \geq 0 \end{aligned} \quad (5)$$

Tri-class classification: We adopted the One vs. All approach (OvA, also called One vs. Rest, OvR). This method consists of building one SVM per class, which is trained to distinguish the samples of one class from the samples of all the other classes. The decision is made according to the maximum output among all SVMs (Milgram et al., 2006). This approach requires that each model predict a probability score per class. The max argument of these scores (class index with the highest score) is then used to predict a class.

Regression: We implemented a Support Vector Regressor (SVR) to predict the value of each label assigned to the personality traits. An SVR is an extension of an SVM, where, instead of integer-valued labels, real-valued labels are predicted. Particularly, an ϵ -SVR aims to find a linear function $f(x)$ where only samples outside the ϵ -radius 'tube' are penalized (Smola and Schölkopf, 2004) (Figure 7). The linear regression function $f(x)$ is represented in Equation 6 as:

$$f(x) = \langle w, x \rangle + b \quad (6)$$

where $\langle \cdot, \cdot \rangle$ denotes the dot product and $b \in \mathbb{R}$. The resulting optimization problem is written as follows:

$$\begin{aligned} &\text{minimize} && \frac{1}{2} \|w\|^2 \\ &\text{subject to} && y_i - \langle w, x_i \rangle - b \leq \epsilon \\ &&& \langle w, x_i \rangle + b - y_i \leq \epsilon \end{aligned} \quad (7)$$

The assumption in Equation 7 is that the function $f(x)$ exists and that the convex optimization problem is feasible. However, this is not always the case. Thus, similarly to the soft-margin SVM, one can introduce slack variables ξ_i and ξ_i^* to cope with otherwise infeasible constraints of the optimization problem in Equation 7. The resulting optimization problem is as follows (Vapnik, 1995):

$$\begin{aligned} &\text{minimize} && \frac{1}{2} \|w\|^2 + C \sum_{i=1}^l (\xi_i + \xi_i^*) \\ &\text{subject to} && y_i - \langle w, x_i \rangle - b \leq \epsilon + \xi_i \\ &&& \langle w, x_i \rangle + b - y_i \leq \epsilon + \xi_i^* \\ &&& \xi_i, \xi_i^* \geq 0 \end{aligned} \quad (8)$$

In Equation 8, the constant $C > 0$ determines the trade-off between the flatness of f and the maximum allowed deviation ϵ . This corresponds to the so called ϵ -insensitive loss function $|\xi|_\epsilon$, which is described in Equation 9:

$$|\xi|_\epsilon = \begin{cases} 0 & \text{if } |\xi| \leq \epsilon \\ |\xi| - \epsilon & \text{otherwise} \end{cases} \quad (9)$$

Figure 7 illustrates the concept. Note that only points outside the region between the dotted line (the 'tube') contribute to the cost. Deviations are linearly penalized, although it is possible to extend SVM to nonlinear functions (Smola and Schölkopf, 2004; Ranković et al., 2014).

Parameter optimization: For both SVM and SVR, Gaussian kernel and linear kernel were considered in our preliminary experiments. However since the results with the first one were better in most of the cases, only results with the Gaussian kernel are reported (see Appendix with results for the linear kernel). The hyper-parameters C , γ , and ϵ were optimized through a grid-search up to powers of ten between 1×10^{-4} and 1×10^4 . A subject-independent

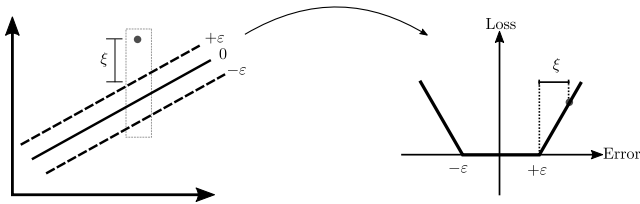


Figure 7. Linear SVR with ε -insensitive loss function
Source: Modified from Smola and Schölkopf (2004)

10-fold Cross-Validation (CV) strategy was followed in the training process, *i.e.*, the data were divided into 10 groups (randomly chosen, but data from the same subject were never included in the train and test fold simultaneously). The CV strategy was repeated 10 times to evaluate the generalization capability of the model (Kohavi, 1995). The reported metrics correspond to the average and standard deviation of the ten repetitions.

Performance evaluation

The classification systems used in this work were evaluated with typical performance metrics including the confusion matrix (Powers, 2020). For the particular case of a two-class classification problem, the matrix is as shown in Table 2.

Table 2. Confusion matrix

Estimated class	True class	
	Class 0	Class 1
Class 0	TP	FP
Class 1	FN	TN

Source: Authors

According to this matrix and taking class 0 as the target one, the following terms are defined:

- **True positive (TP)** refers to the number of samples in class 0 that are correctly classified as class 0.
- **False negative (FN)** corresponds to the number of samples in class 0 that are incorrectly classified as class 1.
- **False positive (FP)** is the number of samples in class 1 that are incorrectly classified as class 0.
- **True negative (TN)** is the number of samples in class 1 that are correctly classified as class 1.

Derived from the aforementioned terms, different performance measures are defined and taken into account, including accuracy (ACC), sensitivity (SEN), specificity (SPE), and the F1-score (F1). Apart from the aforementioned measures, the receiver operating characteristic curves (ROC) were used as a graphical representation that summarizes the performance of binary-classification systems. The performance of the multi-class classification systems was evaluated with the Unweighted Average Recall (UAR) and Cohen's kappa coefficient (κ).

The regression systems of this study were evaluated according to Spearman's correlation coefficient (ρ).

Additionally, to allow comparisons with different works in the literature that report results with different measures, we decided to include other metrics such as the Mean Absolute Error (MAE), the Root Mean Square Error (RMSE), and the coefficient of determination, R^2 .

Experiments, results, and discussion

This section presents the three main experiments performed in this work: i) personality trait estimation according to the scores of the OCEAN model; ii) classification between weak presence vs. strong presence of each personality trait; and iii) classification of three levels in the manifestation of each personality trait (low, medium, and high). Before providing details of each experiment, the next subsection presents the details of the strategy followed to distribute the data, together with statistical analyses that evaluate the suitability of the proposed approach prior to training the classifiers.

Data distribution and statistical analyses

The personality trait estimation considers the values assigned to each sample for each trait. Their distribution per trait is presented in Figure 2, and the corresponding statistics are presented in Table 1. For the binary classification scenario, the scores of each trait are divided around their median, *i.e.*, samples with values below the median are considered weak, while those above are labeled as strong. This distribution criterion allows for a balanced number of samples per trait. The median threshold is shown in Figure 8 as a red dotted line. The distribution of the data for the tri-class classification problem is made according to the tertiles of the distribution of the scores per trait. This strategy guarantees balance among the three resulting subgroups. The distribution of these three subgroups is shown in Figure 8 as the three shadowed regions. The number of samples per class and subgroup (two for the bi-class problem and three for the tri-class problem) is summarized in Table 3.

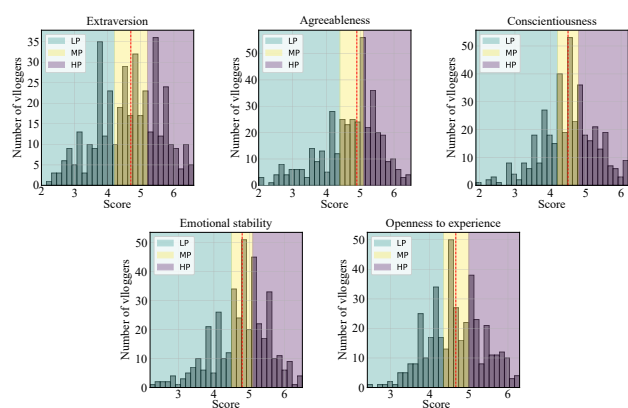


Figure 8. Score thresholds for the bi-class and tri-class classification problems. LP: low presence; MP: medium presence; HP: high presence.

Source: Authors

Two statistical tests were performed. The first one was the Kruskal-Wallis test regarding the feature matrices extracted per sample and trait. This test was performed for the two scenarios: weak vs. strong presence of each trait, and the three levels of manifestation of the traits. In all

Table 3. Number of subjects for the bi-class and tri-class classification problem

Trait	Number of subjects for the bi-class problem		Number of subjects for the tri-class problem		
	Weak presence	Strong presence	Low presence	Medium presence	High presence
Extraversion	209	195	144	137	123
Agreeableness	218	186	137	138	129
Conscientiousness	209	195	146	132	126
Emotional stability	203	201	136	137	131
Openness to experience	203	201	135	148	121

Source: Authors

cases, the null hypothesis was rejected with $p \ll 0,01$. The second statistical test aimed to evaluate whether the gender of subjects biased the distribution of the extracted features. We performed χ^2 tests for both the bi-class and the tri-class scenarios. A possible bias regarding gender was discarded for the 'extraversion', 'conscientiousness', 'emotional stability', and 'openness to experience' traits, whereas a possible bias was found for the 'agreeableness' trait.

Experiment 1: personality trait estimation

This experiment was mainly based on SVR systems with Gaussian kernel. Experiments with linear kernel were also performed, and the results can be found in the Appendix. As mentioned before, to allow comparisons with respect to other works in the literature that use the same corpus as this study, the results are reported in Table 4 regarding the four metrics mentioned in the performance evaluation subsection, where the results in bold letters correspond to the best for each trait. Note that, in three out of the five traits, the best result was obtained when merging the Word2Vec and GloVe embeddings, except for the 'extraversion' trait, whose best result was obtained with the BERT-base embeddings, and 'openness to experience' whose best result was obtained with GloVe embeddings. When observing R^2 and ρ , the best result was obtained for the 'agreeableness' trait ($R^2 = 0,24$ and $\rho = 0,43$), followed by 'conscientiousness' ($R^2 = 0,16$ and $\rho = 0,41$). The worst result was for the 'openness to experience' trait, with $R^2 = 0,05$ and $\rho = 0,21$. The lowest MAE = 0,55 was obtained with 'conscientiousness', and the lowest RMSE value was obtained with 'openness to experience', with a value of RMSE = 0,70.

Experiment 2: weak vs. strong presence of each trait

In this case, SVM classifiers with Gaussian kernel were used, and the results are reported in Table 5, where the results in bold letters correspond to the best for each trait. Note that four out of the five traits (all except 'openness to experience') obtained the best result when considering word embeddings based on BERT, three of them with the base model ('extraversion', 'agreeableness', and 'emotional stability') and the remaining one ('conscientiousness') with the large model. Furthermore, note that three out of the five traits exhibit accuracies above 60%. The best result was obtained for 'extraversion', with an accuracy of 64,7%, followed by 'agreeableness', with an accuracy of 64,3%, and 'conscientiousness', with 63,9%. As seen a few lines below, these results are similar to most of the results reported in

Table 4. Results for personality trait estimation

Trait	Feature	C, γ, ϵ	R^2	ρ	MAE	RMSE
Extr	Word2Vec	1e1, 1e-3, 1e-4	0,10 \pm 0,00	0,30 \pm 0,01	0,77 \pm 0,00	0,93 \pm 0,00
	GloVe	1, 1e-4, 1e-4	0,10 \pm 0,00	0,31 \pm 0,02	0,77 \pm 0,01	0,93 \pm 0,01
	Fusion	1, 1e-4, 1e-4	0,12 \pm 0,00	0,35 \pm 0,01	0,75 \pm 0,01	0,92 \pm 0,01
	BERT-b	1, 1e-4, 1e-1	0,14 \pm 0,00	0,37 \pm 0,02	0,74 \pm 0,00	0,91 \pm 0,01
	BERT-l	1, 1e-4, 1e-1	0,13 \pm 0,00	0,36 \pm 0,01	0,74 \pm 0,01	0,91 \pm 0,01
Agr	Word2Vec	1, 1e-4, 1e-1	0,24 \pm 0,00	0,43 \pm 0,01	0,61 \pm 0,00	0,79 \pm 0,00
	GloVe	1, 1e-4, 1e-1	0,16 \pm 0,00	0,38 \pm 0,02	0,63 \pm 0,01	0,81 \pm 0,01
	Fusion	1, 1e-4, 1e-1	0,24 \pm 0,00	0,43 \pm 0,02	0,60 \pm 0,00	0,77 \pm 0,01
	BERT-b	1e1, 1e-4, 1e-1	0,22 \pm 0,00	0,44 \pm 0,01	0,62 \pm 0,00	0,78 \pm 0,01
	BERT-l	1e1, 1e-4, 1e-1	0,19 \pm 0,00	0,39 \pm 0,01	0,63 \pm 0,01	0,79 \pm 0,01
Cons	Word2Vec	1, 1e-4, 1e-1	0,16 \pm 0,00	0,40 \pm 0,01	0,55 \pm 0,00	0,71 \pm 0,00
	GloVe	1, 1e-4, 1e-1	0,13 \pm 0,00	0,37 \pm 0,02	0,56 \pm 0,01	0,72 \pm 0,01
	Fusion	1, 1e-4, 1e-1	0,16 \pm 0,00	0,41 \pm 0,01	0,55 \pm 0,00	0,71 \pm 0,00
	BERT-b	1, 1e-4, 1e-1	0,15 \pm 0,00	0,40 \pm 0,01	0,55 \pm 0,00	0,71 \pm 0,00
	BERT-l	1, 1e-4, 1e-1	0,15 \pm 0,00	0,40 \pm 0,01	0,55 \pm 0,00	0,71 \pm 0,01
Emot	Word2Vec	1, 1e-4, 1e-1	0,05 \pm 0,00	0,18 \pm 0,02	0,60 \pm 0,01	0,76 \pm 0,01
	GloVe	1e1, 1e-3, 1e-4	0,07 \pm 0,00	0,22 \pm 0,02	0,59 \pm 0,00	0,75 \pm 0,00
	Fusion	1, 1e-4, 1e-1	0,08 \pm 0,00	0,24 \pm 0,02	0,59 \pm 0,01	0,75 \pm 0,01
	BERT-b	1e1, 1e-4, 1e-1	0,06 \pm 0,00	0,21 \pm 0,02	0,59 \pm 0,01	0,76 \pm 0,01
	BERT-l	1e1, 1e-4, 1e-1	0,06 \pm 0,00	0,22 \pm 0,02	0,60 \pm 0,03	0,76 \pm 0,00
Open	Word2Vec	1, 1e-3, 1e-4	0,04 \pm 0,00	0,18 \pm 0,02	0,57 \pm 0,00	0,70 \pm 0,00
	GloVe	1, 1e-3, 1e-4	0,05 \pm 0,00	0,21 \pm 0,02	0,56 \pm 0,00	0,70 \pm 0,00
	Fusion	1, 1e-4, 1e-1	0,02 \pm 0,00	0,16 \pm 0,02	0,57 \pm 0,00	0,71 \pm 0,00
	BERT-b	1, 1e-4, 1e-4	0,00 \pm 0,00	0,06 \pm 0,04	0,58 \pm 0,01	0,72 \pm 0,01
	BERT-l	1, 1e-4, 1e-4	0,00 \pm 0,00	0,04 \pm 0,02	0,58 \pm 0,00	0,72 \pm 0,00

Fusion: Word2Vec + GloVe; BERT-b: BERT base; BERT-l: BERT large.

Source: Authors

the literature. The results also show that there is no a clear model that leads to the best results. This means that there is still a lot of work to be done in this field, which, apart from the challenge of extracting information from text, imposes an additional constraint due to the consistency of the labels, i.e., the evaluation of personality is very hard task for both humans and machines.

Table 5. Results for bi-class system: weak presence vs. strong presence of the trait

Trait	Feature	C, γ	Accuracy	Sensitivity	Specificity	F1-score	AUC
Extr	Word2Vec	1e1, 1e-3	60,9 \pm 0,8	53,2 \pm 1,7	68,1 \pm 1,6	60,7 \pm 0,9	0,63 \pm 0,01
	GloVe	1e1, 1e-3	63,8 \pm 1,2	54,7 \pm 1,0	72,3 \pm 2,1	63,5 \pm 1,2	0,67 \pm 0,01
	Fusion	1e1, 1e-4	63,4 \pm 1,1	62,9 \pm 1,6	64,7 \pm 1,8	63,4 \pm 1,1	0,68 \pm 0,01
	BERT-b	1e1, 1e-4	64,7 \pm 0,6	63,5 \pm 0,9	65,8 \pm 1,6	64,7 \pm 0,6	0,70 \pm 0,01
	BERT-l	1e1, 1e-4	63,4 \pm 1,0	62,3 \pm 1,3	64,4 \pm 1,8	63,4 \pm 1,0	0,68 \pm 0,01
Agr	Word2Vec	1e1, 1e-4	59,8 \pm 1,4	53,3 \pm 3,3	65,2 \pm 1,9	59,6 \pm 1,4	0,64 \pm 0,01
	GloVe	1e1, 1e-4	60,3 \pm 1,5	52,2 \pm 2,3	67,2 \pm 2,8	60,0 \pm 1,5	0,64 \pm 0,01
	Fusion	1e1, 1e-4	60,9 \pm 1,6	56,7 \pm 2,7	64,5 \pm 2,4	60,8 \pm 1,6	0,67 \pm 0,02
	BERT-b	1e1, 1e-4	64,3 \pm 0,8	59,4 \pm 1,7	68,5 \pm 1,5	64,2 \pm 0,8	0,69 \pm 0,08
	BERT-l	1e1, 1e-4	61,7 \pm 1,2	57,3 \pm 2,2	65,4 \pm 1,9	61,6 \pm 1,2	0,67 \pm 0,01
Cons	Word2Vec	1e1, 1e-3	62,5 \pm 0,8	53,6 \pm 1,2	70,8 \pm 1,6	62,2 \pm 0,8	0,67 \pm 0,01
	GloVe	1e1, 1e-3	63,4 \pm 0,7	57,9 \pm 1,2	68,6 \pm 1,3	63,3 \pm 0,7	0,67 \pm 0,01
	Fusion	1, 1e-4	63,0 \pm 1,1	66,5 \pm 1,7	59,8 \pm 1,4	62,9 \pm 1,1	0,69 \pm 0,01
	BERT-b	1, 1e-4	63,6 \pm 1,7	64,4 \pm 1,8	62,9 \pm 1,8	63,6 \pm 1,7	0,68 \pm 0,01
	BERT-l	1, 1e-4	63,9 \pm 1,0	63,9 \pm 1,4	63,8 \pm 1,6	63,9 \pm 1,0	0,68 \pm 0,01
Emot	Word2Vec	1, 1e-4	56,7 \pm 1,9	52,4 \pm 2,9	60,9 \pm 3,5	56,6 \pm 1,9	0,59 \pm 0,02
	GloVe	1, 1e-3	55,5 \pm 1,2	53,8 \pm 1,2	57,1 \pm 2,1	55,5 \pm 1,2	0,57 \pm 0,02
	Fusion	1, 1e-4	55,9 \pm 1,1	54,2 \pm 2,1	57,6 \pm 1,8	55,9 \pm 1,1	0,59 \pm 0,02
	BERT-b	1e1, 1e-4	56,8 \pm 1,0	54,0 \pm 1,4	59,6 \pm 1,6	56,8 \pm 1,0	0,60 \pm 0,01
	BERT-l	1e1, 1e-4	56,5 \pm 1,3	54,5 \pm 2,7	58,4 \pm 2,9	56,4 \pm 1,3	0,58 \pm 0,01
Open	Word2Vec	1, 1e-3	56,4 \pm 1,9	51,7 \pm 2,9	60,9 \pm 1,9	56,3 \pm 1,9	0,58 \pm 0,02
	GloVe	1e1, 1e-3	56,4 \pm 1,2	52,8 \pm 2,3	59,9 \pm 2,1	56,3 \pm 1,3	0,58 \pm 0,02
	Fusion	1e1, 1e-4	56,5 \pm 1,5	49,9 \pm 2,5	63,0 \pm 3,3	56,3 \pm 1,5	0,58 \pm 0,02
	BERT-b	1e1, 1e-4	55,2 \pm 1,2	48,5 \pm 2,4	61,9 \pm 3,8	55,0 \pm 1,2	0,57 \pm 0,01
	BERT-l	1, 1e-4	54,0 \pm 1,6	52,2 \pm 4,2	55,9 \pm 2,1	54,0 \pm 1,6	0,55 \pm 0,01

Fusion: Word2Vec + GloVe; BERT-b: BERT base; BERT-l: BERT large.

Source: Authors

Results are shown more compactly in Figure 9, where the ROC curves resulting from the bi-class experiments are included. Each panel in the figure includes the results obtained with the three feature extraction approaches. The AUC values show that, in the majority of the cases, better results are obtained for 'extraversion' and 'conscientiousness', and also that the best AUC values are obtained by the Fusion of Word2Vec and GloVe embeddings, as well as by embeddings based on BERT.

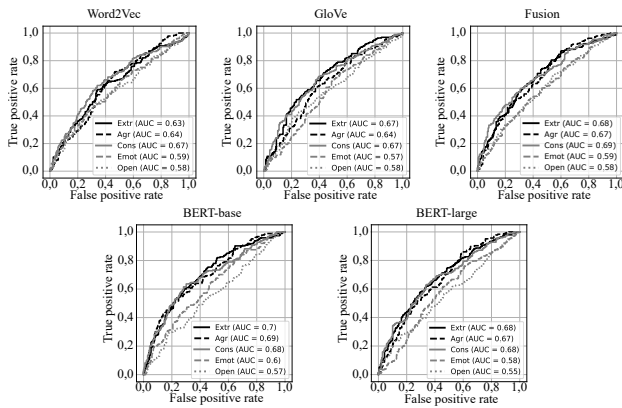


Figure 9. ROC curves obtained with Word2Vec, GloVe, Fusion (Word2Vec + GloVe), BERT-base and BERT-large embeddings
Source: Authors

Experiment 3: classification of personality traits into three levels

Three groups were created according to the scores in the personality traits, as it was explained in the data distribution and statistical analyses subsection: LP (low presence), MP (medium presence), and HP (high presence). The results of the tri-class classification are presented in Table 6 in terms of accuracy, F1-score, UAR, and κ , where the results in bold letters correspond to the best for each trait. Note that, in four out of the five traits, the best results were obtained with the Fusion of Word2Vec and GloVe embeddings. Only in the case of 'conscientiousness' was the best result obtained with Word2Vec. It can also be observed that the models trained with BERT embeddings did not improve the performance of the models in comparison with the classical word embeddings (Word2Vec and GloVe) in any of the OCEAN traits. However, with a close look at the numbers, one can notice that the difference among different approaches is not that high, and the results are similar across different traits, *i.e.*, between 40 and 46%.

To facilitate a detailed look at the results, confusion matrices are presented in Table 7, where, again, the results in bold letters correspond to the best for each trait. The results do not show a clear pattern when comparing the three trait levels. One would expect to see a relatively clear separation between LP and HP samples. However, in all cases, the target class shows the largest percentage, but the remaining portion is almost always equivalently distributed between the other two classes. Even though the models presented in this study could be improved, while also acknowledging that the addressed problem is very challenging, the behavior of the observed results may reflect possible labeling problems. We believe that there is a big gap in the study of personality traits based on linguistic patterns, which makes it necessary to work on collecting and labeling data considering the knowledge of expert psychologists and psycholinguists (Sun *et al.*, 2019; Guan *et al.*, 2020).

The best results obtained throughout the regression and classification experiments are summarized in Figure 10. The first column of sub-figures shows the regression results. It can be observed that the regressor is doing a good job, especially in the first three traits, where Spearman's correlation is above 0,35. In the second and third columns,

Table 6. Tri-class classification results

Trait	Feature	Accuracy	F1-score	UAR	κ
Extr	Word2Vec	42,6 ± 1,4	42,0 ± 1,3	42,2 ± 1,3	0,13 ± 0,02
	GloVe	44,2 ± 1,4	43,5 ± 1,4	43,7 ± 1,4	0,15 ± 0,02
	Fusion	44,3 ± 1,2	44,1 ± 1,2	44,7 ± 1,3	0,17 ± 0,02
	BERT-b	41,8 ± 1,1	41,7 ± 1,1	41,8 ± 1,1	0,12 ± 0,02
	BERT-l	41,9 ± 1,0	41,8 ± 1,0	41,8 ± 1,0	0,12 ± 0,02
Agr	Word2Vec	46,0 ± 1,5	45,9 ± 1,5	45,8 ± 1,5	0,19 ± 0,02
	GloVe	46,1 ± 2,0	46,0 ± 2,0	45,9 ± 2,0	0,19 ± 0,03
	Fusion	46,2 ± 1,3	46,3 ± 1,3	46,2 ± 1,3	0,19 ± 0,02
	BERT-b	45,9 ± 0,9	45,8 ± 0,82	45,9 ± 0,8	0,19 ± 0,01
	BERT-l	44,7 ± 1,3	44,5 ± 1,2	44,6 ± 1,3	0,17 ± 0,02
Cons	Word2Vec	46,6 ± 1,2	45,1 ± 1,2	45,8 ± 1,2	0,19 ± 0,02
	GloVe	46,7 ± 0,8	44,9 ± 0,9	45,8 ± 0,9	0,19 ± 0,01
	Fusion	45,6 ± 1,4	45,8 ± 1,4	45,5 ± 1,4	0,18 ± 0,02
	BERT-b	45,5 ± 1,5	45,3 ± 1,5	45,1 ± 1,5	0,18 ± 0,02
	BERT-l	43,6 ± 0,8	43,5 ± 0,8	43,3 ± 0,8	0,15 ± 0,01
Emot	Word2Vec	39,2 ± 1,4	38,9 ± 1,3	39,1 ± 1,4	0,09 ± 0,02
	GloVe	39,1 ± 1,3	39,0 ± 1,3	39,1 ± 1,3	0,09 ± 0,02
	Fusion	40,4 ± 1,3	40,4 ± 1,3	40,5 ± 1,3	0,11 ± 0,02
	BERT-b	38,3 ± 0,7	38,0 ± 0,6	38,2 ± 0,7	0,07 ± 0,01
	BERT-l	34,7 ± 1,6	34,4 ± 1,5	34,6 ± 1,5	0,02 ± 0,02
Open	Word2Vec	37,9 ± 1,9	37,6 ± 1,9	37,4 ± 1,9	0,06 ± 0,03
	GloVe	40,6 ± 2,6	40,1 ± 2,6	39,9 ± 2,6	0,09 ± 0,04
	Fusion	41,2 ± 0,8	41,0 ± 0,9	40,8 ± 0,8	0,11 ± 0,01
	BERT-b	35,0 ± 2,1	34,2 ± 2,1	34,3 ± 2,0	0,01 ± 0,03
	BERT-l	34,6 ± 1,4	33,9 ± 1,5	34,0 ± 1,4	0,01 ± 0,02

Fusion: Word2Vec + GloVe; **BERT-b:** BERT base; **BERT-l:** BERT large.

Source: Authors

Table 7. Confusion matrix for the classification of personality traits into three levels (results in %)

		Extr			Agr			Cons			Emot			Open		
		LP	MP	HP	LP	MP	HP	LP	MP	HP	LP	MP	HP	LP	MP	HP
Word2Vec	LP	58	31	11	56	26	18	66	21	13	47	32	21	36	45	19
	MP	46	32	22	25	45	30	51	26	23	38	37	25	35	47	18
	HP	36	28	36	23	40	37	34	20	46	32	34	34	32	38	30
GloVe	LP	60	28	12	53	25	22	70	18	12	42	32	26	44	37	19
	MP	47	33	20	27	44	29	53	24	23	36	34	30	31	48	21
	HP	34	28	38	23	36	41	31	25	44	29	30	41	28	45	27
Fusion	LP	45	33	22	51	26	23	49	35	16	41	33	26	42	36	22
	MP	31	35	34	25	43	32	31	41	28	35	37	28	29	46	25
	HP	19	26	55	19	37	44	18	35	47	27	29	44	30	36	34
BERT-b	LP	49	36	15	55	28	17	56	29	15	47	27	26	41	39	20
	MP	44	32	24	32	38	30	53	34	33	37	34	29	40	41	19
	HP	28	28	44	23	33	44	24	31	45	32	34	34	36	37	27
BERT-l	LP	48	34	18	53	24	23	53	33	14	43	34	23	41	40	19
	MP	39	34	27	33	39	28	36	31	33	36	34	30	42	39	19
	HP	27	30	43	22	36	42	23	31	46	31	42	27	41	37	22

Fusion: Word2Vec + GloVe; **BERT-b:** BERT base; **BERT-l:** BERT large.
LP: Low presence; MP: Medium presence; HP: High presence.

Source: Authors

the resulting representation spaces from the bi-class and tri-class scenarios are shown, respectively. Note that, in these two cases, the Figures illustrate the result of applying a dimensionality reduction based on Principal Component Analysis (PCA). In the bi-class scenario, the hyper-planes shown in the Figure correspond to those found with the optimal parameters of the SVM, *i.e.*, using the parameters reported in Table 5. Notice the high dispersion of the samples along the representation space. This is one of the reasons for the low accuracies found in the classification experiments. Finally, the tri-class scenario is shown in the third column of sub-figures, where three different colors are used to represent the three classes (LP, MP, and HP). These are also representations resulting from the PCA projection of the feature space. Even though the results appear to be low, the representation spaces show that the three sub-groups are found. These results, as well as the summarizing Figures, motivate us to continue working on this topic considering other approaches from fields such as language features and deep learning.

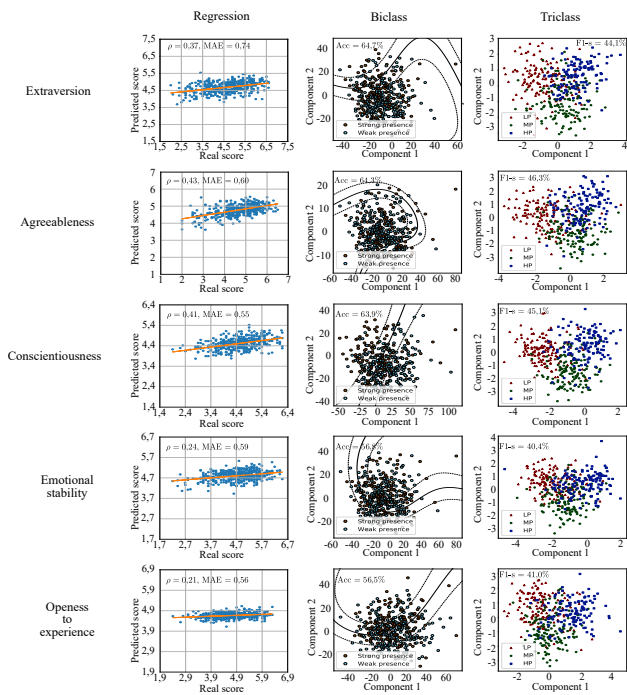


Figure 10. Graphical summary of the best results
Source: Authors

Comparison with recent works

The results reported in this study were compared with respect to different works in the state of the art. We did not find any study working on the tri-class classification problem, so comparisons are only reported for regression and the bi-class results.

The summary of our regression results and those reported by others in the literature are included in Table 8. According to the average results reported in the last row of the table, our approach shows similar performance to others reported in the literature. Our results are in fact better with regard to the MAE value in about 0,02. Now, in the case of RMSE, our results are 0,03 below (worst) and 0,04 below (worst) with respect to the previous result reported for R^2 . Although other works in the literature did not report results for Spearman's correlation, we decided to examine it because this measure is more intuitive, especially when the 'actual vs. predicted' plot is shown (Figure 10).

Table 8. Comparison of our regression model with recent works

Trait	Our approach				Biel <i>et al.</i> (2013)	Sun <i>et al.</i> (2019)	Guan <i>et al.</i> (2020)
	R^2	ρ	RMSE	MAE	R^2	RMSE	MAE
Extr	0,14	0,37	0,91	0,74	0,13	0,89	0,72
Agre	0,24	0,43	0,77	0,60	0,31	0,77	0,67
Cons	0,16	0,41	0,71	0,55	0,18	0,69	0,57
Emot	0,08	0,24	0,75	0,59	0,17	0,69	0,60
Open	0,05	0,21	0,70	0,56	0,04	0,68	0,58
Average	0,13	0,33	0,77	0,61	0,17	0,74	0,63

Source: Authors

The comparison regarding the bi-class classification scenario is reported in Table 9. Note that, on average, our results are slightly better than the other works, except for those obtained by Das-Kumar and Das-Dipankar (2017). Unfortunately, the authors of that work only report the average accuracy along with the five traits, which does

not allow for direct comparisons in specific traits. If we consider the average performance in terms of the F1-score compared to the performance reported by Salminen *et al.* (2020), we were able to improve the performance by 6,5%, which is relevant considering that we did not use neural networks. This gives us an idea that, for certain traits ('agreeableness', 'conscientiousness', and 'emotional stability'), classical methods such as those used in this paper (SVM with Gaussian kernel) yield better results than those found with other methods like the one reported by Salminen *et al.* (2020).

Table 9. Comparison of our bi-class classification model with recent works

Trait	Sarkar <i>et al.</i> (2014)		Alam and Riccardi (2014)	Das-Kumar and Das-Dipankar (2017)	Salminen <i>et al.</i> (2020)
	Acc	F1-score	F1-score	Acc	F1-score
Extr	64,7	64,7	60,5	-	71,9
Agre	64,3	64,2	65,7	-	44,4
Cons	63,9	63,9	65,8	-	48,5
Emot	56,8	56,8	47,7	-	40,3
Open	56,5	56,3	60,8	-	68,6
Average	61,2	61,2	60,1	62,3	54,7

Source: Authors

Conclusions and future work

This work considered the transliterations of multimedia recordings obtained from YouTube and explored the use of three word embedding methods (Word2Vec, GloVe, and BERT) to model the five different personality traits included in the OCEAN model. Standard regression and classification methods were considered to facilitate the analysis regarding the embedding methods. Three different evaluation scenarios were presented in this work: i) estimation of the personality scores by creating a regression system, ii) automatic classification of the strong vs. weak presence of each personality trait, and iii) the classification of three levels of personality traits. According to our findings in the regression experiments, Spearman's correlation coefficients ranging from 0,21 to 0,43 were obtained between the predicted personality scores and the ones assigned by the labeling system. Other performance measures such as MAE, RMSE, and R^2 were also reported to allow comparisons with respect to other studies in the state of the art. The classification between strong vs. weak presence of the traits shows that the accuracy and F1-score of the proposed approach are in the same range as those reported in the literature, and, in some traits ('extraversion', 'conscientiousness', and 'emotional stability'), our results outperform those of previous works in terms of the F1-score metric. Finally, the classification of three levels of personality traits (low, medium, and high) shows accuracies between 40,4 and 46,6%.

In general terms, our findings suggest that Word2Vec and GloVe embedding methods may be combined to obtain better results, and that the addition of the BERT-base and BERT-large models did not improve the performance in regression or in tri-class classification experiments. However, they considerably improved the performance in the two-class classification experiments with respect to the performance of the models based on Word2Vec, GloVe, or a fusion of both. It can also be concluded from the results that models based on word embeddings obtained with BERT-base generally outperform models based on word embeddings with BERT-large, which is in line with the work

by Mehta et al. (2020a), who found that the use of a larger linguistic model does not always result in a better performance. Further research is required to increase the results. Additionally, although the use of the data and labels considered in this work is relatively standard, we believe that there is also a big gap that needs to be filled in the labeling process. We are aware of the fact that these processes are expensive, time-consuming, and require sophisticated knowledge (especially from psychologists); joint efforts are required to create realistic databases labeled with more natural personality scores.

Acknowledgements

This work was funded by CODI from Universidad de Antioquia, grant no. PRG2017-15530.

References

- Alam, F. and Riccardi, G. (2014). Predicting personality traits using multimodal information. In ACM (Eds.), *Proceedings of the 2014 ACM multi media on workshop on computational personality recognition* (pp. 15-18). ACM. <https://dl.acm.org/doi/10.1145/2659522.2659531>
- Alammar, J. (June 27, 2018). The illustrated transformer. Jay Alammar. <http://jalammar.github.io/illustrated-transformer/>
- Allport, G. W. (1937). *Personality: A psychological interpretation*. Holt.
- Bellei, C. (2018). The backpropagation algorithm for Word2Vec. *Marginalia* <http://www.claudiobellei.com/2018/01/06/backprop-word2vec/>
- Biel, J. I., Tsiminaki, V., Dines, J., and Gatica-Perez, D. (2013). Hi YouTube! Personality impressions and verbal content in social video. In ACM (Eds.) *Proceedings of the 15th ACM on International conference on multimodal interaction* (pp. 119-126). ACM. <https://doi.org/10.1145/2522848.2522877>
- Buhrmester, M., Kwang, T., and Gosling, S. D. (2016). Amazon's Mechanical Turk: A new source of inexpensive, yet high-quality data? In A. E. Kazdin (Ed.), *Methodological issues and strategies in clinical research* (pp. 133-139). American Psychological Association. <https://doi.org/10.1037/14805-009>
- Cambria, E., Das, D., Bandyopadhyay, S., and Feraco, A. (2017). Affective computing and sentiment analysis. In E. Cambria, D. Das, S. Bandyopadhyay, and A. Feraco (Eds.), *A practical guide to sentiment analysis* (pp. 1-10). Springer. <https://doi.org/10.1007/978-3-319-55394-8>
- Celli, F. (2012). Unsupervised personality recognition for social network sites. In ICDS (Eds.), *ICDS 2012: The Sixth International Conference on Digital Society* (pp. 59-62). IARIA. <https://citeseerx.ist.psu.edu/viewdoc/download?doi=10.1.1.723.5551&rep=rep1&type=pdf>
- Celli, F., Lepri, B., Biel, J. I., Gatica-Perez, D., Riccardi, G., and Pianesi, F. (2014). The workshop on computational personality recognition 2014. In ACM (Eds.), *Proceedings of the 22nd ACM international conference on Multimedia* (pp. 1245-1246). ACM. <https://doi.org/10.1145/2647868.2647870>
- da Silva, B. B. C. and Paraboni, I. (2018). Personality recognition from Facebook text. In A. Villavicencio, V. Moreira, A. Abad, H. Caseli, P. Gamallo, C. Ramisch, H. G. Oliveira, and G. H. Paetzold (Eds.) *International Conference on Computational Processing of the Portuguese Language* (pp. 107-114). Springer. https://doi.org/10.1007/978-3-319-99722-31_1
- Das, K. G., and Das, D. (2017, December). *Developing lexicon and classifier for personality identification in texts* [Conference presentation]. 14th International Conference on Natural Language Processing (ICON-2017), Kolkata, India. <https://aclanthology.org/W17-7545.pdf>
- Devlin, J., Chang, M. W., Lee, K., and Toutanova, K. (2018). Bert: Pre-training of deep bidirectional transformers for language understanding. *arXiv preprint*. <https://arxiv.org/abs/1810.04805>
- Dey, S. (2018, April). Implementing a soft-margin kernelized support vector machine binary classifier with quadratic programming in R and Python. *Simple Data Science*. <https://sandipanweb.wordpress.com/2018/04/23/>
- Gosling, S. D., Rentfrow, P. J., and Swann Jr., W. B. (2003). A very brief measure of the Big-Five personality domains. *Journal of Research in Personality*, 37(6), 504-528. [https://doi.org/10.1016/S0092-6566\(03\)00046-1](https://doi.org/10.1016/S0092-6566(03)00046-1)
- Guan, Z., Wu, B., Wang, B., and Liu, H. (2020). Personality2vec: network representation learning for personality. In IEEE (Eds.) *2020 IEEE Fifth International Conference on Data Science in Cyberspace (DSC)* (pp. 30-37). IEEE. <https://doi.org/10.1109/DSC50466.2020.00013>
- Hassanein, M., Hussein, W., Rady, S., and Gharib, T. F. (2018). Predicting personality traits from social media using text semantics. In IEEE (Eds.) *2018 13th International Conference on Computer Engineering and Systems (ICCES)* (pp. 184-189). IEEE. <https://doi.org/10.1109/ICCES.2018.8639408>
- Jiang, H., Zhang, X., and Choi, J. D. (2020). Automatic text-based personality recognition on monologues and multiparty dialogues using attentive networks and contextual embeddings (Student Abstract). *Proceedings of the AAAI Conference on Artificial Intelligence*, 34(10), 13821-13822. <https://doi.org/10.1609/aaai.v34i10.7182>
- John, O. P., Donahue, E. M., and Kentle, R. L. (1991). Big Five inventory (BFI) [Database record]. *APA PsycTests*. <https://doi.org/10.1037/t07550-000>
- John, O. P., Naumann, L. P., and Soto, C. J. (2008). Paradigm shift to the integrative Big Five trait taxonomy: history, measurement, and conceptual issues. In O. P. John, R. W. Robins, and L. A. Pervin (Eds.), *Handbook of Personality: Theory and Research* (pp. 114-158). The Guilford Press.
- Kazameini, A., Fatehi, S., Mehta, Y., Eetemadi, S., and Cambria, E. (2020). Personality trait detection using bagged svm over bert word embedding ensembles. *arXiv preprint*. <https://arxiv.org/abs/2010.01309>
- Kohavi, R. (1995). A study of cross-validation and bootstrap for accuracy estimation and model selection. *IJCAI'95: Proceedings of the 14th International Joint Conference on Artificial Intelligence*, 14(2), 1137-1145. <https://dl.acm.org/doi/10.5555/1643031.1643047>

- Kosinski, M., Matz, S. C., Gosling, S. D., Popov, V., and Stillwell, D. (2015). Facebook as a research tool for the social sciences: Opportunities, challenges, ethical considerations, and practical guidelines. *American Psychologist*, 70(6), 543. <https://doi.org/10.1037/a0039210>
- Mao, Y., Zhang, D., Wu, C., Zheng, K., and Wang, X. (2018). Feature analysis and optimisation for computational personality recognition. In IEEE (Eds.), *2018 IEEE 4th International Conference on Computer and Communications (ICCC)* (pp. 2410-2414). IEEE. <https://doi.org/10.1109/CompComm.2018.8780801>
- Mehta, Y., Fatehi, S., Kazameini, A., Stachl, C., Cambria, E., and Eetemadi, S. (2020a). Bottom-up and top-down: Predicting personality with psycholinguistic and language model features. In IEEE (Eds.) *2020 IEEE International Conference on Data Mining (ICDM)* (pp. 1184-1189). IEEE. <https://doi.org/10.1109/ICDM50108.2020.00146>
- Mehta, Y., Majumder, N., Gelbukh, A., and Cambria, E. (2020b). Recent trends in deep learning based personality detection. *Artificial Intelligence Review*, 53(4), 2313-2339. <https://doi.org/10.1007/s10462-019-09770-z>
- Milgram, J., Cheriet, M., and Sabourin, R. (2006, October). "One against one" or "one against all": Which one is better for handwriting recognition with SVMs? [Conference presentation]. Tenth International Workshop on Frontiers in Handwriting Recognition, La Baule, France. <https://hal.inria.fr/inria-00103955>
- Mikolov, T. (2015). word2vec: Tool for computing continuous distributed representations of words. *Google Code*. <https://code.google.com/archive/p/word2vec/>
- Mikolov, T., Chen, K., Corrado, G., and Dean, J. (2013). Efficient estimation of word representations in vector space. *arXiv preprint*. <https://arxiv.org/abs/1301.3781>.
- Mohammad, S. and Kiritchenko, S. (2013). Using nuances of emotion to identify personality. *Seven International AAAI Conference on Web and Social Media*. <https://doi.org/10.48550/arXiv.1309.6352>
- Onan, A. (2015). Classifier and feature set ensembles for web page classification. *Journal of Information Science*, 42(2), 150-165. <https://doi.org/10.1177/0165551515591724>
- Onan, A. (2016). An ensemble scheme based on language function analysis and feature engineering for text genre classification. *Journal of Information Science*, 44(1), 1-20. <https://doi.org/10.1177/0165551516677911>
- Onan, A. (2017a). Hybrid supervised clustering based ensemble scheme for text classification. *Kybernetes*, 46(2), 330-348. <https://doi.org/10.1108/K-10-2016-0300>
- Onan, A. (2017b). A K-medoids based clustering scheme with an application to document clustering. In IEEE (Eds.), *2017 International Conference on Computer Science and Engineering (UBMK)* (pp. 354-359). IEEE. <https://doi.org/10.1109/UBMK.2017.8093409>
- Onan, A. (2018). Sentiment analysis on Twitter based on ensemble of psychological and linguistic feature sets. *Balkan Journal of Electrical and Computer Engineering*, 6(2), 69-77. <https://doi.org/10.17694/bajece.419538>
- Onan, A. (2019a). Two-stage topic extraction model for bibliometric data analysis based on word embeddings and clustering. *IEEE Access*, 7, 145614-145633. <https://doi.org/10.1109/ACCESS.2019.2945911>
- Onan, A. (2019b). Mining opinions from instructor evaluation reviews: a deep learning approach. *Computer Applications in Engineering Education*, 28(1), 117-138. <https://doi.org/10.1002/cae.22179>
- Onan, A. (2020). Sentiment analysis on product reviews based on weighted word embeddings and deep neural networks. *Concurrency and Computation: Practice and Experience*, e5909. <https://doi.org/10.1002/cpe.5909>
- Onan, A., and Korukoglu, S. (2015). A feature selection model based on genetic rank aggregation for text sentiment classification. *Journal of Information Science*, 43(1), 25-38. <https://doi.org/10.1177/0165551515613226>
- Onan, A., Korukoğlu, S., and Bulut, H. (2016a). Ensemble of keyword extraction methods and classifiers in text classification. *Expert Systems with Applications*, 57, 232-247. <https://doi.org/10.1016/j.eswa.2016.03.045>
- Onan, A., Korukoğlu, S., and Bulut, H. (2016b). LDA-based topic modelling in text sentiment classification: An Empirical Analysis. *International Journal of Computational Linguistics and Applications*, 7(1), 101-119. <https://doi.org/10.1016/j.eswa.2016.06.005>
- Onan, A., Korukoğlu, S., and Bulut, H. (2016c). A multiobjective weighted voting ensemble classifier based on differential evolution algorithm for text sentiment classification. *Expert Systems with Applications*, 62, 1-16. <https://doi.org/10.1016/j.eswa.2016.06.005>
- Pennebaker, J. W. and King, L. A. (1999). Linguistic styles: language use as an individual difference. *Journal of Personality and Social Psychology*, 77(6), 1296-1312. <https://doi.org/10.1037/0022-3514.77.6.1296>
- Pennington, J. (2014). GloVe: Global Vectors for Word Representation. <https://nlp.stanford.edu/projects/glove/>
- Pennington, J., Socher, R., and Manning, C. D. (2014, October). GloVe: Global vectors for word representation [Conference presentation]. 2014 Conference on Empirical Methods in Natural Language Processing (EMNLP), Doha, Qatar. <http://dx.doi.org/10.3115/v1/D14-1>
- Pérez, P. A. (2020). WEBERT: Word Embeddings using BERT. <https://doi.org/10.5281/zenodo.3964244>
- Powers, D. M. (2020). Evaluation: From precision, recall and F-measure to ROC, informedness, markedness and correlation. *arXiv preprint*. <https://arxiv.org/abs/2010.16061>
- Pratama, B. Y. and Sarno, R. (2015). Personality classification based on Twitter text using Naive Bayes, KNN and SVM. In IEEE (Eds.) *2015 International Conference on Data and Software Engineering (ICoDSE)* (pp. 170-174). IEEE. <https://doi.org/10.1109/ICoDSE.2015.7436992>
- Ranković, V., Grujović, N., Divac, D., and Milivojević, N. (2014). Development of support vector regression identification model for prediction of dam structural behaviour. *Structural Safety*, 48, 33-39. <https://doi.org/10.1016/j.strusafe.2014.02.004>
- Rehurek, R. and Sojka, P. (2010, May 2). *Software framework for topic modelling with large corpora* [Conference presentation]. LREC 2010 Workshop on New Challenges for NLP Frameworks, Valletta, Malta.

Salminen, J., Rao, R. G., Jung, S. G., Chowdhury, S. A., and Jansen, B. J. (2020). Enriching social media personas with personality traits: a deep learning approach using the Big Five classes. In H. Degen, L. Reinerman-Jones (Eds.), *International Conference on Human-Computer Interaction* (pp. 101-120). Springer. https://doi.org/10.1007/978-3-030-50334-5_7

Sarkar, C., Bhatia, S., Agarwal, A., and Li, J. (2014, November). Feature analysis for computational personality recognition using youtube personality data set. In ACM (Eds.), *Proceedings of the 2014 ACM Multi Media on Workshop on Computational Personality Recognition* (pp. 11-14). ACM. <https://doi.org/10.1145/2659522.2659528>

Schölkopf, B., Smola, A. J., and Bach, F. (2002). *Learning with kernels: support vector machines, regularization, optimization, and beyond*. MIT press.

Smola, A. J. and Schölkopf, B. (2004). A tutorial on support vector regression. *Statistics and computing*, 14(3), 199-222. <https://doi.org/10.1023/B:STCO.0000035301.49549.88>

Sun, X., Liu, B., Meng, Q., Cao, J., Luo, J., and Yin, H. (2019). Group-level personality detection based on text generated networks. *World Wide Web*, 23(3), 1887-1906. <https://doi.org/10.1007/s11280-019-00729-2>

Vapnik, V. (1995). *The nature of statistical learning theory*. Springer. <https://doi.org/10.1007/978-1-4757-2440-0>

Vinciarelli, A. and Mohammadi, G. (2014). A survey of personality computing. *IEEE Transactions on Affective Computing*, 5(3), 273-291. <https://doi.org/10.1109/TAFFC.2014.2330816>

White, J. K., Hendrick, S. S., and Hendrick, C. (2004). Big Five personality variables and relationship constructs. *Personality and individual differences*, 37(7), 1519-1530. <https://doi.org/10.1016/j.paid.2004.02.019>

Xue, D., Hong, Z., Guo, S., Gao, L., Wu, L., Zheng, J., and Zhao, N. (2017). Personality recognition on social media with label distribution learning. *IEEE Access*, 5, 13478-13488. <https://doi.org/10.1109/ACCESS.2017.2719018>

Table 10. Results for personality trait estimation with linear kernel

Trait	Feature	C, ϵ	R^2	ρ	MAE	RMSE
Extr	Word2Vec	1e-4, 1e-1	0,08 ± 0,00	0,29 ± 0,01	0,77 ± 0,00	0,94 ± 0,00
	GloVe	1e-4, 1e-1	0,10 ± 0,00	0,31 ± 0,01	0,76 ± 0,00	0,93 ± 0,00
	Fusion	1e-4, 1e-4	0,11 ± 0,00	0,33 ± 0,00	0,76 ± 0,00	0,92 ± 0,00
	BERT-b	1e-4, 1e-1	0,14 ± 0,00	0,37 ± 0,01	0,74 ± 0,01	0,91 ± 0,01
	BERT-l	1e-4, 1e-1	0,09 ± 0,00	0,30 ± 0,01	0,76 ± 0,00	0,94 ± 0,00
Agr	Word2Vec	1e-4, 1e-2	0,18 ± 0,00	0,41 ± 0,03	0,62 ± 0,01	0,80 ± 0,01
	GloVe	1e-4, 1e-1	0,14 ± 0,00	0,36 ± 0,02	0,64 ± 0,01	0,83 ± 0,01
	Fusion	1e-4, 1e-1	0,26 ± 0,00	0,45 ± 0,01	0,59 ± 0,00	0,77 ± 0,00
	BERT-b	1e-4, 1e-4	0,21 ± 0,00	0,43 ± 0,01	0,62 ± 0,01	0,79 ± 0,01
	BERT-l	1e-4, 1e-1	0,17 ± 0,00	0,38 ± 0,01	0,63 ± 0,00	0,81 ± 0,01
Cons	Word2Vec	1e-4, 1e-1	0,14 ± 0,00	0,39 ± 0,01	0,55 ± 0,00	0,71 ± 0,00
	GloVe	1e-4, 1e-1	0,14 ± 0,00	0,38 ± 0,01	0,56 ± 0,00	0,72 ± 0,00
	Fusion	1e-4, 1e-1	0,15 ± 0,00	0,41 ± 0,01	0,55 ± 0,00	0,71 ± 0,00
	BERT-b	1e-4, 1e-1	0,14 ± 0,00	0,38 ± 0,01	0,56 ± 0,01	0,72 ± 0,01
	BERT-l	1e-4, 1e-1	0,14 ± 0,00	0,39 ± 0,01	0,55 ± 0,01	0,71 ± 0,01
Emot	Word2Vec	1e-3, 1	0,07 ± 0,00	0,19 ± 0,03	0,60 ± 0,00	0,75 ± 0,01
	GloVe	1e-4, 1e-1	0,04 ± 0,00	0,16 ± 0,05	0,60 ± 0,01	0,77 ± 0,01
	Fusion	1e-4, 1	0,06 ± 0,00	0,19 ± 0,02	0,59 ± 0,01	0,76 ± 0,01
	BERT-b	1e-4, 1e-1	0,07 ± 0,00	0,23 ± 0,02	0,58 ± 0,01	0,75 ± 0,01
	BERT-l	1e-4, 1e-1	0,03 ± 0,00	0,16 ± 0,04	0,61 ± 0,01	0,77 ± 0,01
Open	Word2Vec	1e-4, 1e-4	0,01 ± 0,00	0,14 ± 0,01	0,57 ± 0,00	0,71 ± 0,00
	GloVe	1e-4, 1e-4	0,02 ± 0,00	0,19 ± 0,02	0,56 ± 0,00	0,71 ± 0,00
	Fusion	1e-4, 1e-4	0,02 ± 0,00	0,17 ± 0,03	0,57 ± 0,01	0,72 ± 0,00
	BERT-b	1e-4, 1	0,00 ± 0,00	-0,04 ± 0,03	0,59 ± 0,00	0,73 ± 0,01
	BERT-l	1e-4, 1e-1	0,01 ± 0,00	-0,05 ± 0,03	0,59 ± 0,00	0,73 ± 0,01

Fusion: Word2Vec + GloVe; **BERT-b:** BERT base; **BERT-l:** BERT large.

Source: Authors

Table 11. Results for bi-class system: weak presence vs. strong presence of the trait considering linear kernel

Trait	Feature	C	Accuracy	Sensitivity	Specificity	F1-score	AUC
Extr	Word2Vec	1e-3	60,3 ± 1,7	58,3 ± 1,6	62,2 ± 2,3	60,3 ± 1,6	0,63 ± 0,01
	GloVe	1e-3	61,6 ± 1,3	63,8 ± 1,9	59,4 ± 1,2	61,6 ± 1,3	0,65 ± 0,01
	Fusion	1e-4	61,0 ± 1,1	63,1 ± 1,4	59,0 ± 1,8	61,0 ± 1,1	0,65 ± 0,01
	BERT-b	1e-3	60,8 ± 1,1	62,5 ± 1,8	59,2 ± 1,6	60,8 ± 1,0	0,66 ± 0,01
	BERT-l	1e-4	61,2 ± 1,3	65,6 ± 1,6	57,0 ± 2,0	61,1 ± 1,3	0,67 ± 0,01
Agr	Word2Vec	1e-3	59,4 ± 1,4	59,4 ± 1,4	59,4 ± 1,9	59,4 ± 1,3	0,65 ± 0,01
	GloVe	1e-3	61,6 ± 1,0	60,3 ± 2,3	62,7 ± 1,2	61,6 ± 1,0	0,66 ± 0,01
	Fusion	1e-3	59,0 ± 1,3	55,9 ± 2,5	61,7 ± 1,9	59,0 ± 1,3	0,64 ± 0,01
	BERT-b	1e-3	62,4 ± 1,6	60,3 ± 1,5	64,3 ± 2,5	62,4 ± 1,5	0,67 ± 0,01
	BERT-l	1e-4	60,7 ± 1,8	59,2 ± 3,1	61,9 ± 1,8	60,7 ± 1,8	0,66 ± 0,01
Cons	Word2Vec	1e-4	61,9 ± 1,8	68,6 ± 2,4	55,7 ± 2,2	61,8 ± 1,8	0,66 ± 0,02
	GloVe	1e-4	61,8 ± 1,1	66,4 ± 1,0	57,5 ± 1,9	61,8 ± 1,1	0,66 ± 0,01
	Fusion	1e-4	62,7 ± 0,7	69,1 ± 1,9	56,8 ± 1,2	62,6 ± 0,7	0,69 ± 0,01
	BERT-b	1e-4	61,8 ± 1,0	66,5 ± 1,2	57,5 ± 1,3	61,8 ± 1,0	0,67 ± 0,01
	BERT-l	1e-4	62,2 ± 0,6	66,4 ± 1,2	58,2 ± 1,7	62,1 ± 0,6	0,67 ± 0,1
Emot	Word2Vec	1e-3	55,3 ± 1,4	49,2 ± 3,6	61,3 ± 2,4	55,1 ± 1,5	0,58 ± 0,01
	GloVe	1e-2	50,9 ± 1,9	46,2 ± 2,6	55,7 ± 2,9	50,8 ± 1,9	0,55 ± 0,01
	Fusion	1e-4	54,9 ± 1,5	43,7 ± 2,0	65,9 ± 2,3	54,3 ± 1,5	0,59 ± 0,01
	BERT-b	1e-3	57,6 ± 2,5	56,1 ± 3,4	59,1 ± 2,5	57,6 ± 2,5	0,62 ± 0,02
	BERT-l	1e-4	55,5 ± 1,3	53,1 ± 2,0	57,9 ± 1,3	55,5 ± 1,3	0,58 ± 0,02
Open	Word2Vec	1e-3	54,6 ± 1,5	53,8 ± 3,0	55,5 ± 2,7	54,6 ± 1,5	0,56 ± 0,01
	GloVe	1e-3	53,1 ± 1,5	50,7 ± 2,8	55,6 ± 2,2	53,1 ± 1,5	0,55 ± 0,02
	Fusion	1e-4	57,4 ± 1,9	53,5 ± 2,1	61,3 ± 2,1	57,4 ± 1,9	0,58 ± 0,02
	BERT-b	1e-3	55,0 ± 1,9	51,8 ± 3,1	58,1 ± 1,4	54,9 ± 1,9	0,56 ± 0,01
	BERT-l	1e-4	55,1 ± 1,8	51,5 ± 2,0	58,9 ± 2,6	55,1 ± 1,8	0,56 ± 0,01

Fusion: Word2Vec + GloVe; **BERT-b:** BERT base; **BERT-l:** BERT large.

Source: Authors

Table 12. Tri-class classification results with linear kernel

Trait	Feature	Accuracy	F1-score	UAR	κ
Extr	Word2Vec	40,7 ± 1,0	40,7 ± 1,1	40,7 ± 1,1	0,11 ± 0,02
	GloVe	41,6 ± 1,3	41,5 ± 1,3	41,6 ± 1,3	0,12 ± 0,02
	Fusion	43,4 ± 1,1	43,1 ± 1,1	43,7 ± 1,2	0,15 ± 0,02
	BERT-b	39,4 ± 1,0	39,4 ± 1,0	39,4 ± 1,0	0,09 ± 0,02
	BERT-l	43,0 ± 0,9	43,0 ± 0,9	43,2 ± 0,9	0,15 ± 0,01
Agr	Word2Vec	44,6 ± 1,5	44,6 ± 1,5	44,5 ± 1,5	0,17 ± 0,02
	GloVe	47,1 ± 1,3	47,0 ± 1,3	47,0 ± 1,3	0,20 ± 0,02
	Fusion	46,2 ± 1,2	46,3 ± 1,3	46,1 ± 1,2	0,19 ± 0,02
	BERT-b	45,3 ± 1,4	45,2 ± 1,3	45,3 ± 1,3	0,18 ± 0,02
	BERT-l	45,6 ± 1,2	45,5 ± 1,2	45,5 ± 1,2	0,18 ± 0,02
Cons	Word2Vec	41,7 ± 1,1	41,8 ± 1,1	41,6 ± 1,1	0,13 ± 0,02
	GloVe	43,9 ± 1,2	43,9 ± 1,1	43,8 ± 1,1	0,16 ± 0,02
	Fusion	45,3 ± 1,6	45,6 ± 1,6	45,4 ± 1,6	0,18 ± 0,02
	BERT-b	45,0 ± 1,6	45,2 ± 1,6	44,9 ± 1,6	0,17 ± 0,02
	BERT-l	43,3 ± 1,2	43,5 ± 1,2	43,2 ± 1,2	0,15 ± 0,02
Emot	Word2Vec	41,3 ± 1,3	41,2 ± 1,3	41,3 ± 1,2	0,12 ± 0,01
	GloVe	40,3 ± 1,4	40,2 ± 1,4	40,4 ± 1,4	0,10 ± 0,02
	Fusion	39,4 ± 1,5	39,4 ± 1,5	39,4 ± 1,5	0,09 ± 0,02
	BERT-b	37,8 ± 1,6	37,6 ± 1,5	37,8 ± 1,6	0,07 ± 0,02
	BERT-l	36,8 ± 2,1	36,5 ± 2,0	36,7 ± 2,1	0,05 ± 0,03
Open	Word2Vec	38,0 ± 1,4	38,1 ± 1,4	37,9 ± 1,4	0,07 ± 0,02
	GloVe	38,6 ± 1,5	38,6 ± 1,6	38,6 ± 1,5	0,08 ± 0,02
	Fusion	38,9 ± 0,7	38,8 ± 0,7	38,6 ± 0,7	0,08 ± 0,01
	BERT-b	32,5 ± 1,0	31,9 ± 1,0	31,8 ± 1,0	-0,03 ± 0,02
	BERT-l	36,2 ± 1,4	35,8 ± 1,3	35,7 ± 1,3	0,03 ± 0,02

Fusion: Word2Vec + GloVe; **BERT-b:** BERT base; **BERT-l:** BERT large.

Source: Authors

Appendix: results obtained with linear kernels

This section shows the results obtained in the three main experiments of this work regarding linear kernels.

First Aid Approaches, Teaching, and Knowledge and Technology Transfer to Undergraduate Engineering Students

Enfoques de primeros auxilios, enseñanza y transferencia de conocimiento y tecnología a estudiantes de pregrado en ingeniería

Rosângela de França Bail¹, Ariel Orlei Michaloski², João Luiz Kovaleski³,
Daiane Maria de Genaro Chiroli⁴, Vander Luiz da Silva⁵, and Regina Negri Pagani⁶

ABSTRACT

First aid and prehospital care practices are fundamental in helping victims, often saving lives. This study aims to present the results of a bibliometric analysis regarding first aid, as well as a case report on teaching in first aid to a group of undergraduate students. The latter presents a project developed at a Brazilian public university for engineering students. The core modules addressed in the project were: first aid concepts, specialized distress calling, site safety, injury mechanism, primary and secondary approaches, bleeding control, cardiopulmonary resuscitation, clinical emergencies, seizures, intoxications, fractures, burns, immobilizations, and victim transport. A systematic literature review was conducted, which was based on structured protocols, in four databases: Scopus, Web of Science, PubMed, and ScienceDirect. Significant data were analyzed, such as years of publication, main journals, and more frequent terms in first aid teaching. The SOS-UTFPR Project aims to provide scholars of engineering and related fields with theoretical-practical knowledge about first aid. As of 2021, it has three graduated groups, thus generating relevant data for this research. Its main purpose is to train citizens capable of making assertive decisions in emergency situations, whether at the university, work, home, etc. With this, it was possible to promote the dissemination of the Transfer of Knowledge and Technology (KTT) by training individuals to multiply information, techniques, and acquired knowledge, in order to act preventively and save lives.

Keywords: First aid, teaching, engineering, collective health

RESUMEN

Las prácticas de primeros auxilios y atención prehospitalaria son fundamentales para ayudar a las víctimas, a menudo salvando vidas. Este estudio tiene como objetivo presentar los resultados de un análisis bibliométrico en primeros auxilios, así como un informe de caso sobre la enseñanza de primeros auxilios a un grupo de estudiantes de pregrado. Este último presenta un proyecto desarrollado en una universidad pública brasileña para estudiantes de ingeniería. Los módulos centrales abordados en el proyecto fueron: conceptos de primeros auxilios, llamadas especializadas de socorro, seguridad del sitio, mecanismo de lesiones, enfoques primarios y secundarios, control de hemorragias, reanimación cardiopulmonar, emergencias clínicas, convulsiones, intoxicaciones, fracturas, quemaduras, inmovilizaciones y transporte de víctimas. Se realizó una revisión sistemática de la literatura, basada en protocolos estructurados, en cuatro bases de datos: Scopus, Web of Science, PubMed y ScienceDirect. Se analizaron datos significativos como años de publicación, revistas principales y palabras más frecuentes en la enseñanza de primeros auxilios. El Proyecto SOS-UTFPR pretende proporcionar conocimientos teórico-prácticos sobre primeros auxilios a académicos de ingeniería y campos relacionados. Hasta 2021, el proyecto ha graduado a tres grupos, generando datos relevantes para esta investigación. Su objetivo principal es formar ciudadanos capaces de tomar decisiones asertivas en situaciones de emergencia, ya sea en la universidad, en el trabajo, el hogar, etc. Con ello se logró impulsar la difusión de la Transferencia de Conocimiento y Tecnología (KTT), capacitando individuos para que multipliquen la información, las técnicas y los conocimientos adquiridos, a fin de actuar de manera preventiva y salvaguardar vidas.

Palabras clave: Primeros auxilios, enseñanza, ingeniería, salud colectiva

Received: January 28th, 2020

Accepted: July 26th, 2021

¹ Federal University of Technology of Paraná, Brazil. Affiliation: Ph.D candidate in Production Engineering, Federal University of Technology of Paraná, Brazil. Email rosangelabail@hotmail.com

² Federal University of Technology of Paraná, Brazil. Affiliation: Associate professor of the Post-Graduate Program in Production Engineering, Federal University of Technology of Paraná, Brazil. Email ariel@utfpr.edu.br

³ Federal University of Technology of Paraná, Brazil. Affiliation: Associate professor of the Post-Graduate Program in Production Engineering, Federal University of Technology of Paraná, Brazil. Email kovaleski@utfpr.edu.br

⁴ Federal University of Technology of Paraná, Brazil. Affiliation: Associate professor at the Production Engineering Department, Federal University of Technology of Paraná, Brazil. Email daianechiroli@utfpr.edu.br

⁵ Federal University of Technology of Paraná, Brazil. Affiliation: Ph.D candidate at Production Engineering, Federal University of Technology of Paraná, Brazil. Email luizvnder@gmail.com

⁶ Federal University of Technology of Paraná, Brazil. Affiliation: Associate professor at Post-Graduate Program in Production Engineering, Federal University of Technology of Paraná, Brazil. Email reginapagani@utfpr.edu.br

How to cite: Bail, R. F., Kovaleski, J. L., Michaloski, A. O., Chiroli, D. M. G., Silva, V. L., and Pagani, R. N. (2022). First aid approaches, teaching, and knowledge and technology transfer to undergraduate engineering students. *Ingeniería e Investigación*, 42(2), e84495. <http://doi.org/10.15446/ing.investig.v42n2.84788>



Attribution 4.0 International (CC BY 4.0) Share - Adapt

Introduction

The significant increase in world population, technological innovations, and the expansion of economic and industrial growth, in addition to the aspect of urban violence and environmental conditions, are the main causes of accidents. Since self-care actions cannot be fully applied to protect against the risks of daily living, they do not depend solely on individuals, but also on their context (Veronese and Oliveira, 2006).

Regardless of the danger, it has become necessary to identify hazards whenever possible and manage them accordingly. Therefore, preventive actions are essential, followed by corrective actions, in order to minimize impacts and damages to humans or administer the necessary care as a person, citizen, worker, or user (Bail et al., 2019). Day to day, thousands of people go through medical emergencies experiencing and/or witnessing adversities. In these moments, spectators usually provide spontaneous aid (Velde et al., 2006).

First aid is a knowledge science that is part of the greater area of health and safety at work (Veronese and Oliveira, 2006). It is of extreme importance, as it makes it possible to save lives, seeing that people are increasingly exposed to dangers and risks of different types and intensities in their commute from a place to another, in their work environment, at the university, among others (Bail et al., 2019). Danger can be defined as a potential threat to one's physical and psychic integrity and welfare, whereas hazard is the probability of adversities or accidents (Velde et al., 2006). Risk arises not only from how the future can be described, but from the uncertainty surrounding that description (Eiser et al., 2012).

First aid comprises assistance offered in cases involving accidents, search and rescue, removal of victims from dangerous locations, requests for help, infection control, bleeding, injuries, spine and head trauma, musculoskeletal trauma, oral poisoning, and other needs (Velde et al., 2006). It basically involves emergency care or procedures applied before medical treatment (Cuttle et al., 2009).

First aid teaching, training, and approaches are essential to prepare people for adversities (Velde et al., 2006). In order to reach everyone, researchers and experts recommend approaching first aid in schools (Engeland et al., 2002) and universities to reduce untimely deaths caused by accidents and other adversities (Khan et al., 2010). The more people are prepared for providing first aid, the safer the environment becomes for everyone.

In developed countries, the knowledge about first aid practices has been introduced to not only healthcare professionals, but also to basic education for children at schools, thus shaping citizens who are aware of how to act in case of emergency (Azhar and Choudhry, 2016). One of reasons for this is the high incidence of natural disasters, even though they are not the only causes of accidents and damage to human beings.

On the other hand, in developing countries such as Brazil, this type of training is limited to healthcare professionals in specific aid and rescue organizations or in companies via basic tutorials. It is necessary to transfer knowledge, both to healthcare staff and the general public, bearing in mind that the United Nations (UN) determines that ensuring the community's health, safety, and welfare, especially through prevention, is mandatory (Leiva et al., 2014).

The aim of this paper is to present the results of a bibliometric analysis regarding first aid, as well as a case report on teaching in first aid involving a group of undergraduate students. The case report presents a project developed at a Brazilian public university for engineering students. Unlike degree programs in the field of health such as nursing and medicine, engineering degrees do not feature first aid approaches, which entails a deficiency for students regarding this knowledge, seeing as Brazilian schools do not approach first aid teaching for children and teenagers either.

With this goal, this paper aims to answer the following questions:

- i. In the international scope, are there reports of studies about first aid teaching in engineering degrees?
- ii. Are engineering undergraduate students knowledgeable about first aid?
- iii. How can this knowledge be specifically transferred to engineering students?

The university where the study was conducted offers a greater number of undergraduate programs in this field, such as mechanical, electrical, chemical, computer, and production engineering. For this reason, the first aid case report focuses on engineering courses. It is the result of an extension project developed at the Federal Technological University of Paraná, Ponta Grossa, Brazil.

As emphasized, first aid teaching is important for individuals and professionals, not limited to undergraduate health courses, as is the case in Brazil. Through this project, we have expanded the teaching to engineering students.

Methodology

Initially, a systematic literature review was conducted, which was based on the structured protocols by Pagani et al. (2015) called *Methodi ordinatio*. This method is a multi-criteria decision aid tool, which allows researchers to ponder using three variables: impact factor, number of citations, and year of publication. The pondering on these variables generates an index, the InOrdinatio, which indicates the scientific relevance of the paper. From this index, it is possible to rank the papers individually (Pagani et al., 2015; Silva et al., 2020). Studies that applied the *Methodi ordinatio* include

Pagani *et al.* (2019), Bail (2019), Bail *et al.* (2020), Soares *et al.* (2020), Moura *et al.* (2020), Silva *et al.* (2021), and Corsi *et al.* (2021), among others.

Figure 1 illustrates the three paper portfolios defined, each with a more specific purpose.

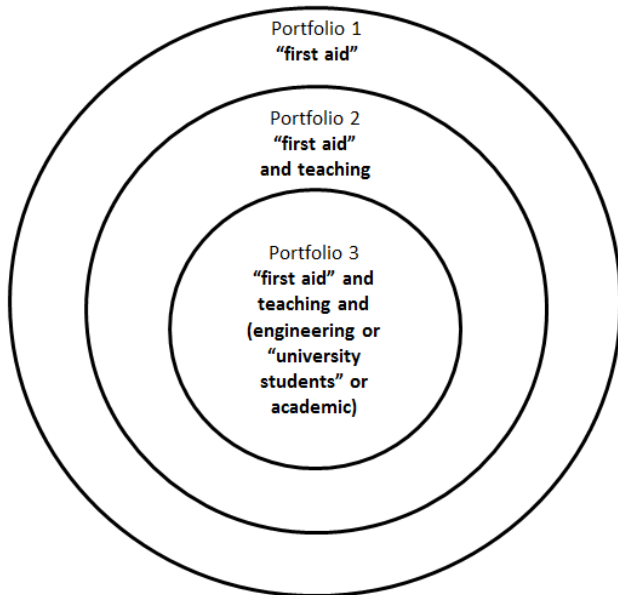


Figure 1. Definition of bibliographic portfolio
Source: Authors

Portfolio 1 was created for the bibliometric analysis of papers by consulting four international databases (Scopus, Web of Science, ScienceDirect, and PubMed). Systematic research works from a qualitative perspective, as it analyzes the alignment of articles with the focus of the research objective. However, in the context of the research, there is also a quantitative point of view that is related to bibliometric study (Chirolí *et al.*, 2016). The basic filtering criteria employed in each database comprised a keyword inserted in titles, a time period including all years, and the type of document (such as journal papers). The search on the databases was conducted in January 2020, so only data from 2019 and previous years were included, with no other restrictions. The papers were exported in the bibtex format to the Mendeley reference manager software, eliminating all duplicate results.

The bibliometric analysis explored data related to the papers about first aid, defining the years of publication, the central journals in the field considering the number of publications, and the terms most employed in the papers.

Portfolio 2 aimed to find papers for reading in full, both to better understand the studies about first aid teaching in the international scope and to prioritize the relevant subjects in the discussion. This portfolio employed a combination of keywords, “first aid” and “teaching”, also inserted in titles, followed by the aforementioned basic filtering criteria. After discarding duplicate papers, the *Methodi ordinatio* was applied. It is a tool that sorts scientific papers based on

impact factor, year of publication, and number of citations, and it is managed by Equation (1):

$$InOrdinatio = \left(\frac{IF}{1000} \right) + \left(\alpha \times (10 - (ResearchYear - PublishYear)) \right) + ci \quad (1)$$

where IF is the impact factor, α is a weighting factor ranging from 1 to 10 to be attributed by the researcher; ResearchYear is the year in which the bibliographic research was developed; PublishYear is the year in which the selected paper was published; and Ci is the number of times the paper has been cited on Google Scholar (Pagani *et al.*, 2015).

In this way, the articles with the highest InOrdinatio values of the *Methodi ordinatio* were selected.

Portfolio 3 sought to explore, in the literature, the existence, formalization, and further approaches of first aid teaching in engineering degrees. This portfolio is directly aligned with a case report in this study, focusing on the teaching and knowledge transfer to a specific group of students. Unlike the other portfolios, the keywords were inserted in the papers’ titles, abstracts, or keywords, and six databases were consulted (Scopus, Web of Science, ScienceDirect, PubMed, Emerald, and SciELO). The papers were exported to Mendeley, eliminating duplicates, and then read in full.

After the systematic literature review (bibliometric and content analysis of the papers), an extension project developed at a Brazilian public university was described.

The project, called SOS – UTFPR, was created in August 2017 at the Federal Technological University of Paraná. As of today, the course encompasses theoretical (lectures, simulations, and classroom seminars) and practical classes (monthly training sessions, emergency drills, and technical visits to local companies). The project established partnerships between the university, companies, and public organizations such as the fire brigade, focusing on the Mutual Assistance Plan (PAM) and obeying international standards, according to the World Protocol of Prehospital Care of the American College of Surgeons’ Committee on Trauma (PHTLS) and the American Heart Association (AHA).

The case report on project SOS explores data and information such as the knowledge level of engineering students, the modules included in the project, relevant subjects that are inherent to first aid, and how they are significant for those students, as well as the Brazilian context of first aid teaching and other aspects. The students involved in the case report are participants in the project. They carried out their registrations according to interests on the subject. Therefore, no sampling selection was carried out, as all enrollees were automatically incorporated into the project.

Results and discussion

The numbers of articles entered in each portfolio are presented in Table 1.

Table 1. Number of papers in the literature review

Portfolio 1. "first aid"	
- Scopus	3 232
- Web of Science	775
- ScienceDirect	180
- PubMed	2 834
Total of journal papers	7 021
Duplicate papers removed	2 006
Total of papers	5 015

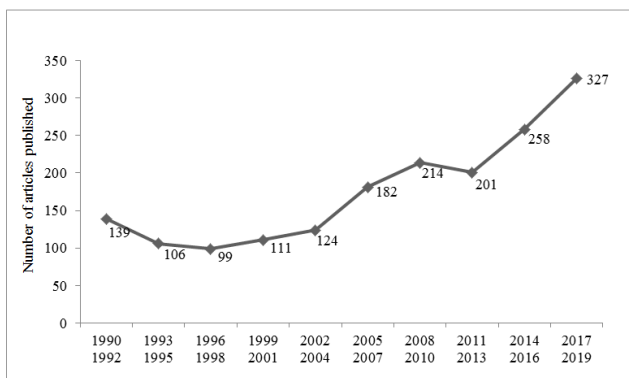
Portfolio 2. "first aid" and teaching	
- Scopus	46
- Web of Science	36
- ScienceDirect	4
- PubMed	22
Total of journal papers	108
Duplicate papers removed	36
Total of papers	72

Portfolio 3. Combination of keywords "first aid" and teaching and (engineering or "university students" or academic)	
- Scopus	6
- Web of Science	0
- ScienceDirect	0
- PubMed	1
- Emerald	0
- SciELO	0
Total of journal papers	7

Source: Authors

Bibliometric analysis: Portfolio 1

A total of 5 015 journal articles was analyzed, which have direct foci in first aid. Their publication over the years is shown in Figure 2.

**Figure 2.** Number of articles published on first aid in general

Source: Authors

The period between 2017 and 2019 presented the largest number of articles published in journals: 327 articles, succeeding 2014-2016 with 258 articles, and 2008-2010 with 214 articles. In an interrupted period from 1927-1989, another 3 216 were indexed in the consulted databases, in addition to years prior to 1927, with records of 38 articles.

The main journals, according to the quantities of published articles on first aid, are listed in Table 2.

Table 2. Main journals of articles on first aid in general

Scientific journal	ISSN	Cite Score (2019)	Impact Factor (2019)	Number of articles
Fel'dsher i akusherka	0014-9772	-	-	272
Sovetskoe zdravookhranenie	0038-5239	-	-	114
Meditsinskaia sestra	0025-8342	-	-	114
Sovetskaia meditsina	0038-5077	-	-	51
Nursing times	0954-7762	-	-	50
Burns Journal	0305-4179	3,6	2,066	48
Zdravookhranenie Rossiiskoi Federatsii	0044-197X	0,1	-	43
Hefte zur Unfallheilkunde	0085-1469	-	-	42
British Medical Journal	1756-1833	6,5	30,233	40
Zeitschrift fur Allgemeinmedizin	1439-9229	0,5	-	39
Minerva Medica	0026-4806	3,7	3,031	37
The Expository Times	1745-5308	-	-	37
Vrachebnoe delo	0049-6804	-	-	34
Occupational Health	1348-9585	3,0	2,289	33
Fortschritte der Medizin	1613-3560	-	-	33
Tijdschrift voor ziekenverpleging	0303-6456	-	-	32
Zeitschrift fur Arztliche Fortbildung	0044-2178	-	-	32
Nursing mirror	0029-6511	-	-	30
Nursing standard	0029-6570	-	-	30
Tidskrift for Sveriges sjukskoterskor	0037-6027	-	-	30
Vestnik khirurgii imeni I. I. Grekova	0042-4625	-	-	30
Occupational Health & Safety	0362-4064	-	-	29
Munchener Medizinische Wochenschrift	1886-1999	-	0,360	29
Nederlands Tijdschrift voor Geneeskunde	1876-8784	0,3	-	29
MMW Fortschritte der Medizin	1613-3560	0,1	-	28
Schwester Revue	0048-9549	-	-	28
Zentralblatt fur Arbeitsmedizin und Arbeitsschutz	2198-0713	1,2	-	27
Resuscitation	0300-9572	6,8	4,215	25
Ugeskrift for laeger	1603-6824	0,1	-	25
Minerva Chirurgica	1827-1626	1,2	0,765	25

Source: Data collected from Scopus, PubMed, Web of Science, and ScienceDirect

The most frequent terms inserted in the portfolio with 5 015 articles are presented in Figure 3.

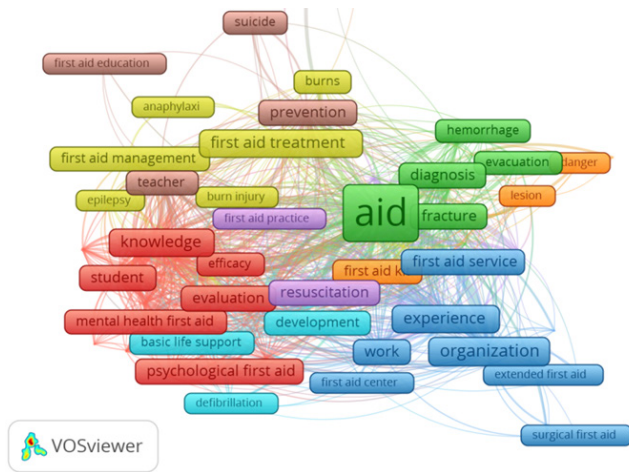


Figure 3. Most frequent terms in published articles on first aid approaches

Source: Authors

Analysis of articles: Portfolios 1 and 2

Velde *et al.* (2006) define first aid as a set of fundamental practices to apply efforts and provide aid until professionals (e.g., doctors) are available for specialized services. According to the authors, it is the immediate assistance given to a sick or injured person, comprising procedures and techniques that require little to no equipment. A first aid provider must be able to assess the situation as fast, albeit adequately, as possible, deal with life-threatening conditions, and contact medical assistance (Abbas *et al.*, 2011).

Lack of knowledge or inadequate training may result in inefficient or even harmful interventions (Velde *et al.*, 2006). In case of adversities, delays in the treatment may entail severe consequences for the patient, so proper knowledge in first aid is useful (Ertl and Christ, 2007).

First aid courses are not limited to the treatment of physical injuries; they also include emotional support and dealing with stress and collective and individual anxiety (Velde *et al.*, 2006). Teaching and learning in first aid are established through lectures, demonstrations, theoretical and practical classes (experiments or drills with dummies or candidates), videos, and formal materials elaborated by experts and competent institutions (Das and Elzubeir, 2009).

Thus, first aid applications seek to reduce suffering, stop the clinical condition of the patient from worsening, prevent deaths, relieve pain, minimize physical and mental damage, and reduce edemas (Cuttle *et al.*, 2009).

The topic of first aid is full of theoretical and practical approaches useful for instructing various audiences, some of which are listed in Table 3.

Some studies have focused on more specific approaches to first aid, highlighting mental health first aid (Hart *et al.*, 2018), drug and alcohol first aid (Allan *et al.*, 2016; Kostadinov *et al.*, 2018), hypothermia and evaluation of clinical symptoms (Pyšný *et al.*, 2015), domestic accidents (Ergenekon, 2012), among others.

To provide knowledge about first aid in general, some modules have been proposed by government institutions. Table 4 describes the modules regulated and addressed by Brazilian institutions.

Table 3. Participants involved in first aid studies

Group	Source
Teenagers at a school	Hart <i>et al.</i> (2018), Walsh <i>et al.</i> (2016).
Physical education students (children and adolescents)	Lago-Ballesteros <i>et al.</i> (2018)
Community	Kostadinov <i>et al.</i> (2018)
University students	Hamid (2018)
Medical students	Jagdish <i>et al.</i> (2005)
Children	Bánfai <i>et al.</i> (2018) Ammirati <i>et al.</i> (2014) Lubrano <i>et al.</i> (2005)
Teachers	Paton <i>et al.</i> (2015)
Trained healthcare professionals	Thomas and Schild (1980)

Source: Authors

In addition to the first aid approaches presented in Table 4, the Brazilian Mobile Emergency Care Service (2002) provides detailed actions and instructions for first aid and prehospital treatment. Their material is in-depth and complete, especially concerning basic occurrences in first aid.

In order to determine whether undergraduate engineering students have knowledge about first aid, a new search was conducted, exploring six different databases. It sought to ascertain whether there were studies related to this matter, but it found that no papers focused on the permanent and continuous teaching of first aid; instead, there were only brief talks on the subject. Table 5 presents the total of papers found via each keyword combination.

Studies on the teaching of first aid and prehospital care in engineering courses, or in higher education at large, are lacking except in fields related to human health, according to the paper analysis (Table 6).

The studies above are lacking in certain aspects. The target public of the instruction was the faculty rather than the students, and the techniques employed were shallow and simple. Moreover, they lacked practical lessons, limiting themselves to tutorial videos and lectures.

Education is a strong tool in the systematic construction and promotion of knowledge and skills in all fields, as well as in creating desired attitudes towards issues of occupational

Table 4. Main modules on first aid

First Aid Manual by the Brazilian Ministry of Health (2003)
1. General basic occurrences
<ul style="list-style-type: none"> - Assessment of the accident location - Victim protection – Safety in the location - Assessment and examination of the victim - Functions, vital signs, and support - Asphyxiation - Cardiopulmonary resuscitation - Transportation of victims - Hemorrhage - Airway obstruction
2. Clinical Emergencies
<ul style="list-style-type: none"> - Acute pulmonary edema - Myocardial infarction - Hypertensive crisis - Renal colic - Diabetic coma (hyperglycemia) - Hyperthermia - Heat stroke - Heat exhaustion - Heat cramps - Diarrhea - Electric shock - Syncope - Mental alterations - Convulsion - Hysterical neurosis - Acute alcoholism
3. Trauma Emergencies
<ul style="list-style-type: none"> - Injuries - Head injuries - Eye injuries - Chest trauma - Abdominal trauma - Soft tissue injuries - Contusions - Abrasions - Crush injuries - Amputations - Burns
4. Poisoning and Intoxication
<ul style="list-style-type: none"> - Drug intoxication - Poisonous plants - Accidents with poisonous and venomous animals
5. Other occurrences
Emergency childbirth Radioactive accidents Rescues
First aid approaches of the Integrated Service of Emergency Trauma Care (2014)
1. Vital signs 2. Airways 3. Cardiopulmonary resuscitation (CPR) 4. Hemorrhage and Shock 5. Injuries and bandages 6. Burns 7. Venomous animals 8. Brown spider 9. Convulsive crisis 10. Injuries caused by electricity 11. Clinical emergencies 12. Materials employed in prehospital treatment

Source: Authors

safety and health (OSH), including the environment, the safety of technical equipment, the optimization of working conditions, and first aid (Bail *et al.*, 2019; Chiroli *et al.*, 2019; Kozík and Bulla, 2013).

Table 5. Number of papers found in each database

Keyword combination	ScienceDirect	Scopus	Web of Science	Emerald	PubMed	SciELO
"Teaching" AND "engineering" AND "first aid"	0 papers	6 papers	0 papers	0 papers	1 paper	0 papers
"Teaching" AND "prehospital care" AND "engineering academics"	0 papers	0 papers	0 papers	0 papers	0 papers	0 papers
"Prehospital care" AND "engineering course" AND "discipline"	0 papers	0 papers	0 papers	0 papers	0 papers	0 papers
"Teaching" AND "prehospital care" AND "university students"	0 papers	0 papers	0 papers	0 papers	0 papers	0 papers
"First aid" AND "engineering academics"	0 papers	0 papers	0 papers	0 papers	0 papers	0 papers
"Discipline" AND "first aid" AND "university academics"	0 papers	0 papers	0 papers	0 papers	0 papers	0 papers
"Primeiros socorros" AND "acadêmicos" AND "engenharia"	0 papers	0 papers	0 papers	0 papers	0 papers	0 papers

Source: Authors

Table 6. Studies about the teaching of first aid to engineering majors

Author	Title of the paper	Focus
Tian (2018)	<i>The Development of Electronic Assembly Technology Course Aided by Video and Flash Courseware and Teaching Effectiveness Verified by Radio Assembly and Shakedown Test</i>	Method for electrical engineering majors comprising the precautions required in working with electric/electronic machinery, magnetic fields, and professionals of the area.
Hamid (2018)	<i>Effectiveness of Structured Teaching Program on Academics' Knowledge about First Aid at University of Baghdad</i>	Experimental study involving two distinct groups of students, each adopting different procedures for first aid programs.
Kureckova (2017)	<i>First aid as an important traffic safety factor – evaluation of the experience-based training</i>	First aid training offered to driver's education students and traffic dispatchers in the Czech Republic.
Pate (2014)	<i>Promoting Safety in High School Supervised Agricultural Experiences: Teachers' Training and Student Injury Experiences</i>	The school provides rural technical training for teenagers. And the teachers were trained in first aid, so that they can assist students in diverse situations, like snake bites, wounds, injuries, among others.
Hubert (2001)	<i>Texas Entry-Year Agriculture Teachers' Perceptions, Practices, and Preparation Regarding Safety and Health in Agricultural Education</i>	Report on the first aid training of agricultural education teachers. The training sessions were theoretical and involved tutorial videos.

Source: Authors

Considering that engineering is a necessary industry to maintain current social standards, maintain infrastructure and advance innovations, knowledge and preparation for first aid situations is important and necessary. Engineers work in a variety of environments where professionals are under different types of pressure (industrial, technical, political, economic, environmental, and financial), which poses many risks.

Knowledge and practices in first aid are necessary for all types of professionals, and, for engineers who work in leadership, this knowledge favors more effective actions. It is important to highlight that, when first aid actions are performed on an accident victim, the worsening of the clinical condition is avoided, and a life can be saved.

Therefore, training professionals on the notions of first aid becomes essential in the work environment and is never in vain, as it is not only at work that this knowledge can be useful; there are risks everywhere, and accidents can occur unexpectedly, regardless of time or place. Therefore, it is always good to be prepared and help save lives (Pergola and Araújo 2008; de Sousa, 2018; Rosa *et al.*, 2001).

In the next subsection, the results of a project developed in a Brazilian public university about teaching first aid practices will be presented.

Case report: first aid project in engineering

Project SOS from UTFPR, Brazil, is an extension mode that comprises 124 hours of theoretical and practical classes about first aid. The project's goal is to provide engineering students with theoretical and practical knowledge about the main first aid techniques, such as acting in emergencies and adversities, the crucial attitudes to be taken, and other basic pertinent matters until the arrival of medical professionals or health experts. After its planning and didactic-pedagogical structuring, the project began and was announced through the institution's social networks. To enroll, the students were required to fill out a questionnaire with basic information (name, age, and academic degree), as well as their level of knowledge about first aid through questions centered on the topic. The questionnaire consisted of a mechanism to understand the participants' profiles.

The project has no limit for enrollments. Although it was an unprecedented project in Brazil, students enrolled according to their level of interest in the subject.

In the first edition, from August 2017 to July 2018, a total of 61 students enrolled in the project. Most of the students (70%) were between 19 and 25 years old, followed by freshmen aged 18 or younger (21,70%). Only 8,30% of the students were over 25 years old.

Out of 61 enrolled students, 45 answered the questionnaire and applied before the project started. It contained ten basic questions regarding the central modules of first aid, with the

purpose of assessing the knowledge level of the participants in terms of the course modules, which are presented in Figure 4.

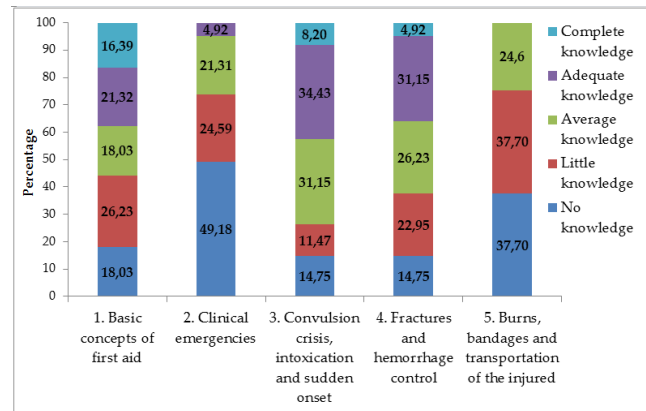


Figure 4. Students' level of knowledge on first aid in the first edition of project

Source: Authors

In the second edition, from August 2018 to July 2019, a total of 77 students enrolled in SOS – UTFPR. Most of them (70%) were between 19 and 25 years old.

Out of the 77 enrolled students, 61 answered the questionnaires and applied before the project started. It contained ten basic questions regarding the central modules of first aid, with the purpose of assessing the knowledge level of the participants (Figure 5).

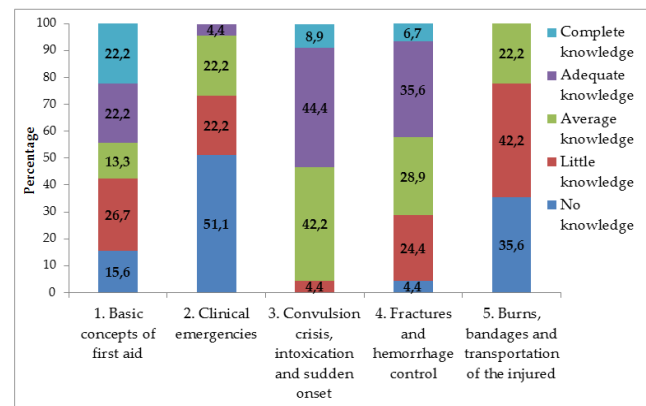


Figure 5. Students' level of knowledge on first aid in the second edition of project

Source: Authors

Figures 4 and 5 show that the initial assessment sought to ascertain the students' intrinsic knowledge about the subject, judging whether their answers adequately met the guidelines of the world protocol of prehospital care (PHTLS). The questionnaire also found that the students had the least knowledge about the modules involving clinical emergencies and burns, bandages, and transportation.

In addition to engineering courses, the project included two other UTFPR courses: biology and natural sciences; as well as the technological courses. Therefore, all courses available

at the Ponta Grossa, Brazil, campus of UTFPR participated in the SOS project. This included the following programs: Chemical Engineering (15 and 21 students, in the first and second edition, respectively); Mechanical Engineering (11 and 14 students); Production Engineering (8 students in both editions); Electronic Engineering (8 students in both editions); Biotechnology Engineering (5 students in both editions); Computer Engineering (3 and 5 students, respectively); Natural Sciences (3 and 4 students); Biological Sciences (3 students in both editions); Food Technology (2 students in both editions); and three other technological courses with one student each, resulting in 138 total participants.

In Table 7, a simplification of student data and information is presented.

Table 7. Simplification of the main data and information on the students

Project edition 1	Project edition 2
61 participating students	77 participating students
45 students returned the questionnaire	61 students returned the questionnaire,
Most of them (70%) were between 19 and 25 years old.	
Engineering courses with higher numbers of project participants	
- Chemical Engineering (15 students) - Mechanical Engineering (11 students) - Production Engineering (8 students)	- Chemical Engineering (21 students) - Mechanical Engineering (14 students) - Production Engineering (8 students)
Predominance of results; analysis of students' knowledge about first aid	
No knowledge related to the following modules: - Clinical Emergencies: 51,1% of students - Burns, Bandages, and Transportation of the Injured: 35,6% of students - Basic Concepts of First Aid: 15,60% of students	No knowledge related to the following modules: - Clinical Emergencies: 47,54% of students - Burns, Bandages, and Transportation of the Injured: 37,7% of students - Basic Concepts of First Aid: 18,03 % of students

Source: Authors

The project featured the participation of 138 students (for two editions) in lectures, workshops, drills of natural disasters and accidents, external training with the Fire Department (Brazilian institution trained in first aid, rescue, and fires), seminars, congresses, events, recreation locations, and inserting the students into the Higher Education Institutions of the region, acting as active participants and extras (victims and simulation voluntaries). This first aid training included members of the PAM (Fire Department, employees of 47 participant companies, and hospital staff). The students acted as victims, thus deepening their knowledge.

The didactic and pedagogic materials were provided for the participants, so that they were able to solve their doubts and practice aid and rescue techniques. The students could also exchange countless experiences with collaborators from several companies, observing aspects of health and work safety, as well as how to act in prevention and cases of emergency.

Each complete edition of the project was conducted over 12 months, with theoretical-practical classes that took place on one Saturday every month (8 hours). The classes featured instructors specialized in the field of aid and rescue. It encompassed the following topics:

- Basic concepts of human anatomy and physiology;
- On-site security (the student's, the victim's and other people's);
- Primary approach:
 - A- Airway (cervical control with identification);
 - B- Breathing (seeing, hearing, and feeling);
 - C - Circulation and bleeding control;
 - D - Disability - neurological state and/or level of consciousness;
- Cardiopulmonary resuscitation (CPR), use of automated external defibrillator (AED);
- Secondary approach, immobilizations, and transportation;
- Clinical emergency (adult and pediatric);
- Convulsion crisis, intoxication, and sudden onset;
- Fractures, hemorrhage control;
- Burns, bandages, and transportation of the injured;
- Firefighting and basic notions of Fire Brigade;
- Evacuation plan and escape routes;
- Emergency drills.

The knowledge of the student group evolved gradually, developing over months of theoretical and practical classes, tests, simulated, emergency drills, and joint participation with the companies belonging to the PAM, which have appreciated the initiative and have been providing the students from the project with opportunities, first hiring them as interns and then as collaborators. Although knowledge was not measured through questionnaires, advances were measured in practical classes and interviews with company representatives, where student activities took place.

The first positive report about project SOS – UTFPR came from a few of the participant companies, which stated that the students would be able to work in the industry at the end of one year of training because they acquired not only industry knowledge, but also complementary skills concerning health and safety. The students thus became much more competitive in the job market, as shown by the hiring of several of them by the leading multinationals of the city. Moreover, the project also included approaches to natural disasters, often observed in developed and developing countries.

Secondly, the project students worked jointly with graduate students in occupational safety engineering, stimulating the exchange of experiences with professional engineers who are already part of the job market. Simulations were carried out to stimulate joint work in creating mock-ups and possible accident victims, as close as possible to injuries and trauma. They enabled the care provided to the victims to have a high quality, agility, and dexterity, minimizing major impacts on life.

Conclusions

The teaching of first aid in developed countries takes place since childhood, as it is part of the school curriculum. In this way, the individual fully learns how to act in emergency situations, whatever their nature, knowing the exact steps to be followed until the arrival of specialized help, attempting to mitigate risks that may involve an individual in the event of an accident, and striving to save lives. In Brazil, this teaching is not yet part of the curricula, even within universities, as is the case of engineering programs, so it is essential to include these studies in the academic life of everyone.

This study pointed out that there are few works that address the teaching of first aid for students in higher education courses, especially those in engineering. In Brazil, this training is still not seen as a priority in all spheres of education, unlike from developed countries, which have priority in their school grids and propose this education and training from childhood.

The key points of the practices offered by the SOS – UTFPR project addressed, the following contents in the course modules: first aid concepts, calling for specialized care, on-site safety, injury mechanism, primary and secondary approach, bleeding control, cardiopulmonary resuscitation, clinical emergencies, convulsions, intoxications, injuries, fractures, burns, immobilizations, and transport of victims.

Therefore, it was possible to observe that engineering students receive the necessary technical training to fulfill their professional duties, but they lack certain basic first aid concepts. The SOS – UTFPR project has revealed that it is possible to prepare and train them in this regard, albeit more succinctly than a nursing major, for example, without discarding the basic, fundamental approaches.

Basic knowledge of the risks, their consequences, and their management is essential in the care of victims, as well as for people who are injured or in need of assistance or guidance. This paper is relevant in this sense, pointing out the need to expand first aid teaching in higher education in general. Even further, it showed that higher education programs generally lack studies on the subject, with the exception of medicine and nursing.

This study refers to future work when it focuses on the importance of teaching first aid to an entire society, seeking

to train citizens who are able to take corrective decisions in cases of emergency, as is already the case in developed countries, and training individuals who multiply information, who know how to act to safeguard lives, inside and outside the workplace, teaching, or elsewhere. Such knowledge can no longer be aimed only at health professionals, but at the entire academic community and students in general. It has become an integral part of school curricula in Brazil and other developing countries.

References

- Abbas, A., Bukhari, S. I., and Ahmad, F. (2011). Knowledge of first aid and basic life support amongst medical students: a comparison between trained and un-trained students. *The Journal of the Pakistan Medical Association*, 61(6), 613-616. <https://pubmed.ncbi.nlm.nih.gov/22204227/>
- Allan, J., Roche, A., Pidd, K., McEntee, A., and Kostadinov, V. (2016). Can you teach alcohol and drug first aid? *Drug And Alcohol Review*, 35, 23-23. <http://onlinelibrary.wiley.com/doi/10.1111/dar.2016.35.issue-S1/issuetoc>
- Alli, B. O. (2008). *Fundamental principles of occupational health and safety*. International Labour Organization. https://www.ilo.org/global/publications/ilo-bookstore/order-online/books/WCMS_093550/lang--en/index.htm
- Ammirati, C., Gagnayre, R., Amsellem, C., Némitz, B., and Gignon, M. (2014). Are schoolteachers able to teach first aid to children younger than 6 years? A comparative study. *BMJ open*, 4(9), 005848. <https://doi.org/10.1136/bmjopen-2014-005848>
- Azhar, S. and Choudhry, R. M. (2016). Capacity building in construction health and safety research, education, and practice in Pakistan. *Built Environment Project and Asset Management*, 6(1), 92-105. <https://doi.org/10.1108/BE-PAM-09-2014-0044>
- Bail, R. F., Kovalski, J. L., Chirolí, D. M. G., and Silva, V. L. (2019). Knowledge transfer and teaching of First Aid and Prehospital Care in the Engineering Courses. *Revista Eletrônica Científica Ensino Interdisciplinar*, 5(15), 489-500. <https://doi.org/10.21920/recei72019515489500>
- Bail, R. F. (2019). *Identification of the anthropotechnological aspects in the mutual assistance plan (MAP)* [Master's thesis, Federal University of Technology, Paraná]. <https://repositorio.utfpr.edu.br/jspui/handle/1/3991>
- Bail, R. F., Kovalski, J. L., Silva, V. L., Pagani, R. N., and Chirolí, D. M. G. (2020). Internet of Things in disaster management: technologies and uses. *Environmental Hazards*, 1867493. <https://doi.org/10.1080/17477891.2020.1867493>
- Bánfai, B., Deutsch, K., Pandur, A., Bánfai-Csonka, H., and Betlehem, J. (2018). Preliminary results of teaching first aid to 5-6 year old children – a longitudinal study. *Kontakt*, 20(2), e120-e125. <https://doi.org/10.1016/j.kontakt.2018.03.003>
- Brazilian Ministry of Health (2003). *Manual de Primeiros Socorros*. Fundação Oswaldo Cruz. <http://www.fiocruz.br/biosseguranca/Bis/manuais/biosseguranca/manualdeprimeirosocorros.pdf>
- Chirolí, D. M. D. G., Rodrigues, H. F., and Mayerle, S. F. (2016). Problemas de programação e roteamento de caminhões com restrições de horários de motoristas: Um estudo da

- produção científica. *Espacios*, 37(4), 1. <https://www.revista-espacios.com/a16v37n04/16370418.html>
- Chiroli, D. M. G., Baú, A. C., Deschamps, F., Sakakibara, E., and Christóforo, L. C. (2019). Work safety management applied to a lab used by a junior company of chemical engineering. *Independent Journal of Management & Production*, 10(1), 281-300. <https://doi.org/10.14807/ijmp.v10i1.787>
- Corsi, A., Barboza, B. M. L., Pagani, R. N., De Genaro Chiroli, D. M., & Kovaleski, J. L. (2021). Technology transfer oriented to sustainable development: Barriers and opportunities. *Journal of Information & Knowledge Management*, 20(02), 2150015. <https://doi.org/10.1142/S0219649221500155>
- Cuttle, L., Pearn, J., McMillan, J. R., and Kimble, R. M. (2009). A review of first aid treatments for burn injuries. *Burns*, 35(6), 768-775. <https://doi.org/10.1016/j.burns.2008.10.011>
- Das, M. and Elzubeir, M. (2009). First aid and basic life support skills training early in the medical curriculum: curriculum issues, outcomes, and confidence of students. *Teaching and Learning in Medicine*, 13(4), 240-246. https://doi.org/10.1207/S15328015TLM1304_05
- Eiser, J. R., Bostrom, A., Burton, I., Johnston, D. M., McClure, J., Paton, D., Pligt, J., and White, M. P. (2012). Risk interpretation and action: A conceptual framework for responses to natural hazards. *International Journal of Disaster Risk Reduction*, 1, 5-16. <https://doi.org/10.1016/j.ijdr.2012.05.002>
- Emergency Mobile Care Service. (2002). *Life support protocol*. <http://bvsm.sau.gov.br/>
- Engeland, A., Røysamb, E., Smedslund, G., and Sjøgaard, A. J. (2002). Effects of first-aid training in junior high schools. *Injury Control and Safety Promotion*, 9(2), 99-106. <https://doi.org/10.1076/icsp.9.2.99.8702>
- Ergenekon, Y. (2012). Teaching basic first-aid skills against home accidents to children with autism through video modeling. *Educational Sciences: Theory and Practice*, 12(4), 2759-2766. <https://eric.ed.gov/?id=EJ1002874>
- Ertl, L. and Christ, F. (2007). Significant improvement of the quality of bystander first aid using an expert system with a mobile multimedia device. *Resuscitation*, 74(2), 286-295. <https://doi.org/10.1016/j.resuscitation.2007.01.006>
- Hamid, H. J. (2018). Effectiveness of structured teaching Program on students' knowledge about first aid at university of Baghdad. *Indian Journal of Public Health Research & Development*, 9(8), 1364-1370. <https://doi.org/10.5958/0976-5506.2018.00921.X>
- Hart, L. M., Cox, G. R., and Lees, L. (2018). Teaching mental health first aid in the school setting: A novel approach to improving outcomes for common adolescent mental disorders. *Current Opinion in Pediatrics*, 30(4), 478-482. <https://doi.org/10.1097/MOP.0000000000000639>
- Hubert D. J., Ullrich, D. R., Murphy, T. H., and Lindner, J. R. (2001). Texas entry-year agriculture teachers' perceptions, practices, and preparation regarding safety and health in agricultural education. *Journal of Agricultural Safety and Health*, 7(3), 143-53. <https://doi.org/10.13031/2013.5440>
- Integrated Trauma Emergency Service. (2012). *Teaching materials*. <http://www.bombeiros.pr.gov.br>
- Jagdish, S., Kadambari, D., Pai, D., Kundra, P., Nalini, P., and Swaminathan, R. P. (2005). First aid teaching for undergraduate medical students. *Medical Teacher*, 27(7), 658. <https://pubmed.ncbi.nlm.nih.gov/16374927/>
- Khan, A., Shaikh, S., Shuaib, F., Sattar, A., Samani, S. A., Shabbir, Q., and Rasheed, A. Z. (2010). Knowledge attitude and practices of undergraduate students regarding first aid measures. *Journal of the Pakistan Medical Association*, 60(1), 68. <https://pubmed.ncbi.nlm.nih.gov/20055288/>
- Kostadinov, V. R., Roche, A. M., McEntee, A., Allan, J. M., Meumann, N. R., and McLaughlin, L. L. (2018). Brief workshops to teach drug and alcohol first aid: A pilot evaluation study. *Drug and Alcohol Review*, 37(1), 23-27. <https://pubmed.ncbi.nlm.nih.gov/29345083/>
- Kozík, T. and Bulla, R. (2013). Aktualny stan prawny dotyczący ochrony pracy w Republice Słowackiej w kształceniu i przygotowaniu zawodowym pracowników. *Problemy Profesjologii*, 2, 193-206. https://bazhum.muzhp.pl/media/files/Problemy_Profesjologii/Problemy_Profesjologii-r2013-t-n2/Problemy_Profesjologii-r2013-t-n2-s193-216/Problemy_Profesjologii-r2013-t-n2-s193-216.pdf
- Kureckova, Veronika, Gabrhel, V., Zamecnik, P., Rezac, P., Zaoral, A., and Hobl, J. (2017). First aid as an important traffic safety factor evaluation of the experience-based training. *European Transport Research Review*, 9, 1-5. <https://doi.org/10.1007/s12544-016-0218-4>
- Lago-Ballesteros, J., Basanta-Camino, S., and Navarro-Patón, R. (2018). First aid teaching in physical education: a systematic review about the materials for its implementation. *Retos - Nuevas Tendencias en Educación Física, Deporte y Recreación*, 2018(34), 349-355. <https://doi.org/10.47197/retos.v0i34.65683>
- Leiva, C. A., Seda, J. M., Prado, M. C., and Sottoriva, P. R. S. (2014). *Atendimento de saúde a múltiplas vítimas e em catástrofes*. SAMU Brasil.
- Lubrano, R., Romero, S., Scoppi, P., Cocchi, G., Baroncini, S., Elli, M., and Cristaldi, S. (2005). How to become an under 11 rescuer: a practical method to teach first aid to primary schoolchildren. *Resuscitation*, 64(3), 303-307. <https://doi.org/10.1016/j.resuscitation.2004.09.004>
- McKenna, S. P. and Hale, A. R. (1981). The effect of emergency first aid training on the incidence of accidents in factories. *Journal of Occupational Accidents*, 3(2), 101-114. [https://doi.org/10.1016/0376-6349\(81\)90003-1](https://doi.org/10.1016/0376-6349(81)90003-1)
- Moura, E., Cruz, B. T., and Chiroli, D. M. G. (2020). A framework proposal to integrate humanitarian logistics practices, disaster management and disaster mutual assistance: A Brazilian case. *Safety Science*, 132, 104965. <https://doi.org/10.1016/j.ssci.2020.104965>
- Navarro-Patón, R., Arufe-Giraldez, V., and Basanta-Camino, S. (2015). Descriptive research about first aid teaching by physical education teachers in Elementary School. *Sportis - Scientific Technical Journal of School Sport Physical, Education, and Psychomotricity*, 1(1), 35-52. https://minerva.usc.es/xmlui/bitstream/handle/10347/22087/2015_sportis_navarro-descriptive_research_english.pdf?sequence=2&isAllowed=y
- Pagani, R. N., Kovaleski, J. L., and Resende, L. M. (2015). Methodi ordinatio®: a proposed methodology to select and rank relevant scientific papers encompassing the impact factor, number of citation, and year of publication. *Scientometrics*, 105(3), 2109-2135. <https://doi.org/10.1007/s11192-015-1744-x>

- Pagani, R. N., Ramond, B., Da Silva, V. L., Zammar, G., and Kovalski, J. L. (2019). Key factors in university-to-university knowledge and technology transfer on international student mobility. *Knowledge Management Research & Practice*, 18(4), 405-423. <https://doi.org/10.1080/14778238.2019.1678415>
- Pate, M. L. and Lawver, R. G. (2014). Promoting safety in high school supervised agricultural experiences: Teachers' Training and Student Injury Experiences. *American Society of Agricultural and Biological Engineers*, 141901562. <https://elibrary.asabe.org/abstract.asp?aid=44459>
- Pergola, A. M. and Araújo, I. E. M. (2008). O leigo em situação de emergência. *Revista da Escola de Enfermagem da USP*, 42(4), 769-776. <https://doi.org/10.1590/S0080-6234200800040002>
- Pyšný, L., Petrů, D., and Pyšná, J. (2015). Selected Aspects of The first aid during teaching of physical education and sport in winter activities. *Procedia - Social and Behavioral Sciences*, 186, 815-819. <https://doi.org/10.1016/j.sbspro.2015.04.040>
- Rosa, D. D. O., Bérnago, N. M., and Dorini, S. R. (2001). *Organização de primeiros socorros na empresa*. Fundação de Apoio à Pesquisa e Extensão Universitária.
- Silva, V. L. Kovalski, V. L., Pagani, R. N., Silva, J. M., and Corsi, A. (2020). Implementation of Industry 4.0 concept in companies: empirical evidences. *International Journal of Computer Integrated Manufacturing*, 33(4), 325-342. <https://doi.org/10.1080/0951192X.2019.1699258>
- Silva, V. L. Kovalski, V. L., and Pagani, R. N. (2021). Fundamental elements in technology transfer: An in-depth analysis. *Technology Analysis & Strategic Management*, 1894328. <https://doi.org/10.1080/09537325.2021.1894328>
- Soares, A. M., Kovalski, J. L., Gaia, S., and Chiroli, D. M. de G. (2020). Building sustainable development through technology transfer offices: An approach based on levels of maturity. *Sustainability*, 12(5), 1795. <https://doi.org/10.3390/su12051795>
- De Sousa, L. M. M. (2018). *Primeiros Socorros-Conduas Técnicas*. Saraiva Educação SA.
- Thomas, P. and Schild, M. (1980). First aid: Teaching the teacher. *Occupational Health; a Journal for Occupational Health Nurses*, 32(10), 532. <https://pubmed.ncbi.nlm.nih.gov/6904923/>
- Tian, Y., Wu, Y., and Zhu, H. (2018). The development of electronic assembly technology course aided by video and flash courseware and teaching effectiveness verified by radio assembly and shakedown test. *Proceedings of the International Conference on Digital Technology in Education, Thailand, 2018*, 41-48. <https://doi.org/10.1145/3284497.3284510>
- Velde, V. S., Broos, P., van Bouwelen, M., De Win, R., Sermon, A., Verduyck, J., and van den Steene, P. (2006). European first aid guidelines. *Resuscitation*, 72(2), 240-251. <https://doi.org/10.1016/j.resuscitation.2006.10.023>
- Veronese, A. M. and Oliveira, D. L. L. C. (2006). The risks of traffic accidents from the perspective of motorcycle boys: subsidies for health promotion. *Cadernos de Saúde Pública*, 22(12), 2717-2721. <https://doi.org/10.1590/S0102-311X2006001200021>
- Walsh, K., Hili, S., and Dheansa, B. (2016). Compulsory teaching of first aid in UK schools-A missed opportunity? *Burns*, 42(4), 946-947. <https://doi.org/10.1016/j.burns.2015.12.002>

Typifying Students' Help-Seeking Behavior in an Intelligent Tutoring System for Mathematics

Tipificación de comportamientos de estudiantes relacionados con la búsqueda de ayuda en un sistema inteligente de tutorías para matemáticas

Roberto A. Meléndez-Armenta¹, Genaro Rebolledo-Méndez², and N. Sofía Huerta-Pacheco³

ABSTRACT

The use of tutoring systems has become normalized in secondary schools (grades 7-9) in many parts of the world. There have been studies analyzing the students' behavior, their affective responses, or the abuse of the system, but little has been done to discover other types of behavior. This paper presents evidence that there are different types of help-seeking behavior which can be typified in Mexican students interacting with the Scooter intelligent tutoring system (ITS), which was designed to teach mathematics at secondary-level. The implemented methodology consisted of applying discovery algorithms and data mining to typify students in terms of their help-seeking behaviors. The results and contributions of this work suggest that gaming the system with the aforementioned ITS may not always be useful. Future work will analyze other student groups who have used this software in other parts of the world to correlate these typologies to students' traits or opinions about mathematics and learning.

Keywords: educational technology, educational innovation, mining sequence data, intelligent tutoring system, behavioral education

RESUMEN

En muchas partes del mundo se ha normalizado el uso de sistemas de tutoría en las escuelas de secundaria (grados 7 a 9). Se han realizado estudios que analizan el comportamiento de los estudiantes, sus respuestas afectivas o el abuso del sistema, pero se ha hecho poco para descubrir otros tipos de comportamiento. Este artículo presenta evidencia de que existen diferentes tipos de comportamiento de búsqueda y solicitud de ayuda, los cuales pueden tipificarse en estudiantes que interactúan con el sistema tutor inteligente (STI) Scooter, diseñado para enseñar matemáticas a estudiantes de secundaria. La metodología implementada consistió en aplicar algoritmos de descubrimiento y minería de datos para tipificar a los estudiantes en términos de sus comportamientos de búsqueda de ayuda. Los resultados y las contribuciones de este trabajo sugieren que "jugar con el sistema" del STI ya mencionado no siempre es útil. El trabajo futuro analizará otros conjuntos de estudiantes que han utilizado el tutor inteligente en otras partes del mundo para correlacionar estas tipologías con los rasgos u opiniones de los estudiantes sobre las matemáticas y el aprendizaje.

Palabras clave: tecnología educativa, innovación educativa, secuencia de datos, sistema tutor inteligente, educación conductual

Received: January 9th, 2020

Accepted: July 30th, 2021

Introduction

Nowadays, educational tools based on artificial intelligence (AI) can collect a great number of data points without the need for human intervention. These data points include a compilation of test results, performance indicators, teachers' opinions, comments, and even students' behaviors

and learning. The identification of patterns in data can be a complicated task, as behavior is frequently associated to performance and is estimated by how capable the student is or will be to achieve a specific task, reach a specific learning goal, or respond adequately to a particular learning situation (Peña-Ayala, 2014). In this article, a student's ability (described as p-know) is defined as the number of correct actions that are carried out within the educational tool. Correct actions are associated with the probability that a student knows the involved ability in a determined action, which is obtained using the Bayesian knowledge tracing algorithm (Corbett, 1997).

¹ PhD in Computer Sciences, Universidad Veracruzana, México. Affiliation: Research Professor, División de Estudios de Posgrado e Investigación, Tecnológico Nacional de México/Instituto Tecnológico Superior de Mianla, México. E-mail: ramelendeza@itsm.edu.mx

² PhD in Computer Science and Artificial Intelligence, University of Sussex, England. Affiliation: Professor of Research, Writing Lab, Institute for the Future of Education, Vicerrectoría de Investigación y Transferencia de Tecnología, Tecnológico de Monterrey, Mexico. E-mail: g.rebolledo@tec.mx

³ PhD in Computer Sciences, Universidad Veracruzana, México. Affiliation: Research Professor, Consejo Nacional de Ciencia y Tecnología - Ciencia Forense, Facultad de Medicina, Universidad Nacional Autónoma de México, Mexico. E-mail: nshuerta@cienciaforense.facmed.unam.mx

How to cite: Meléndez-Armenta, R. A., Rebolledo-Méndez, G., and Huerta-Pacheco, N. S. (2022). Typifying Students' Help-Seeking Behavior in an Intelligent Tutoring System for Mathematics. *Ingeniería e Investigación*, 42(2), e84495. <http://doi.org/10.15446/ing.investig.v42n2.84495>



Attribution 4.0 International (CC BY 4.0) Share - Adapt

The variety of technological tools applied to learning is wide, and they comprise the understanding of the content they convey and the objectives students achieve. There are research studies that analyze student behavior in different types of activities in educational environments, with the purpose of detecting specific interaction patterns (Juhaňák *et al.*, 2019). The diversity of uses for technological tools in learning suggests that there is value in analyzing registers of user interactions (Apaolaza and Vigo, 2019). The ASSISTment on-line intelligent tutor provides a tool that facilitates the development of tutors based on rules called CTAT (Cognitive Tutor Authoring Tools). CTAT initially asks authors for behavior examples to solve problems, which are used by the tutor to help students learn a determined domain. Taking ASSISTment (Pardos and Heffernan, 2001) as a basis, our study aims to develop a model that could predict if a student's achievement is associated to help-seeking behavior.

In the field, there is evidence that students who request help from the system are not always the ones that have correct actions associated to their learning (Tabandeh and Sami, 2010). However, it has been observed that the use of help can be harmful for learning. Help-seeking in tutoring systems has been associated with students whose main objective is to finish the activity at hand and not to acquire knowledge. This phenomenon has been called 'gaming the system' (Baker *et al.*, 2004). This behavior leads to looking for correct answers and to continue making progress in the system rather than learning from the experience. One of the most important findings in this research is that students who frequently game the system have significantly lower scores than the students who never do.

Most educational tools generate interaction files (log files) which store data points that could lead to the analysis of behaviors when solving specific activities. Analyzing this information is important since data mining could lead to new findings in educational research. The aim of educational data mining is to identify patterns in the data, including frequent elements, frequent subsequences, and frequent substructures (Baker and Inventado, 2014). There are several data mining techniques for the identification of patterns in data that come from educational settings, which generate associative, predictive, and even behavioral models (Falakmasir and Habibi, 2010; Jovanovic *et al.*, 2012). These models have allowed education institutions to make decisions towards improving the student's educational experiences and their learning. The objectives of this research are: 1) to typify student behaviors when interacting with intelligent tutors for mathematics and 2) to associate the identified typologies with help-seeking and achievement. The overall aim is to present an outlook of user behaviors, so that further personalization through scaffolding can be defined in newer versions of the system. The hypotheses that guide this research are:

- H1: There are typologies for help-seeking students with the intelligent tutor.

- H2: Students with different typologies have significant differences regarding the actions they perform with help, success, failure, and by gaming the system.

Related works

The literature review is dedicated to the processing of data generated by the interaction between students and an Intelligent Tutor System (ITS), which reflects the decisions made by the students when solving the problems presented in the system. In this context, the research presented by D'Aniello *et al.* (2016) focuses on awareness learning, allowing students to understand the concepts they acquire during their daily activities. The authors propose an approach to situational awareness based on Endsley's model, which employs conceptualization of the learning environment through concept maps.

Afterwards, Lara-Muñoz *et al.* (2019) found that students who work collaboratively when using an ITS can gain learning from their social environment. This means that students learn from the interaction with fellow learners when performing a collaborative activity. Additionally, the results show that students with the same learning style have significant learning gains once they have found the most suitable groups in a collaborative activity, in contrast to those who worked with partners with different learning styles.

In the same way, but with a focus on individual student performance, Rebollo-Méndez *et al.* (2021) analyzed students' meta-affective capacity in learning and how it influences the knowledge acquisition process. This research presents typologies that study the relationship between meta-affect, students' knowledge, and their affective transitions during the use of an intelligent tutor system for mathematics. The results demonstrate that having a meta-affective ability is positively associated with students' learning during ITS use.

Moreover, Padayachee (2002) identified that ITSs have several generic characteristics and behaviors related to specific architectural components that can affect the learning process: 1) domain model, 2) tutor model, 3) learner model, and 4) user interface. In this sense, Chang *et al.* (2020) presented a semantic web-based approach for obtaining pedagogical rules for the tutor module component, which can be integrated with other models in an ITS. The authors build ontology-based tutor models that will allow future ITSs to implement strategies for generating and managing predetermined rules and actions.

Additionally, help-seeking is studied, which is an important process in an ITS, as it is a recurring activity of students when they use technological tools, and it has been proven that appropriate help-seeking behavior can positively influence student learning gain (Tai *et al.*, 2016).

Help-seeking influences students' learning when interacting with ITS because intelligent tutor systems often provide answers to students' requests. The interaction between metacognitive skills and cognitive factors is important for help-seeking, according to the work by Aleven *et al.* (2003). The authors conclude that help-seeking skills are fundamental for learners, enabling them to face new learning objectives. In addition, some researchers have suggested that meta-cognitive feedback on help-seeking behavior is related to acquiring better learning skills (Roll *et al.*, 2011).

In another line of research, Vaessen *et al.* (2013) presented a list of help-seeking strategies that students used in an ITS, as well as the relationship between the use of these strategies and performance goals. Based on his results, Aleven (2013) argued that feedback on help-seeking helped students to use help more deliberately, even after feedback was no longer provided, considering that the goal of helping students is one of the big challenges in ITS research. Besides, it is important to address social motivational and meta-cognitive aspects, as they may influence help-seeking (Aleven *et al.*, 2016).

It is important to note that help-seeking in ITS is not a new issue, but, so far, these approaches have not presented evidence of data processing from the log files (student performance) resulting from the interaction between students and the ITS. In this research, the log files were used to typify students' help-seeking behavior.

Method

Participants

The participants in this study were secondary school students from Escuela Federal No. 2 Julio Zárata, in the city of Xalapa, Veracruz, México. The evaluation was carried out during the 2016-2017 school year with selected students from the morning shift population (N=132). The selection of students followed a random sampling that considered a 95% trust level and an acceptable maximum error of 6.5%, providing a final sample size (n=50). The school administration office gave its approval to carry out this study, and neither personal nor sensitive data were collected from the students.

Materials

The materials used in the experimental design included ITSs as a technological tool and the TraMineR package (Gabadinho *et al.*, 2011) in the R programming language. The Scooter intelligent tutoring system is an interactive software developed by Baker *et al.* (2004), which combines teaching given by a teacher with problems that each student has to solve. These problems are presented as different practice exercises in the learning of types of variables (categorical and numerical) and their graphic representation. Scooter has two working modalities: 1) reactive, in which the tutor reacts to gaming the system instances; and 2) non-reactive, where the tutor is not shown to the student, so that it does

not interfere in the learning process. Scooter clearly specifies the objectives that each student must reach, knows the students' needs, and can correct the student immediately when they make a mistake. The TraMineR R packages are used to extract, describe, and visualize states or event sequences. This package allows managing longitudinal data, tracing sequences, removing subsequences of frequent events, and associating found subsequences by means of rules (Gabadinho *et al.*, 2011)

Phases

The experimental design phases included activities such as collecting the information based on the students' interaction logs with Scooter when doing an exercise. This included dispersion, selection, cleaning, information transformation, and, finally, data mining algorithms for the typification of students:

1. Phase 1- Interaction: During this stage, the students interacted with Scooter in a research scenario, where the participants worked with the tutor for 20 minutes. Each student was assigned a computer so that they could work at their own pace. This took place in the school's media room, and the exercises were of the following type:

"Samanta is trying to find out what brand of dog food her pet likes best. Each day, she feeds it a different brand and checks how many bowls it eats, but then her mother says that maybe her dog only eats more on the days it does more exercise. Please, draw a dispersion diagram to show how many bowls the dog eats depending on the level of exercise it does that day".

2. Phase 2 – Cleaning and integration: In this stage, the interaction logs are analyzed, the data is cleaned, and it is integrated in a csv file. The interaction logs show the actions students do with Scooter, for example, if they answer a question correctly (or not), if they ask for help, the time they take to do a scenario, among others. The number of requests per student varies depending on the number of times he or she interacts with the tutor when solving an exercise. These data are stored based on a time sequence. The interaction logs contain too much information related to student performance in the ITS.
3. Phase 3 – Selection and transformation: The objective of this research is to use the students' interaction logs in a non-reactive way, specifically when they solve graphic representation exercises (SPLOT). In this type of exercises, Scooter asks the students to identify the dependent and independent variables in a Cartesian plane, as well as the relations between them. It is important to mention that the main variable of the research is the learning probability (p-know). Additionally, in this stage, the data has to be transformed into categorical variables in order to typify the students based on the cases.

4. Phase 4 – Data mining: Once the data are collected, cleaned, transformed, and integrated in a csv file, the patterns of interest to the research are extracted by means of the implementation of data mining algorithms. This stage consists of two activities: 1) grouping each of the instances by assigning them a label (category), and 2) identifying the typologies associated with each type of student.

Results

Based on the interactions between the students and Scooter, 50 interaction logs were obtained. In each file, approximately 31 characteristics were identified per interaction with the intelligent tutor. The main characteristic identified was the p-know value, which expresses a student's probability to learn when doing an activity. p-know is assigned within an interval of $[-1, 1]$ where the value of -1 means that a student performed an incorrect action (WRONG), 0 means that the student did not learn from his/her last interaction, and, finally, 1 means that the student performed a correct action (RIGHT). This research uses the p-know value, the main input variable, as a means to apply the data mining technique. The interaction sequences were defined as follows:

- Each register in the knowledge base consists of 20 attributes that correspond to one minute of interaction, thus resulting in 20 minutes for each sequence.
- The defined group of labels in each sequence is: positive, negative, and neutral.
- The p-know value was registered in one-minute periods, defining the state as positive (if the majority of p-know is positive), negative (if the majority of p-know is negative), or neutral (in case they have the same number of frequencies per tendency).

To typify the interaction behavior sequences, a clustering exercise using the Ward method was followed. As a result of the grouping implementation, four typologies were identified. These typologies are related to the p-know value of the actions the students made when interacting with Scooter. Once the most representative groups were identified, the sequence analysis technique provided by TraMineR was used to typify the students' interaction behaviors. Figure 1 shows the sequences associated to the student behavior clusters (typologies) according to p-know when interacting with the intelligent tutor.

Table 1 shows the breakdown of the proportions of associated actions per typology. Each one receives a name according to the students' predominant actions. To define the identified clusters or typologies, the following variables related to interaction were used: help-seeking, success, failure, and the system abuse shown during the interaction. Figure 2 shows the most representative sequences per each one of the typologies, which are categorized as good performance, average performance, hardworking, and poor performance.

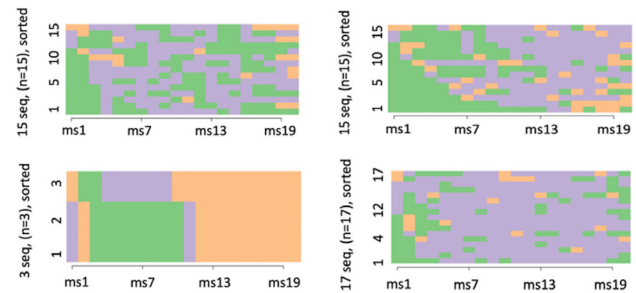


Figure 1. Sequences associated to the students' behavior clusters by p-know

Source: Authors

Table 1. Action proportions per typology

	Typology 1	Typology 2	Typology 3	Typology 4
Right %	36,8	25,33	5,33	32,54
Help %	23	21,27	2,6	53,13
Gaming %	29,14	25,83	0,67	44,36
Wrong %	27,84	25,7	2,01	44,45

Note: The highest values are marked in bold and the lowest are marked in italics

Source: Authors

1. **Type 1 (Good performance):** students in this typology have a good performance regarding correct and incorrect actions, as well as help-seeking (30% Cluster size; $n1=15$).
2. **Type 2 (Average performance):** in this group, students can be labeled as regular, since they represent a total of correct actions (20,6) that is below the total mean (23,89) (30% Cluster size; $n2=15$).
3. **Type 3 (Hardworking):** students who have an excellent performance during their interaction with the tutor and thus make the least number of mistakes. They also report the maximum amount of correct actions without system abuse (6% Cluster size; $n3=3$).
4. **Type 4 (Poor performance):** students who abuse the system during most of their interaction time. In addition, they are the group of students who make more mistakes in the average number of correct actions (34% Cluster size; $n4=17$).

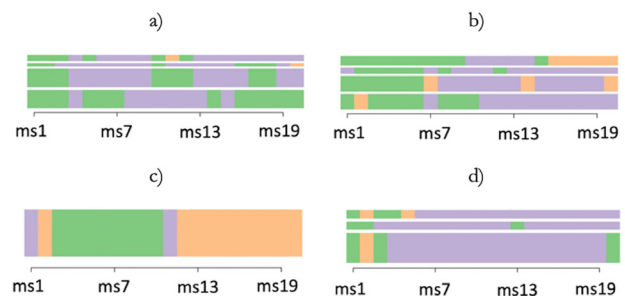


Figure 2. All behavior sequences typologies: a) good, b) average, c) hardworking and d) poor

Source: Authors

Once the typologies were identified, independent sample comparisons were made to study H2. In Table 2, descriptive statistics of each of the typologies regarding the actions: RIGT, HELP, GAMING, and WRONG can be observed.

Table 2. Averages and standard deviations ($M \pm SD$); achievement by typology

	n	Right	Help	Gaming	Wrong
Type 1	15	29,93 \pm 16,89	5,33 \pm 4,67	2,93 \pm 1,86	23,06 \pm 10,80
Type 2	15	20,60 \pm 8,99	4,93 \pm 6,64	2,6 \pm 1,54	21,26 \pm 13,41
Type 3	3	21,67 \pm 10,97	3 \pm 0	0,33 \pm 0,57	8,66 \pm 2,30
Type 4	17	23,35 \pm 11,15	10,88 \pm 8,16	3,94 \pm 2,48	32,47 \pm 20,44

Source: Authors

Kruskal-Wallis tests were conducted to check the differences in the variables of interest. The results show significant differences for the four typologies in help-seeking, gaming, and wrong answers ($p < 0,05$). A new Kruskal-Wallis test was carried out excluding type 3 students, and the results showed a significant difference only in help-seeking ($p < 0,05$).

Conclusions

The results suggest that student behaviors can be typified according to p-know value. Four groups were identified and labeled as good, average, hardworking, and poor. According to the proportions shown in Table 2, we accept H1, as it can be inferred that, according to the students' help-seeking typologies, they request less help from the tutor, and, as a consequence, they tend to have better performance. In Table 1, it can be observed that there is no significant difference in the comparison of typologies regarding the errors ($p = 0,1564$), correct actions ($p = 0,3264$), and system abuse ($p = 0,2407$). On the other hand, a significant difference was identified in the help-seeking typologies ($p = 0,0175$). Moreover, our results suggest that there are behaviors such as those described in the literature (HersHKovitz and Nachmias 2010). For example, Jovanovic *et al.* (2012) specify that student behaviors allow teachers to identify hardworking students based on their performance regarding a specific subject. Additionally, Taub *et al.* (2019) present the impact of performing activities in e-learning environments on the students' learning development. In this sense Romero *et al.* (2013) discuss how web mining can be applied in learning environments to predict the grades that students will obtain in a final exam.

Our results relate to the work by Romero *et al.* (2013) because they focus on analyzing the behavior of students in an educational environment with the objective of associating it with their learning within the classroom. During our research, association tests were carried out. We observed that there was a significant association between

typologies related to help-seeking ($p = 0,03277$), which confirms that help-seeking typologies with ITS not only exist but explain part of the learning accrued with this type of systems. Additionally, it was observed that "Wrong" has a high association with system abuse ($p < 0,01$), which is why it is important that these values are associated with type 4 students, who show more system abuse, thus leading them to seek more help and thus make more mistakes than the rest.

Additionally, students with poor performance tend to behave in a particularly unproductive manner: they start by doing positive and neutral actions, but, after a short time, they revert to only having negative learning probabilities (p-know) even if they perform correct actions. The findings in the literature (Duffy and Azevedo, 2015; Radford *et al.*, 2015; Angeli and Valanides, 2019) suggest that students benefit from scaffolding techniques; a positive effect has been detected in the interaction of students in learning environments in this regard. These results are important because they show the strategies students use to deal with the complexity of a specific task. In this context, in our research, the typologies associated to the students' behaviors during their interaction with the tutor can be observed (Figure 2). These typologies define our contribution to literature since:

- They represent a case study in which behavior typologies based on students' actions and the learning probability (p-know) are identified.
- These typologies help define personalized help-seeking strategies. In other words, system abuse is not necessarily negative for learning, since there is a group of students that benefit from it (type 4). This new educational scaffolding will allow acknowledging the probability that a new student belongs to any of the typologies, and so, in this way, the interaction with intelligent tutors will be even more personalized.

Future research should involve analyzing these typologies in an experimental situation, aiming to identify students' learning and verify the hypothesis that there is a direct relation between these typologies and student performance with an intelligent tutor.

Acknowledgements

The first author acknowledges the financial support from the Mexican Council of Science and Technology (CONACYT, Scholarship 442422). The corresponding author acknowledges the financial support of Writing Lab, TecLabs, Tecnológico de Monterrey, México, in the production of this work. The authors gratefully acknowledge the financial research support from CONACYT. This paper is dedicated to the memory of PhD Sergio Hernández González.

References

- Aleven, V. (2013). Help seeking and intelligent tutoring systems: Theoretical perspectives and a step towards theoretical integration. In R. Azevedo and V. Aleven (Eds.) *International Handbook of Metacognition and Learning Technologies* (pp. 311-335). Springer. https://doi.org/10.1007/978-1-4419-5546-3_21
- Aleven, V., Roll, I., McLaren, B. M., and Koedinger, K. R. (2016). Help helps, but only so much: Research on help seeking with intelligent tutoring systems. *International Journal of Artificial Intelligence in Education*, 26(1), 205-223. <https://doi.org/10.1007/s40593-015-0089-1>
- Aleven, V., Stahl, E., Schworm, S., Fischer, F., and Wallace, R. (2003). Help seeking and help design in interactive learning environments. *Review of Educational Research*, 73(3), 277-320. <https://doi.org/10.3102/00346543073003277>
- Angeli, C. and N. Valanides (2019). Developing young children's computational thinking with educational robotics: An interaction effect between gender and scaffolding strategy. *Computers in Human Behavior*, 105, 105954. <https://doi.org/10.1016/j.chb.2019.03.018>
- Apaolaza, A. and Vigo, M. (2019). Assisted Pattern Mining for Discovering Interactive Behaviours on the Web. *International Journal of Human-Computer Studies*, 130, 196-208. <https://doi.org/10.1016/j.ijhcs.2019.06.012>
- Baker, R. S., Corbett A. T., and Koedinger K. R. (2004). Detecting student misuse of intelligent tutoring systems. In J. C. Lester, R. M. Vicari, and F. Paraguaçu (Eds.) *Intelligent Tutoring Systems, ITS 2004* (pp. 531-540). Springer. https://doi.org/10.1007/978-3-540-30139-4_50
- Baker, R. S., Corbett, A. T., Koedinger, K. R., and Wagner, A. Z. (2004). Off-task behavior in the cognitive tutor classroom: when students game the system. In ACM (Eds.) *Proceedings of the SIGCHI conference on Human factors in computing systems* (pp. 383-390). Association for Computer Machinery. <https://doi.org/10.1145/985692.985741>
- Baker, R. S. and Inventado, P. S. (2014). Educational data mining and learning analytics. In J. A. Larusson and B. White (Eds.) *Learning Analytics* (pp. 61-75). Springer.
- Chang, M., D'Aniello, G., Gaeta, M., Orciuoli, F., Sampson, D., and Simonelli, C. (2020). Building ontology-driven tutoring models for intelligent tutoring systems using data mining. *IEEE Access*, 8, 48151-48162. <https://doi.org/10.1109/ACCESS.2020.2979281>
- D'Aniello, G., Gaeta, A., Gaeta, M., and Tomasiello, S. (2018). Self-regulated learning with approximate reasoning and situation awareness. *Journal of Ambient Intelligence and Humanized Computing*, 9(1), 151-164. <https://doi.org/10.1007/s12652-016-0423-y>
- Duffy, M. C. and Azevedo, R. (2015). Motivation matters: Interactions between achievement goals and agent scaffolding for self-regulated learning within an intelligent tutoring system. *Computers in Human Behavior*, 52, 338-348. <https://doi.org/10.1016/j.chb.2015.05.041>
- Falakmasir, M. H. and Habibi, J. (2010). Using educational data mining methods to study the impact of virtual classroom in e-learning. In R. S.J.d. Baker, A. Merceron., P. I. Pavlik Jr. (Eds.) *Educational Data Mining 2010* (pp. 241-248). ERIC. <https://files.eric.ed.gov/fulltext/ED538834.pdf>
- Gabadinho, A., Ritschard, G., Mueller, N. S., and Studer, M. (2011). Analyzing and visualizing state sequences in R with TraMineR. *Journal of Statistical Software*, 40(4), 1-37. <https://doi.org/10.18637/jss.v040.i04>
- Hershkovitz, A. and R. Nachmias (2010). Is Students' Activity in LMS Persistent? In R. S.J.d. Baker, A. Merceron., P. I. Pavlik Jr. (Eds.) *Educational Data Mining 2010* (pp. 295-296). ERIC. <https://files.eric.ed.gov/fulltext/ED538834.pdf>
- Jovanovic, M., Vukicevic, M., Milovanovic, M., and Minovic, M. (2012). Using data mining on student behavior and cognitive style data for improving e-learning systems: a case study. *International Journal of Computational Intelligence Systems*, 5(3), 597-610. <https://doi.org/10.1080/18756891.2012.696923>
- Juhaňák, L., Zounek, J., and Rohlíková, L. (2019). Using process mining to analyze students' quiz-taking behavior patterns in a learning management system. *Computers in Human Behavior*, 92, 406-506. <https://doi.org/10.1016/j.chb.2017.12.015>
- Lara-Muñoz, E., Rebolledo-Méndez, G., and Rojano-Cáceres, J. (2019). Mejorando el aprovechamiento de las actividades colaborativas por pares de estudiantes utilizando tecnología educativa en matemática. *Revista Complutense de Educación*, 30(2), 441-460. <https://doi.org/10.5209/RCED.57597>
- Padayachee, I. (2002). Intelligent tutoring systems: Architecture and characteristics. In SACLA (Eds.) *Proceedings of the 32nd Annual SACLA Conference* (pp. 1-8). South African Computer Lecturers' Association.
- Pardos, Z. A. and Heffernan, N. T. (2001). *Using HMMs and bagged decision trees to leverage rich features of user and skill from an intelligent tutoring system dataset*. Journal of Machine Learning Research W & CP. http://people.csail.mit.edu/zp/papers/pardos_JMLR_in_press.pdf
- Peña-Ayala, A. (2014). Educational data mining: A survey and a data mining-based analysis of recent works. *Expert Systems with Applications*, 41(4), 1432-1462. <https://doi.org/10.1016/j.eswa.2013.08.042>
- Radford, J., Bosanquet, P., Webster, R., and Blatchford, P. (2015). Scaffolding learning for independence: Clarifying teacher and teaching assistant roles for children with special educational needs. *Learning and Instruction*, 36, 1-10. <https://doi.org/10.1016/j.learninstruc.2014.10.005>
- Rebolledo-Mendez, G., Huerta-Pacheco, N. S., Baker, R. S., and du Bolay, B. (2021). Meta-Affective Behaviour within an Intelligent Tutoring System for Mathematics. *International Journal of Artificial Intelligence in Education*. <https://doi.org/10.1007/s40593-021-00247-1>
- Roll, I., Aleven, V., McLaren, B. M., and Koedinger, K. R. (2011). Improving students' help-seeking skills using metacognitive feedback in an intelligent tutoring system. *Learning and Instruction*, 21(2), 267-280. <https://doi.org/10.1016/j.learninstruc.2010.07.004>
- Romero, C., López, M. I., Luna, J. M., and Ventura, S. (2013). Predicting students' final performance from participation in on-line discussion forums. *Computers & Education*, 68, 458-472. <https://doi.org/10.1016/j.compedu.2013.06.009>

- Tabandeh, Y. and A. Sami (2010). Classification of tutor system logs with high categorical features. *JMLR: Workshop and Conference Proceeding*, 8. https://pslccdatashop.web.cmu.edu/KDDCup/workshop/papers/JMLR_Y10.pdf
- Tai, M., Arroyo, I., and Woolf, B. P. (2013) Teammate Relationships Improve Help-Seeking Behavior in an Intelligent Tutoring System. In H. Chad Lane, K. Yacef, J. Mostow, and P. Pavlik (Eds.) *Artificial Intelligence in Education. AIED 2013* (pp. 239-248). https://doi.org/10.1007/978-3-642-39112-5_25
- Taub, M., Azevedo, R., Rajendran, R., Cloude, E. B., Biswas, G., and Price, M. J. (2019). How are students' emotions related to the accuracy of cognitive and metacognitive processes during learning with an intelligent tutoring system? *Learning and Instruction*, 72, 101200. <https://doi.org/10.1016/j.learninstruc.2019.04.001>
- Vaessen, B. E., Prins, F. J., and Jeuring, J. (2014). University students' achievement goals and help-seeking strategies in an intelligent tutoring system. *Computers & Education*, 72, 196-208. <https://doi.org/10.1016/j.compedu.2013.11.001>

Instructions for Authors

The Editorial Committee reserves the copyright to printing any material and its total or partial reproduction, as well as the right to accept submitted material or reject it. It also reserves the right to make any editorial modification which it thinks fit. In such event, the author of the submitted material will receive the evaluators' recommendations in writing. If an author accepts them, the revised (or rewritten) article must be submitted with the suggested changes having been made by the date on the date set by the journal in order to guarantee its publication in the scheduled issue..

The process to be followed for publishing an article in the journal

The article must be uploaded into the journal's OJS website (see the guidelines for article submission in the Authors guide section in our website <http://www.revistas.unal.edu.co/index.php/ingeneinv/article/view/59291/56815>). Any manuscript must be submitted using journal's template (with a maximum length of six pages) and must be accompanied by the license agreement, addressed to the journal's editor, Prof. Andrés Pavas, stating that all authors involved in the work in question agree to its submission for consideration in the *Ingeniería e Investigación* journal.

Article and License templates are available on:

<http://www.revistas.unal.edu.co/index.php/ingeneinv/index>

Once an article has been received by the journal, the corresponding author will be notified by e-mail and the peerreview process will begin. Following this evaluation, authors will then be informed whether their article has been accepted or not. If accepted, authors must deal with the respective corrections recommended by the evaluators and the Editorial Committee's final decision –if the article is to be published.

Content

All articles considered by the committee for possible publication in the *Ingeniería e Investigación* journal must consist of the following parts:

- Title, abstract and keywords must be written in Spanish and English. The title must clearly explain the contents of the article in question, written in normal title form and be preferably brief. The abstract should contain around 200 words in Spanish and English, in addition to the methods and materials used, results obtained, and conclusions drawn.
- An Introduction must be given. It must describe the article's general purpose, including its main objective, referring to any previous work and the scope of the current article.
- Conclusions must be drawn. This section must provide the implications of the results found and their relationship to the proposed objective.
- Bibliographical references must be given (an explanation and example of how to set them out is given later on).
- Acknowledgements (Optional). These should be brief and mention any essential support received for carrying out the work being reported.
- Appendix (Optional).

Scientific and technological research articles must also include:

- Experimental development. This must be written giving sufficient details for the subject to be fully understood by readers, including the descriptions of any procedures involved.

- Results. These must give a clear explanation and interpretation of the findings. If necessary, a brief, focused discussion about how given results can be interpreted.

It is required that the bibliographical references for all articles be included at the end of the article, given in alphabetical order of first authors' surnames, and mentioned in the text and, since May 2014, it is asked that the authors use the American Psychological Association (APA) style for citation and references:

- Articles published in journals:

Author, A. A., Author, B. B., and Author, C. C. (year). Article title. *Journal Title*, volume number (issue number), page numbers.

Del Sasso, L. A., Bey, L. G., and Renzel, D. (1958). Low-scale flight ballistic measurements for guided missiles. *Journal of the Aeronautical Sciences*, 15(10), 605-608

Author, A. A., and Author, B. B. (year). Article title. *Journal Title*, volume number (issue number), page numbers. <http://www.xxxxxxxxxxxxxxxxxx>

Gaona, P. A. (2014). Information visualization: A proposal to improve search and access digital resources in repositories. *Ingeniería e Investigación*, 34(1), 83-89. <http://www.revistas.unal.edu.co/index.php/ingeneinv/article/view/39449>

- Books:

Author, A. A., and Author, B. B. (year). Title of work. Publisher.

Turner, M. J., Martin, H. C., and Leible, R. C. (1964). Further development and applications of the stiffness method, *Matrix Methods of Structural Analysis*. New York: the Macmillan Co.

- Conference papers and symposium contributions:

Naveen, B., and Sivakamasundari, S. (2016). *Study of strength parameters of bacterial concrete with controlled concrete and structural elements made with concrete enriched with bacteria* [Conference presentation]. International conference on engineering innovations and solutions CMS College of Engineering, Tamil Nadu, India.

- Theses or undergraduate projects:

Cazalla, O. (2002). *Morteros de cal. Aplicación en el patrimonio histórico* [Doctoral thesis, Universidad de Granada]. <http://hdl.handle.net/10481/28626>

Further information can be obtained by:

Contacting the Editorial Team (Email: revii_bog@unal.edu.co) or Prof. Andrés Pavas (Editor-in-Chief. Email: fapavasm@unal.edu.co)

The *Ingeniería e Investigación* journal's office is located at: Ciudad Universitaria, Facultad de Ingeniería, Edificio CADE. Telefax: (57-1) 3165000 Ext. 13674. Bogotá - Colombia.